High Temperature Gas Cooled Reactor Fuels and Materials

The following States are Members of the International Atomic Energy Agency:

AFGHANISTAN
ALBANIA
ALGERIA
ANGOLA
ARGENTINA
ARMENIA
AUSTRALIA
AUSTRIA
AZERBAIJAN
BAHRAIN
BANGLADESH
BELARUS
BELGIUM
BELIZE
BENIN
BOLIVIA
BOSNIA AND HERZEGOVINA
BOTSWANA
BRAZIL
BULGARIA
BURKINA FASO
BURUNDI
CAMBODIA
CAMEROON
CANADA
CENTRAL AFRICAN REPUBLIC
CHAD
CHILE
CHINA
COLOMBIA
CONGO
COSTA RICA
CÔTE D'IVOIRE
CROATIA
CUBA
CYPRUS
CZECH REPUBLIC
DEMOCRATIC REPUBLIC OF THE CONGO
DENMARK
DOMINICAN REPUBLIC
ECUADOR
EGYPT
EL SALVADOR
ERITREA
ESTONIA
ETHIOPIA
FINLAND
FRANCE
GABON
GEORGIA
GERMANY
GHANA
GREECE
GUATEMALA
HAITI
HOLY SEE
HONDURAS
HUNGARY
ICELAND
INDIA
INDONESIA
IRAN, ISLAMIC REPUBLIC OF
IRAQ
IRELAND
ISRAEL
ITALY
JAMAICA
JAPAN
JORDAN
KAZAKHSTAN
KENYA
KOREA, REPUBLIC OF
KUWAIT
KYRGYZSTAN
LATVIA
LEBANON
LESOTHO
LIBERIA
LIBYAN ARAB JAMAHIRIYA
LIECHTENSTEIN
LITHUANIA
LUXEMBOURG
MADAGASCAR
MALAWI
MALAYSIA
MALI
MALTA
MARSHALL ISLANDS
MAURITANIA
MAURITIUS
MEXICO
MONACO
MONGOLIA
MONTENEGRO
MOROCCO
MOZAMBIQUE
MYANMAR
NAMIBIA
NEPAL
NETHERLANDS
NEW ZEALAND
NICARAGUA
NIGER
NIGERIA
NORWAY
OMAN
PAKISTAN
PALAU
PANAMA
PARAGUAY
PERU
PHILIPPINES
POLAND
PORTUGAL
QATAR
REPUBLIC OF MOLDOVA
ROMANIA
RUSSIAN FEDERATION
SAUDI ARABIA
SENEGAL
SERBIA
SEYCHELLES
SIERRA LEONE
SINGAPORE
SLOVAKIA
SLOVENIA
SOUTH AFRICA
SPAIN
SRI LANKA
SUDAN
SWEDEN
SWITZERLAND
SYRIAN ARAB REPUBLIC
TAJIKISTAN
THAILAND
THE FORMER YUGOSLAV REPUBLIC OF MACEDONIA
TUNISIA
TURKEY
UGANDA
UKRAINE
UNITED ARAB EMIRATES
UNITED KINGDOM OF GREAT BRITAIN AND NORTHERN IRELAND
UNITED REPUBLIC OF TANZANIA
UNITED STATES OF AMERICA
URUGUAY
UZBEKISTAN
VENEZUELA
VIETNAM
YEMEN
ZAMBIA
ZIMBABWE

The Agency's Statute was approved on 23 October 1956 by the Conference on the Statute of the IAEA held at United Nations Headquarters, New York; it entered into force on 29 July 1957. The Headquarters of the Agency are situated in Vienna. Its principal objective is "to accelerate and enlarge the contribution of atomic energy to peace, health and prosperity throughout the world".

IAEA-TECDOC-1645

High Temperature Gas Cooled Reactor Fuels and Materials

INTERNATIONAL ATOMIC ENERGY AGENCY
VIENNA, 2010

For further information on this publication, please contact:

Nuclear Fuel Cycle and Materials Section
International Atomic Energy Agency
Vienna International Centre
PO Box 100
1400 Vienna, Austria
email: Official.Mail@iaea.org

HIGH TEMPERATURE GAS COOLED REACTOR
FUELS AND MATERIALS
IAEA, VIENNA, 2010
IAEA-TECDOC-1645-CD
ISBN 978-92-0-153110-2
ISSN 1684-2073

Printed by the IAEA in Austria
March 2010

FOREWORD

At the third annual meeting of the technical working group on Nuclear Fuel Cycle Options and Spent Fuel Management (TWG-NFCO), held in Vienna, in 2004, it was suggested “to develop manuals/handbooks and best practice documents for use in training and education in coated particle fuel technology” in the IAEA’s Programme for the year 2006–2007. In the context of supporting interested Member States, the activity to develop a handbook for use in the “education and training” of a new generation of scientists and engineers on coated particle fuel technology was undertaken. To make aware of the role of nuclear science education and training in all Member States to enhance their capacity to develop innovative technologies for sustainable nuclear energy is of paramount importance to the IAEA

Significant efforts are underway in several Member States to develop high temperature gas cooled reactors (HTGR) based on either pebble bed or prismatic designs. All these reactors are primarily fuelled by TRISO (tri iso-structural) coated particles. The aim however is to build future nuclear fuel cycles in concert with the aim of the Generation IV International Forum and includes nuclear reactor applications for process heat, hydrogen production and electricity generation. Moreover, developmental work is ongoing and focuses on the burning of weapon-grade plutonium including civil plutonium and other transuranic elements using the “deep-burn concept” or “inert matrix fuels”, especially in HTGR systems in the form of coated particle fuels. The document will serve as the primary resource materials for “education and training” in the area of advanced fuels forming the building blocks for future development in the interested Member States.

This document broadly covers several aspects of coated particle fuel technology, namely: manufacture of coated particles, compacts and elements; design-basis; quality assurance / quality control and characterization techniques; fuel irradiations; fuel failure mechanisms; accident testing; fuel and fission product chemistry; fuel cycles; fission product transport; spent fuel management; and nuclear hydrogen production. This knowledge base was gained over nearly fifty years of fuel materials research and development in the international HTGR community. The primary intent of this effort is that this documented experience will provide the basis for further development of HTGR fuels and reactor systems. In many ways this book is a unique source of past experience, and hopefully, it will serve as an important part of future development of nuclear energy worldwide for the new generation scientists and engineers.

The authors for the preparation of this report were drawn from a large number of countries involved today in HTGR research and development. Subsequently, consultancy meetings in December 2006 (Vienna), December 2007 (NRG, Petten) and November, 2008 (Vienna) were held to review and finalize this report. The IAEA is grateful to the experts who contributed to this publication (listed at the end of this publication). Special thanks to H. Nabielek of Germany for chairing this working group and to Ü. Colak of Turkey and M.J. Kania of the USA for their critical review of this report. The IAEA officer responsible for this publication was H.P. Nawada of the Division of Fuel Cycle and Waste Technology.

CONTENTS

1. INTRODUCTION

A recent forecast by the International Energy Agency considering sustainable energ development vision scenario [1] indicates that nuclear energy can provide a significant role in meeting future energy demand. Years after start-up of the first gas cooled nuclear reactor, Calder Hall in 1956, nuclear energy has gained an important place in the world's electricity generation. There are currently 439 reactors with a total generating capacity of 372 GWe worldwide [2]. Furthermore, 34 units with generating capacity of 28 GWe were under construction as of June 2008.

Within the framework of the project "Prototype Nuclear Process Heat" (PNP), the coal gasification processes for hydrogen production was also investigated in Germany. These activities eventually resulted in the construction and operation of pilot plants for coal gasification utilizing nuclear heat source. Catalytic and non-catalytic steam-coal gasification of hard coal was verified in the 1.2 MW WKV facility using 950°C helium as the energy source. The process of hydro-gasification of brown coal (lignite) was realized in the 1.5 MW HKV plant operated for ~ 27 000 h with a total amount of 1800 tons of lignite being gasified.

More and more countries look into the nuclear option, and countries in which nuclear was to be phased-out have called for renewed evaluations. The economic record of nuclear power plants is good, and new units promise even better economics. Against this excellent record of environmental friendly electricity generation stands the fear of a catastrophic nuclear accident.

The Generation IV International Forum was founded to study and promote the fourth generation of advanced reactors with enhanced safety features, superior proliferation resistance attributes, efficient fuel resource utilization and improved economics. Among the concepts is the Very High Temperature Reactor, VHTGR, with gas outlet temperatures of 900 to 1000°C. The high temperature in the primary cycle enables the realization of efficient thermal conversion cycles like the superheated steam cycle and the gas turbine cycle.

Net thermal efficiencies greater then 45% are within reach in some of the designs of High Temperature Gas-cooled Reactors (HTGR). The high outlet gas temperatures may also be utilized as a thermal heat source in endothermic chemical processes. Examples are in coal chemistry and upgrading of hydrocarbons. Hydrogen production is another promising field for deployment of the HTGR (Annexure). The foremost motivation for the development of HTGR technology is its enhanced safety features along with its high temperature capabilities. The enhanced safety of the HTGR fuel is based on its coated fuel particle design consisting of minute uranium particles coated with layers of carbon and silicon carbide. Coated particles can withstand high internal gas pressure without releasing their fission products to the environment. The understanding gained through the design, fabrication, and testing of HTGR fuel is the goal of this book.

1.1. HTGR technology

1.1.1. History of HTGR development and concepts

The HTGR has a long history going back to the earliest days of nuclear energy development. Commercial gas-cooled nuclear power for electricity production started in 1956 with the operation of the first 50 MWe unit at Calder Hall, UK. The design, which came to be known as Magnox, featured carbon-dioxide as the pressurized coolant and magnesium alloy cladding for the fuel. Thermal efficiency was still limited to ~ 20%. To raise thermal efficiency, later

designs switched to stainless steel cladding, enriched uranium oxide fuel, higher CO_2 pressures, and higher operating temperatures in what came to be known as the Advanced Gas Reactor (AGR).

The use of helium (He) as a coolant was advocated as early as 1944 in a 5 MWt experimental reactor project, also featuring an indirect gas turbine cycle. Later, the prototype DRAGON reactor [2] was put into operation at Winfrith in the UK, between 1965 and 1976. Featuring a steel pressure vessel, coated fuel particles of highly-enriched uranium-thorium carbide and a helium outlet temperature of 750ºC, the 20 MWt prototype reactor served as a test bed providing valuable information on fuel, material and component behavior under high-purity helium conditions.

The starting point of contemporary HTGR design concept is early air and CO_2 cooled reactors. The substitution of He instead of air or CO_2 provided excellent neutronic and thermal characteristics together with a graphite moderator. Historical HTGR technology development is shown in Fig. 1 and Table 1 There are two mainstream HTGR design concepts; the prismatic core design and the pebble bed core design. They both possess common advantages of the HTGR design such as inherent safety and high efficiency. Historically, the initial design efforts were started at the Atomic Energy Research Establishment (AERE) in the United Kingdom in 1956. Simultaneously, another independent study was initiated in Germany to a design pebble bed core version of the system. The work in the UK resulted in the construction of the DRAGON reactor, a 20 MWt test reactor, at Winfrith [3]. This facility was extensively utilized to demonstrate capabilities of HTGRs and coated particle fuel. It operated from 1964 to 1976. The German efforts were also successful in the building and operation of the AVR pebble bed reactor in 1966 at Jülich, Germany [4]. This reactor accumulated 122 000 hours of operation in 21 years.

The main features of HTGRs are enhanced safety, high thermal efficiency, economical competitiveness, and prolifileration resistance and these make this technology a potential candidate for the nuclear power plant deployment. One of the driving forces behind the HTGR philosophy is its utilization in the production of process heat. Net thermal efficiencies greater then 45% are within the reach in some of the designs of HTGRs. The high outlet gas temperatures may also be utilized as a thermal heat source in endothermic chemical processes. Examples are in coal chemistry and upgrading of hydrocarbons. Hydrogen production is another promising field for deployment of the HTGR. The short construction period, modularity and low capital cost are also attractive characteristics of HTGRs. The foremost motivation for the development of HTGR technology is its enhanced safety features along with its high temperature capabilities. The enhanced safety of the HTGR fuel is based on its coated fuel particle design consisting of uranium oxide / carbide particles coated with layers of pyrolytic carbon and silicon carbide. Coated particles are so designed that they can withstand high internal gas pressure without releasing any fission products to the environment. The understanding gained through the design, fabrication, and testing of HTGR fuel is the goal of this book.

1.1.2. Characteristics and utilization of HTGRs

There are many advantages of HTGRs over conventional water cooled reactors from the safety point of view. First of all, the large mass of the graphite moderator provides high heat capacity. Core materials are made of ceramic materials and usable at elevated temperatures. The helium coolant is single phase and an inert fluid. Thus, chemical interactions between fuel, moderator, and coolant can be avoided. However, these same chemical interactions are

the primary concern in water cooled reactors, especially during transients since water-zirconium reactions are exothermic at elevated temperatures and such reactions become autocatalytic. According to the HTGR fuel design philosophy, the SiC layer in TRISO particles serve as the primary pressure boundary. Modern TRISO particles have very high fission product retention capability.

Even though the two HTGR concepts have a similar design approach, their structural and operational characteristics are quite different. The main difference is in their fuel form, either prismatic block type or spherical pebble type fuel. The prismatic HTGR concept with hexagonal-graphite block fuel elements has been used in prototype and commercial HTGRs in USA and is also currently utilized in the design of the High Temperature Test Reactor (HTTR) [5] in Japan and the Gas Turbine – Modular Helium Reactor (GT-MHR) design shown in Fig. 2. The GT-MHR Project [6] is an international effort between the US Department of Energy (DOE) and the Russian State Corporation, Rosatom. (The GT-MHR Project was initiated in the mid-1990s between General Atomics of the US and Minatom of Russia. In 1989 the US-DOE began to provide support for the project.) In this design, a gas cooled modular helium reactor is coupled with a Brayton cycle gas turbine to provide high efficiency energy conversion in the order of 47%.

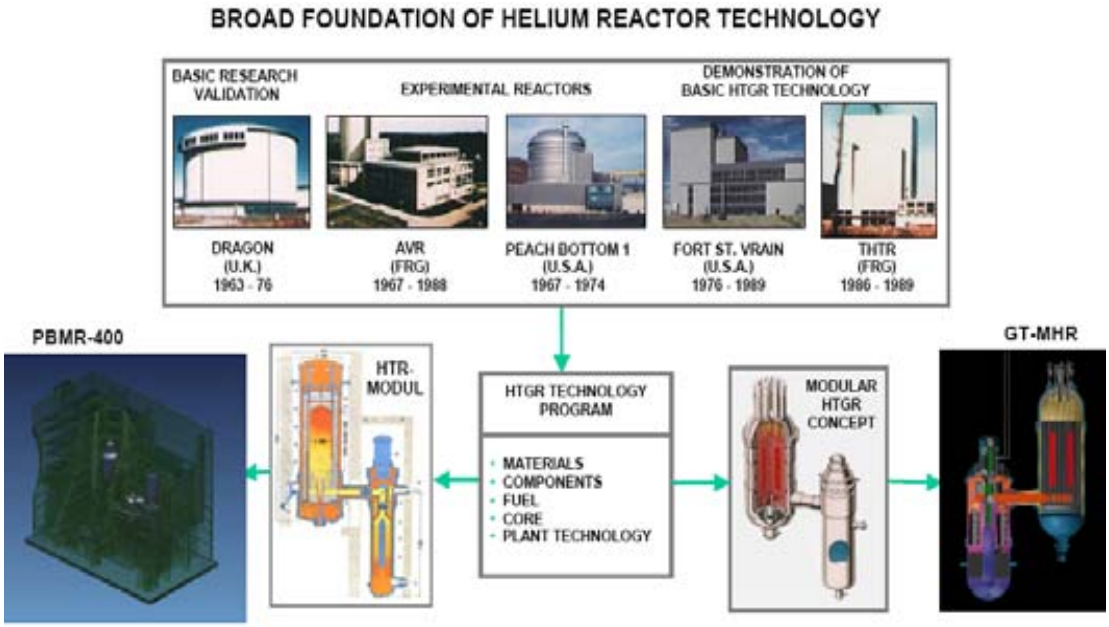

Fig. 1. HTGR technology development.

Table 1. HIGH TEMPERATURE REACTORS:
Key operation and design data that characterize the early and modern experimental HTGRs, prototype HTGRs, their follow-on commercial HTR projects, and current commercial prototype HTR projects

Experimental HTGRs					
	Peach Bottom (USA)	**Dragon** (UK)	**AVR** (Germany)	**HTTR** (Japan)	**HTR-10** (China)
Operational	1967-74	1968-75	1967-88	1998-xx	2000-xx
Status	safe encl.	safe encl.	Defueled	in operation	in operation
Thermal/electric power [MW_{th}/MW_{el}]	115/40	20/-	46/15	30/-	10/-
Fuel element type	pin	pin	Spherical	pin-in-block	Spherical
Power density [$MW_{th}.m^{-3}$]	8.3	14	2.6	2.5	2
He-inlet/ outlet temperature [°C]	377/750	350/750	270/950	385/850 and 950	250/350/ 700/900
Mean He pressure [MPa]	2.5	2	1	4	3
Enrichment	HEU	HEU/ LEU	HEU/ LEU	LEU	LEU
Fuel	Carbide	Oxide	Carbide/ Oxide	Oxide	Oxide
Coating	BISO	TRISO	BISO/ TRISO	TRISO	TRISO
Pressure vessel	steel	steel	Steel	steel	Steel

Prototype HTGRs		
	Fort St. Vrain (USA)	**THTR** (Germany)
Operational	1976-1989	1986-1989
Status	Decommissioned	safe enclosure
Thermal/electric power [MW_{th}/MW_{el}]	842/330	750/300
Fuel element type	Prismatic	Spherical
Power density [$MW_{th}.m^{-3}$]	6.3	6
He-inlet/-outlet temperature [°C/°C]	405/784	270/750
Mean He pressure [MPa]	4.5	3.9
Steam temperature [°C]	530	530
Electricity production [MWh]	5500	2890
Enrichment	HEU	HEU
Fuel	Carbide	Oxide
Coating	TRISO	BISO
Pressure vessel	PCRV	PCRV

Commercial HTGR Projects					
German designs	**PNP**	**HHT**	**HTR-500**	**HTR-Modul**	**HTR-100**
Thermal/electric power [MW_{th}/MW_{el}]	500/-	1240/500	1250/500	200/80	258/100
Fuel element type	spherical	block/ spherical	spherical	spherical	Spherical
Power density [$MW_{th}m^{-3}$]	4	5,5	7	3	3
He-inlet/-outlet temperature [°C/°C]	300/950	440/850	280/700	250/750	250/740
He pressure [MPa]	3.9	5.0	4.7	5.0	7.0
Steam temperature[°C]	850	-	530	530	530
Enrichment	LEU	LEU	LEU	LEU	LEU
Fuel	Oxide	Oxide	Oxide	Oxide	Oxide
Coating	TRISO	TRISO	TRISO	TRISO	TRISO
Pressure vessel	PCRV	PCRV	PCRV	Steel	Steel
International designs	**MHTGR** (USA)	**VGR-50** (Russia)	**VGM-400** (Russia)	**PBMR** (SA)	**GT/MHR** (USA/Russia)
Thermal/electric power [MW_{th}/MW_{el}]	350/140	136/50	1060/300	400/165	600/285

Fuel element type	prismatic	spherical	spherical	spherical	prismatic
Power density [$MW_{th}.m^{-3}$]	6	?	?	4.8	6.5
He-inlet/-outlet temperature [°C]	319/685	296/810	350/950	500/900	510/850
He pressure [MPa]	9	4	5	9	7
Enrichment	LEU	HEU	LEU	LEU	U/Pu
Fuel	UCO	Oxide	Oxide	Oxide	Oxide
Coating	TRISO	TRISO	TRISO	TRISO	TRISO
Pressure vessel	steel	steel	PCRV	steel	steel

	HTR-PM (China)	**HTR/VHTR [ANTARES]** (France)	**NGNP (VHTR)** (USA)	
Thermal/electric power [MW_{th}/MW_{el}]	2x250/ 200	600/-	600 (max)/-	500/200
Fuel element type	spherical	prismatic	prismatic	spherical
Power density [$MW_{th}.m^{-3}$]	3.215	?	undecided	6.0
He-inlet/-outlet temperature [°C/°C]	250/700	400/1000	-/ 850 to 950	350/ 850 to 950
He pressure [MPa]	7	5	undecided	9
Enrichment	LEU	LEU	LEU	LEU
Fuel	Oxide	UCO or UO_2	UCO	UO_2
Coating	TRISO	TRISO	TRISO	TRISO
Pressure Vessel	Steel	Steel	Steel	Steel

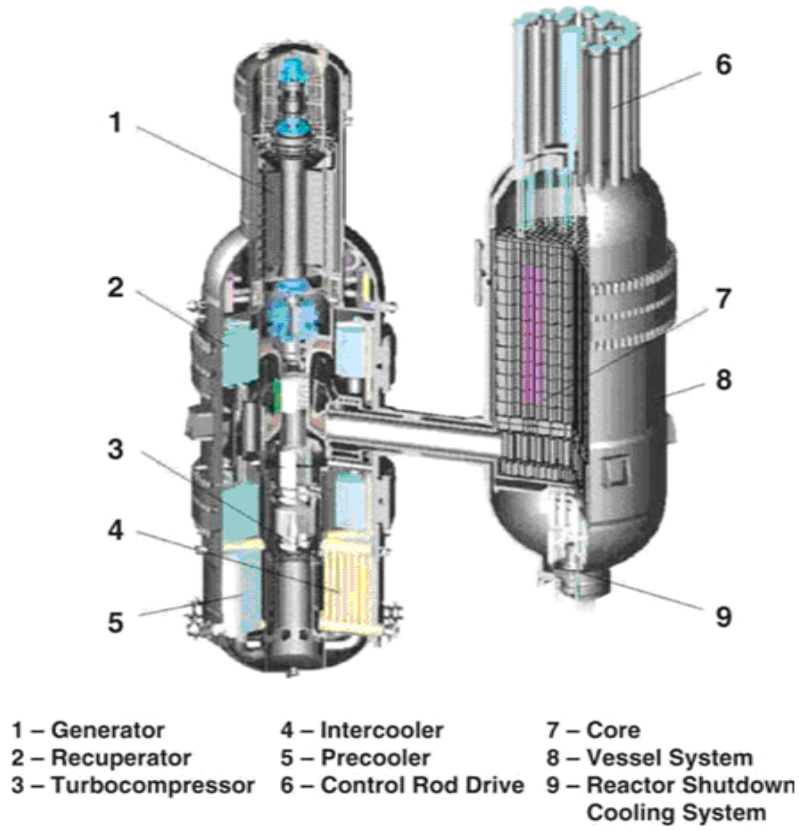

Fig. 2. GT-MHR module [6].

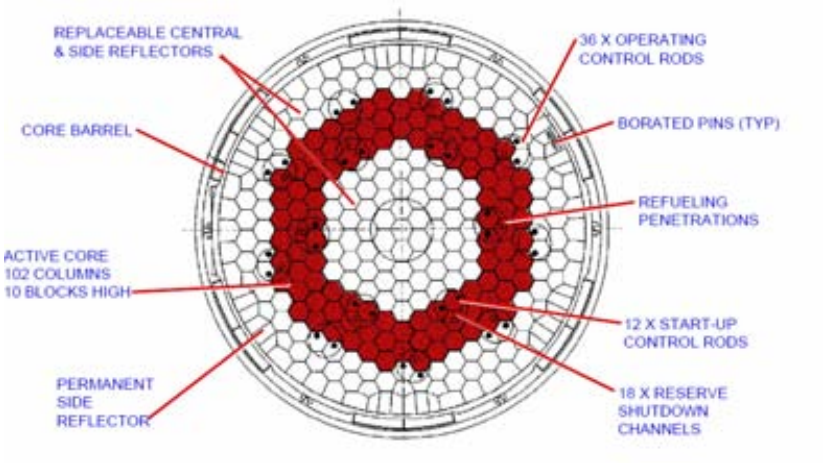

Fig. 3. GT-MHR annular core [6].

Fuel for the GT-MHR is in the form of TRISO-coated particles embedded in a carbonaceous matrix and then formed into cylindrical fuel compact. These compacts are approximately 13 mm in diameter and 51 mm long. They are then inserted, one on top of the other into fuel holes, machined in the hexagonal graphite fuel elements, 793 mm long and 360 mm across sides. An annular core is formed by stacking ten layers of blocks, each layer containing 102 hexagonal fuel elements, surrounding a replaceable un-fueled center of graphite blocks. The fueled region is then surrounded by un-fueled side reflector graphite blocks as shown in Fig. 3.

The GT-MHR core possesses some excess reactivity because the batch wise refueling and fuel shuffling operations are carried out off-line. This reactor design has the flexibility of utilizing different fuel cycles. Plutonium fuel, originated from dismantled nuclear weapon stockpiles, will be burned in the GT-MHR. The transmutation of LWR spent fuel is another prospective fuel cycle scenario.

The second HTGR concept is the pebble bed reactor. A successful prototype which also supplied 15 MWe of electricity to the grid was the AVR reactor which was operated at Juelich, Germany (1967-1988) [4]. This particular HTGR design incorporated on-line refueling with 100 000 spherical fuel elements traveling downwards through the core and achieved a gas outlet temperature of 950ºC. During its years of operation, the AVR was used to perform tests related to HTGR performance and safety.

In the US, the Peach Bottom Unit 1 was the first HTGR demonstration plant [7]. Rated at 40 MWe, the unit was operated between 1967 and 1974. Early operation experience prompted significant coated fuel particle design changes with the introduction of the buffer layer to the coated particle. All along, two distinctive HTGR concept designs were emerging, namely, the pebble-bed type and the prismatic block type. Two power prototypes, each rated around 300 MWe were operated in the 1980s. The German Thorium Hochtemperature Reaktor (THTR-300) [8] represented the pebble-bed concept, while the US Fort St. Vrain (FSV) Power Station [9] represented the prismatic concept. Funding and technical problems led to the early closure of both reactors.

The South African HTGR design, the Pebble Bed Modular Reactor (PBMR) [10], is the successor of early generation, small German pebble bed reactors (AVR and HTR-MODUL designs). The PBMR (Fig. 4) is designed to run on a direct Brayton cycle using a gas turbine to generate electricity. There is also another prospective pebble bed reactor design which is underway in China. The Chinese reactor HTR-PM (High Temperature Gas Cooled Reactor-Pebble Bed Module) [11] will initially operate on a steam cycle to shorten the design period and utilize Chinese expertise with steam turbines. The demonstration plant is expected to be completed around 2013.

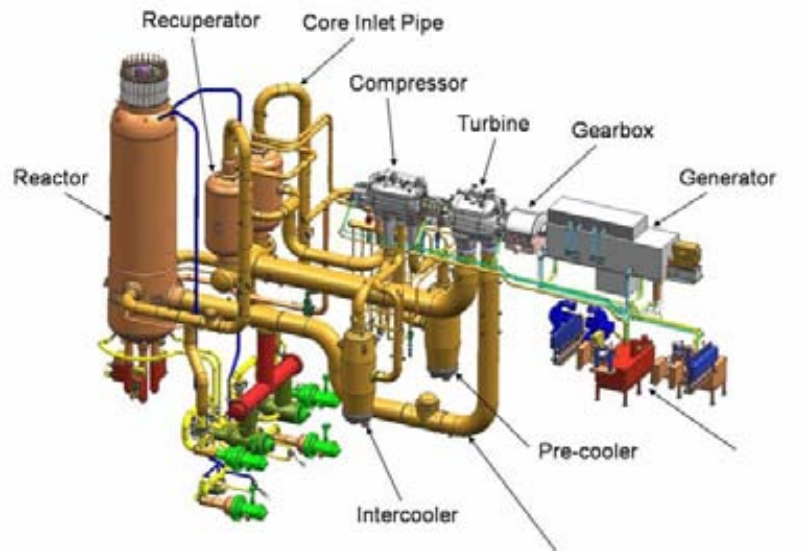

Fig. 4. Pebble Bed Modular Reactor PBMR main components [10].

Modular pebble bed reactors employ fuel elements similar to those used in the AVR. The fuel element is spherical in shape and 60 mm diameter. The fueled portion of the element is 50 mm diameter and contains coated fuel particles imbedded into a graphite matrix. The number of coated particles and their enrichment may change according to the design considerations. It is possible to mix or arrange fuel spheres with pure graphite moderator spheres and B4C-containing absorber spheres in the core. Alternatively, a solid central graphite column at the center and control rods in the side reflector may be employed as in the design of the PBMR. Maximum fuel temperatures are kept at a low level by the presence of a solid central reflector. This provides an extra margin of safety.

An important difference of pebble bed reactors compared to the prismatic reactor is the capability to do on-line refueling. Thus, the reactor can be run without having to be shut down for long period for refueling. This may increase plant capacity factors. Another advantage of on-line refueling is that the reactor can operate with very little excess reactivity and reduced enrichment.

One of the conceptual Generation IV reactor designs, the VHTR is a further evolution of HTGR concepts with enhanced safety and increased helium outlet temperature. Thus, heat can be supplied for process heat applications including hydrogen production and other chemical processes. Electricity generation using a direct Brayton cycle gas turbine also remains an option of this reactor system [12].

The TRISO-coated particles have an overall diameter in the range of 500 to 1000 μm. Each particle contains a spherical fuel kernel (350 to 600 μm diameter) of fissile or fertile fuel materials, usually in the form of uranium dioxide (UO_2), plutonium dioxide (PuO_2), or an uranium oxycarbide (UCO) mixture. (Fertile thorium compounds, either alone or mixed with uranium or plutonium, can be used as fuel kernel material.) Typical fuel enrichments vary from 8 to 20%, as dictated by power rating and safety considerations. The fuel kernels are then coated with successive layers of pyrocarbon (PyC) and silicon carbide (SiC). First, a low-density PyC buffer coating is applied that provides void volume to accommodate fission gas and attenuates fission product recoils released from the fuel kernel. This layer is surrounded by successive coatings consisting of an inner PyC layer (IPyC), a silicon carbide (SiC) layer and an outer PyC layer (OPyC). The irradiation behavior of the PyC coatings on either side of the SiC provides prestressing to assist in accommodating internal pressure. The SiC layer is the primary pressure vessel and is an effective barrier to fission product release. The coated particles are overcoated with a resinated graphite powder to prevent particle-to-particle contact during either sphere making or compact formation.

In the prismatic design, the overcoated TRISO particles are imbedded within a graphite matrix to form cylindrical compacts. Approximately 3200 of these compacts are inserted into a hexagonal graphite fuel element. In the pebble bed design, overcoated TRISO particles are also imbedded in a graphite matrix; however, in this case, in the form of a spherical element with hundreds of thousands of them making up the core.

Fission product release rates are kept very low during normal operation and off-normal transients as long as the maximum fuel temperature is kept below 1600ºC. The main features behind the design philosophy of HTGR concepts are passive and inherent safety, small and medium size, and modularity. The HTGR cores are quite large in size; therefore, their core power density is appreciably low. With their low power density, the HTGR can accommodate decay heat removal passively from the reactor core by means of the large graphite volume without causing any radioactivity release. This is a critical issue in the case of off-normal transients such as the loss-of-coolant, or loss of flow, to keep the coated fuel particles intact by not exceeding their accident fuel temperature limit, typically 1600ºC for a short period of time. The highest normal operating fuel temperature should not be greater than 1250ºC. Fuel failure rates are extremely low below these temperatures and increases rapidly at much higher temperatures. However, accident fuel performance depends on temperature progressions, duration, burnup, fabrication quality, and must be demonstrated by specific fuel irradiation experiments, followed by out-of-reactor accident simulation testing.

The unique features and safety characteristics of the HTGR will make it a reliable source of energy. The role of HTGRs in the future will not be limited just too generating electricity safely and with a competitive cost. Another potential of high temperature reactors is their utilization in process heat applications. Hydrogen production, oil extraction from oil shales, and coal gasification are possible applications. Desalination is also a possible process heat application using waste heat of HTGRs.

The placement of HTGRs can be as stand alone units as well as coupled with LWRs. There is a synergy between LWR and HTGR fuel cycles. Currently, LWRs are extensively used in nuclear electricity generation. Meanwhile, the generation of minor actinides seems to be an issue in the LWR spent fuel. However, LWR spent fuel can be burnt in HTGRs as proposed in the “Deep Burn” concept. Thus, long lived minor actinides will be transmuted into short lived isotopes and waste management will be easier to handle. Furthermore, some extra energy will be generated as a by-product [13]. As noted earlier, another potential use of

HTGRs is in the disposition of weapon grade plutonium as fuel. The characteristics of HTGR fuel provide an important advantage over conventional nuclear reactor fuel forms because of its improved proliferation resistance attributes. The isotopic configuration of spent fuel, a small amount of fuel distributed in a large graphite matrix, barrier characteristics of coated particles, closed fuel handling, and storage facilities all make it difficult to extract fissile or fertile material out of spent coated particle fuel. The typical small size and modularity of HTGRs make them preferred in small grid use. Therefore, HTGRs are possible candidate systems to be deployed within the concepts of Small and Medium Sized Reactors (SMRs). HTGRs are examined to implement innovative fuel cycle such as application of inert matrix fuels and thorium fuel cycles [14], [15].

1.2. Fuels for HTGRs

1.2.1. Conventional fuels for HTGRs

The original idea of coated fuel particles was suggested by R. Huddle in 1957. Since then, different forms of coated fuel particles have been developed, manufactured, and utilized worldwide. An important advantage of the HTGR is the flexibility of using different fuel cycles. Hence, High Enriched Uranium (HEU) and Low Enriched Uranium (LEU), Uranium-Thorium (U, Th), Uranium-Plutonium (U-Pu), and Plutonium (Pu) fuel cycles have been employed in various applications. Until the 1980s, two types of fuel designs were used extensively, namely, bi-isotropic (BISO) and tri-isotropic (TRISO) particles as shown in Fig. 5. From the 1980s forward, only the TRISO coated fuel particle has been capable of meeting the fuel quality and performance required for modern HTGRs.

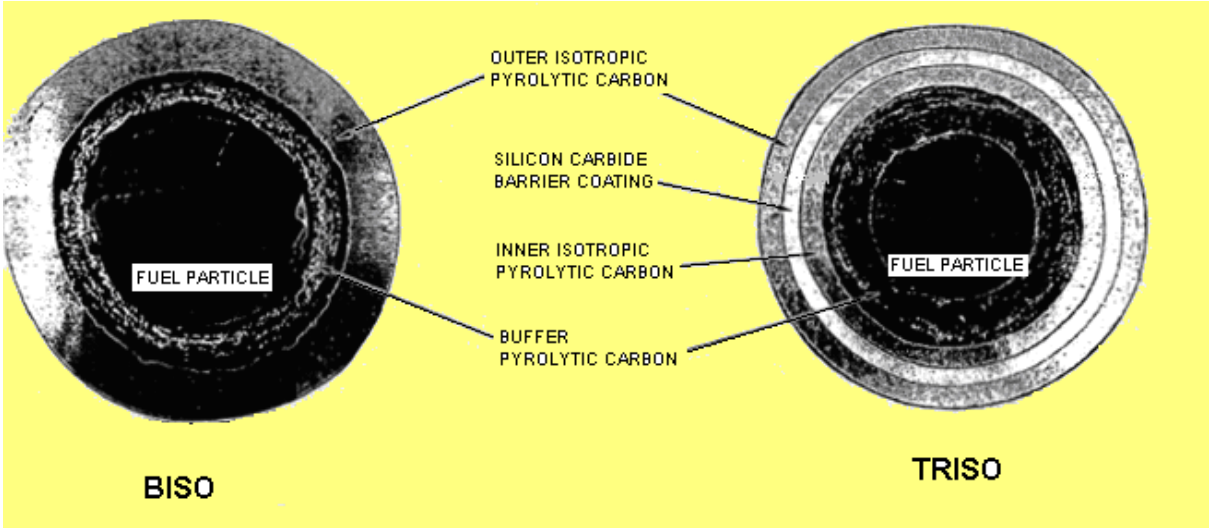

Fig. 5. BISO and TRISO coated fuel particles (General Atomics Co.).

Coated fuel particles are tiny fuel elements on the order of one millimeter in diameter. There are more than a billion (10^9) coated fuel particles employed in a typical HTGR. The essential safety concern is preserving the integrity of individual coated particles and their fission product retention capability. The BISO-coated particle design consisted of two layers of pyrocarbon surrounding a spherical fuel kernel. The first layer was a porous buffer layer and it was surrounded by a dense pyrocarbon (i.e., “pyrolytic” carbon or PyC), layer. In a TRISO-

coated particle there are four layers consisted of a porous buffer layer, an inner PyC layer (IPyC), a SiC layer, and another outer PyC layer (OPyC), sequentially. Both BISO- and TRISO-coated particles have gaseous fission product retention capability; however, the use of BISO particles has been limited to low temperature and low burnup operations. The TRISO-coated particle can retain metallic fission products at HTGR operational, transient, and design accident temperatures; therefore, the TRISO-coated particle has become the logical choice for reduced fission product release, extended burnup and higher fuel temperature applications.

Prior to their use in power reactors, BISO- and TRISO-coated fuel particles were extensively irradiated and tested in prototype and material test reactors. The AVR (Arbeitsgemeinschaft Versuchsreaktor) was a prototype HTGR with a pebble bed core having 46 MWt and 15 MWe power with typical coolant inlet and outlet temperatures of 270°C and 950°C, respectively, at 1 MPa pressure. The AVR was operated between 1967 and 1988 in Germany. The fuel types irradiated in AVR were (Th, U)C_2, (Th,U)O_2, and UC_2 BISO-coated particles and (Th,U)O_2 and UO_2 (LEU and HEU) TRISO-coated particles.

The Peach Bottom Reactor in the United States operated between 1967 and 1974 and utilized BISO-coated particles containing HEU and fertile thorium fuel materials in carbide compounds dispersed in a graphite moderator in fuel compact form. The Peach Bottom fuel element was a solid graphite cylinder 3.5 inches in diameter and 144 inches long as shown in Fig. 6. Annular fuel compacts (1.75 inches inner diameter by 2.75 inches outer diameter, and 1.5 inches long) were stacked inside the cylindrical graphite sleeve as an annular ring. The Peach Bottom reactor produced 115 MWt and 40 MWe power with a helium coolant temperature of 377°C inlet and 750°C outlet at 2.5 MPa pressure.

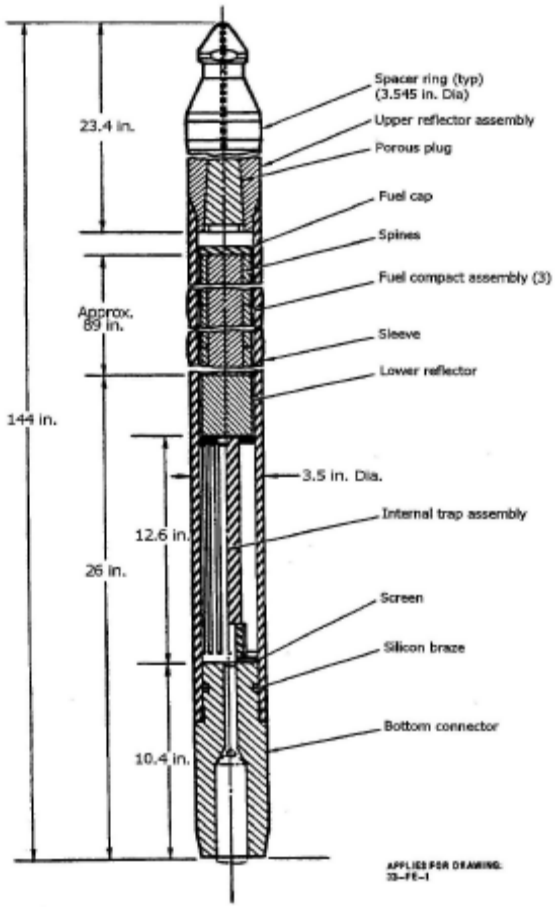

Fig. 6. Schematic of the Peach Bottom Reactor fuel element.

An important international project which made a significant contribution to HTGR fuel development was the DRAGON Reactor in the UK. This reactor was fueled with different forms of driver fuel elements. Various driver fuel combinations with UO_2 TRISO particles were tested in the DRAGON Reactor Experiment between 1968 and 1975. The DRAGON reactor operated at 20 MWt power and a power density of 14 MW/m^3, with helium coolant temperatures of 350°C inlet and 750°C outlet at 1MPa pressure.

In addition to these test reactors, there were two historical prototype HTGR power reactors, namely, the Fort St. Vrain (FSV) Power Station and Thorium High Temperature Reactor (THTR). The Fort St. Vrain reactor was built by General Atomics co. and operated by Colorado Public Utility (between 1976 and 1989). It was the first commercial gas cooled reactor to produce electricity. The fuel consisted of HEU (Th, U)C_2 fissile fuel kernels and ThC_2 fertile fuel kernels, both as TRISO-coated particles imbedded in carbonaceous matrix compact and placed in prismatic block fuel elements. The FSV core operated at 842 MWt and 6.3 MW/m^3 power density, with 405°C inlet and 785°C outlet helium temperatures at 4.5 MPa pressure. The THTR utilized uranium-thorium mixed oxide, (Th, U)O_2 fuel kernels with BISO-coated fuel particles in spheres or fuel `pebbles. The THTR operated in Germany (between 1986 and 1989) with 750 MWt and 300 MWe power, with 270°C inlet and 750°C outlet helium coolant temperatures at 3.9 MPa pressure.

The individual coating layers of TRISO fuel are designed for particular functions related to fission product retention, creep strength, shrinkage under irradiation, and irradiation performance. Most fission products are produced and retained inside the fuel kernel itself. The porous buffer layer serves as a sacrificial layer to stop energetic fission products thus protecting IPyC from radiation damage, and provides sufficient void volume to accommodate fission gases and kernel swelling. The IPyC layer is a barrier against (a) gaseous fission product diffusion and (b) chlorine gas, generated during the SiC deposition process, infiltration into the kernel; and helps to keep the SiC layer under compression. The SiC layer is the main pressure boundary, retains metallic fission products, and provides strength. The OPyC serves as a gaseous fission product barrier, reduces the tensile stress on SiC layer, and forms a bonding surface for the overcoating or matrix material. The SiC layer should preserve its containment function up to approximately ~ 1800°C; however, transient and accident temperatures in HTGR designs are typically limited to 1600°C. It should be noted that a small amount of uranium may become trapped inside the coating layers during coating processes, known as 'tramp' uranium that eventually may produce fission product releases in-reactor. Also, a very small amount of uranium impurities may exist in the graphitic matrix material and source material for pyrolytic carbon layers. Together the tramp uranium and the uranium contamination in the matrix material represents only ~ 10^{-5} fraction of the total uranium contained in the fuel element.

1.2.2. Advanced fuels for HTGRs

The Very High Temperature Reactor (VHTR) or the Next Generation Nuclear Plant (NGNP) concept has been introduced for the future nuclear power plant deployment. Such VHTR concepts would operate at increased temperatures in order to produce outlet temperatures of ~950°C for hydrogen production, process heat applications, and Brayton cycle electricity production, while increasing fuel discharge burnup for better uranium utilization. One possible method of achieving the higher operating temperature conditions and increased burnup, i.e., FIMA, is to replace the conventional UO_2 fuel kernel with a stoichiometric two-phase mixture of UO_2 and UC_2, namely UCO. The UCO fuel kernel provides resistance against fuel kernel migration and internal pressure buildup caused by excessive CO formation. The presence of a sufficient number of carbon atoms in the fuel kernel assures the consumption of excess oxygen atoms inside the kernel preventing CO buildup thereby eliminating kernel migration (or the 'amoeba effect') and excess internal pressures at high burnups.

Another TRISO particle design, designated as UO_2*, with a dense pyrocarbon seal coat and thin ZrC coating applied directly onto a UO_2 kernel followed by the traditional TRISO coatings, as shown in Fig. 7 was fabricated and tested in the late 1970s and early 1980s. This thin ZrC layer acts as an oxygen getter to limit CO production and retards the kernel migration. The UO_2* TRISO particles were irradiated side-by-side with standard TRISO particles having kernels of UO_2, UC_2, and UCO in fuel compact specimens in the ORNL HFIR reactor. These tests designated as HRB ranged from 860°C to 1210°C, achieved burnups from 19 to 29% FIMA, and accumulated fast fluences from 3.7 to 6.5×10^{25} n/m^2 (E>29 fJ), specifically HRB-15A HRB-15B, and HRB-16 [16]. The UO_2* particles showed superior performance during the irradiations and in post-irradiation annealing tests. These HRB tests indicate that the UO_2* TRISO fuel design may be useful for VHTR/NGNP high temperature applications.

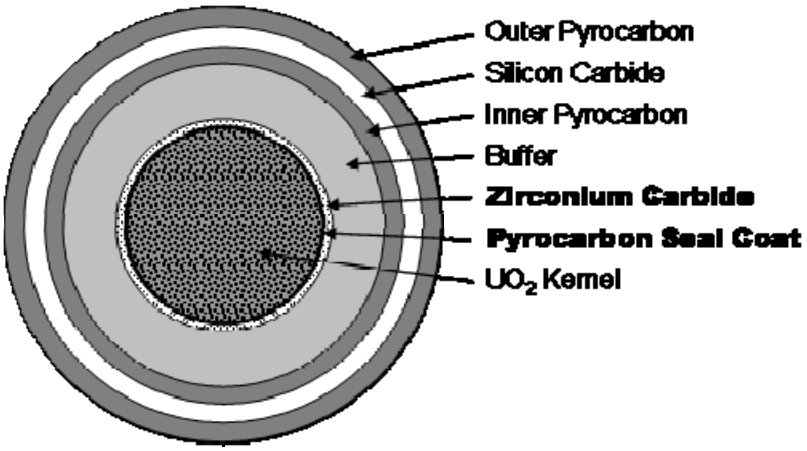

Fig. 7. Schematic cross-sectional view of the UO_2 coated fuel particle.*

Another possible TRISO-coating design improvement, particularly for mixed oxide Pu and minor actinide fuel is to replace the SiC layer with a ZrC layer in order to minimize Pd attack in SiC. The ZrC layer has higher refractory material properties so that fuel temperature limits may be increased by ~ 200°C. This possible TRISO-coating design improvement still requires significant development followed by extensive irradiation testing and post-irradiation accident simulation testing.

2. MANUFACTURE OF TRISO COATED PARTICLES

This chapter covers the manufacture of UO_2 and UCO fuel kernels as well as the coating of the fuel kernels to produce TRISO coated particles. Several countries have initiated fuel development and qualification programs with the coated particle as the basic unit [16], [17].

2.1. Historic development

The objectives of the coated particle development program at UKAEA [18], [20] which began in 1961, were to define the essential processing steps of a production route for the manufacture of nuclear fuel kernels and coated particles. This effort included identifying the important parameters and developing techniques that characterize the coated particle properties that influence their irradiation performance. Detailed assessments of the various components of the coated particle have led to advanced designs. The versatility of the UKAEA powder agglomeration process to fabricate highly spherical fuel kernels of carbide and oxide compounds is verified by its ability to produce monosized kernels in the range of 200 μm to 1000 μm diameter, with controlled porosities from 5% to 20%. Identification and understanding of the important parameters controlling the coating deposition process resulted in specifications for coating furnace designs and process routes that ensure a high degree of sphericity was maintained throughout the CVD deposition processes with an acceptable range in properties. More recent investigations of process variables have identified factors controlling PyC microstructure and the effect of defects and substrate shapes have on the quality of SiC layer. The proportion of defective particles in modern HTGR coated particle fabrication is now less than 10^{-5} by adherence to strict process controls and product specifications. The UKAEA fuel fabrication development effort was terminated in 1974.

To produce fully dense spherical fuel kernels, liquid processes were developed that offered substantial advantages over the powder agglomeration process. These include the production of oxide, carbide or mixed (oxycarbide) fuel kernels of almost any desired composition, pore-size distribution and density. Researchers in the US and Germany were responsible for developing a number of aqueous processes in the 1960s and 1970s. The so-called "sol-gel" process has gained particular importance. In the sol-gel process a colloidal liquid of fuel material – called the "sol" –is dropped into a liquid, immiscible with water. The near spherical droplets are then solidified by a gelation process – called the "gel" – and after washing; they can be dried and sintered to obtain fuel kernels over a wide range of properties. The colloidal solution contains an oxide of the fuel material in the form of very small crystallites (~50Å). After gelation, these crystallites form a stable structure, saturated with water. The fine distribution in the colloidal form makes it possible to obtain oxides of near theoretical density by sintering at high temperatures (≥1200°C) in a reducing atmosphere without applying pressure. Both external and internal gelation processes are available to convert the sol into a geometrical stable gel.

In the late 1970s, Germany had achieved unprecedented quality levels for its HEU (Th,U)O_2 TRISO fuel particle fabricated into spherical elements in large-scale commercial production facilities (HOBEG, GmbH.). By 1980, Germany had discarded the high-enriched thorium-uranium fuel cycle for HTGR applications and adopted the low-enriched uranium-plutonium fuel cycle. The reference particle design for the German pebble-bed HTGR became the LEU UO_2 TRISO-coated particle. Beginning in 1980, Germany initiated a new fuel development effort to qualify their reference LEU UO_2 TRISO fuel particle. By the late 1980s, Germany had successfully demonstrated fission product retention under all normal and off-normal design condition for its reference fuel concept. The LEU UO_2 TRISO-coated particle fuel produced during this period represents "modern HTGR fuel" characterized as near defect free along with very low contamination. Improvements in coated particle and fuel element fabrication processes, quality assurance and quality control, and characterization resulted in the commercial production of fuel elements with defect levels at the 10^{-5} level, and similar U_{free}/U_{total} contamination levels. The final fuel development effort in Germany was the production and proof-testing of fuel elements under Modul HTR specifications and operating conditions. The German LEU UO_2 TRISO fuel particles produced by HOBEG remain the standard of excellence within the worldwide HTGR community. In 1988 all fuel fabrication activities were terminated.

The evolution of coated particle fuel development over more than four decades of effort has led to the adoption of the LEU TRISO-coated particle as the reference particle design used in HTGR development world wide. Although the hexagonal block fuel element used in prismatic core HTGRs differs significantly from the spherical elements used in pebble-bed HTGRs, the basic TRISO-coated particle design is the same for both. Today, a number of active HTGR fuel development programs are underway in China, France, South Korea, Russia, South Africa and the United States.

The kernel fabrication process employed in Germany was based on the sol-gel, internal gelation process. This process was developed for production of the highly spherical, dense HEU (Th,U)O_2, ThO_2 and LEU UO_2 fuel kernels. Further developments led to a modified sol-gel, external gelation microsphere fabrication process which is a drip- casting process, also called "gel-precipitation" process. This process was used by NUKEM to produce the HTR Modul Proof Test fuel prior to the termination of fuel production activities in Germany. This gel-precipitation process (or nearly the same) is the reference fuel kernel fabrication process used to produce LEU UO_2 fuel kernels in spherical elements manufactured for the HTR-10

experimental reactor in China, and as the reference LEU UO_2 kernel making process for the PBMR Project in South Africa. The latter is outlined in the remaining sections of this chapter.

2.2. Manufacture of UO2 kernels

2.2.1. Process schematic

The process schematic for UO_2 fuel kernels is given in Fig. 8. This process is based on the external gelation process (also known as the "gel-precipitation" process). The feed material is uranyl nitrate solution and is prepared by dissolving fine U_3O_8 powders in nitric acid.

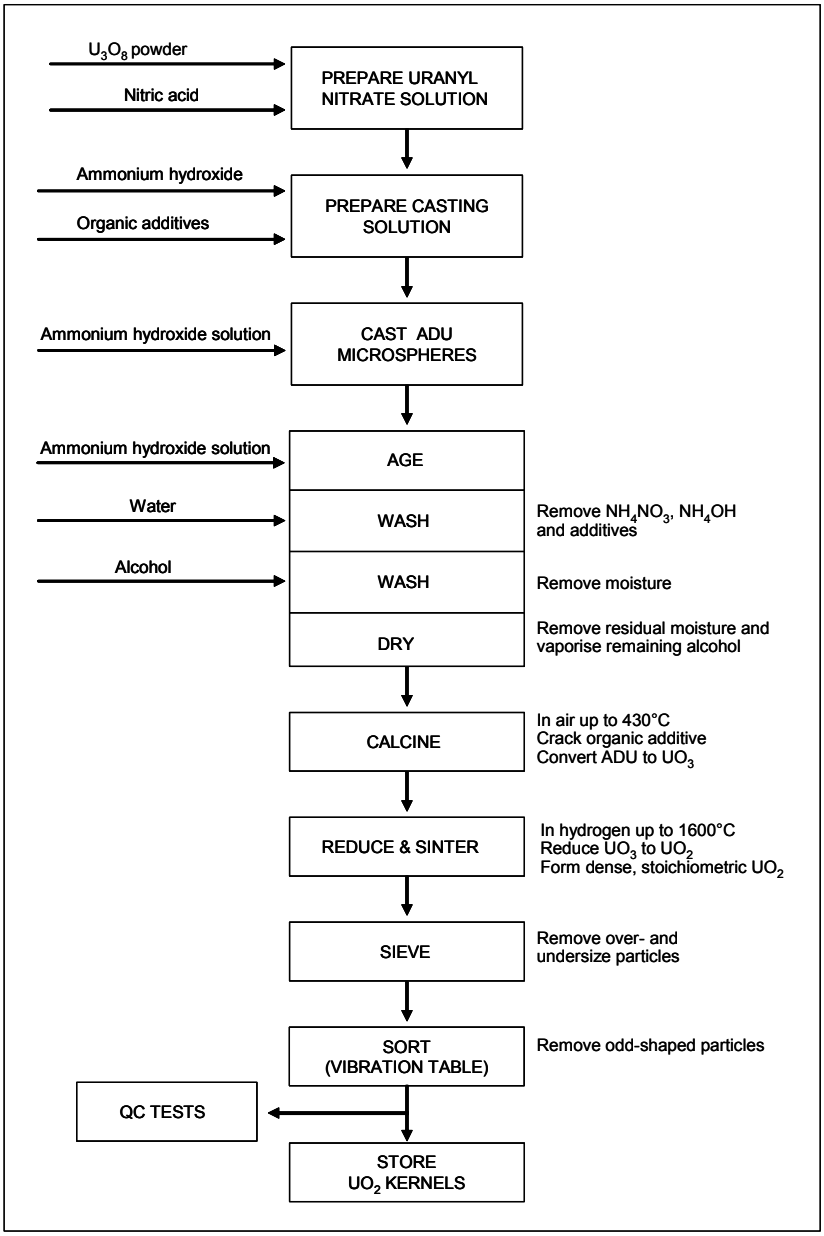

Fig. 8. UO_2 kernel production.

2.2.2. Preparation of the feed solution

The U_3O_8 feed powder is dissolved in nitric acid to form a uranyl nitrate solution according to the chemical reaction:

$$3U_3O_8\ (s) + 20HNO_3\ (aq) \rightarrow 9UO_2(NO_3)_2\ (aq) + 10H_2O + 2NO\ (g). \quad (2.1)$$

The uranyl nitrate solution is pre-neutralized with dilute ammonium hydroxide to just prior to precipitation of the uranium according to the following reaction:

$$2UO_2(NO_3)_2\ (aq) + NH_4OH\ (aq) \rightarrow 2UO_2(NO_3)_{1.5}(OH)_{0.5}\ (aq) + NH_4NO_3\ (aq) \quad (2.2)$$

A casting solution is prepared by adding small amounts of polyvinyl alcohol and tetrahydrofurfuryl alcohol to the pre-neutralized uranyl nitrate solution. These additives adjust the surface tension and viscosity to ensure proper droplet formation and also assist with later uniform shrinkage of the kernels as well as crystals growth.

2.2.3. Casting of microspheres

Casting is carried out in a glass column filled with the concentrated ammonium hydroxide precipitation solution (refer to Fig. 9). The casting solution is pneumatically fed to the nozzles (typically between 4 and 6) at the top of the column, where a vibrator “shakes off" droplets from the feed stream at a rate of. ~100 discrete droplets per second from each nozzle.

The droplets first fall a short distance through air where they attain a spherical shape as a result of surface tension. The spherical droplets then fall a further short distance through an ammonia atmosphere (ammonia gas is blown directly onto the droplets), where a chemical reaction occurs with the uranyl nitrate on the surface of the droplets. The uranyl nitrate precipitates as ammonium diuranate (ADU) in the outer layer of the droplet, forming a protective film. This protective skin enables the droplets to retain their spherical shape on impacting the precipitation solution (without deforming).

As the reaction continues in the casting column ADU forms throughout the kernels, with ammonium nitrate as a by-product:

$$2UO_2(NO_3)_{1.5}(OH)_{0.5}\ (aq) + 2NH_4OH\ (aq) \rightarrow (NH_4)2U2O7\ (s) + NH_4NO_3\ (aq) + H_2O. \quad (2.3)$$

The precipitation solution is circulated from the bottom of the casting column to the top of the column via a cooled circulation line. The precipitation solution is saturated in the circulation line to ensure a high ammonia concentration at the top of the column where the chemical reaction in the droplet initiates. The precipitation solution in the casting column is also saturated by bubbling ammonia through the solution. Ammonia vapors from the casting process are scrubbed with water in a glass column filled with stainless steel rings.

The kernels are kept in the casting column until they are strong enough to be processed further. The diameter of a cast gelled sphere is about 1.8 mm (UO_2 kernels that have a final diameter of 500 μm after sintering).

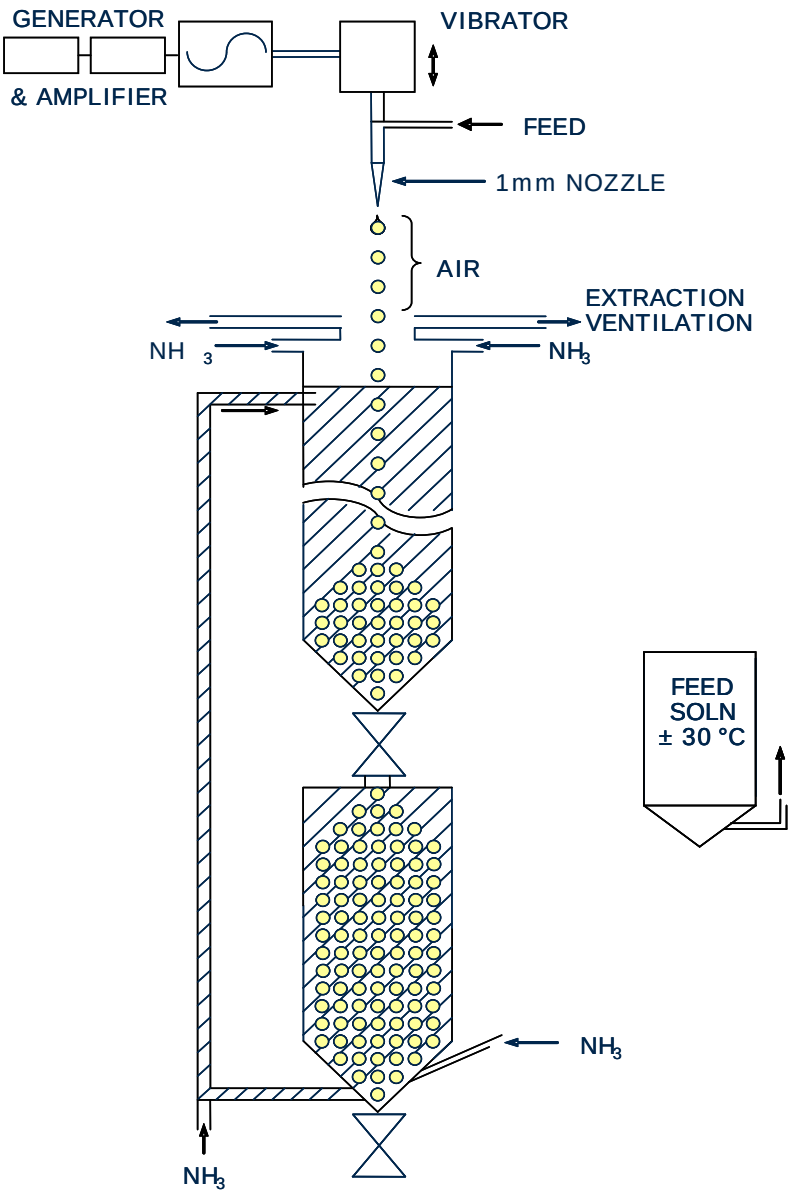

Fig. 9. Casting process.

2.2.4. Ageing, washing and drying

After casting, the wet kernels and the accompanying precipitation solution are transferred from the casting column to a jacketed rotary flat vessel for ageing, washing, and drying.

During ageing, the vessel rotates and is heated with steam to 80°C. The ageing process fully converts the gelled spheres to solid ADU kernels, and initiates crystal growth in the kernels. The precipitation solution may be used as an ageing solution, or fresh diluted precipitation solution may be prepared for use as the ageing solution.

After ageing, the solution is drained from the vessel. The ADU kernels are washed in this vessel with water, at a slightly faster rotation speed, to remove the ammonium nitrate as well as ammonium hydroxide and tetrahydrofurfuryl alcohol. Thereafter the kernels are washed

with isopropyl alcohol (IPA) to remove moisture and any remaining ammonium nitrate, ammonium hydroxide and tetrahydrofurfuryl alcohol.

The final step is to dry the kernels at 80°C under vacuum at a slow rotation speed. The dried ADU kernels have a diameter of about 1 mm.

2.2.5. Calcining

After completion of the ageing, washing, and drying processes, the ADU kernels are calcined in air up to 430°C in a batch furnace. The remaining organic additives are cracked and driven off during a gradual temperature increase. Above 300°C the ADU is converted to UO_3 according to the following reaction:

$$(NH_4)_2U_2O_7\ (s) + O_2\ (g) \rightarrow 2UO_3\ (s) + 2H_2O\ (g) + NO\ (g). \quad (2.4)$$

The mean diameter of a calcined kernel is about 750 μm.

2.2.6. Reduction and sintering

After calcining, reduction and sintering follows at a high temperature to reduce the UO_3 to UO_2, remove remaining impurities and densify the kernels. This process is carried out under a hydrogen atmosphere.

The reduction step takes place between 450°C and 650°C according to:

$$UO_3\ (s) + H_2\ (g) \rightarrow UO_2\ (s) + H_2O\ (g). \quad (2.5)$$

Thereafter, the temperature is increased to 1 600°C in order to form dense, stoichiometric UO_2 kernels that have a diameter of 500 μm and a density just below the theoretical value of 10.96 Mg/m^3.

2.2.7. Sieving and sorting

The final production steps are sieving to remove any under and over sized kernels, followed by sorting to remove any odd-shaped particles. The latter is performed on a sorting table that is slightly inclined to allow spherical kernels to roll downhill while odd-shaped particles are vibration transported along a perpendicular direction and collected for recycling. The vibration sorting is a very slow but effective method to ensure that any odd-shaped kernels are removed from the batch.

2.3. Manufacture of UCO kernels

Uranium oxycarbide (UCO) microspheres are formed by an internal gelation sol gel process [24], [25]. Internal gelation is a non-equilibrium process that converts uranyl nitrate to green microspheres of UO_3 containing dispersed carbon. The kernel fabrication process is outlined in the block flow diagram shown in Fig. 10. The feedstock for the internal gelation process is a “broth” consisting of an aqueous solution of acid deficient uranyl nitrate (ADUN), fine carbon black, and an ammonia donor, hexamethyltetramine (HMTA), to initiate gelation. Discrete aqueous droplets of the broth are formed by ejection through a vibrating orifice into a heated trichloroethylene (TCE) column containing a surfactant, in which the constituents of the broth droplets are insoluble. The interfacial tension between the TCE and the aqueous droplets causes them to spheridize, while the heat of the TCE initiates the thermal

decomposition of the ammonia donor. The ammonia in turn initiates the gelation of the liquid microspheres. The formed microspheres are aged in the stirred TCE to complete the gelation process and partially extract water. The gelled microspheres are removed from the TCE, washed to remove the gelation byproducts, and dried to remove additional water.

At this stage in the process the dry gelled spheres are of large diameter, low density, high specific surface area, and consist of hydrated UO_3 ($UO_2(OH)_2 \bullet xH_2O$) and dispersed carbon. These "green" kernels are then placed in a furnace for subsequent calcination, carbothermic reduction, and sintering.

Calcination is carried out in 100% hydrogen at 550°C and removes the water of hydration from the oxide matrix of the green kernel (reaction 3.6), decomposes the uranium oxyhydroxide to UO_3 (reaction 3.7), and reduces the UO_3 to UO_2 (reaction 3.8):

$$UO_2(OH)_2 \bullet xH_2O \rightarrow UO_2(OH)_2 + x\ H_2O \quad (2.6)$$

$$UO_2(OH)_2 \rightarrow UO_3 + H_2O \quad (2.7)$$

$$UO_3 + H_2 \rightarrow UO_2 + H_2O \quad (2.8)$$

$$2\ UO_3 + C \rightarrow 2\ UO_2 + CO_2 \quad (2.9)$$

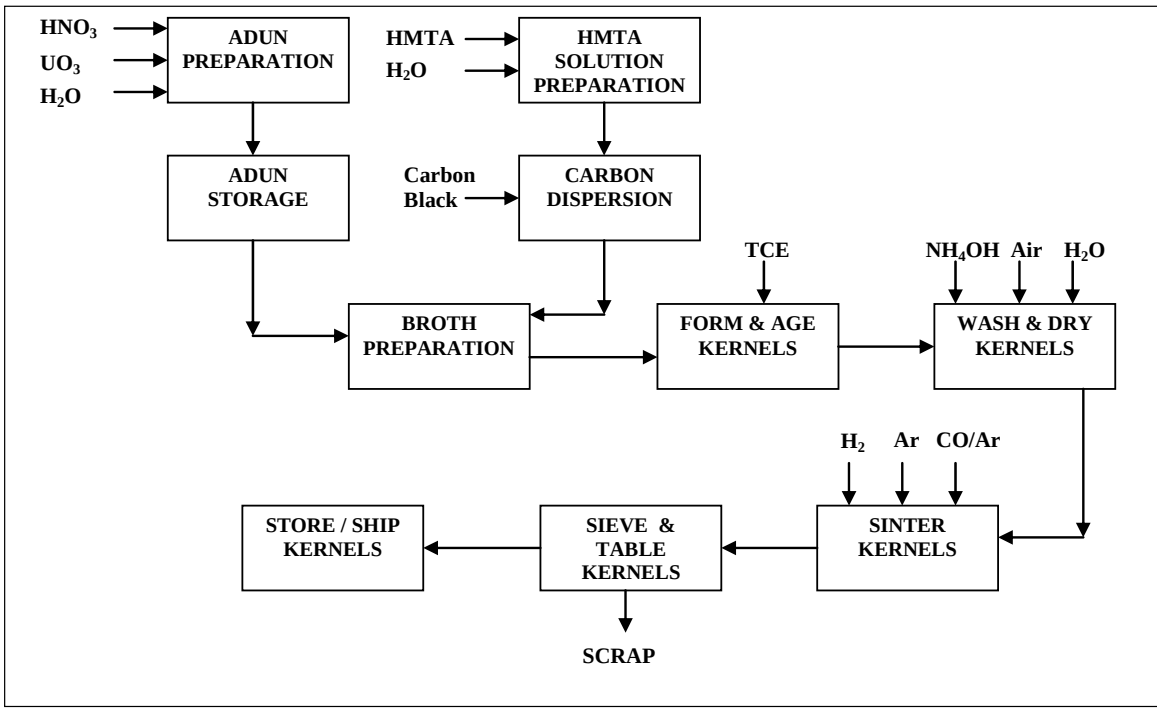

Fig. 10. Block flow diagram of the UCO kernel fabrication process.

The hydrogen atmosphere favors reaction 3.8 and thereby minimizes the effects of reaction 3.9, which otherwise could strip substantial amounts of carbon from the mixture. The dehydration, decomposition, and reduction process (reactions 3.6, 3.7, and 3.8) produces water as a byproduct, which could react with carbon by the gas shift reaction:

$$C + H_2O \rightarrow CO + H_2 \quad (2.10)$$

Because the gas shift reaction is an equilibrium reaction with hydrogen gas as a product, the hydrogen overpressure helps to suppress the reaction and minimize this mode of carbon loss.

In the carbothermic reduction step, the temperature is ramped to 1680°C in an argon atmosphere. This step also has a hold period at 1680°C in a mixed CO/Ar atmosphere. Uranium carbides are formed according to reactions 3.11 and 3.12:

$$UO_2 + 4\,C = UC_2 + 2\,CO \quad (2.11)$$

$$UO_2 + 3\,UC_2 = 4\,UC + 2\,CO \quad (2.12)$$

The temperature is increased again, to 1 890°C, and held at this temperature for one hour to densify the kernels. A CO-Ar atmosphere is used to minimize the formation of UC during this sintering step.

A typical final composition of sintered kernels is 74 mol% UO_2, 12 mol% UC_2 and 14 mol% UC. A range of compositions, namely 65-85 mol% UO_2, 0-27 mol% UC_2 and 0-35 mol% UC, are allowed by the specification, which is expressed as limits for O/U and C/U ratios.

Following cooling, the kernels are unloaded from the furnace, sieved to remove undersize and oversize kernels, tabled to remove aspherical kernels, and sampled and analyzed to ensure conformance to specifications.

2.4. Manufacture of TRISO coated particles

The main focus in this section is on the proven TRISO coating technology previously developed in the German HTGR program and is considered the reference coating technology for modern HTGR fuel development programs [26], [27].

2.4.1. Process schematic

The process schematic for TRISO coating deposition is given in Fig. 11. The four coating layers are deposited on kernels in a heated furnace (see Fig. 12) by a process called chemical vapor deposition (CVD). Flowing gases in the furnace suspend the kernels so that they form a fluidized bed. Coating gases are chosen which decompose and deposit, at temperatures up to 1600°C, certain of their constituents on the surfaces of the kernels. The materials of the layers formed by this process are described as pyrolytic, because they are formed by a chemical decomposition, brought about by heat.

2.4.2. Coating process

The process for depositing the four coating layers is as follows:

- Deposit a porous pyrocarbon (PyC) layer (the "buffer" layer) on the kernels by the decomposition of acetylene (ethine, C_2H_2) according to:

  $$C_2H_2(g) \rightarrow 2C(s) + H_2(g) \quad (2.13)$$

- Deposit an inner, dense layer of isotropic pyrocarbon (IPyC) on the porous carbon layer by the decomposition of a mixture of acetylene and propylene (propene, C_3H_6):

  $$C_2H_2(g) \rightarrow 2C(s) + H_2(g). \quad (2.14)$$

$C_3H_6(g) \rightarrow 3C(s) + 3H_2(g)$. (2.15)

- Deposit a dense, isotropic layer of SiC on the IPyC layer by the decomposition of methyltrichlorosilane (CH_3SiCl_3) according to the following reaction:

  $CH_3SiCl_3\ (g) \rightarrow SiC(s) + 3HCl\ (g)$. (2.16)

- Deposit an outer, dense layer of isotropic pyrocarbon (OPyC) on the SiC layer by the decomposition of acetylene and propylene (similar to the inner dense layer).

The IPyC and OPyC layers have also been deposited by decomposition of only propylene.

Values of the key process parameters used for the deposition of a TRISO coating onto a LEU UO_2 fuel kernel are provided in Table 2.

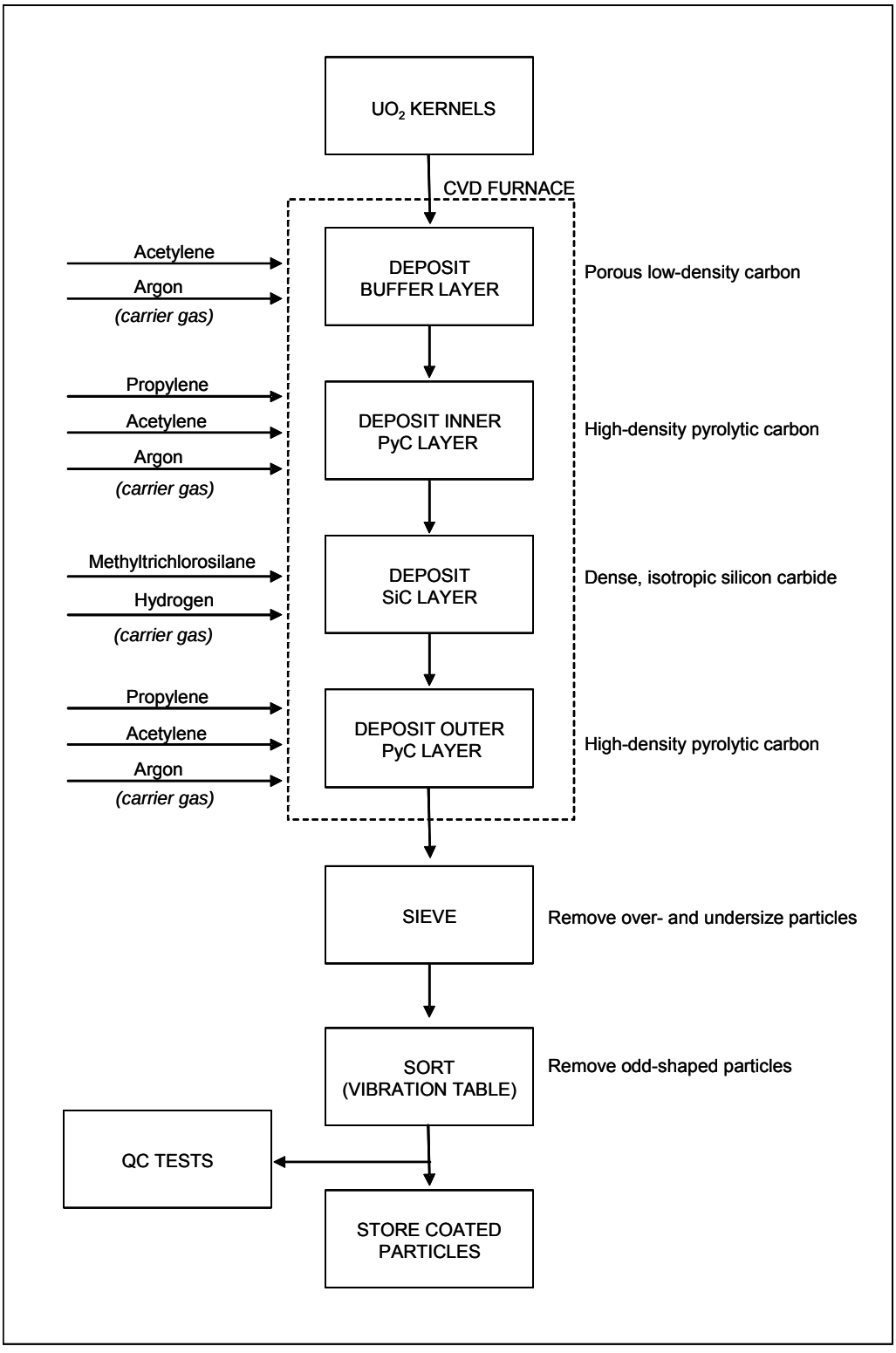

Fig. 11. Coating process.

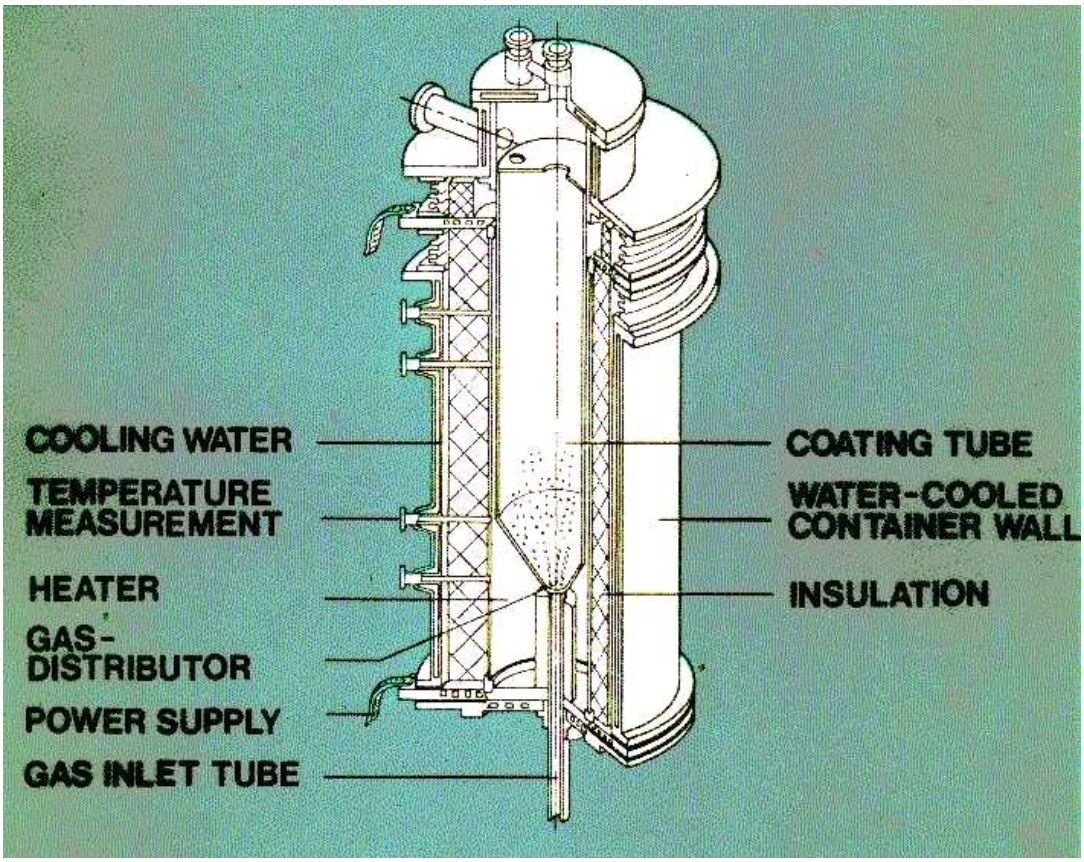

Fig. 12. Schematic of a High temperature fluidized bed coating reactor used in HTGR fuel fabrication.

Table 2. PROCESSING PARAMETERS FOR THE DEPOSITION OF A TRISO COATING ONTO A LEU UO_2 FUEL KERNEL

Coating Layer	Decomposition Gas	Carrier Gas	Approximate Temperature (°C)	Approximate Deposition Rate (μm/min)
Low-density carbon	C_2H_2	Argon	1250	10
Inner dense isotropic PyC	Mixture of C_2H_2 and C_3H_6	Argon	1300	5
Isotropic SiC	CH_3SiCl_3	Hydrogen	1500	0.2
Outer dense isotropic PyC	Mixture of C_2H_2 and C_3H_6	Argon	1300	5

All the layers are coated in an uninterrupted sequential process in the same fluidized bed reactor.

The conditions under which layer deposition takes place are very important as these deposition parameters determine the properties of the coated particle formed. Parameters such as temperature, pressure, gas composition and gas ratios all play an important role in fixing the coated particle properties.

The following coating layer thicknesses were applied to the reference German HTGR LEU UO_2 TRISO-coated fuel particle design [28]:

- Buffer layer: 95 μm;
- IPyC layer: 40 μm;
- SiC layer: 35 μm;
- OPyC layer: 40 μm.

Key material property requirements for good irradiation performance for the dense isotropic PyC layers and the SiC layer are:

PyC Layer:
- must be impermeable;
- have an isotropic texture;

SiC Layer:
- β-SiC with a cubic structure;
- a density > 3.19 Mg/m^3 [29];
- equiaxed microstructure with fine grains and as few flaws as possible;
- PyC-SiC interfaces must be of sufficient strength.

2.4.3. Sieving and sorting

The final production steps are sieving to remove any under and over sized particles, followed by sorting to remove any odd-shaped particles. The latter is performed on a sorting table that is slightly inclined to allow spherical particles to roll down-hill while odd-shaped particles are vibration transported along a perpendicular direction and collected for recycling.

3. MANUFACTURE OF SPHERICAL FUELS

Two HTGR reactor concepts have evolved in the international development arena: (1) pebble bed reactor has been adopted by Germany, China, and South Africa; and (2) prismatic design has been adopted by the USA and Japan. A basic difference between the two designs is the geometry of their fuel elements. The pebble-bed design uses spherical fuel elements. The prismatic block design uses cylindrical ‘fuel compacts’ inserted into hexagonal graphite block fuel elements. The spherical fuel element, as shown in Fig. 13, consists of a spherical fuel zone of 50 mm diameter, in which the TRISO particles are homogeneously distributed in a graphite matrix material, and then, surrounded by a fuel-free shell of graphite matrix of 5 mm thick.

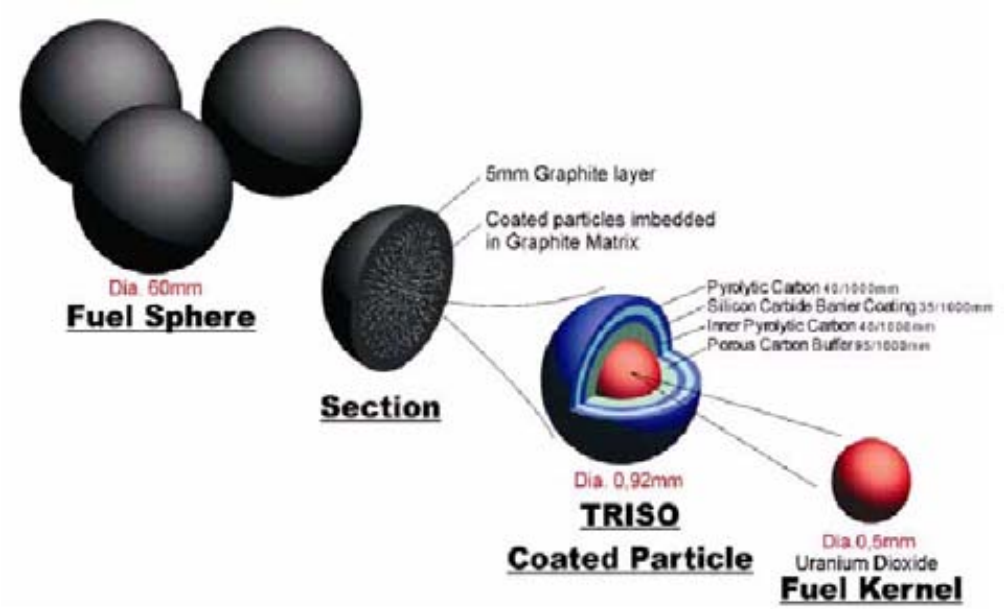

Fig. 13. Spherical fuel element.

The spherical fuel matrix material consists of carbonized organic binder and nuclear-grade graphite material which acts as a fission neutron moderator, heat transfer medium, and protection against external forces. The graphitic matrix material should exhibit high density, high thermal conductivity, high mechanical strength, low thermal expansion, low anisotropy, low Young's modulus, good corrosion resistance, good dimensional stability under neutron irradiation, and low concentration of impurities.

3.1. Fabrication technology

The fabrication process for fuel spheres was developed and improved by NUKEM, Germany and consists of the following steps: (1) resinated graphitic matrix powder preparation; (2) overcoating of particles; (3) pre-molding of fuel zone and high-pressure isostatic pressing of the complete fuel element; (4) machining; and (5) carbonization at 800°C and heat treatment at 1900-1950°C. Figure 14 describes the different process steps in the fabrication of fuel spheres.

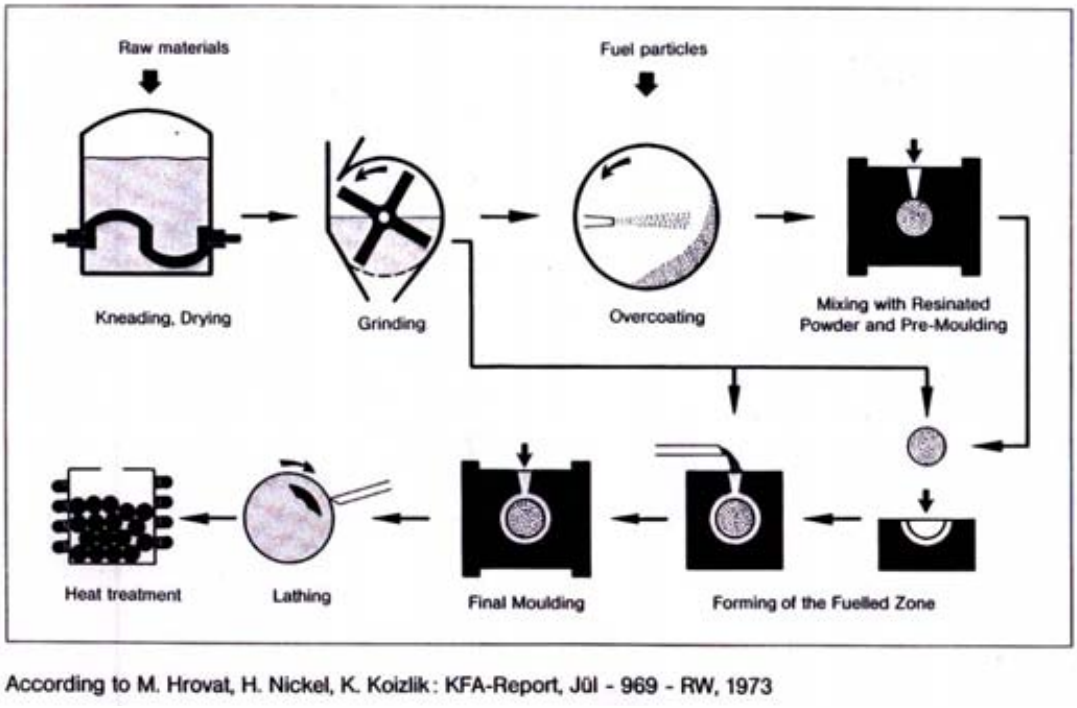

Fig. 14. Fabrication method for fuel spheres.

3.1.1. Preparation of resinated graphitic matrix powder

The matrix graphite for the spherical fuel consists of approximately 64% natural graphite, 16% electro-graphite powders, and 20% phenolic resin binder. The fabrication process includes the mixing of natural graphite and electro-graphite powders, and kneading of the graphite powders and binder, drying and milling.

The manufacturing process of the graphitic matrix powder is as follows:

1. Natural graphite and electro-graphite powders are mixed in a four-to-one ratio in a conical mixer.

2. The mixture is fed into a kneading machine where phenolic resin binder, dissolved in alcohol, is added and the mixture is homogenized.

3. The paste-like mixture is extruded through a punched screen creating strings that are cut into small pieces.

4. These small pieces are placed in drying trays which are heated to approximately 100°C.

5. The dried graphitic mass is transferred into a hopper that feeds a hammer mill used to grind the material into powder of the desired grain size.

6. The milled powder is homogenized and ready for pressing.

3.1.2. Overcoating of TRISO coated particles

Overcoating the TRISO particles prevents direct particle-to-particle contact which may induce cracking of the particle coating layers during sphere formation. The overcoating graphitic matrix material is about 200 μm thick and is applied to TRISO coated particles already placed in a rotating drum. The overcoating dry resinated graphitic matrix material and solvent are added simultaneously into the rotating drum in order to maximize adherence and obtain a uniform thickness. Then, the moist overcoated particles are dried at about 80°C to remove any remaining solvent. The dried overcoated particles are sieved to select proper sized particles within the range of 1.1 mm and 1.5 mm. An inclined vibrating table is used to remove oddly shaped, twin, or nonspherical overcoated particles.

3.1.3. Molding and pressing of fuel spheres

The fuel spheres are manufactured by quasi-isostatic pressing at room temperature using silicon rubber molds. The pressing operation consists of taking overcoated TRISO particles together with graphite matrix powder and molding them in a pre-pressing operation to form the internal fueled zone. Then additional matrix material is added to form the fuel-free shell around the fueled core using a final high pressure molding process. Figure 15 is a photograph of the sphere pressing line, based on the NUKEM process, in place at the Institute of Nuclear Energy Technology (INET) at Tsinghua University in China. The sphere molding and pressing process consists of the following steps:

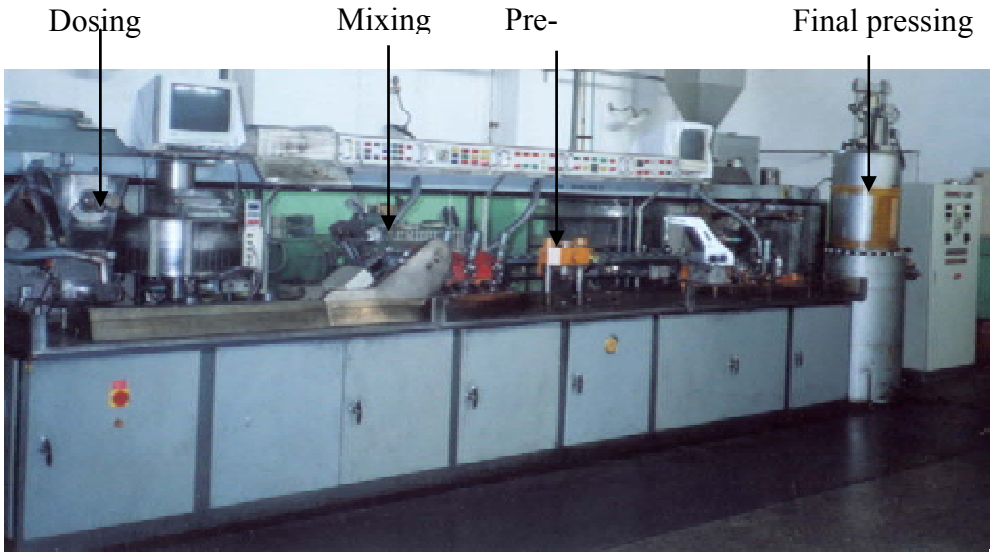

Fig. 15. The molding and pressing line for green fuel spheres at the Institute of Nuclear Energy Technology (INET) at Tsinghua University in China.

1. Combine overcoated particles with matrix graphite powder to form the fueled zone. The matrix graphite powder volume is carefully controlled along with the overcoated particle volume and the mixture homogenized.

2. The homogenized mixture is injected into the pre-pressing mold and pressed at approximately 5 MPa pressure.

3. The pressed fuel zone spheres are then transferred into the final mold. The lower half of the final mold contains matrix graphite powder. The fuel zone sphere is placed into the center and the second half of the mold is placed on top. More matrix material is added through a feeder and final pressing process is performed at about 300 MPa pressure.

3.1.4. Lathing the elements

After pressing, the green fuel spheres are transported to the lathing process where they are machined in a two step process to obtain uniform spheres with specified dimensions.

3.1.5. Carbonization and removal of impurities

After machining, the spheres are heat-treated in two distinct processes; carbonization and annealing. In the carbonizing process, the green fuel spheres are heated to 800°C in an inert argon atmosphere furnace in order to carbonize the phenolic resin binder to provide strength. The annealing process is carried out under vacuum at a temperature range between 1900-1950°C for one hour to eliminate residual impurities in the matrix graphite. After a cool down phase, the fuel spheres are removed for inspection.

4. QUALITY ASSURANCE / QUALITY CONTROL AND THE CHARACTERIZATION OF TRISO COATED PARTICLES

This section covers the Quality Assurance (QA), Quality Control (QC) and characterization of TRISO coated particles, including the fuel kernels.

4.1. Quality assurance

Coated fuel particles for development and testing purposes must be manufactured and controlled in accordance with a documented QA program that has been established in accordance with an appropriate standard, for example, ASME NQA-1 (American Society of Mechanical Engineers - Quality Assurance Requirements for Nuclear Facility Applications).

Among other things, the QA program must provide for:

- Product and material specifications to prescribe the technical and quality requirements that must be met,
- Appropriate sampling procedures and acceptance criteria for determining that the specified values have been met,
- Performance of work in accordance with written manufacturing and test instructions,
- Calibration and control of measuring and test equipment,
- Identification and control of materials and product, and
- Generation of reports in accordance with established formats and maintenance of appropriate QA records.

4.2. Statistical quality control

As in any industry, Quality Assurance, Quality Control and Testing go hand in hand to ensure the quality of the product and client satisfaction. The Nuclear industry, however, is far more rigid and stringent in defining its requirements, standards and specifications as 'the client' always involves the safety of the greater public.

Quality Control is in essence a set of procedures laid down to evaluate a work product. Products are evaluated by testing against stringent specifications whether they are raw materials, intermediate products or final products. Quality Assurance is the process by which development and/or production is 'guided' to ensure the system will attain the objectives set for it.

In the evaluation of a material there are always a multitude of possible errors present – sampling, being perhaps the most critical. The test itself will have a 'random error' present. The development of testing methods strives to reduce all of the errors to a manageable quantity whilst ensuring the parameter value ascribed to any sample is the best possible estimate of the whole batch. This process involves validation of the test method applied to a specific type of material. In order to achieve ultimate confidence in the results of testing, standard statistical processes are used to quantify the uncertainty (of the test value) and the consequences of this uncertainty.

Confidence levels are created by application of statistical processes to ensure that any material in use meets the specification set by the assurance program. By this process the likelihood of unexpected failure is reduced to a remote probability which can be quantified and accepted in the design. Variability of these critical confidence levels is monitored by the Assurance process and manufacturing will be guided by 'trend analyses' of the process. An example of specific information on statistical methods, quality control, and quality assurance as applied to TRISO fuel QA/QC characterization and testing is provided in the reference [50] for the US AGR Fuel Development Program.

4.3. QC and characterization test methods

Tables 4 and 5 contain a list of typical QC tests and the preferred techniques used to diagnose TRISO coated particles [51]. Some of the more unique tests are discussed in the sections below.

4.3.1. TRISO particle size and shape analysis (PSA)

The benchmark apparatus for measuring particle diameters (and their associated volumes) for spherical particles in the size range applicable to kernels and coated particles is an automated optical particle analyzer with pneumatic particle transport, custom developed by Seibersdorf for NUKEM. It is a reliable, accurate and precise method that relies on the intensity dip observed by a detector when a particle passes through a light beam. For spherical particles, it is possible to achieve a linear response between an appropriately defined function of the intensity dip and the particle diameter. Accurate calibration of the system is achieved by means of standard steel balls. Particles are pneumatically transported, separated and passed through the light beam where they are counted and measured. Although a maximum rate of about 50 particles per second is achievable, the feed rate is chosen to match the desired accuracy and precision of the application.

Kernels and coated particles are not perfect spheres. Spherical pressure vessels provide maximum strength and therefore, sphericity, defined as the ratio of a particle's maximum diameter to its minimum diameter, has to be within specified bounds. To measure sphericity many randomly selected orientations of the same particle are presented to the measurement system by cycling the same particle many times through the light beam. The next particle is then selected and so on. In practice, particle sphericity tends to have a log-normal distribution indicating that multiplicative accumulation of random errors conspire during manufacture to cause deviation from a perfect sphere.

Table 3. LIST OF FUEL KERNEL PROPERTIES AND THE PREFERRED TEST TECHNIQUES

Fuel kernel property	Test techniques
Uranium enrichment	Mass spectrometric analysis using thermal ion mass spectrometry or gamma-ray spectrometry
Equivalent boron content (impurities)	Spectroscopic analysis using plasma source mass spectrometry or emission spectrometry
Stoichiometry (O:U ratio)	Thermo-gravimetric analysis
Diameter and sphericity	Particle Size Analyzer (PSA) Shadowscope techniques using an optical microscope and image analysis system
Density	Geometrical determination by means of PSA Mass by helium pycnometry or mercury porosimetry
Microstructure	Microscopy on ceramographic sections
Shape defect distribution (odd shapes)	Sorting table fraction analysis

Particle size and shape is also often determined using a shadowscope technique. In this method, a sample of particles is arranged in a monolayer on a transparent plate. An optical microscope is used in bright field transmitted mode to image the silhouette of each particle. Manual or computer automated image analysis is performed to measure the minimum, maximum, and average diameters of each particle. The shadowscope technique can provide particle size and shape to an accuracy that is equivalent to or better than the PSA, but sample analysis rate is more limited.

Table 4. LIST OF COATING PROPERTIES AND THE RECOMMENDED TEST TECHNIQUES USED TO CHARACTERIZE THEM

Property	Techniques
Layer thickness and symmetry	Micro-radiography Ceramography using image analysis techniques
Density of buffer layer	Geometrical determination by means of PSA and mass change between the coated and uncoated particles Mercury porosimetry
Density of other layers	Gradient column (sink-float method)
Anisotropy of the inner and outer	Optical anisotropy measurement

PyC layers	Advanced Two-Modulator Generalized Ellipsometry Microscope (2-MGEM) [52], [53]
SiC layer integrity	Burn-leach testing Micro-radiography
Microstructure and chemical composition of layers	Transmission electron microscope (TEM) Scanning electron microscope (SEM) Electron probe X-ray micro-analyzer (EPMA) Auger electron spectroscopy (AES) Scanning transmission electron microscope (STEM) Ceramography
Uncontained uranium	Burn-leach testing
Shape defect distribution (odd shapes)	Sorting table fraction analysis

4.3.2. Optical anisotropy

High density pyrolytic carbon is a graphitic material with a complex extended structure. Roughly speaking it behaves in a way similar to a polycrystalline material where each crystallite has inherently anisotropic properties, such as thermal expansion and fast neutron induced shrinkage. It is imperative to strive for isotropic macroscopic orientation in order to have average macroscopic properties that are homogeneous and isotropic. For macroscopic graphite samples, X-ray diffraction can be used to define and measure a so-called Bacon Anisotropy Factor (BAF) that directly relates to macroscopic material anisotropy. On the tiny layers of coated particles, normal X-ray diffraction is not possible. Fortunately, it happens that the intensity of reflected, polarized light differs depending on the orientation of the polarization direction relative to the crystallographic axes of the graphite crystal. Measurement of the ratio of the reflected intensities of a light beam, polarized first along one direction and then perpendicular to that direction will yield an optical anisotropy factor (OAF). It can be shown that this OAF can be related in a consistent way to the BAF, which in turn relates to actual expected anisotropy and fuel performance. As a light beam can easily be focused onto a polished metallurgical section of a coated particle under a light microscope, an OAF profile across a pyrolytic carbon layer can conveniently be determined.

This principle was utilized by researchers at the Seibersdorf Austrian Research Center to develop an OAF instrument for the German fuel manufacture NUKEM, GmbH. which can now be viewed as the primary standard for determination of anisotropy of pyrolytic carbon layers.

Recently, advanced ellipsometry techniques have been applied to the measurement of pyrocarbon anisotropy in TRISO fuels. A system developed by Oak Ridge National Laboratory (ORNL) called the Two-Modulator Generalized Ellipsometry Microscope (2-MGEM) was designed to completely determine the polarization effect on light reflected off of a polished pyrocarbon cross-section [52], [53]. This ellipsometer provides very accurate determination of the pyrocarbon anisotropy with a selectable spatial resolution down to a few micrometers.

4.3.3. Kernel, buffer and layer density determination

Silicon carbide and pyrocarbon (PyC) densities are measured by means of suitable density gradient columns [54]. A density gradient column is created by filling a glass column with two liquids of different density, where the ratio of the two liquids is varied during filling in order to create a linear density gradient as a function of the column height. This linear density gradient is determined by measuring the zero buoyancy position of calibrated floats. Samples of the Inner-PyC (IPyC), SiC, and outer-PyC (OPyC) layers are obtained by fracturing the coatings of individual TRISO particles. Pieces of free-standing OPyC fragments usually can be easily picked out of the fractured coatings because of the weak bonding between the SiC and OPyC layers. Free-standing IPyC fragments usually can not be obtained after deposition of the SiC because of the infiltration of SiC into the open porosity of the IPyC, which results in a strong interface. For this reason, IPyC density must be determined using hot sampling or interrupted batches. Free-standing SiC is obtained by picking out multiple layer fragments and heating in air to about 850°C to remove the attached PyC.

Density of the other two TRISO components (i.e., fuel kernels, and buffer layer) must be obtained by other methods. Suitable liquids spanning the density of the fuel kernels are not available. Liquid penetration of the buffer material results in the determination of the skeletal density of that layer, which is not of interest. A particle size analyzer (PSA) can be used to determine kernel density. The mass of a sample of (pre-sieved and sorted) kernels can be determined accurately. The sample is then passed through the PSA and the sum of the volume of all the kernels in the sample is divided by the sample mass to yield the mean kernel geometric density. The geometric density is a reasonable approximation of the envelope density if the particles are close to spherical. The density of the buffer layer can be determined in a similar way after subtracting the mean kernel volume from the mean total volume and using the appropriate mass values. Apart from the relative standard deviation caused by variation in buffer volume, the relative standard deviation in kernel density becomes amplified (by about six times for nominal TRISO particles) and adds to the over-all relative error. This places a strict upper limit on the required accuracy and precision of kernel density determination. Alternately, mercury porosimetry can be utilized to determine the envelope volume of the kernels and buffer-coated particles. This technique can provide improved measurement accuracy, especially for non-spherical particle shapes.

4.3.4. Layer thickness determination: Micro-radiography

Although PSA analysis can be used to derive layer thickness, the method becomes increasingly imprecise for outer layers due to error propagation. To achieve good statistics of intrinsic layer variation over a large number of particles (100 – 200), X-ray microradiography can be utilized [55], [56]. A single layer of particles is positioned directly on the emulsion of a high resolution photographic film (about 1 µm resolution) and illuminated with an X-ray source approximately 300 mm away. With such an arrangement, sharp projected images of layers can be achieved even with an X-ray tube that does not behave like a true point source, so that there is no need for a fine focus source. To distinguish between the buffer and the adjacent pyrolytic carbon layer, low energy X-rays are needed and the exposure must be in vacuum. Tube voltage and current are selected to give the required contrast needed for the intended layers. The developed and mounted film is analyzed under a transmission light microscope equipped with a CCD camera. Layer thickness analysis is achieved by means of standard image processing software. Coating thickness is also often determined by preparing metallographic cross-sections and directly imaging with an optical microscope using bright

field reflected light [57]. Resolutions of 1 μm can be obtained and analysis can again be performed by standard image processing software.

4.3.5. SiC layer integrity: Burn-leach testing

A very important test for SiC layer integrity is the burn-leach test. A representative sample of coated particles of statistically significant size is selected. Under clean laboratory conditions these are burned down to the SiC layers and the remaining particles and ash are leached under reflux for an extended time period in a nitric acid solution. A sample of the liquid is then pre-concentrated in a rotary evaporator and analyzed for uranium with extremely sensitive analytical technique such as fluorimetry, mass spectrometry methods, or delayed neutron counting (after activation in a reactor). When there are no defective SiC coatings, the analytical result reflects the unconfined uranium content. The number of broken particles or defective SiC layers can be calculated after division of the total concentration by the expected contribution per particle.

The intrusion method has also been applied to determine particle defect or failure fraction. This method involves surrounding the particles with a liquid under pressure. The liquid intrudes into the pores of the particles and the measurement of the extent of the intrusion yields information about the existence or size of the pores. The intrusion liquid can be a wetting or non-wetting liquid (e.g. mercury), halogenated carbons or aqueous solutions. For wetting liquids, the liquid will flow into the pores depending on the relative interior/exterior pressure of the pores and for non-wetting liquids pressure will have to be applied. For mercury (a non-wetting liquid) intrusion, commercial mercury porosimeters are available.

4.3.6. Thermal conductivity

The most important property for predicting the in-reactor fuel temperature is the thermal conductivity. For the graphite element (compact or sphere) this property can easily be obtained by the conventional laser flash method. The thermal properties of coated particles must also be evaluated to improve the prediction of the in-reactor behavior.

Photo-thermal experiments are particularly suitable for determining thermal diffusivity between micrometer and millimeter scale simply by varying the modulation frequency [58]. The currently selected technique is thermo-reflectance microscopy, based on detecting a photo-thermal effect and therefore, allowing no-contact thermal diffusivity measurement. The thermal conductivity is the product of the experimentally measured thermal diffusivity by the heat capacity and density, according to the following relation:

$$K = \rho \, \alpha \, Cp. \tag{4.1}$$

Where K is the thermal conductivity ($W.m^{-1}\cdot K^{-1}$), α is the measured thermal diffusivity ($m^2\cdot s^{-1}$), ρ is the density ($kg\cdot m^{-3}$), and Cp is the heat capacity ($J\cdot kg^{-1}\cdot K^{-1}$).

4.3.6.1. Description of thermo-reflectance microscopy

The thermo-reflectance microscopy technique [59] is based on measuring and analyzing the periodic temperature increase induced by the absorption of an intensity-modulated laser beam (pump beam). By detecting the thermally induced reflection coefficient variations with the help of a secondary continuous laser beam (probe beam), the temperature increase is measured at the sample surface with a sensitivity better than 10^{-3} $kHz^{-1/2}$. Unlike other photo-thermal methods, this contactless technique has micrometric spatial resolution.

The experimental setup (Fig. 16) consists of three main parts: an optical system for focusing and positioning the pump and probe beams, a device for measuring the reflected probe beam intensity, and several electronic devices for detecting the signal and driving the experiment.

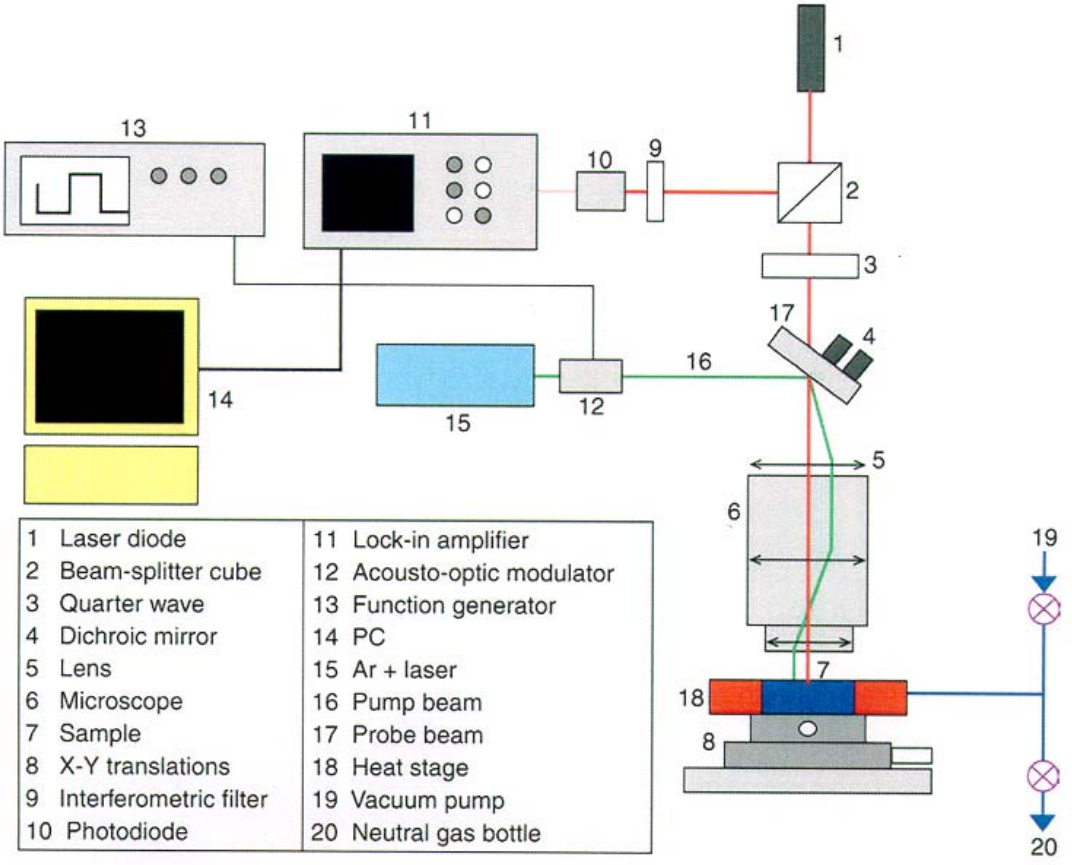

Fig. 16. Thermal microscope set-up [59].

The pump beam is a continuous-wave Ar+ laser with a maximum power of 2 W. Its intensity is modulated by a frequency generator-driven acousto-optic modulator operated at frequencies up to 2 MHz. The pump beam is then oriented by a dichroic mirror and finally focused onto the sample surface in the heating stage with a microscope.

The probe beam is a laser diode that passes through a quarter-wave plate and the dichroic mirror, and is then focused onto the sample surface with the same microscope. After reflection, it passes through the quarter-wave plate again and is then sent to the photodiode by a beam splitter cube. An optical filter prevents any pump beam photons from reaching the detector. A lock-in amplifier extracts the amplitude and phase of the periodic photodiode signal. A computer controls the dichroic mirror orientation and consequently the distance r between probe and pump beam location.

The fused silica heating stage window transmits 93% of the intensities of the two beams. An objective with suitable magnification and a large working distance is used to correct the spherical aberrations due to the heating stage window. The highest temperature that the heating stage can reach is 1500°C with a heating rate of 0.1–130°C/min. The sample must be

polished to a mirror finish to ensure good reflection. In our case, the measurements were performed on polished particle cross-sections.

When an isotropic, homogeneous medium is heated by a periodic point-like heat source of power Q, the periodic temperature increase, also called the "thermal wave", at a distance r from the pump location is described by the following equation:

$$\delta T(r) = \frac{Q}{4\pi kr} \exp\left(-\frac{r}{\mu}\right) \cos\left(\omega t - \frac{r}{\mu}\right), \tag{4.2}$$

and

$$\mu = \sqrt{\frac{\alpha}{\pi f}}. \tag{4.3}$$

Where, μ is the thermal diffusivity length, f the modulation frequency of the harmonic heat source, α is the thermal diffusivity of the material, and k its thermal conductivity. The argument of δT (i.e. its phase) is $-r/\mu$; the slope of the phase versus r curve is $-1/\mu$, which is used to estimate the thermal diffusivity of the medium using a simple linear regression. The thermal diffusivity can thus be determined with a precision often better than 5%.

4.3.6.2. Thermal characterization applied to dense PyC layers

Thermoreflectance microscopy has been applied to characterize dense pyrolytic carbon layers of TRISO particles. Measurements have been performed at room temperature [60], and tests at temperatures of up to 1500°C are currently in progress. The thermal diffusivity is estimated from the 1D least-squares fit of the phase profiles. An example for IPyC is illustrated in Fig. 17. The results obtained on TRISO particles are given in Table 6. These results give an order of magnitude to thermal diffusivity values which can be used in modeling of TRISO particles. Differences in the diffusivity values observed between the IPyC and the OPyC may be correlated with annealing of the IPyC around 1500–1600°C during the SiC deposition process, which tends to increase its diffusivity.

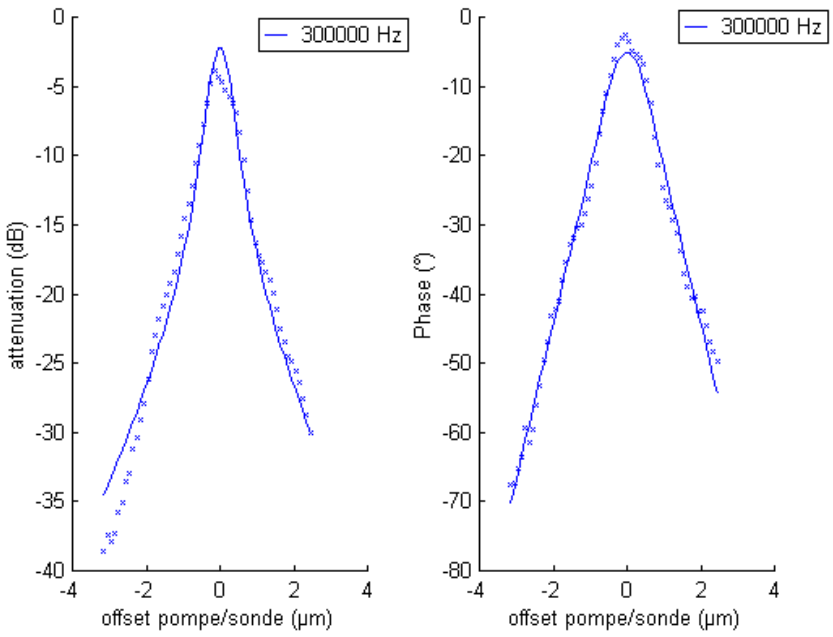

Fig. 17. 1D Scanning and its related squares adjustment [60].

Table 5. THERMAL DIFFUSIVITY OF DENSE PYROLYTIC CARBON LAYERS [60]

Property	TRISO particles	
	Inner PyC	Outer PyC
Diffusivity ($mm^2.s^{-1}$)	7,6 ± 3,2	3,6 ± 0,2

4.3.6.3. Thermal characterization applied to the buffer layer

Buffer layer thermal property measurements can be performed at room temperature. The diffusivity obtained for the dense parts of the buffer layer is 5.2 ± 0.5 $mm^2.s^{-1}$ [60]. A numerical model of steady-state thermal conduction inspired from the guarded hot plate method is used to determine the thermal diffusivity of the buffer layer. This approach, coupling local measurement and numerical homogenization, has been validated as shown in [61]. The diffusivity value obtained on the buffer layer is 4 $mm^2.s^{-1}$.

4.3.7. Elasticity modulus

Elastic modulus measurements were performed with a Nanoindenter® NT 600 (Micro Materials Limited) that allows indentation displacement of 50 µm. The penetration of the non-deformable diamond indenter is measured by a capacitive sensor with about 0.01 nm accuracy.

Thirty indentations were performed in each layer on a polished equatorial cross-section. The average results obtained are given in Table 7, and compared with literature data based on nanoindentation measurements. These values are in agreement with literature data [16], [62], [65]. They give an order of magnitude to the Young's modulus values for the IPyC and OPyC which can be used in modeling. Differences are observed between the Young's modulus of

the IPyC and the OPyC. As for the thermal properties, this difference may be correlated with annealing of the IPyC during the SiC deposition process.

Table 6. YOUNG MODULUS OF DENSE PYROLYTIC CARBON LAYERS [60]

Property	TRISO particles	
	Inner PyC	Outer PyC
Young's Modulus (GPa)	18 ±1,1	23 ±1,4

5. FABRICATION OF FUEL COMPACTS

Fuel compacts are typically cylindrical fuel forms that are placed into graphite hexagonal blocks for prismatic HTGR designs. Because the shape of the Japanese fuel compact is annular there are significant differences between the Japanese compacting process and those of the French and US. Each of these compacting processes will be described separately.

5.1. The Japanese process

The High Temperature Engineering Test Reactor (HTTR) at the Japan Atomic Energy Agency utilizes prismatic type fuel with UO_2 TRISO-coated fuel particles. Coated fuel particles are dispersed in a graphite matrix and sintered to form an annular fuel compact as shown in Fig. 18 [30]. Fuel compacts are contained in a graphite sleeve to form a fuel rod. These fuel rods are inserted into vertical holes bored into the prismatic graphite block. The Japanese process for the manufacture of fuel compacts is shown in Fig. 19 [31].

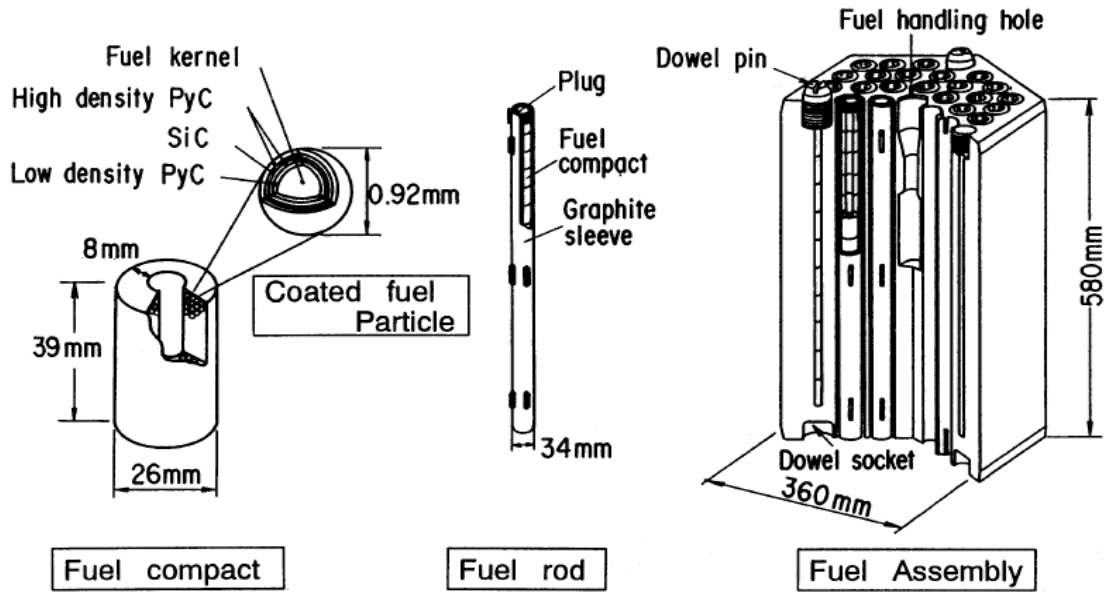

Fig. 18. Pin-in-block prismatic fuel element for the High Temperature Engineering Test Rector (HTTR) in Japan.

1. TRISO coated fuel particles are overcoated with graphitic matrix material. The overcoating matrix material is prepared by mixing electro-graphite powder, natural graphite powder, and phenolic resin as a binder in the ratio of approximately 16%, 64%, 20% (by weight), respectively and ground into a powder with specific particle grain sizes. Overcoating of the TRISO particles prevents particle- to-particle contact. The thickness of overcoating layer is about 200 μm for the Japanese process, in order to achieve a specified 30% TRISO fuel particle-to-total compact volume after pressing and heat treatment processes.
2. The overcoated particles are warm-pressed in metallic dies to form annular compacts.
3. The compacts are heated to approximately 800°C in an inert nitrogen atmosphere furnace to carbonize the phenolic resin binder.
4. The compacts are heat-treated at 1800°C in an annealing furnace under vacuum to remove impurities and to de-gas the fuel compacts [32].

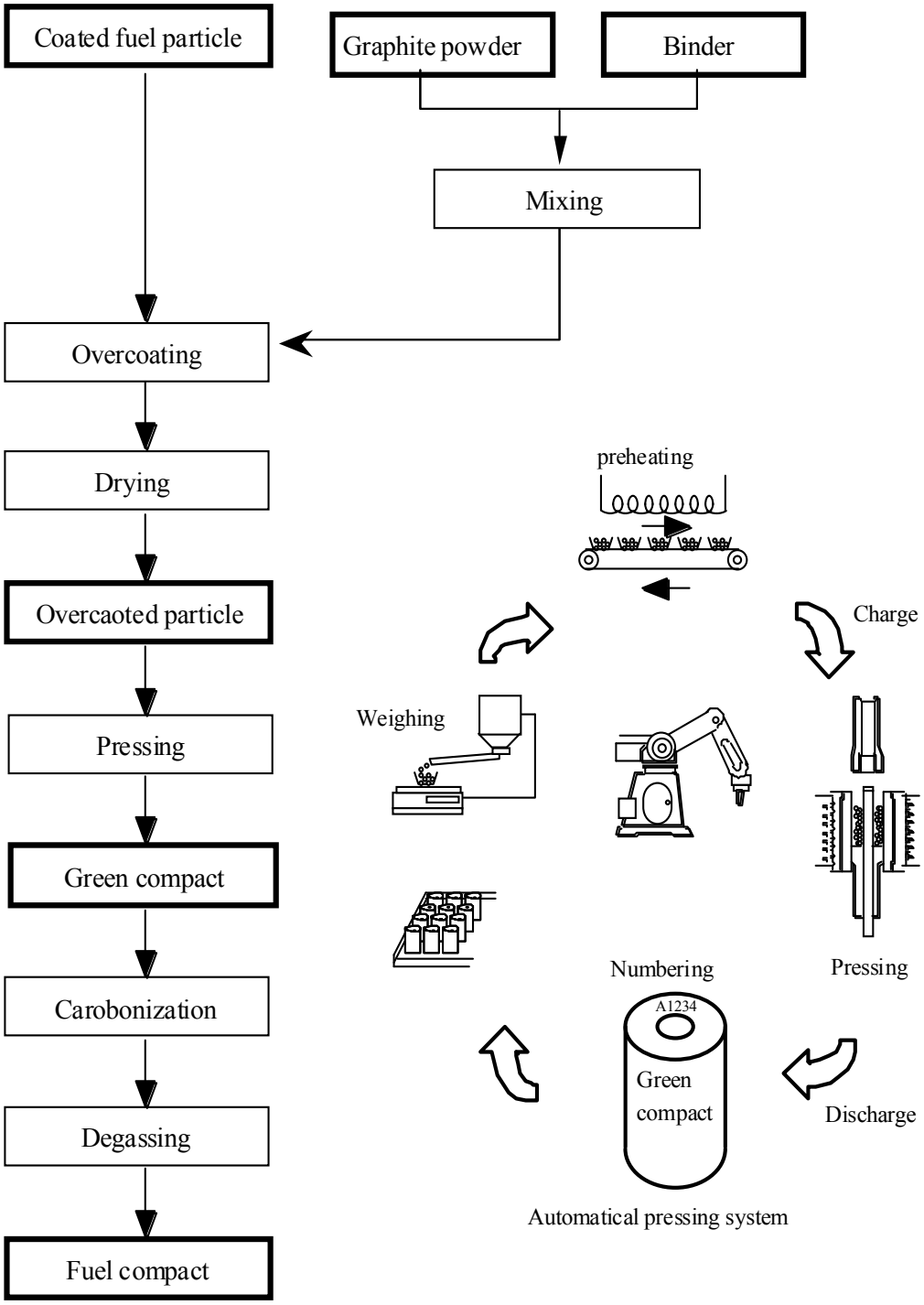

Fig. 19. Summary of fabrication process for fuel compacts.

This fabrication method was used for the first [31], [32] and the second HTTR fuel core loadings [33]. Characterization results of the second TRISO fuel core loading demonstrated that the average through-coatings defect fraction was 2×10^{-6} and the SiC defective fraction was 1.7×10^{-4} [33]. The Japanese fabrication process successfully produced, on a commercial scale, first and second fuel core loadings with high quality, low defect fraction TRISO fuel compacts, and fuel rods that contained a total of 2 tonnes of uranium.

5.2. The French process

The French compacting process [34], as implemented by CERCA, a subsidiary of AREVA NP, France, does not use an overcoating process. In the CERCA process, the matrix material is poured into the cylindrical compact mold simultaneously with bare TRISO coated particles.

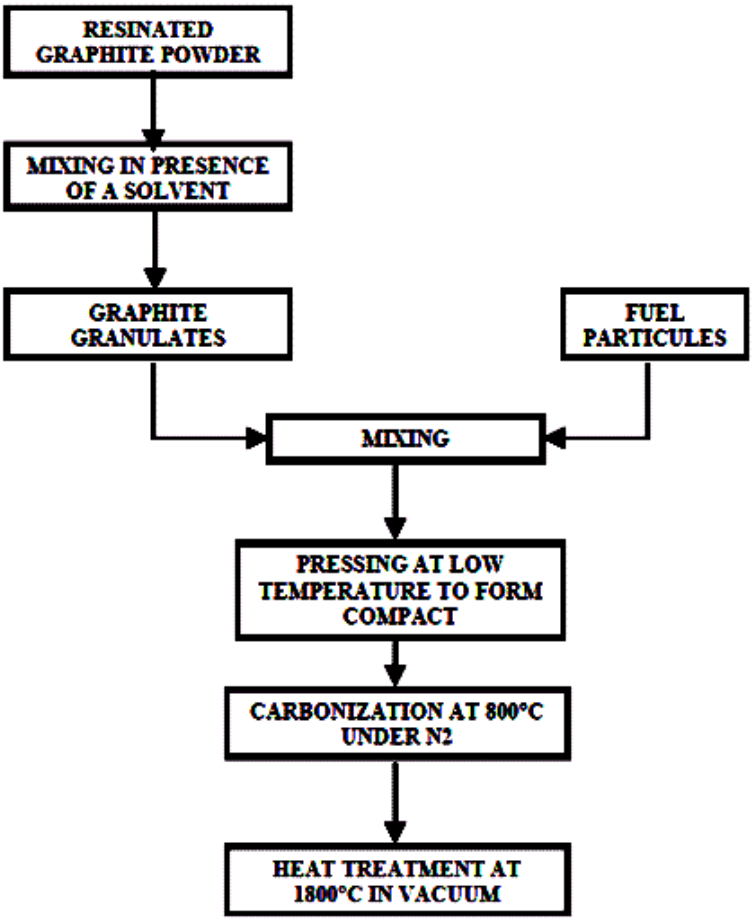

Fig. 20. Diagram of the CERCA compacting process.

The French process as shown in Fig. 20 involves the following steps:

1. A resinated graphite powder is first prepared by mixing graphite powder and phenolic resin.
2. This graphitic mixture is then fed into a rotating drum by a vibrating bowl and alcohol is sprayed directly on the powder, and produces small agglomerates of resinated graphite called granulates.
3. These granulates are then dried to remove the alcohol and sieved.
4. Dry granulates and TRISO particles are placed into a specific CERCA device with two holders. TRISO particles and dry granulates are pushed into a CERCA die to reach the specified packing fraction and to achieve a highly uniform TRISO particle distribution.

The mixture in the CERCA die is warm pressed to form the cylindrical compact and heat treated.

1. A low temperature heat treatment process is used to polymerize the resin at 200°C.

2. A second heat treatment at 800°C is performed in an inert nitrogen atmosphere furnace to de-gas the volatile organic products and carbonizes the compact.

3. A final heat treatment at 1800°C is performed under vacuum to insure hardening of the matrix and further degassing of the cylindrical compacts.

The French CERCA process heat treatment temperatures are directly linked with dimensional change behavior of the compacts, final physical properties, structure, and density of the graphite matrix.

5.3. The US process

The US is developing its TRISO fuel for the HTGR reactor (Next Generation Nuclear Plant, NGNP) in Idaho which will demonstrate very high temperature gas reactor technology for hydrogen, process heat, and electricity applications by 2018. The US Advanced Gas Reactor (AGR) fuel development program [35] is fabricating and testing UCO and UO_2 TRISO fuel in the Idaho National Laboratory (INL) Advanced Test Reactor (ATR) to demonstrate the irradiation performance and safety characteristics of the NGNP fuel.

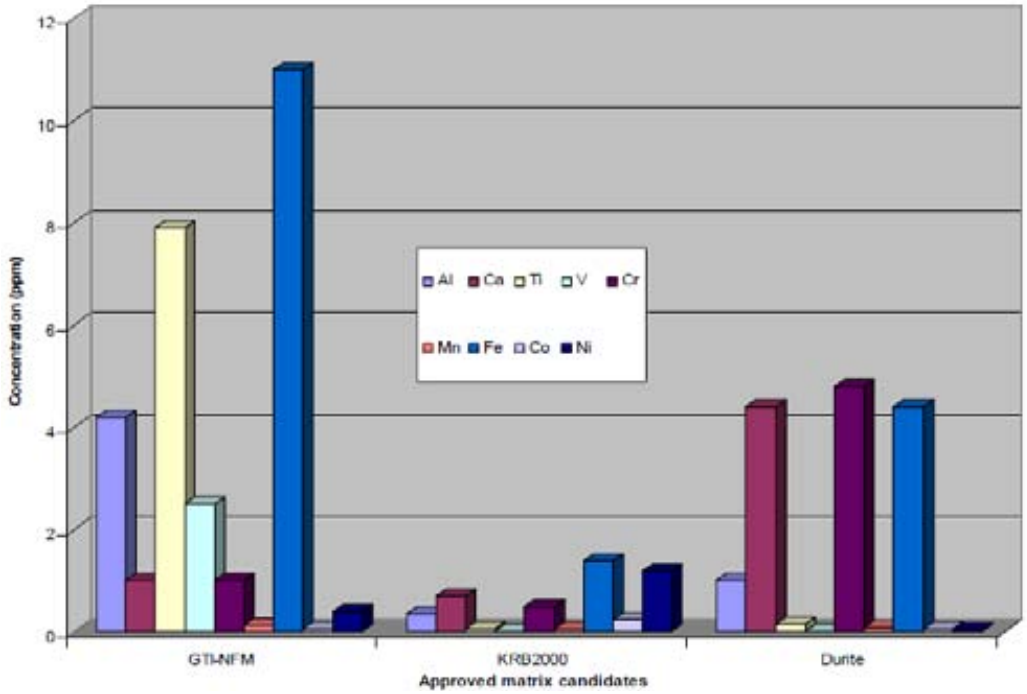

Fig. 21. Impurities content of natural graphite, synthetic graphite, and thermosetting resin used to make the matrix for the AGR-1 test articles [36].

The AGR fuel program uses overcoated TRISO fuel particles pressed into cylindrical compacts and heat treated. The steps are delineated below, with greater details to explain the rationale behind the process.

5.3.1. Graphite matrix material formulation

The graphitic matrix material is formulated by mixing natural graphite, synthetic graphite, and a thermosetting resin in the ratio of 64, 16 and 20% (by weight), respectively.

Natural graphite is highly anisotropic, but can be milled into a fine particle size and re-formed into a graphitic matter that is macroscopically isotropic. Synthetic graphite is less anisotropic than natural graphite, but also can be milled and re-formed in order to produce overall isotropic graphite. By mixing the natural graphite with the synthetic graphite, a material with some compressibility (as a result of the natural graphite) and some toughness (as a result of the synthetic graphite) is achieved, so less binder (thermosetting resin) is needed. The thermosetting resin is used to provide some adhesion to the mixture and help it adhere to the TRISO particles during overcoating, and will harden into a solid during the carbonization. The selection of natural graphite, synthetic graphite, and resin candidates must involve the evaluation of impurity concentrations to avoid chemical species that may attack the outer pyrolytic layer or diffuse into the SiC layer causing corrosion. Figure 21 shows the impurity concentrations of specific graphitic materials in ppm [36].

5.3.2. Overcoating TRISO coated fuel particles

The overcoating process developed by the Germans involved slowly rotating the TRISO particles and matrix in a large steel drum. Methanol jets were also incorporated into the drum so that at the desired time a mist of methanol could be sprayed onto the TRISO particle/graphite matrix bed. The methanol aids in the matrix adhering to the TRISO particle.

Fig. 22. Top secured overcoater used in early development stages of AGR-1 test article development [36].

The AGR program's original laboratory scale overcoating device is shown in Fig. 22. Figure 23 is an image of a TRISO particle overcoated by this method. The first ATR test specimens prepared for the AGR irradiation program (AGR-1) were overcoated in the setup shown in Fig. 24.

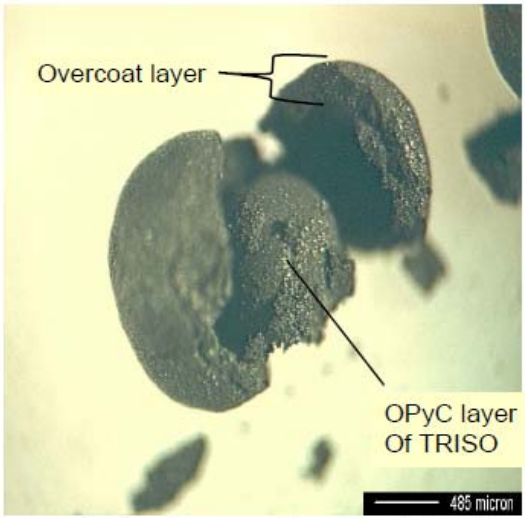

Fig. 23. Overcoated particle prepared in the top secured overcoater and slow rolling method. The overcoat was intentionally broken off to show the TRISO particle [36].

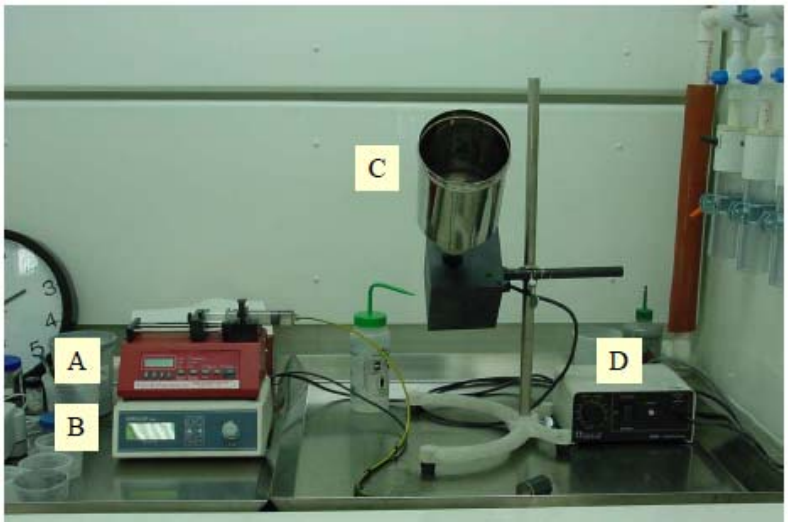

Fig. 24. Overcoater setup, where "A" is the syringe pump, "B" is the ultrasonic atomizer, "C" is the overcoating chamber, and "D" is the motor [36].

Through experimentation the best overcoating method was found to be a centrifugal rotating drum that produced well mixed particles and matrix with an added agent to aid in the adherence of matrix to the particles. The key aspects of the centrifugal overcoating method are: (1) the particles and matrix are pre-mixed in a set ratio, (2) the particle/matrix mixture is spun at high enough speed to force the mixture to the walls of the overcoater, and (3) upon insertion of the agitator arm, the mixture comes off the wall of the overcoater as a spray

which passes through a fine mist of methanol. The methanol mist is delivered by a syringe pump and ultrasonic atomizer. A schematic of the centrifugal overcoating process is shown in Fig. 25.

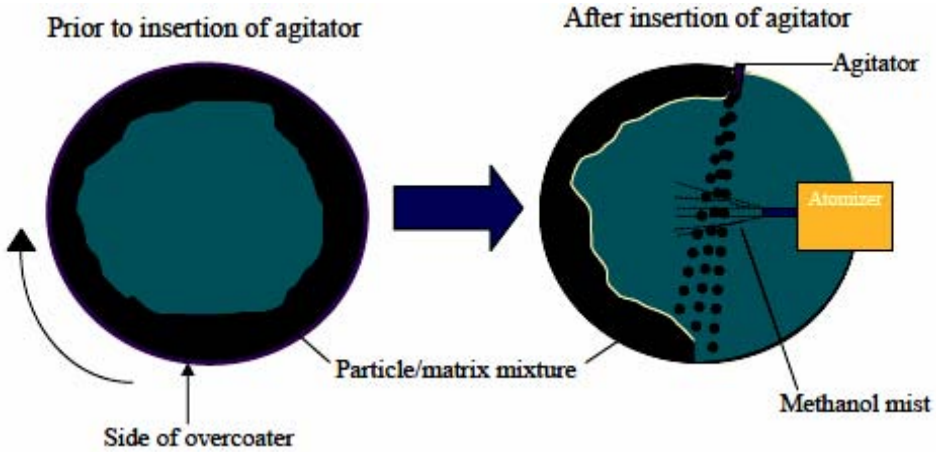

Fig. 25. Schematic diagram of the centrifugal overcoating process developed at ORNL. Development of this overcoating method was needed for the smaller UCO TRISO particles.

The pre-mixing of the particles and matrix in a set ratio allows for good contact between the matrix and the particles, and a lesser probability that matrix clumps will form because essentially no excess matrix is present that could lead to clump formation. Spinning the particle/matrix mixture ensures that the set mixture ratio will be maintained during overcoating, as the particles and matrix are not moving because they are pinned to the wall of the overcoater. The use of the agitator arm to spray the particles off the wall and through a mist of methanol ensures that the methanol is delivered at a time when the correct ratio of particles and matrix is present. This method makes certain that the matrix will adhere to the OPyC layers of the particles, and not to itself. The mist of methanol helps to evenly coat the particles so that an uniform layer of matrix is deposited over the entire surface area of the particles.

The overcoating method must produce overcoated particles with the proper outer diameter required to meet the fuel particle packing fraction requirement, after compacting, pressing, and heat treatment. The number of particles, quantity of overcoating materials, volume of methanol, size of the overcoater, angle of the overcoater, and speed of overcoating must be determined experimentally, for laboratory bench-scale, pilot-scale, and commercial fuel production lines.

5.3.3. Compact fabrication

The AGR fuel program makes compacts in a similar manner as the Japanese method, but with a methanol soaking step added. Steps in the compact forming process are:

1. The overcoated particles are saturated with methanol prior to compacting to improve compact material flow into open spaces under pressure.
2. The overcoated particles are warm-pressed in metallic dies to form cylindrical compacts.

3. The compacts are heated to 950°C in an inert helium furnace for one hour to carbonize the thermosetting resin binder. The compacts are then heat-treated at 1800°C in an annealing furnace under vacuum for one hour to remove impurities.

Figure 26 is an image of the outer surface of a compact that was formed without the overcoated particles being exposure to methanol prior to compacting. Notice the pits and open spaces between particles because the overcoat did not effectively flow under pressure into the inter-particle spaces. Figure 27 is an image of a compact whose overcoated particles were saturated with methanol prior to compacting. The surface finish of this compact appears smoother and more uniform because the overcoat was more malleable and able to fill the void spaces between particles.

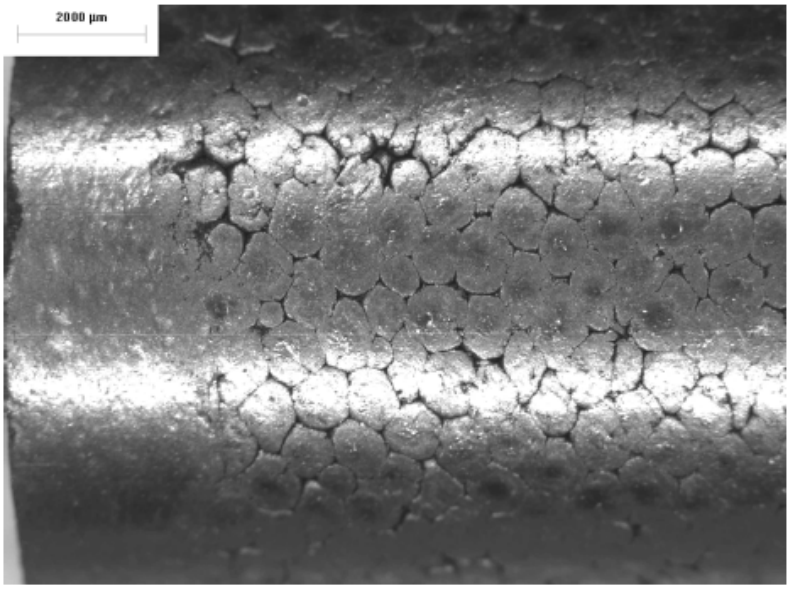

Fig. 26. Image of compact side showing incomplete pressing due to lack of methanol saturation in the original overcoated particles [36].

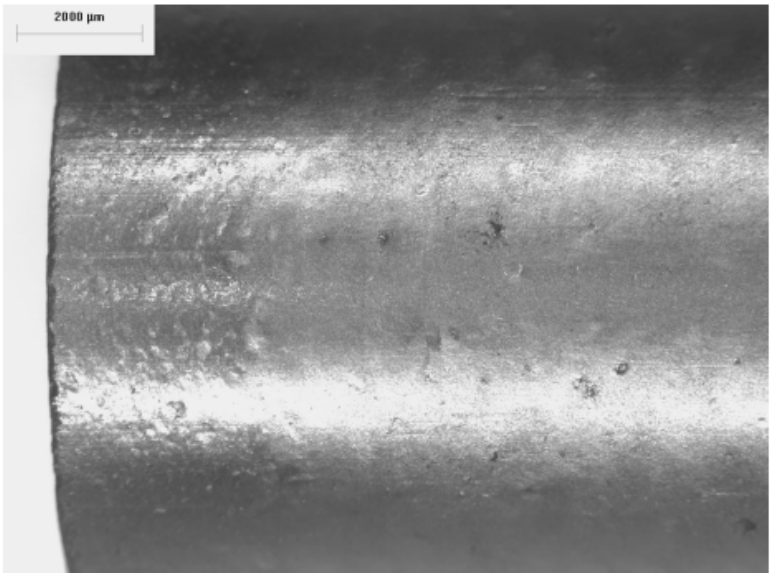

Fig. 27. Image of compact side showing complete compression due to proper saturation of overcoated particles prior to compacting [36].

The final compacts are evaluated and characterized to determine their quality in terms of defect fractions, 'tramp' uranium content, with various methods. Since some of the characterization methods are destructive (e.g., leach-burn-leach process destroys the compact and removes all existing uranium using acids), only a statistical sampling method can be used to evaluate adherence to specifications within a specific tolerance. The compacts produced for the AGR-1 irradiation test exhibited few defects during TRISO particle fabrication and the subsequent compacting process.

The AGR-1 fuel test experiment included baseline fuel that had "German-type" TRISO coatings and three variants with process parameter changes during the coating process. Table 3 provides the upper limit of the 95% confidence interval of the defect fraction for exposed kernels. Note that no exposed kernels were detected in any of the compact lots and there was no other indication that this low pressure compacting process will break particles. Table 3 also gives the upper limit of the 95% confidence interval of the defect fraction for particles with defective SiC layers, before and after compacting. No defective SiC was detected in Variants 1 and 3. The Baseline showed two defective particles and Variant 2 showed one. Details of the AGR-1 fuel irradiation tests are described in Chapter 8 (TRISO-Coated Particle Fuel Irradiations).

Table 7. THE 95% CONFIDENCE PREDICTIONS FOR THE MAXIMUM DEFECT FRACTIONS FOR EACH FUEL COMPACT LOT PRODUCED FOR AGR-1

Property	Baseline[a]	Variant 1[a]	Variant 2[a]	Variant 3[a]
Exposed Kernel Fraction	$\leq 3.1 \times 10^{-5}$ (0/99470)	$\leq 4.1 \times 10^{-5}$ (0/74699)	$\leq 3.1 \times 10^{-5}$ (0/99110)	$\leq 3.1 \times 10^{-5}$ (0/99032)
Defective SiC Coating Fraction after Compacting	$\leq 1.4 \times 10^{-4}$ (2/49735)	$\leq 6.1 \times 10^{-5}$ (0/49799)	$\leq 9.6 \times 10^{-5}$ (1/49555)	$\leq 6.1 \times 10^{-5}$ (0/49516)

Defective SiC Coating Fraction Before Compacting	$\leq 2.5 \times 10^{-5}$ (0/120688)	$\leq 4.0 \times 10^{-5}$ (1/121117)	$\leq 9.5 \times 10^{-5}$ (1/50265)	$\leq 4.0 \times 10^{-5}$ (1/120660)

[a] Values in parentheses are the actual measured defects over the number of particles in the analyzed compacts.

6. IN-CORE STRUCTURAL MATERIALS AND COMPONENTS

Performance of materials is the main factor limiting the achievable gas temperature in HTGRs, especially in-core materials which are exposed to high helium and fuel temperatures during normal operation and transients. Also, in-core components are exposed to high irradiation damage and in an impure helium environment. The Japanese High Temperature Engineering Test Reactor (HTTR) has operated at temperatures of 950°C. Higher temperatures may be envisaged in the future HTGRs; however, temperatures exceeding 950°C present challenges especially for metallic structural materials, graphitic structures, ceramics, and composite materials. This section will introduce general information about in-core materials requirements and suggest further references for more details.

6.1. Hexagonal block fuel elements for the prismatic HTGR design

The first gas cooled reactor designed by General Atomics (GA) was the Peach Bottom Atomic Power Plant which utilized long cylindrical fuel elements that extended the full length of the core. The fuel elements in the Peach Bottom reactor which operated at 115 MWt could not be used for larger reactors producing more than 300 MWt power.

The Peach Bottom Core 1 fuel elements contained very simple fuel particles that were coated by a thin layer of pyrolytic carbon. These pyrolytic carbon coatings were applied so that the uranium-thorium carbide fuel particles would not hydrolyze during manufacture and storage. The Peach Bottom fuel elements were individually purged by a stream of helium gas that swept escaping fission products to an external capture system [40], [41]. The Peach Bottom Core 2 fuel elements contained typical BISO-coated (i.e., two-layer buffer and isotropic pyrolytic carbon) particles, which retained most fission products; however, significant amounts of Cs and Sr isotopes diffused through the intact BISO particles. The fuel element purge system and outer graphite sleeve was used to limit the release of these volatile fission metals into the primary circuit [42].

The hexagonal block fuel element was designed at GA in 1965, for the Fort St. Vrain (FSV) Nuclear Generating Station, which was constructed near Denver, Colorado [37], [38]. The goal for the fuel element design was to utilize a simple geometry that could be adapted to larger reactor cores.

Early gas-cooled reactor designs utilized ceramic materials in the core, including coated fuel particles, helium coolant, and a helium coolant outlet temperature of 700°C, or greater. The change from individually sweep gas purged fuel elements to the hexagonal block fuel element design was possible mainly because of the evolution of coated fuel particle designs that could retain large fractions of fission products. This coated particle fuel evolution is culminated in the TRISO design (tri-layer coatings of buffer carbon, silicon carbide and isotropic pyrocarbon). The TRISO fuel particle was developed in the 1960s at the OECD DRAGON Project in England, and at General Atomics and Oak Ridge National Laboratory in the U.S.

The hexagonal blocks allowed for the stacking of fuel elements into approximately cylindrical reactor core configurations while accommodating control rods into symmetric core positions. The hexagonal blocks can be arranged in roughly cylindrical patterns that minimizes neutron leakage at the outer edge of the reflector. The hexagonal blocks fit relatively closely together, and therefore limit helium coolant flow inside gaps between the blocks, i.e., by-pass flow.

Details of a standard Fort St. Vrain (FSV) fuel element hexagonal block arrangement is shown in Fig. 28 [38], [39]. The width (dimension across flats) of the standard hexagonal block fuel element was determined by reactor neutronics calculations, power and neutron flux distributions, control rod worth, and criticality constraints for reactor scrams during normal operations and transients, refueling and shut down conditions. The FSV core contained 247 separate columns of fuel elements, each six blocks high, and these columns were arrayed within 37 regions. Thirty-one regions each contained seven columns, and six regions at the edge of the core contained five columns. At the center of each region was a pair of control rods, suspended by cables from penetrations in the top head of the reactor vessel, and a flow control valve.

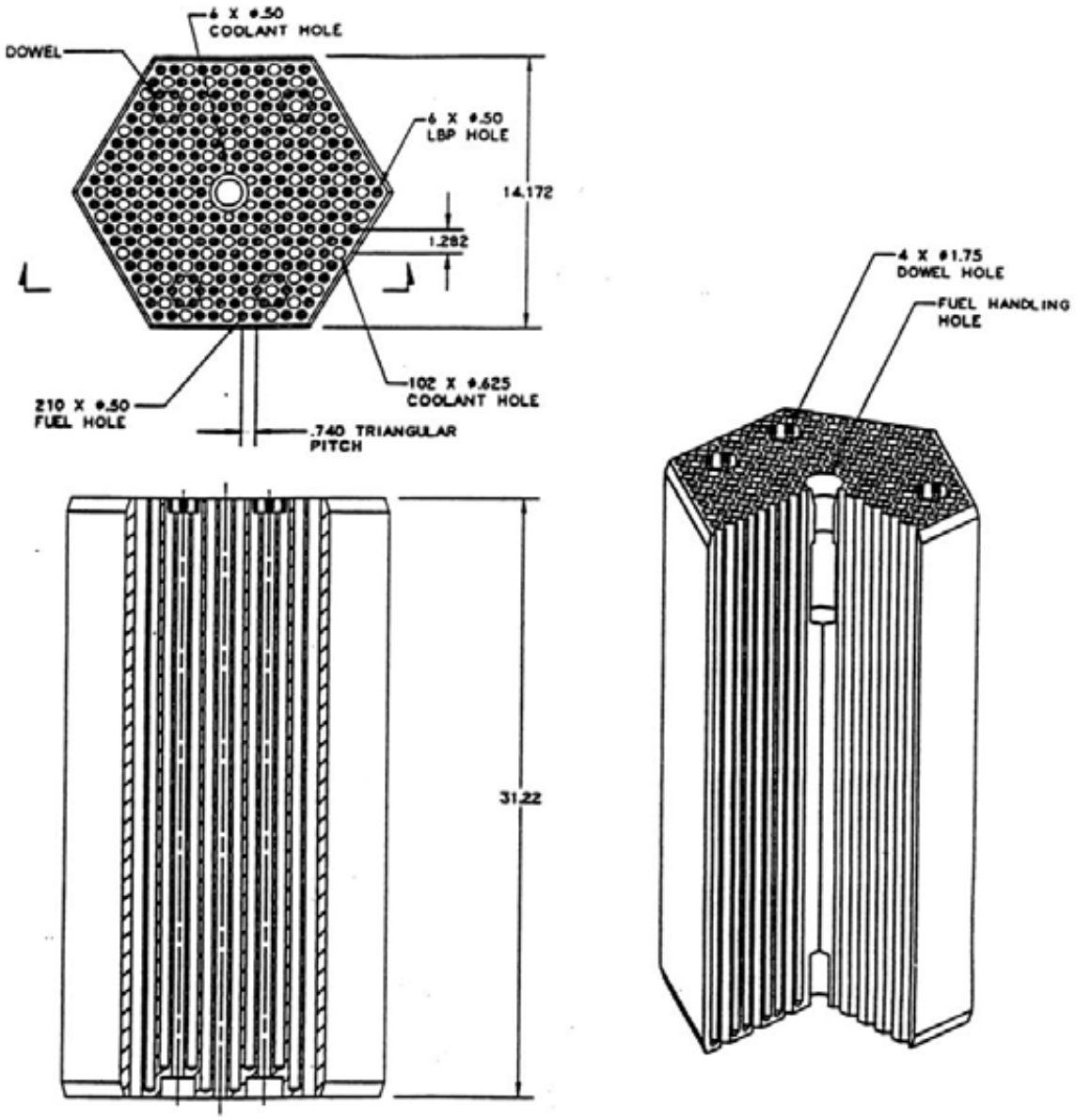

Fig. 28. Hex-block fuel element assembly [38].

The FSV fuel element width of 360 mm across the flats (14.172 inches) was within limits of a block that could be manufactured using the maximum diameter of nuclear grade graphite logs that could be obtained during the 1960s. The FSV hexagonal block was selected on the basis of experimental tests for drilling small diameter holes for locating fuel compacts and coolant passages within the fuel element. The acceptable length was limited by the drift of the holes off-center when drilled from one end of the block. A fuel element length of 790 mm (31.2 inches) was selected. The pattern for fuel and coolant holes within the fuel element was determined on the basis of thermal design analyses, core pressure drop estimates, and to produce a block structure that would not crack from thermal stresses or seismic forces.

The hexagonal block provides the possibility for a wide variety of coolant hole-fuel hole patterns to control fuel temperature, core pressure drop and fuel cost depending on the particular application. Short dowel pins were placed in the top of each fuel element that mated

with corresponding cavities on the bottom surface of blocks to align the coolant and control rod passages from one fuel element to another.

The hexagonal block fuel elements for the FSV reactor and for later test elements for developmental reactor designs were manufactured at the General Atomics Fuel Manufacturing Facility in San Diego, California. The FSV fuel cycle was based on highly enriched uranium (HEU) as the fissile material and thorium as the fertile material. Approximately 30 metric tones of uranium and thorium were processed at GA for the FSV initial core and four reload segments.

The graphite blocks for the FSV fuel elements were machined by GLCC, in Morganton, WV, at the same location where the graphite was manufactured. A machine for drilling precision holes was jointly developed by GA and GLCC, which was capable of drilling one-third of the fuel and coolant holes in a single pass.

A grade of extruded needle-coke graphite, designated as Great Lakes Carbon Company (GLCC) Grade H-327, was selected for the initial core and first reload segment for the FSV reactor. This graphite had anisotropic materials properties in the directions parallel and perpendicular to the extrusion axis. However, this grade was chosen at an early stage of development because it had high density, good strength and good dimensional stability during irradiation. A later grade that was more isotropic in structure was developed by

GLCC, and designated as Grade H-451. This material was selected for subsequent reload fuel segments in the FSV reactor. Grade H-451 continued to be selected as the reference grade for fuel element and reflector components in later GA Modular Helium Reactor (MHR) designs in the U.S.

The final stage in the fuel assembly process is to load stacks of fuel compacts into the machined graphite blocks. For each fuel refueling segment charged into a modular reactor core, a total of 10 to 15 different fuel compact loadings are typically specified to meet the requirements for shaping the power distribution. Once all of the fuel holes in each block have been filled, the compacts are sealed in place with graphite end plugs.

In summary, the processes have been developed and qualified for manufacturing hexagonal block fuel elements in larger scale production facilities. The hexagonal graphite block fuel elements demonstrated very good performance in the Fort St. Vrain Nuclear Power Station [44]. The FSV hexagonal block geometry, design, and past experience provide a foundation for future prismatic HTGR designs.

6.2. In-core graphitic materials

A significant issue for nuclear in-core graphite is high neutron irradiation damage which causes major changes in mechanical and physical properties. In a prismatic core, the hexagonal fuel blocks are inspected periodically during core fuel reloading. These blocks may be reusable if fuel compacts can be removed easily; thus the individual fuel blocks have lower damage rates than reflector blocks which may be required to remain in-service over many years. Hexagonal graphite blocks, without fuel, are used in the neutron reflector region and are replaced when required. Nuclear grade graphite experiences radiation-induced creep which causes it to shrink and then swell, at different rates along crystallographic orientations [45]. Since the properties of nuclear grade graphite is very dependent on the source carbon (i.e., coke) and manufacturing process, irradiation damage testing is required for each

reactor's specific graphite type prior to deployment. Details of specific structural graphite and radiation testing are available [46], [48].

6.3. In-core ceramic and ceramic composite materials

Ceramic composite materials (SiC and C based ceramics) in various forms can be used inside the HTGR core and reflector regions because they can maintain their structural integrity even at high temperatures (greater than 900°C), high neutron fluences (nvt), and high damage levels (dpa). Composite materials and structures are fabricated so that strength is not impacted by irradiation damage. Composite ceramics of C/C, SiC/C and SiC/SiC (where the matrix material (M) is filled into a woven fiber structure (F) to form the (F/M) composite) are advanced materials that can be used for specific in-core structural parts and liners. One specific HTGR application for ceramic composites is control rod guide tubes, sheathing, and the control rod segments themselves. Ceramic composites and superplastic ceramics can be used in-core locations that experience large thermal gradients, motion, flexure and vibration. Ceramic composite and advanced ceramic materials may be needed for instrumentation and control housing and instruments themselves. Some in-core applications may require complex shaped parts difficult to machine out of solid ceramics. Zirconia (ZrO_2)-based fine grained superplastic ceramics can be shaped into complex structures much easier [46]. Details of specific ceramic composite materials and in-core applications are available in the literature[47],[49].

7. TRISO-COATED PARTICLE FUEL IRRADIATIONS

7.1. Past irradiation performance

Numerous in-reactor irradiation experiments with TRISO-coated particle have been conducted world-wide with a significant number conducted in both the US and Europe as part of US and German TRISO-coated particle fuel development programs [27], [66],[68]. These irradiation tests were conducted at a variety of burnups, temperatures, and fluences. The rate of accumulation of burnup and fast fluence (i.e., the degree of acceleration) during the irradiation test relative to that expected in a HTGR reactor is also an important parameter. For most of these fuels, the time to reach design service burnup and fast fluence is approximately 1095 days (3 years), whereas in the experimental irradiation tests the time to reach peak conditions were accelerated by factors of two to ten.

A review of the US and German irradiation programs indicate that the programs were implemented quite differently with very different results. The German program's focus since 1980 was on UO_2-TRISO fuel for AVR and all future designs such as HTR Modul, whereas the US program examined many different particle variants (different coatings, different kernels). Also, the German irradiation tests were conducted with acceleration factors mostly under a factor of three, while US acceleration factors were as high as ten. Differences in in-reactor irradiation performance are evident from a plot of the on-line fission gas release-to-birth ratios (R/B) as shown in Fig. 29. The in-reactor performance indicates that German fuel exhibits about a factor of 1000 lower fission gas release under irradiation at end-of-life (EOL) than the US fuel over a broad range of conditions (temperature, burnup, fluence).

7.2. State of the art in TRISO-coated particle fuel irradiations

The historical experience in irradiation testing of coated particle fuels suggest that multi-cell capsules wherein fuel can be tested in separate, independent compartments under different temperature, burnup and fluence conditions allows tremendous flexibility and can actually save time and money in an overall fuel qualification program. Current multi-capsule irradiation testing capability exists in Russia (IVV-2M), Europe (HTR-Petten) and the US [Idaho National Laboratory (INL) Advanced Test Reactor (ATR)]. Although there are differences in details of the test trains used in each reactor, they share a number of important similarities that represent the state-of-the-art with respect to irradiation testing of this fuel form. In this section these important similarities are presented to give the reader a sense of the technical considerations in executing this type of testing.

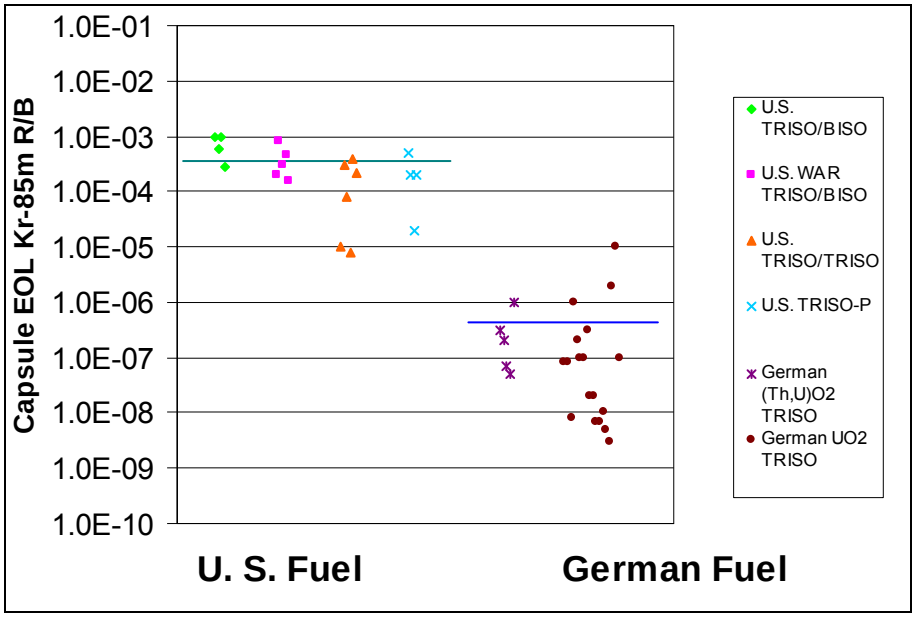

Fig. 29. Comparison of End-of-Life (EOL) 85 mKr fission gas release-rate to birth-rate ratio (R/B) from historic German and U.S. irradiations.

7.2.1. Reactor considerations

Because almost all of the material test reactors around the world are water cooled and moderated reactors, it is important to determine a test location that is most prototypic of a gas reactor spectrum, has the requisite flux to perform the irradiation in a reasonable amount of time, and a fast-to-thermal ratio that does not result in too severe an acceleration of the irradiation. If space is available, neutron absorbers can be used to help suppress the thermal flux and moderate the heat generation during the irradiation. For example, the large B positions (38 mm diameter) in the US ATR (see Fig. 30) were chosen for the US Department of Energy's (DOE) Advanced Gas Reactor (AGR) Fuel Development Program [27], [68], [69] fuel irradiations. In the ATR large B positions the rate of fuel burnup and fast neutron fluence accumulation provide an acceleration factor of less than three times that expected in the DOE HTGR Next Generation Nuclear Plant (NGNP) demonstration reactor. This acceleration factor is high enough to accomplish the irradiation within a reasonable time, but yet low enough as to avoid possible premature particle fuel failures similar to those experienced in

past highly accelerated particle fuel tests. Successful TRISO-coated particle fuel irradiations in the European HFR-Petten reactor were conducted using an acceleration of less than a factor of three. By comparison, the previous German irradiations in the FRJ reactor at Jülich had a neutron spectrum that was too thermalized with the result that the fuel received too little fast fluence to be prototypic of a HTGR. Similarly, previous US irradiations in the High Flux Isotope Reactor (HFIR) at Oak Ridge National Laboratory had too high a thermal flux resulting in significant burnup acceleration during the irradiation.

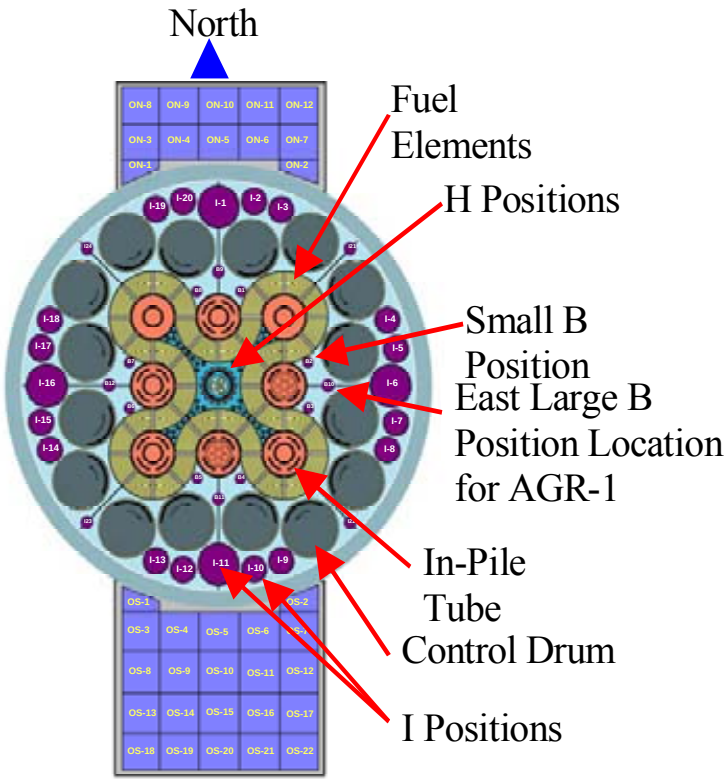

Fig. 30. Cross section of Advanced Test Reactor (ATR) core showing fuel and select irradiation positions.

7.2.2. Thermal and physics analysis considerations

Given the complexity of the capsules currently being designed, the extensive review by safety authorities of the thermomechanical stresses and the importance of each capsule in terms of irradiation data for fuel qualification, three-dimensional physics and thermal analyses are essential and are now expected in irradiation capsule design. These analyses are critical to ensure that the fuel reaches the intended burnup, fluence and temperature conditions. With the goal to achieve high burnups with these fuels, detailed physics calculations are needed to determine the time to reach full burnup. It is not uncommon for such irradiations to take approximately two years to reach full burnup in LEU TRISO-coated particles. In addition, because thermocouples should not be attached directly to the fuel, thermal analysis is used to calculate the fuel temperature during the irradiation.

Temperature control of the capsules is generally accomplished by adjusting the mixture ratio of two gases with differing thermal conductivities to control the heat transfer across an

insulating gas jacket between the heat source (fuel element and gamma heating of capsule materials) and the relatively cold test reactor coolant. Examples of a test train for fuel compacts used in the ATR [70] and spherical elements used in the HFR-Petten [71] are shown in Figs 31 and 32, respectively.

These irradiation capsules have extensive instrumentation to measure temperature, burnup and fast fluence at multiple locations in the test train. Traditional commercial grade (type K, type N, and type C) thermocouples have been used extensively in past irradiations. With the push to higher fuel temperatures for the HTGR (up to 1250°C), existing thermocouple technologies may not survive during the long (two years) fuel qualification irradiations because of drift and/or de-calibration in the reactor. Past experiments have had high uncertainties in fuel element centerline temperatures. Given the importance of establishing fuel temperatures in HTGR fuel qualification irradiations, accurate temperature measurements are critical. High-temperature thermocouples (e.g., refractory thermocouples) have been developed [72] at INL for the AGR Fuel Program underway at the INL. Redundancy in thermocouple measurements is another consideration in light of the low reliability of thermocouples at high temperatures and long times in neutron fields typical of HTGR fuel irradiations. Melt wires are inexpensive and have also been used as a backup to thermocouples where space was available in the capsule. However, melt wires only indicate that a certain peak temperature has been reached and not the time of that peak.

Direct measurements of the temperatures of the coated particles are problematic because direct metal contact (e.g., the thermocouple wires) with the fuel element is not recommended since the metals can attack the TRISO fuel coatings. Thus, temperatures must be calculated based on thermocouples located elsewhere in the capsule. To minimize the uncertainties on the calculated fuel temperatures related to irradiation-induced dimensional change and thermal conductivity changes of the materials in the capsule, thermocouples are generally located as close as possible to the fuel body to minimize the calculational uncertainty associated with the fuel temperature. Encapsulating the fuel element in a graphite sleeve or graphite cup and inserting thermocouples into this graphite has been used successfully in many designs. The high conductivity of graphite minimizes the effect of irradiation-induced dimensional changes on the calculated fuel temperature.

Historically, metal sleeves have not been allowed to touch fuel elements because of previous experiences in which SiC was attacked by transition metals (Fe, Cr and Ni). Although quantitative data on transport rates of such metals into the fuel element and corrosion rates of the SiC are unknown, 2 or 3 mm thickness of graphite between the fuel element and the metallic components (e.g., graphite sleeve) has been found to be effective in minimizing the potential for interaction.

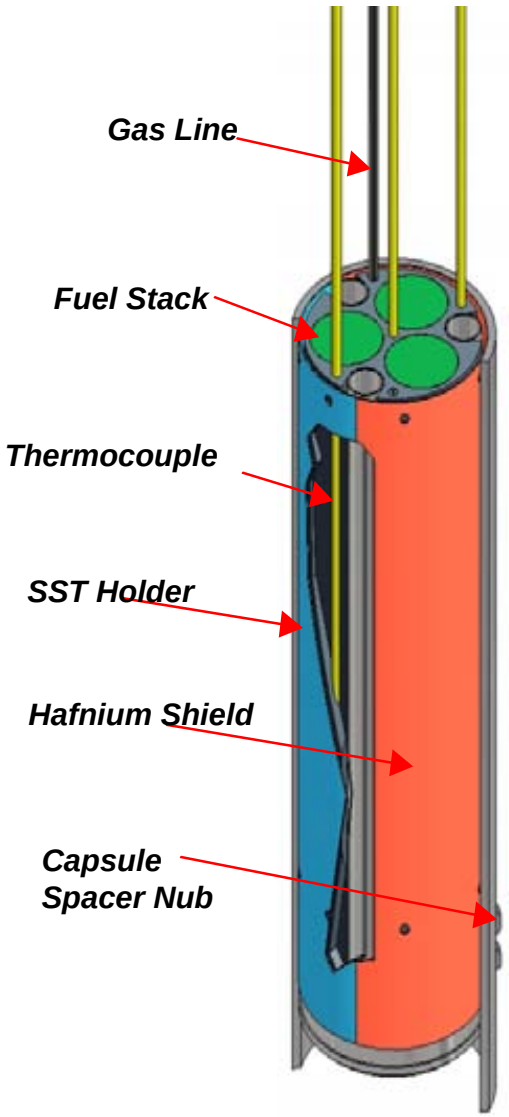

Fig. 31. Schematic of capsule design used in US AGR Fuel Development Program [70].

These irradiation experiments typically include both thermal and fast fluence wires. A number of different fluence wires have been used successfully to measure thermal and fast neutron fluences in coated particle fuel irradiations. The specific type of wire to be used will depend on the measurement need (fast or thermal), the temperature it will experience during the irradiation, and compatibility with the material of encapsulation. Quartz encapsulation is not recommended for high temperature high fluence applications. Neutronically, transparent refractories (e.g., vanadium) are a good alternative material for encapsulation. Inert gas filling of the flux wire encapsulation is recommended to ensure no oxygen interaction with the flux wire. Although fission chambers and self-powered neutron detectors have been used extensively in other reactor irradiations, they may not be practical in the space-constrained capsules expected for HTGR fuel qualification tests.

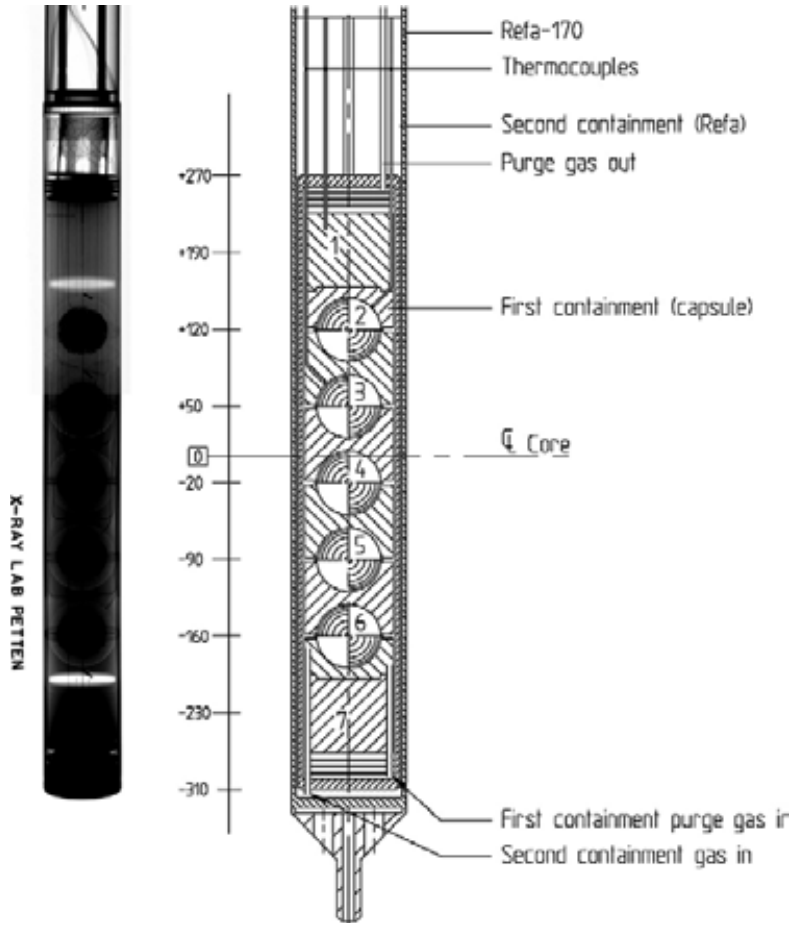

Fig. 32. Schematic of HFR irradiation test rig containing multiple spherical elements [71].

7.2.3. Gas control system considerations

Automated gas control systems to change the gas mixture in the experiment to compensate for the reduction in fission heat and changes in thermal conductivity with burnup minimize human operator error and have proven to be a reliable method of thermal control during these long fuel irradiations. The temperature of each experiment capsule will be controlled by varying the mixture of two gases with differing thermal conductivities in a small insulating gas jacket between the specimens and the experiment containment. Helium and argon have been used in the past, and this combination provides a nice wide temperature control band for the experiments. Unfortunately, argon cannot be used in fuel experiments where on-line fission product monitoring is used because the activated argon (^{41}Ar, $\tau_{½}$ =1.8 h) will reduce detectability of the system. Therefore, helium and neon is used. Computer controlled mass flow controllers are typically used to automatically blend the gases (based upon feedback from the thermocouples) to control temperature. The gas blending approach allows for a very broad range of control. Automatic gas verification (e.g., by a thermal conductivity analyzer) has been implemented in some experiments to prevent inadvertent connection of a wrong gas bottle. This process was incorporated to prevent uncontrollable temperature excursions because of having an insulator gas connected to the conductor gas port. Gas purity is important and an impurity cleanup system should be implemented during each irradiation. Flow rates and gas tubing should be sized to minimize transit times between the mass flow

controllers and the experiment and also between the experiment and the fission product monitors.

Alarm functions are provided in the control system to call attention to circumstances such as temperature excursions or valve position errors. The system can also allow helium purges to cool the individual specimen capsules under automatic control in the unlikely event that measurement or control of the capsule temperature is lost. Manual control capability is also provided at the gas blending panels to provide helium purge in the event of a computer failure. In order to minimize any temperature changes and maintain the most constant temperature as possible, the temperature control gas system provides a separate continuous flow to each specimen capsule, and a means to measure potential fission product releases.

7.2.4. Statistical considerations

A large number of particles must be tested to demonstrate the low failure rates associated with TRISO-coated particles. Traditional binomial statistics are used to determine the number of particles that must be irradiated to demonstrate in a statistically significant manner that a certain failure fraction is achieved. Figure 33 plots the number of particles needed in the irradiation (sample size) as a function of the failure fraction and the number of failed particles expected in the experiment. Thus, to meet a failure probability of 2×10^{-5} at 95% confidence the minimum number of particles to be irradiated is approximately 200 000 particles, assuming none fail during the irradiation.

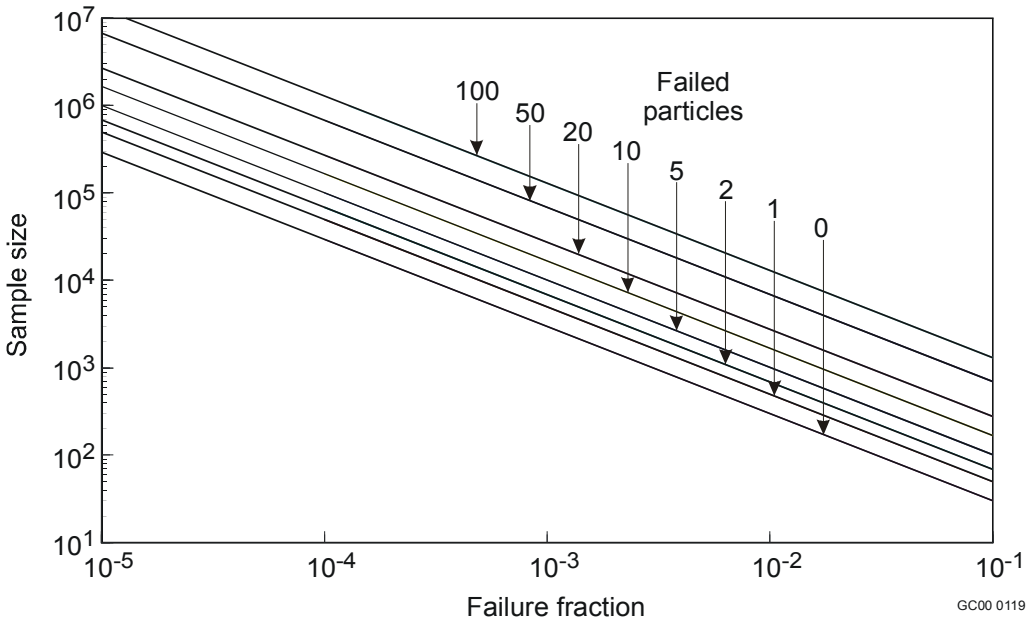

Fig. 33. Failed particle statistics.

7.2.5. Fission product monitoring considerations

In addition to thermal control, the sweep gas is used to transport any fission gases released from the fuel to a fission product monitoring system (FPMS). A number of techniques have been used historically to quantify the release of fission gases from the fuel in these irradiation capsules. Techniques include gross gamma monitoring, on-line gamma spectroscopy, and off-

line gamma spectroscopy of grab samples. On-line gross gamma monitoring of the effluent gas in the experiment is an excellent means to capture any dynamic failures of the coated particles because of the instantaneous release associated with such failures.

Two types of gross gamma detectors have been historically used: ion chambers and sodium iodide scintillation crystals. The scintillation detectors have increased sensitivity relative to the ion chamber approach and therefore allow more space between the gas line to be monitored and the detector. This is especially important if too many fission gas daughter products accumulate (from plate out) in the area viewed by the gross gamma detector. Grab samples can provide excellent noble gas isotopic information. The temporal resolution and the number of isotopes that can be measured depend on the frequency of the grab samples and the delay time between acquisition of the grab sample and the off-line analysis. Weekly grab samples are typical in most irradiations, although daily or even hourly samples are in principle possible if failure has occurred assuming operation and associated analysis costs are not too high. Typical isotopes to be measured include: ^{85m}Kr, ^{87}Kr, ^{88}Kr, ^{131m}Xe, ^{133}Xe, and ^{135}Xe. Measurement of very-long lived isotopes (e.g., ^{85}Kr) would be useful in elucidating fission product release mechanisms from the kernel, but would require waiting for the decay of the shorter-lived isotopes in the sample.

On-line gamma spectroscopy, although the most expensive in terms of hardware costs, can provide the most detailed real-time information with detailed isotopic spectrums as often as necessary subject to data storage limitations of the system. An example of the system used for the US AGR Fuel Development Program is shown in Fig. 34 [70]. With such systems, transit times from the experiment to the detector should be minimized to allow measurement of short- and medium-lived isotopes but long enough to allow decay of any short-lived isotopes associated with the sweep gases (~ 2-3 minutes). With this delay time, ^{89}Kr, ^{90}Kr, ^{135m}Xe, ^{137}Xe, ^{138}Xe, and ^{139}Xe, should also be able to be measured on-line. Measurements of xenon gas release during reactor outages are recommended to provide information on iodine release behavior. Such on-line systems typically use liquid nitrogen-cooled High Purity Germanium (HPGe) detectors, because of their well-established capabilities and reliability. In order to increase the sensitivity of the monitors, especially on the absolute quantity of fission products, the effluent gases should be collected over a long period of time by incorporating a large diameter thin wall gas detection chamber filled with baffles to slow the movement of the gas in front of the spectrometer detector. The use of cryogenically cooled traps could also be employed to collect and concentrate the fission products even more; however, this adds greater complexity. Multiple options for fission gas release measurements should be considered for long irradiations where reliability of the overall fission gas measurement system can be a concern. Redundancy is also recommended for on-line systems so that failure of a spectrometer does not jeopardize the entire experiment.

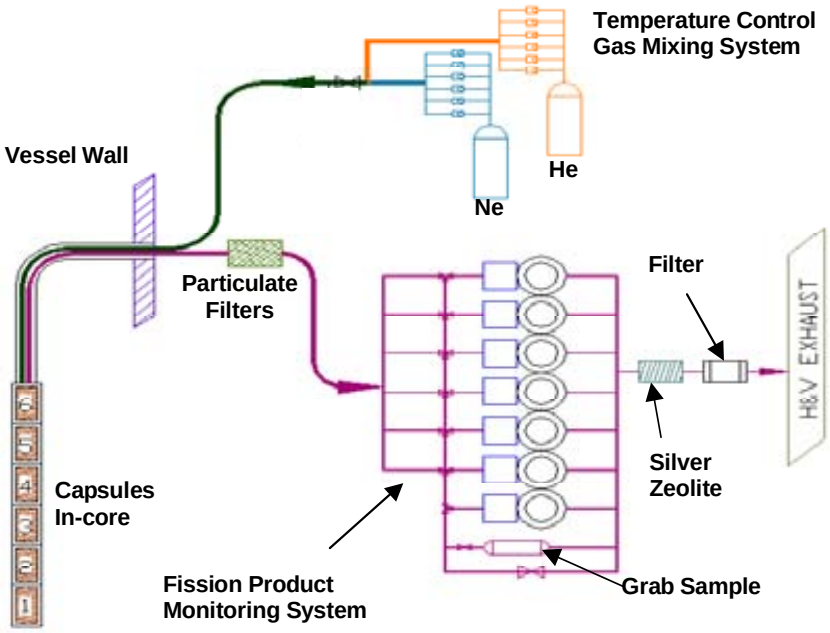

Fig. 34. Integrated Fission Product Monitoring System used in the US Advanced Gas Reactor Program irradiations [70].

Based on the on-line concentration data, we can calculate a release-to-birth ratio (R/B), a key parameter used in reactor fuel behavior studies [73], which can provide some insight into the nature of any particle failures. Examples of the ^{85m}Kr R/B data measured during the NPR-1A fuel irradiation in the INL ATR as a function of irradiation time after particle failure are shown in Fig. 35. Because these instruments are on-line during the entire irradiation, a complete time history of gas release is available. Such temporal information can provide information on the source of the fission gas. Gas release early in the irradiation (i.e., from the start of the irradiation) is indicative of initially failed particles or contamination outside of the SiC layer. Release later in the irradiation is indicative of *in-situ* particle failure. The timing of the failure data can be correlated to temperature, burnup and/or fluence, which when coupled with post-irradiation examination can be used to determine the mechanisms responsible for the fuel failure.

With the anticipated use of TRISO-coated fuel in HTGR applications, fuel irradiation testing will be needed to demonstrate its performance characteristics. Irradiation testing experience and recent advanced in test train instrumentation and control, fission product monitoring, physics and thermal analysis capabilities allows for more complex and improved capsule designs that can provide nearly real-time data that can be used to assess fuel performance. The state-of-the-art techniques mentioned here should be considered to obtain the maximum amount of information from HTGR fuel qualification testing.

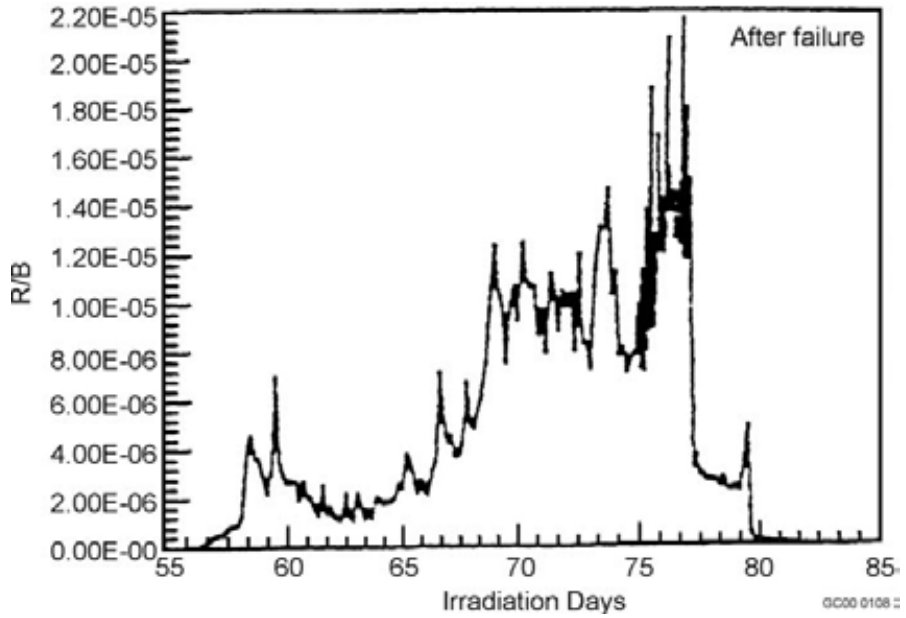

Fig. 35. Release to Birth Ratio for ^{85m}Kr after failure in the NPR-1A irradiation experiment.

8. FUEL FAILURE MECHANISMS

A review of the literature of coated particle fuel reveals a number of potential failure mechanisms under normal and off-normal conditions. In this section, these mechanisms are briefly reviewed and the variables that control them are described.

8.1. Overpressure

Under irradiation coated particle fuel is subjected to a number of forces that put stress on the TRISO coating. One of the earliest recognized mechanisms is overpressure resulting from gas generation under irradiation. During irradiation, fission gases are released from the kernel into the porous buffer layer. The pressure that is generated exerts tensile forces on the SiC layer of the particle. In addition to fission gas, in coated particle fuel with UO_2 kernels, there is excess oxygen released during fission. This excess oxygen will react with carbon from the buffer to form CO and CO_2 gas. The production of these two reactive species and also the fission gas are functions primarily of burnup and temperature. Particles are generally sized with a large enough buffer void volume to ensure that nominal particles do not fail by overpressure during irradiation. Particle failure is postulated to occur as a result of an insufficient or missing buffer layer (i.e., void volume to accommodate the gases) that occurs during the coating process. Thus, fabrication specifications limit the number of particle produced with missing buffer layers. Irradiation experiments should bound the burnup and temperature conditions found in the reactor to ensure that this potential failure mechanism is accounted for. An example of such failure for a fertile particle from a US irradiation is shown in Fig. 36.

8.2. Irradiation-induced IPyC cracking

Under irradiation, pyrocarbon (PyC) shrinks in both the radial and tangential directions. At modest fluences (~ 2 x10^{25} n/m^2) depending on the density, temperature and anisotropy of the material, it begins to swell in the radial direction. This behavior puts the PyC layers into tension in the tangential direction. However, irradiation-induced creep works to relieve the tensile stress in the PyC layer. If the PyC is strongly attached to the SiC layer, the PyC shrinkage provides a strong compressive stress that offsets the tensile stresses generated by gas production in the kernel.

The shrinkage, swelling and creep behavior of PyC materials is complex. Detailed stress calculations are used to model the evolution of stress and strain in all layers of the TRISO coating. In many US irradiation tests, including those from the DOE New Production Reactor Program in the early 1990s, the shrinkage that occurred in the PyC layers was much larger than anticipated and led to tangential stresses in the PyC high enough to cause cracking. These cracks led to stress concentrations in the SiC layer high enough to cause failure of that layer [74].

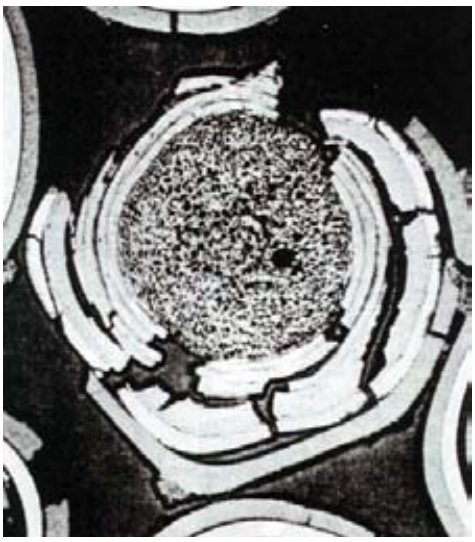

Fig. 36. Overpressure failure of fertile particle from HRB-14.

Photomicrographs of such shrinkage cracks found in the F-30 irradiation used to qualify fuel for the Fort St. Vrain Reactor and the NPR irradiations are shown in Fig. 37. The thicker the PyC layer, the larger are the stresses that develop and the greater the propensity for failure.

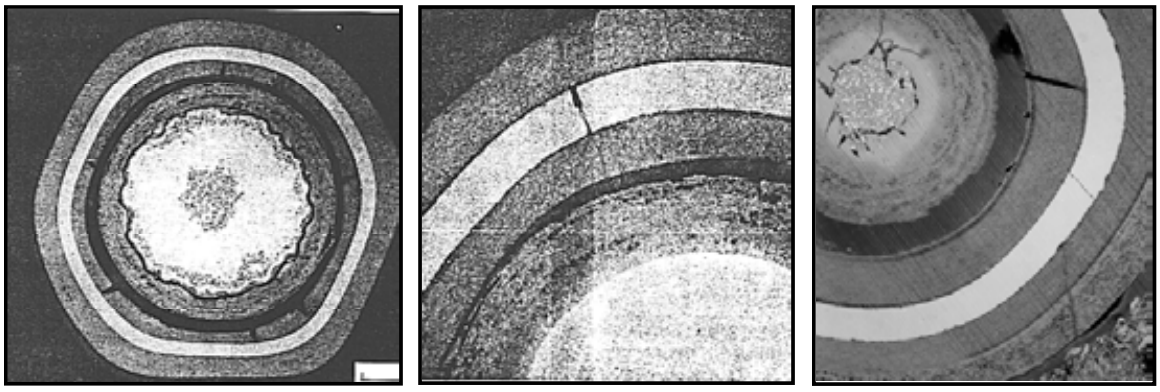

Fig. 37. Irradiation induced cracking of inner PyC in F-30 irradiation (left two photographs) and NPR irradiations.

This failure mechanism has been attributed to high anisotropy in the PyC layer because the deposition of the layer occurred at too low of a coating gas concentration in the coating reactor (corresponding to a very low coating rate) during fuel manufacture in the US. At higher coating rates, the isotropy of the PyC layer is good enough to prevent excessive irradiation induced shrinkage. German fuel is fabricated at higher coating gas concentrations (and corresponding coating rates) than US fuel. Thus, post-irradiation examination of German fuel does not exhibit shrinkage cracks in the IPyC layer as has been observed in US irradiations. This failure mechanism is not expected to be important for isotropic PyC in fuel produced using the German production methods and processing parameters.

8.3. Debonding between IPyC and SiC

In addition to irradiation-induced shrinkage, debonding at the IPyC/SiC interface has been observed in many US irradiations performed over the last 30 years. The debonding is related to the strength of the IPyC/SiC interface. Weakly bonded coating layers can partially detach because of the tensile stresses generated by the IPyC shrinkage under irradiation. A particle for which partial debonding of the IPyC from the SiC has occurred can develop relatively large tensile stresses in the SiC (although significantly smaller than in the case of a cracked IPyC). Tensile stresses occur at the point of IPyC/SiC contact as the IPyC shrinks under irradiation. Irradiation induced creep relieves the stress at longer times. When these tensile stresses are used in concert with SiC elastic properties and Weibull statistics to calculate the SiC failure probability, it is found that the SiC fails at a low, but not insignificant, rate [74]. Variations in the microstructure and surface porosity between the German and the US IPyC layers result in differences in the nature of the bond that exist between the IPyC and the SiC. Photomicrographs of the IPyC/SiC interface in German and US fuels are shown in Fig. 38. This figure shows that the interface in German fuel is more tightly bonded because SiC is deposited into the IPyC, which has apparently greater surface porosity. For historical US fuel, the less porous surface of the IPyC results in a smoother, but less strong bond. The TRISO coating of German fuel never exhibits debonding under irradiation whereas a review of the US irradiation test results indicates that the IPyC and the TRISO coating debonds quite frequently in US fuel.

8.4. Kernel migration

Kernel migration is defined simply as movement of the kernel in the coated particle toward the TRISO-coating [74], [75]. If the migration is excessive, the kernel will penetrate the TRISO-coating leading to failure of the particle. Kernel migration, also known as the "amoeba effect", is actually a misnomer. Kernel migration is associated with carbon transport in the particle in the presence of a temperature gradient. In the fuel kernel, equilibrium exists between C, UO_2, CO and CO_2. When there is a thermal gradient across the particle, the equilibrium is different on each side of the particle. The different equilibrium conditions leads to mass transport of carbon up the temperature gradient. This movement of carbon appears in photomicrographs of fuel as a movement of the kernel down the temperature gradient and hence the name kernel migration as shown in Fig. 39. This phenomenon is strongly dependent on the temperature gradient in the fuel with secondary dependence on temperature and burnup. In prismatic HTGR cores with UO_2 fuel, where particle loadings and power densities are greater, the potential for kernel migration is greater. In pebble bed HTGR cores, the power densities and hence the thermal gradients are much smaller. Kernel migration has only been observed in German irradiation test where conditions were designed to induce this mechanism. Otherwise no indication of kernel migration has occurred during AVR or THTR operation because of the low thermal gradient. In the design of irradiation experiments, it is important to limit the thermal gradient or power per particle to values that are typical of that in the reactor application to ensure that no false positives are observed. As a result, the level of burnup/power acceleration of any coated particle fuel irradiation experiment is recommended to be no greater than three times that expected in the actual reactor application.

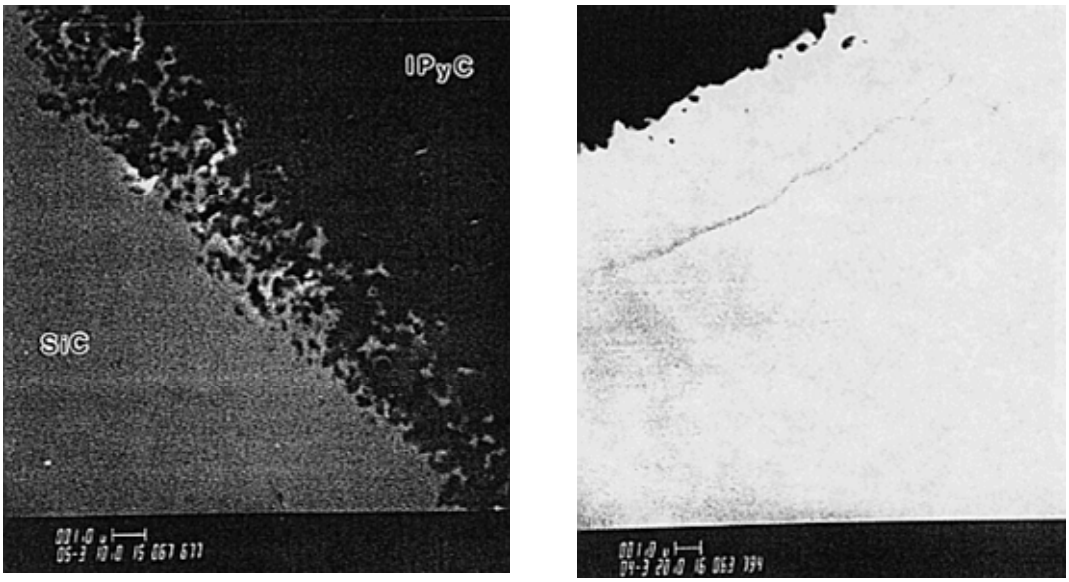

Fig. 38. Comparison of the SiC/IPyC interface in German (left) and US (right) fuel [16]. The different contrast of the two pictures is associated with lighting techniques.

8.5. Fission product attack

Past irradiation experiments indicate that fission products can be transported from the kernel to the inner surface of the SiC where they interact and can damage and potentially fail the SiC layer. In older uranium carbide kernels, rare earth fission product migration was of concern.

In LEU oxide fuel kernels (both UO_2 and UCO), palladium is very important, as are some of the other noble fission products [74]. In UCO kernels, the oxycarbide form of the kernel generally ties up all but the noble fission products (e.g., Pd) as either carbides or oxides, which tend to limit their mobility in the UCO system. However, Pd transport has still been observed in UCO coated particle fuel. In addition, the migration of silver in these particles has been observed.

Fig. 39. Photomicrograph of kernel migration.

Silver can migrate through apparently intact particles and be released into the reactor coolant system where it will deposit on cold surfaces. For direct cycle gas reactors, this cold deposition may take place in the turbine, which has important maintenance and worker dose implications. Studies have been conducted to understand the mechanism for the Ag migration through and Pd attack of the SiC. The migration of the fission products is thought to be functions of time at temperature and burnup as well as temperature gradient. Thus, these fission product attack mechanisms are expected to play a more important role in prismatic reactors where TRISO fuel particles experience higher temperatures and longer times at a given temperature than particles in a pebble bed reactor. A photomicrograph of this fission product attack is shown in Fig. 40. Also of note here is the fact that the enrichment of the fuel is important in defining the magnitude of the Ag and Pd problem. The difference in yield of Ag and Pd between U and Pu is on the order of 25 to 50. Thus, in LEU fuels where at the end of life (EOL) significant fissions comes from Pu, the concentration of Ag and Pd can be much greater than in HEU fuel of similar burnups. As in the case of kernel migration, it is important to limit the thermal gradient or power per particle in the design of irradiation experiments to values that are typical of that expected in the reactor application to ensure that no false positives are observed. As a result, the level of acceleration of any coated particle fuel irradiation is recommended to be no greater than three times real time.

Recent finite element calculations have examined the structural integrity of a coated particle with notches in the SiC layer to represent fission product attack of the SiC coating [79]. The results suggest that independent of the size or number of notches that the failure probability is quite low because so little of the SiC layer is degraded. Of course if the attack causes complete penetration of the SiC layer, the particle may still retain some structural strength; however it would be considered functionally failed since the penetration would allow fission products to easily diffuse from the inside of the particle into the fuel element matrix.

Fig. 40. Photomicrograph demonstrating fission product attack of the SiC layer.

8.6. Matrix-OPyC interactions and OPyC irradiation-induced cracking

In the early days of US coated particle fuel development, infiltration of the liquid graphitic matrix into the porosity of the outer pyrocarbon (OPyC) during manufacture and subsequent dimensional change under irradiation did cause the OPyC layer to fail by cracking and debonding from the SiC layer. In US fuel, irradiation-induced OPyC failure was also observed in many irradiations. This failure was attributed to a combination of unacceptable microporosity and anisotropy of the layer. Specifications on the matrix material and on the microstructure of the OPyC were developed in the US to limit this failure mechanism to ≤3% of all OPyC layers, a level considered acceptable based on fuel performance modeling at the time. No similar behavior was observed in German fuel because of a powdered matrix material (difficult to infiltrate into OPyC) and more a more isotropic OPyC.

8.7. Non-retentive SiC

Although not formally considered structural failure, there are situations where the SiC layer becomes functionally failed or degraded in some way and is no longer retentive of fission products. Two cases are generally considered: (a) diffusive release through intact SiC and (b) degradation of the SiC layer resulting in measurable SiC permeability.

8.7.1. Diffusive release through intact layers

Effective diffusion coefficients have been established for the noble gases and important metallic fission products in PyC and SiC based on numerous heating test data [16], [80]. These data suggest that if fuel temperatures during normal operation approach 1300°C, then some of the fission products that are usually retained by the TRISO coating (e.g., cesium) will be able to diffuse out of the particle during normal operation and could contribute to the normal and/or accident radiological source term.

8.7.2. SiC degradation resulting in permeability to fission products

There is some limited evidence that the permeability of the SiC layer to fission products under irradiation and high temperature heating can change. Spherical fuel elements exposed to

higher fluence (4 x10^{25} -6 x 10^{25} n/m^2) and higher burnup (14% FIMA) have exhibited a greater release of fission products (e.g., cesium) in heating tests than similar spheres exposed to conditions inside the German operating envelope (8-9% FIMA, 2-4 x 10^{25} n/m^2) [76]. Two different mechanisms could be responsible: cesium attack of the SiC and/or CO corrosion of the SiC.

Experiments performed by Coen [76], [77] in the 1970s demonstrate that cesium vapor can attack SiC at temperatures in excess of 1500°C. Silicon carbide samples exposed to cesium vapor indicate a pitting of the SiC layer indicative of an attack of the layer and not simple diffusion. The kinetics of the attack correlate reasonably well with the timing of cesium release from the German spheres. Unfortunately no additional experiments were performed. Carbon monoxide generated during irradiation of UO_2 kernels can attack the SiC layer if the IPyC layer is either permeable or cracked. At low partial pressures of CO, the SiC layer is converted to SiO, which is a gas at normal operating conditions [76]. It is known that German pyrocarbon is somewhat permeable and that CO can be intercalated (trapped) into graphitic structures. The higher burnup of these particles may have produced enough CO that breakthrough of the PyC layer was achieved and a small amount of CO could attack the SiC layer and cause degradation. Thus, the degradation of the SiC layer in this instance may be misinterpreted as either thermal decomposition or some other attack mechanism. The kinetics of the reaction is not known but thermodynamics predicts that such a reaction is possible. This mechanism may be very important at high burnup in UO_2 TRISO-coated particle fuels where CO production is expected to be very large given the large fraction of plutonium fissions at high burnup in LEU UO_2 and the greater oxygen release per fission from plutonium than uranium.

8.8. Creep failure of PyC

Under stress, thermal creep of the PyC will occur. In some postirradiation heating tests, photomicrographs reveal a thinning and failure of the PyC. This is primarily for tests at very high temperatures (> 2000°C) and very long times when thermal creep can operate. Such failure has not led to failure of the SiC layer.

8.9. SiC thermal decomposition

At very high temperatures (> 2000°C), thermodynamics and data from German furnace-heating tests show that the SiC layer undergoes thermal decomposition [16], [76], [78], [80], [81]. The phenomenon is primarily a function of temperature and time and has not played a major role in fuel failure at lower accident temperatures (1600-1800°C).

8.10. Kernel-coating mechanical interaction (KCMI)

At sufficiently high burn-up values, it is inevitable that all gas gaps between the kernel and coatings will close, thereby resulting in a mechanical interaction between the two (KCMI). This is because the kernel will swell inexorably during the course of the irradiation. Modelling studies predict that the SiC layer will fail shortly after the onset of KCMI. To date, this failure mechanism has not been reported experimentally. Possibly this is because even if, at the end of the irradiation, KCMI occurs, a gas gap will always be created as the particle cools to room temperature owing to the kernel's comparatively higher thermal expansion coefficient. Perhaps this fact was overlooked in some PIE investigations. But clearly this failure mechanism could be of increasing importance as attempts are made to achieve higher

burn-up values. The fission products behavious and its role in KCMI are vividly described in literature [16], [80-85].

8.11. Summary

These failure mechanisms have been observed to some extent in TRISO-coated fuel testing activities conducted around the world. A summary of the mechanisms is found in Table 8. They are in general functions of temperature, burnup, fluence and temperature gradient in the particle and details of the particle design. Based on the previous German experience, TRISO-coated fuel is usually designed such that none of the fuel failure mechanisms are expected to be significant. Fission product releases during irradiation and heatup testing will be dominated by pre-existing as-manufactured defects in the production fuel and heavy metal contamination outside of the SiC layer and initially defective particles. Strict process control and proper statistical quality control are used to limit as-manufactured defects in coated particle fuel.

Table 8. SUMMARY OF COATED-PARTICLE FAILURE MECHANISMS

Failure mechanism	Reactor service conditions	Particle design and performance parameters that affect the failure mechanism	Comments
Pressure vessel failure	Temperature Burnup Fast fluence	Strength of SiC Buffer density (void volume) Fission gas release CO production Layer thicknesses Kernel type (UO_2, UCO)	
Irradiation-induced PyC failure	Fast fluence Temperature	Dimensional change of PyC Irradiation-induced creep of PyC Anisotropy of PyC Strength of PyC PyC thickness PyC density	Can be ameliorated by proper coating conditions
IPyC partial debonding	Temperature Fast fluence	Nature of the interface Interfacial strength Dimensional change of PyC Irradiation-induced creep of PyC	Can be ameliorated by proper coating conditions
Kernel migration	Temperature Burnup Temperature gradient	Layer thicknesses Kernel type	UO_2 only. Not important for UCO. Reasonably well understood
Fission product attack	Temperature Burnup Temperature gradient Time at temperature	Fission product transport behavior Diffusion Buffer densification and cracking Chemical state/transport behavior of fission products Microstructure of PyC and SiC	Could be more important at high burnup in LEU fuels because of greater yields of palladium from plutonium fissions
Non-retentive SiC Layer: Diffusive release through intact layers	Temperature Burnup Temperature gradient Time at temperature	Chemical state/transport behavior of fission products Microstructure of SiC SiC thickness	More important at higher temperatures (> 1200*C) where existing data suggest diffusion will contribute to the source term.
Non-retentive SiC layer:	Burnup Temperature Fluence	Kernel type (UO_2, UCO)	CO is generated in particles with UO_2 kernels.

SiC Corrosion by CO	Time at temperature	IPyC performance	At elevated temperatures, CO can attack the SiC layer if the IPyC layer is porous or has failed.
SiC degradation by cesium		Microstructure of SiC Thickness of SiC	Exact mechanism is unclear but limited data suggest cesium may degrade SiC layer
PyC thermal creep	Time at temperature	Thickness of PyC and stress state of PyC	Not important in traditional accident envelope (peak temperature < 1600°C)
SiC thermal decomposition	Temperature Time at temperature	SiC thickness Microstructure of SiC	Not important in traditional accident envelope (peak temperature < 1600°C)
Kernel Coating Mechanical Interaction (KCMI)	Burnup Fast Fluence Temperature	Initial Kernel – Coating Gas Gap Buffer properties IPyC Properties Kernel Swelling Rate	Failure of SiC Layer shortly after Gas Gap closed at sufficiently high Burn-ups

9. ACCIDENT TESTING

Post-irradiation testing of irradiated fuels under accident conditions is needed to assess the quality of fuel concepts and fabrication methods. That means the evaluation of the release behaviour of fission gases (Xe, Kr) and solid fission products (Cs, Sr, Ag, etc.).

For this purpose, the so-called Cold Finger Apparatus (KÜFA) was developed in the Forschungszentrum Jülich (FZJ). Using this device, the fission product released from defect particles could be tested up to 1800°C [86-88].

An upgraded version of the KÜFA has been installed recently in the hot cells of the Institute for Transuranium Elements in Karlsruhe, Germany.

9.1. Test background

The central aspect of the safety philosophy for a High Temperature Reactor (HTR) is the retention of fission products in the fuel elements during operation and accidents. For this reason, the determination of the number of damaged particles constitutes the central objective of measuring the fission gas release in the reactor and in the extensive post-irradiation examinations under accident conditions. In modern production methodologies, the heavy metal contamination of fuel elements is kept very low. Consequently, solely the number of defective particles establishes fission gas or iodine release.

During depressurized loss of forced circulation, the temperature in the core will increase to a maximum of 1620°C in modern small HTRs. With the increase of the core temperature above normal, fission products may be released from the fuel elements into the primary circuit and, eventually, into the environment. For a realistic assessment of the fission product release, the conditions in the reactor core have to be simulated. The relevant fission products to be measured and their relevance in case of accident are given in Table 9.

Table 9. RELEVANT FISSION PRODUCTS TO BE MEASURED

Fission Product	Half life	Relevance assessment
^{131}I	8 days	Greatest significance for design and licensing
$^{137}Cs/^{134}Cs$, ^{90}Sr	30/2 years 29 years	Long term behaviour after extreme accidents and risk analysis
^{110m}Ag	253 days	Small inventory, short half-life. Important for maintenance
^{85}Kr ^{133}Xe	11 years 5 days	Particle defect indicator, conservative upper limit for iodine release

9.2. Description of the cold finger apparatus

9.2.1. General

The test requirements, arising from the necessity of evaluation of HTR-fuel elements for licensing purposes, led in the past to the development in FZJ of this highly specialised test equipment capable of coping with entire fuel elements (pebbles or compacts) as well as individual coated particles.

The basic function of this device is to heat the fuel elements up to the expected temperature in a dynamic He-atmosphere, and then to measure the fission product release. In the current up-graded version, designed for accident simulation tests of future HTRs, temperatures up to 2000°C can be reached.

The fuel element is supported by three pins in the centre of a tantalum tube placed inside the furnace; helium flows through this tube from the bottom to the top (Fig. 41)**.** The tantalum tube and the fuel element are heated by an electrical resistance heater, which likewise consists of tantalum.

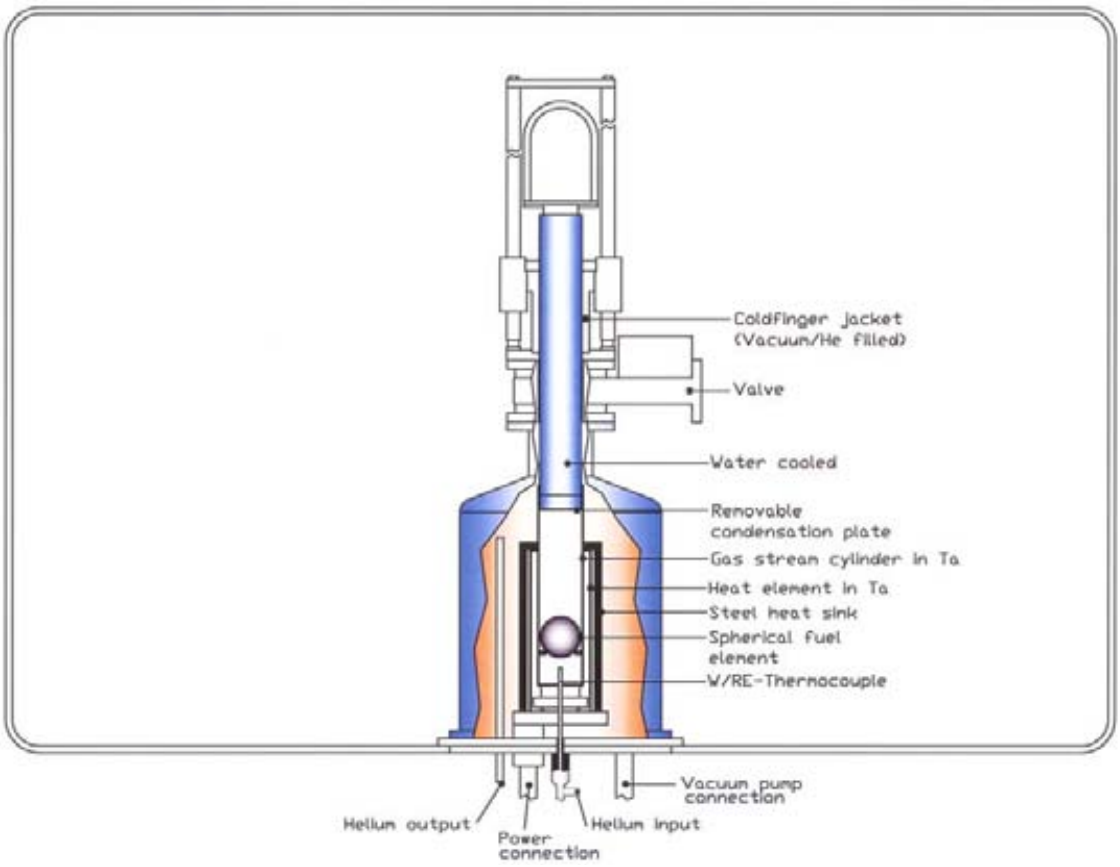

Fig. 41. Cold-finger apparatus (KÜFA).

A W/Re-thermocouple, placed near to the specimen, measures the actual temperature during the tests. This thermocouple can be replaced if needed and serves, simultaneously, for the electronic regulation of the temperature of the furnace.

9.2.2. Measurement of the fission gases release

The measurement of fission gases under accident conditions allows the detection of failed fuel elements. Through the analysis of the release curves, individual failed particles in the fuel element time can be detected as a function of temperature and heating. The two relevant radioactive isotopes ^{85}Kr and ^{133}Xe (see Table 9) are relevant for this measurement. The release of fission gases also indicates the release of other fission products, like Iodine, which is difficult to measure directly but it is known to be released to the same extent as Krypton.

The furnace is installed in an alpha-tight box in a hot cell, containing also the filters for the helium circuit (Fig. 42). Helium carries the fission gases into cold traps where ^{85}Kr and ^{133}Xe are retained. The cold traps are installed outside the hot cell, and the helium is conducted back to the hot cell and released, in a controlled manner, through the ventilation system. The released fission products are adsorbed on an active charcoal filter at liquid nitrogen temperature. The activity in the measuring trap is then determined continuously by on-line gamma-spectrometry throughout the test. In principle, only the long-lived ^{85}Kr can be detected but, provided the cooling period of the fuel elements is less than 4 to 8 weeks, measurements of ^{133}Xe are possible as well. The two cold traps are placed in a room beneath

the hot cell. The second cold trap is solely meant to ascertain that all the ^{85}Kr-activity was retained in the first. As soon as activity is detected in the second cold trap, the first is changed.

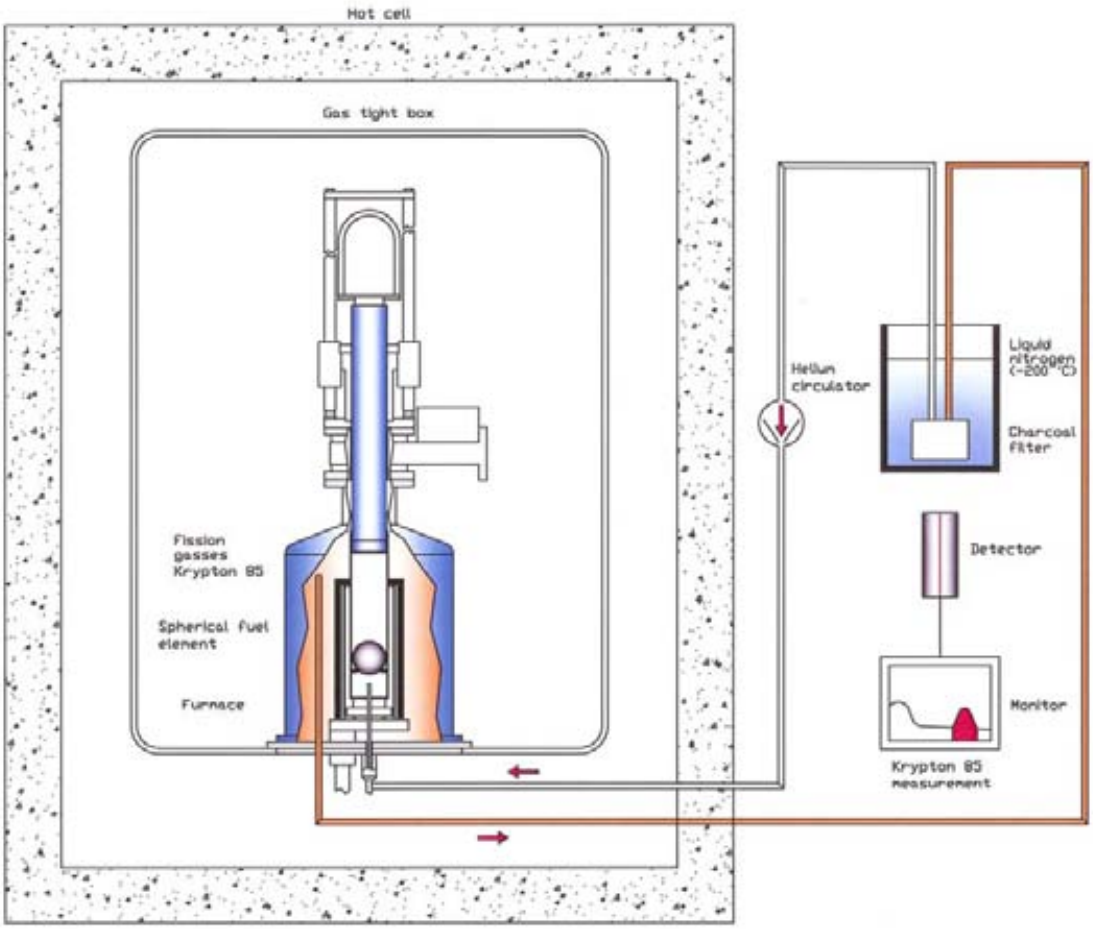

Fig. 42. Scheme of the gaseous fission products release measurement.

9.2.3. Solid fission products release

The determination of solid fission products is slightly more difficult than that of the chemically inert fission gases. At high temperatures they can get into the coolant gas by migration/diffusion and subsequent gaseous desorption, first, from the surface of the coated particles and, afterwards, from the surface of the fuel. On the other hand, such fission products are re-deposited by adsorption on cooler surfaces, and this deposition mechanism is exploited for trapping solid fission products in the cold finger test rig.

To detect the release of solid fission products, a water-cooled cold finger protrudes into the hot tantalum tube, at the end of which an easily replaceable condensation plate is held. The solid fission products released from the fuel element are deposited on this plate which has a temperature of less than 100°C, typically 40 to 80°C depending on the testing temperature. This temperature has to be compared to the specimen temperature, which is in the range of 1600-2000°C.

During the test, the cold finger can be removed from the furnace through an air-lock system (Fig. 43) without needing to cool-down the specimen. In fact, the Helium circulation is

maintained during the plate-changes, which assures the continuous monitoring of the specimen and the detection any coated particle failure.

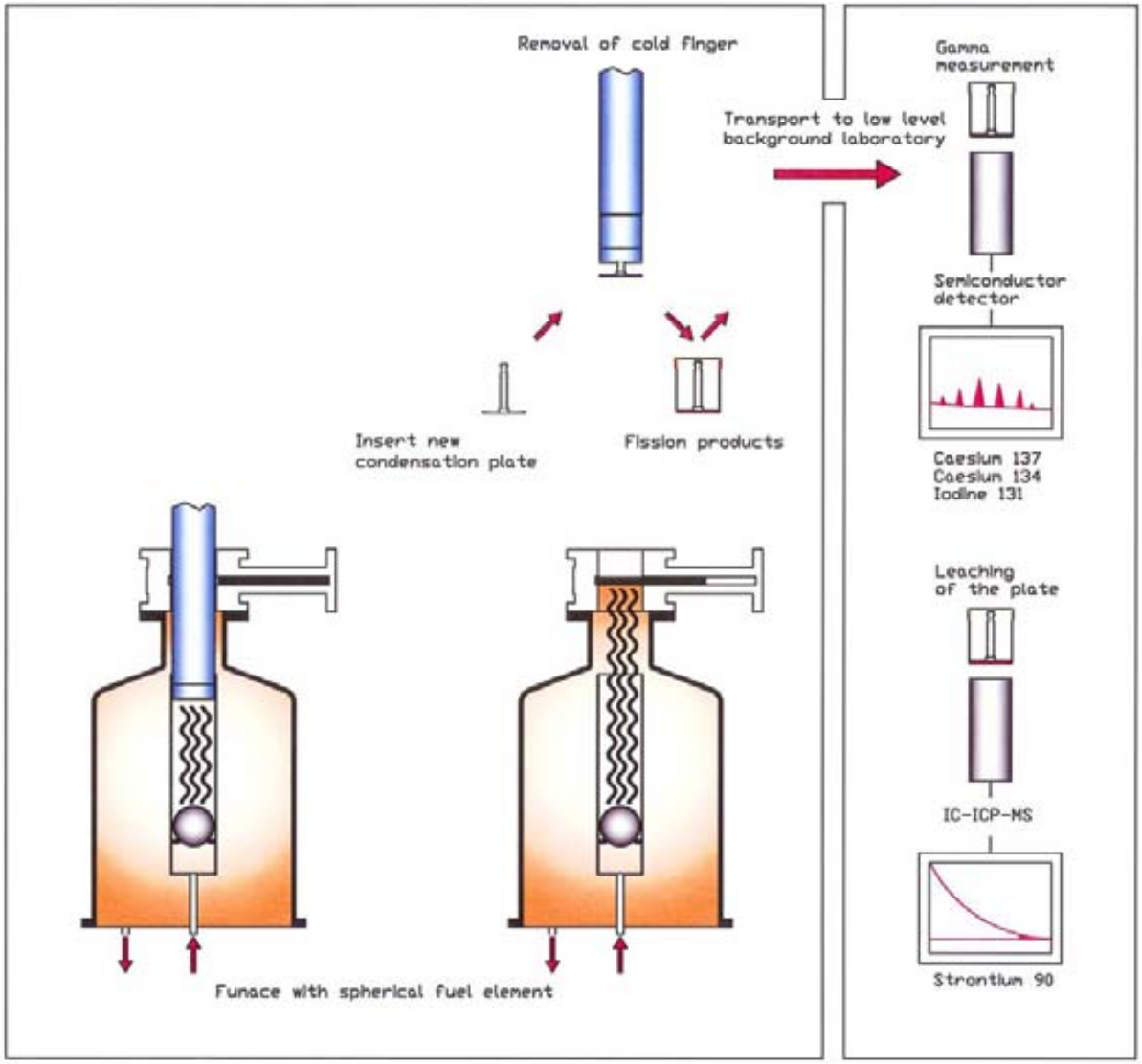

Fig. 43. Scheme of the solid fission products measurement.

After replacing the condensation plate, the cold finger is returned back to its position into the furnace. The plate is normally changed once or twice a day but, if necessary, this operation can be performed more frequently. The changing procedure lasts only few minutes and needs relatively easy manipulation.

The used plates are taken out of the hot cell to be measured by gamma- spectrometry in a low background laboratory to be measured. Measurement of gamma emitters such as ^{137}Cs, ^{134}Cs and ^{131}I is relatively simple, because their individual energy lines can identify them. Strontium 90, a beta emitter nuclide, has to be separated chemically from other fission products for measurement. Since strontium emits beta rays with the highest energy, the activity can also be estimated using a scintillation counter after a special calibration.

This procedure is relatively complicated and did not lead in the past to satisfactory results [88]. Alternatively, the plates can be leached in nitric acid and the resulting solution later analyzed using an Induced Couple Plasma Mass Spectrometer (ICP-MS).

According to the experience gathered in the FZJ, use of the Cold Finger Test Rig allows very low fractional releases, down to 10^{-8}, to be measured [88].

9.2.4. Typical tests

In Fig. 44, a typical heating curve is shown. The highest temperatures in the reactor core occur in depressurisation events with loss of all cooling systems. Depending on reactor design, this temperature can be as high as 1800°C.

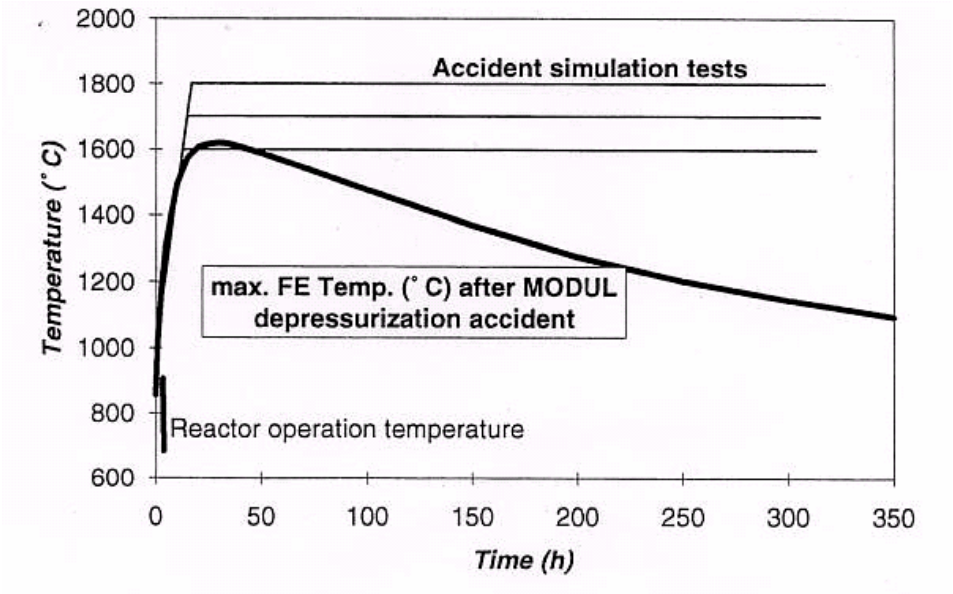

Fig. 44. Temperature evolution during a loss-of-coolant accident in a small HTR and in the heating tests.

9.3. Fission product release in accidents

9.3.1. Bare fuel release

Little fission product retention can be expected in exposed UO_2 fuel kernels at elevated temperatures. Fig. 45 shows that the release of silver, xenon, iodine and cesium quickly approaches 100% during a 1600°C heating test. Beginning in the 30 hours heatup phase to the test temperature, significant release already begins to occur for ^{131}I, ^{133}Xe and ^{137}Cs. After 50 to 100 hours at 1600°C nearly all of the inventories of these fission products have been released from the exposed UO_2 fuel kernels. Only the fission product ^{90}Sr is strongly retained within the oxide kernels at this temperature (but this is not the case for carbide kernels). The primary barrier to the volatile fission products such as iodine, xenon and cesium is by the coating layers on TRISO coated particles, especially the SiC layer.

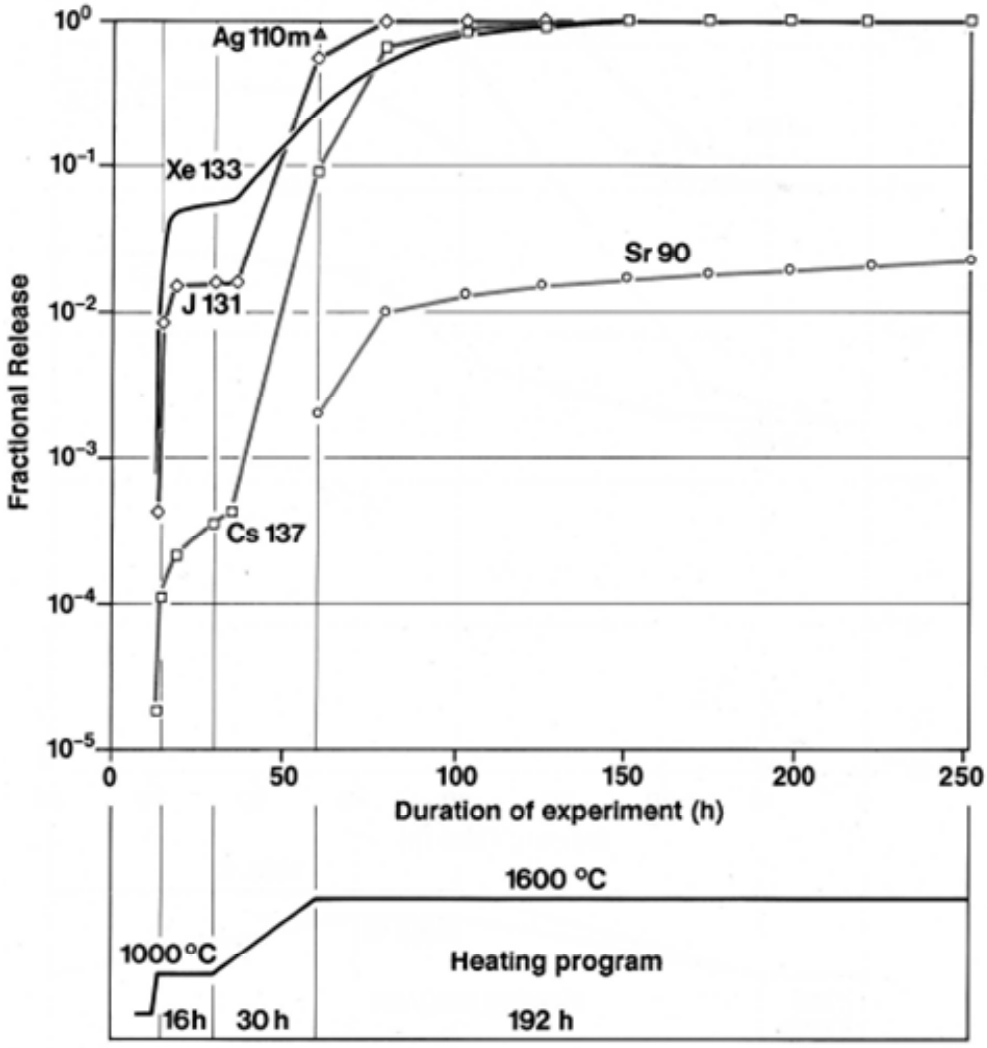

Fig. 45. Fission product release from exposed UO_2 kernels during heating test at 1600°C [87].

Measurement of ^{131}I ($T_{1/2}$= 8.02 d) release from various fuel configurations during heating at, Figure 46, shows three different release behaviors:

(i) exposed UO_2 fuel kernels with ~100% ^{131}I release,

(ii) irradiated fuel elements with TRISO-coated fuel particles that were contaminated in the AVR by old failed fuel from the 1960s and 1970s; ^{131}I release behavior is at 10^{-5} level, and

(iii) fuel elements with modern TRISO-coated fuel particles; ^{131}I release behavior is at the 10^{-9} to 10^{-8} level.

The experimental results represent iodine release from a UO_2 pellet, from contaminated HTR fuel and from modern HTR fuel.

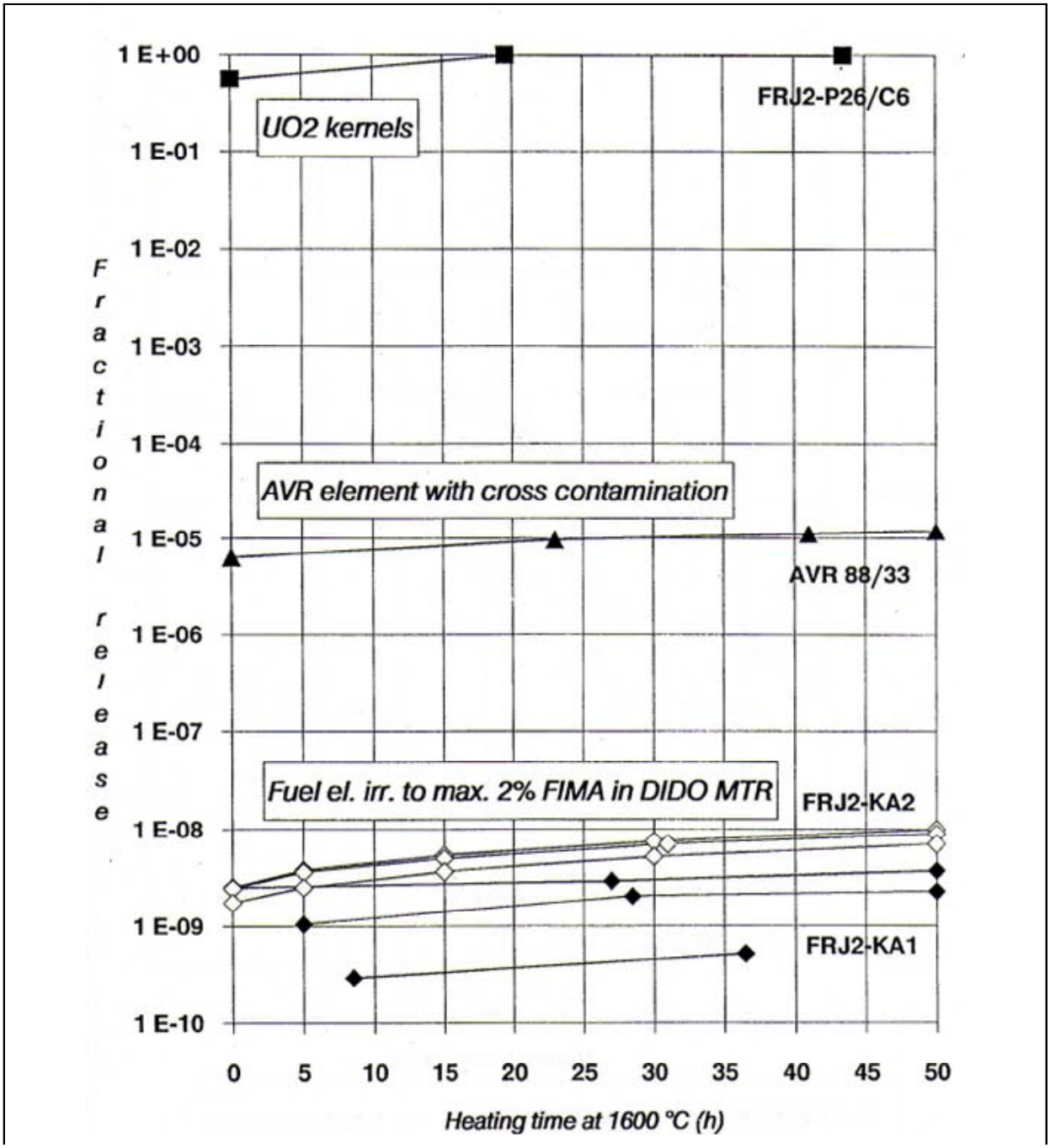

Fig. 46. Iodine (^{131}I) release from various fuel configurations during 1600°C heating tests (Schenk 1991a) shows three classes:

(i) exposed fuel with near 100% release;
(ii) contaminated in the AVR fuel;
(iii) modern clean TRISO fuel.

9.3.2. Release from irradiated spherical fuel elements

In the period 1985 to 1994, a number accident simulation tests in the range of 1600° to 1800°C were carried out in the KÜFA facility [86-88].

Eighteen of these tests — four on irradiated fuel elements from accelerated irradiation tests (HFR-K3 and FRJ2-K13) and 14 on GLE-3 fuel elements irradiated in the AVR — are listed in Table 10. This table identifies the fuel elements tested, their irradiation history, accident temperature simulation and duration, and the fission product results of the accident simulation testing. All of the fuel elements identified here contained modern LEU UO_2 TRISO-coated fuel particles. Figures 47 and 48 show the results of the KÜFA heating tests obtained at the Forschungszentrum Jülich (FZJ). No single particle failure, nor any noticeable cesium or strontium releases, were observed during the first few hundred hours in any of the 1600°C heating tests. The number of particle failures and fission product release do increase as the accident simulation temperatures rises to 1700° and 1800°C.

Table 10. RESULTS OF 1600-1800°C ACCIDENT SIMULATION TESTS WITH IRRADIATED FUEL ELEMENTS CONTAINING LEU UO_2 TRISO PARTICLE FUEL BY KÜFA TESTS PERFORMED AT THE FORSCHUNGSZENTRUM JÜLICH, GERMANY [86-88]

Fuel Element	Burnup %FIMA	Fast Fluence $10^{25}m^{-2}$ E>16fJ	Heating test		Number of failed particles **		Fractional release				
			Temp (°C)	Time (h)	manuf.	heating	^{85}Kr	^{90}Sr	^{110m}Ag	^{134}Cs	^{137}Cs
AVR 71/22	3.5	0.9	1600	500	no	no	4.0E-7	5.3E-6	9.0E-4	6.9E-5	2.0E-5
HFR-K3/1	7.7	3.9	1600	500	no	no	1.8E-6	1.8E-7	2.7E-2	1.3E-4	1.1E-4
FRJ2-K13/2	8.0	0.1	1600	160	no	no	6.4E-7	3.3E-7	2.8E-3	1.0E-4	3.9E-5
AVR 82/20	8.6	2.4	1600	100	no	no	1.5E-7	3.8E-6	4.4E-3	1.2E-4	6.2E-5
AVR 82/9	8.9	2.5	1600	500	no	no	5.3E-7	8.3E-5	1.9E-2	5.9E-4	7.6E-4
AVR 89/13	9.1	2.6	1620 *	~10	no	no	2.0E-7	***	8.3E-4	1.3E-5	1.1E-5
			1620 *	~10		no	1.3E-9	***	1.5E-2	1.6E-6	1.4E-6
AVR 85/18	9.2	2.6	1620 *	~10	no	no	1.4E-7	***	6.5E-3	1.0E-5	1.3E-5
AVR 90/5	9.2	2.7	1620 *	~10	no	no	1.9E-7	***	1.1E-3	7.7E-6	9.0E-6
			1620 *	~10		no	6.6E-9	***	9.0E-4	3.5E-6	3.3E-6
AVR 90/2	9.3	2.7	1620 *	~10	1	2	1.0E-4	***	3.7E-2	5.0E-5	4.6E-5
AVR 90/20	9.8	2.9	1620 *	~10	2	3	2.4E-4	***	7.6E-2	5.6E-6	6.5E-6
AVR 91/31	9.0	2.6	1700 *	~10	2	18	1.2E-3	***	6.2E-1	3.7E-3	2.4E-3
AVR 74/11	6.2	1.6	1700	185	1	no	3.0E-5	8.3E-5	3.2E-2	8.4E-5	7.6E-5
FRJ2-K13/4	7.6	0.1	1600	138	no	no	3.0E-7	2.0E-8	4.5E-4	5.7E-6	2.5E-6
			1800	100		2	7.2E-5	1.4E-3	5.3E-1	9.7E-3	9.9E-3
AVR 88/33	8.5	2.3	1600	50	no	no	1.0E-7	8.4E-6	1.2E-3	1.1E-4	1.2E-4
			1800	20		~4	1.8E-4	2.3E-4	2.1E-1	4.4E-4	4.6E-4
AVR 88/15	8.7	2.4	1600	50		no	6.3E-8	***	9.1E-3	8.8E-6	1.2E-5
			1800	50	1	~6	2.9E-4	1.1E-2	8.1E-1	1.3E-2	1.4E-2
AVR 70/33	1.6	0.4	1800	175	no	28	1.7E-3	***	***	***	2.2E-2
AVR 74/10	5.5	1.4	1800	90	no	30	81.2E-3	***	***	8.5E-2	7.9E-2
AVR 76/18	7.1	1.9	1800	200	no	~3	1.2E-4	6.6E-2	6.2E-1	5.3E-2	4.5E-2
AVR 88/41	7.6	2.0	1800	24	no	no	2.4E-7	1.2E-4	7.7E-2	1.4E-4	1.5E-4

HFR-K3/3	10.2	6.0	1800	100	no	~12	6.5E-4	1.5E-3	6.7E-1	6.4E-2	5.9E-2

* simulating calculated core heatup curve ** out of 16 400 particles *** not measured

Figures 47-48 show the measured time-dependent krypton and cesium release profiles during isothermal heating tests at 1600° to 2100°C. As representatives for a whole series of fission products, there is full retention at 1600°C for the accident specific first hundred hours or more (with ^{110m}Ag being an exception). In particular:

- cesium is retained at 1600°C in kernel, by SiC and by the A3 matrix of the fuel element with SiC providing for the strongest retention. This retention, however, can only be guaranteed by modern high quality TRISO coatings. At 1800°C, there is no delay by the kernel and the matrix, but SiC also becomes more permeable to most fission products;
- krypton is always released later than cesium, because of the additional retention by dense, intact pyrocarbon layers;
- strontium is retained much better in oxide kernels and the sphere matrix than cesium. Therefore, strontium release comes generally later than cesium, although its retention by SiC might not be as good; and
- even in high quality SiC of modern TRISO coatings, silver is already released at irradiation temperatures above 1100°C and release fractions are approaching 100% in the accident condition heating tests.

More recently, KÜFA tests with irradiated LEU UO_2 TRISO spherical fuel elements have been performed at the Joint Research Center of the EU commission, at the Institute of Transuranium (ITU) in Karlsruhe, Germany. These tests are still under evaluation, but results show clearly that there was no single particle failure in all seven heating tests (Table 11 below).

Table 11. RESULTS OF ACCIDENT SIMULATION TESTS WITH IRRADIATED FUEL ELEMENTS CONTAINING LEU UO_2 TRISO BY KÜFA TESTS PERFORMED AT THE INSTITUTE OF TRANSURANIUM

Fuel Element	N= number of particles per spherical fuel element	Heating test temperature (°C)	n= Number of failed particles
AVR 73/21	16400	1600	0
AVR 74/18	16400	1600	0
HFR-K6/2	14580	1600	0
HFR-K6/3	14580	1600	0
HFR-EU1bis/1	9560	1600	0
HFR-EU1bis/3	9560	1600	0
HFR-EU1bis/4	9560	1720	0

A careful analysis of the released of krypton, strontium, silver and cesium allows the quantitative determination of the contribution from particle defects from manufacture and from particle failure induced during irradiation or during heating (Tables 11 and 12). With the statistical analysis of particle failure, it can be shown that the failure fraction during unrestricted core heatup does not exceed significantly the very low levels that exist from the defects in manufacture and the failures during irradiation.

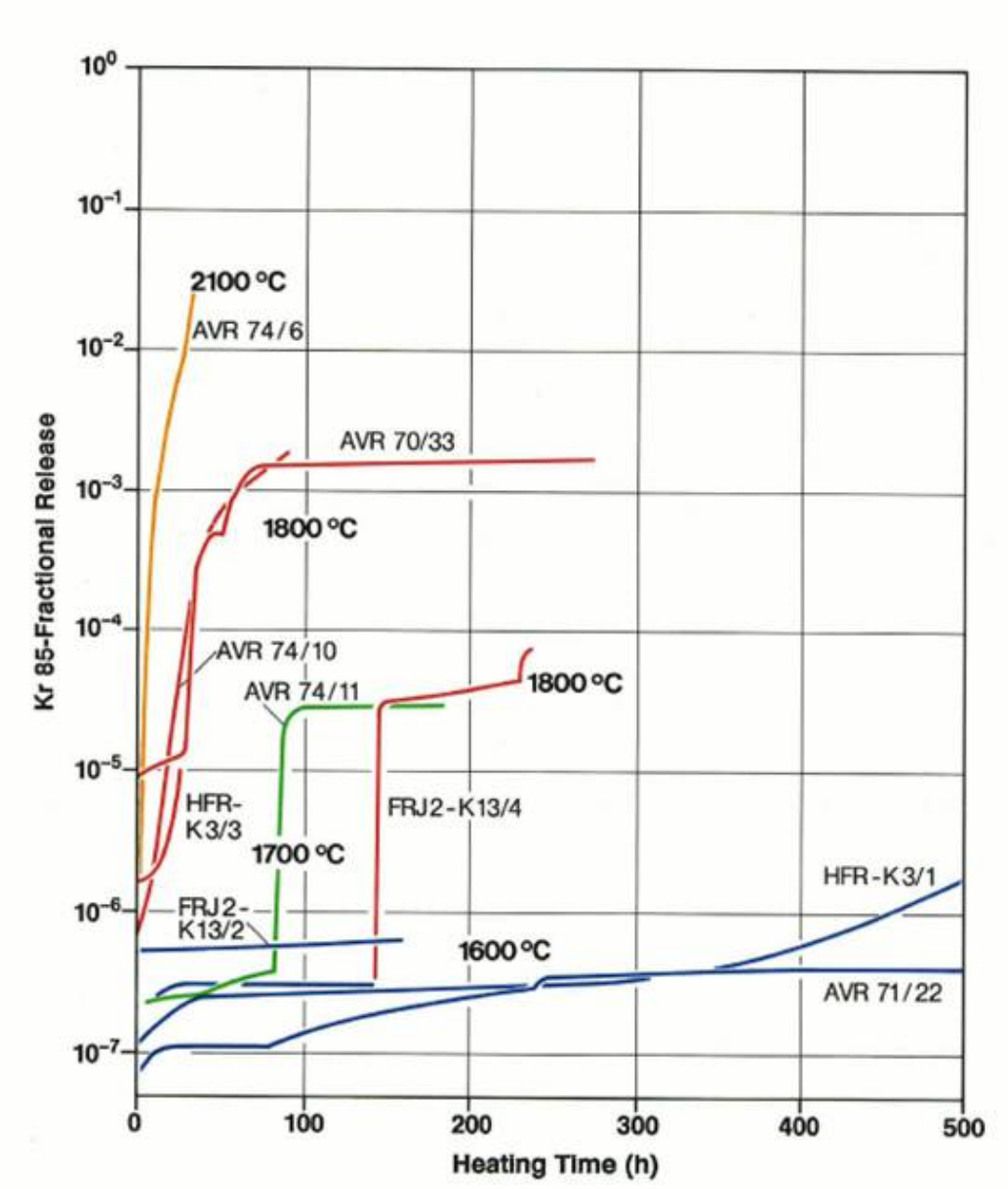

Fig. 47. Krypton release during heating tests with irradiated LEU UO_2 TRISO spherical fuel elements at 1600° to 2100°C [87]: ^{85}Kr release indicates zero particle failures at 1600°C and one single particle failure in the 1700°C test.

Table 12. FAILURE FRACTIONS OBSERVED IN ACCIDENT CONDITION HEATING TESTS AT 1600°C AND UP TO 1620°C. DERIVATION OF EXPECTED FAILURE LEVELS AND THE ONE-SIDED UPPER 95% CONFIDENCE LIMIT

	N= total number of particles	n= number defects/ failures	Expected failure level =n/N	One-sided upper 95% limit of failure level
Isothermal heating tests at 1600°C with various LEU UO_2 LTI TRISO fuel elements	221,840	0	0	1.35E-05
Accident tests simulating MODUL core heatup to 1620°C with 5 AVR GLE-3 fuel elements	82,000	5	6.10E-05	1.28E-04
All heating test results below 1700°C	303,840	5	1.65E-05	3.46E-05

If the maximum burnup is kept strictly below 11% FIMA as is typical for present HTR designs, the allowable fuel temperature limit may be higher than 1600°C and has to be established with new experiments. If UO_2 TRISO-coated particle fuel is irradiated to burnups of 15% FIMA, the fuel temperature must be rigorously limited to ≤1600°C (Fig. 49).

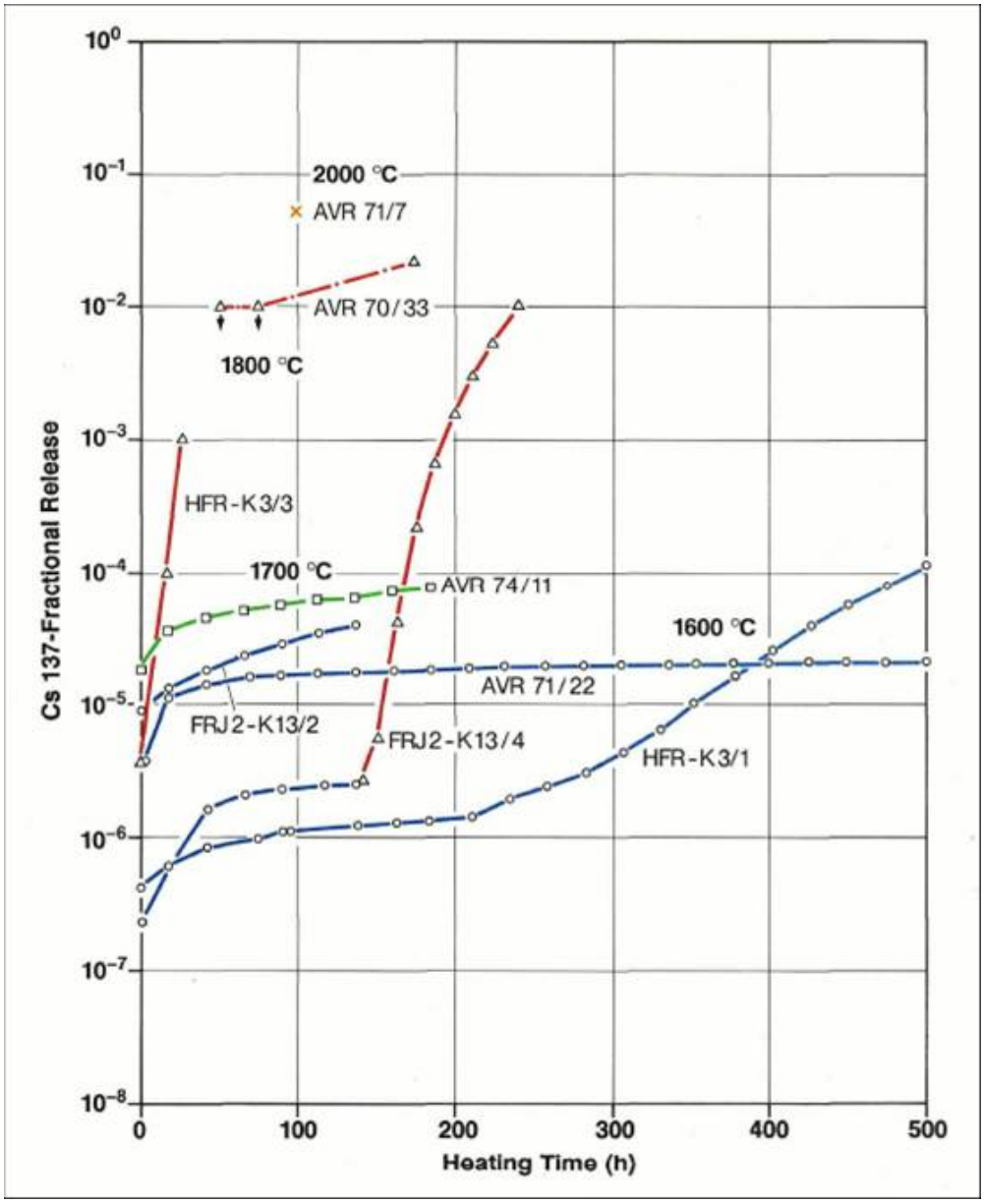

Fig. 48. Cesium release during accident simulation tests with irradiated LEU UO_2 TRISO spherical fuel elements at 1600 to 2000°C [87].

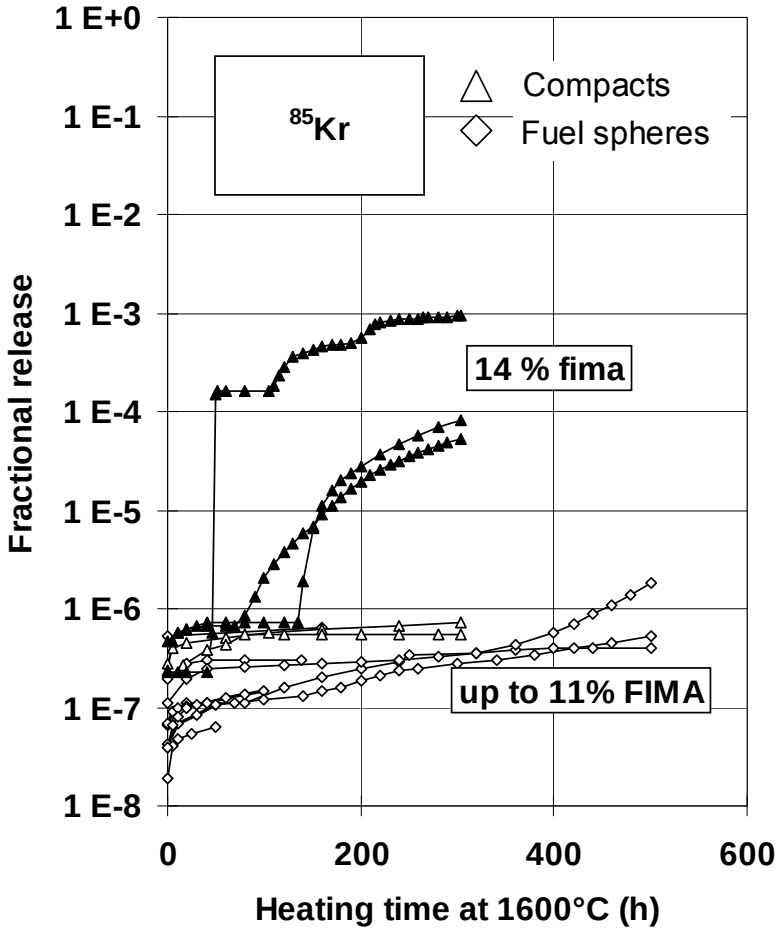

Fig. 49. ^{85}Kr release at 1600°C from compacts with 11 to 14% FIMA burnup in comparison to spherical fuel elements with 3.5 to 9% FIMA burnup.

10. FUEL CHEMISTRY

10.1. Introduction

The wide-ranging phenomena occurring during irradiation of oxide fuels has been more or less understood for a long time [89]. This knowledge can be applied qualitatively to the oxide fuel kernels of the HTGR LEU TRISO coated particles. Fission process in uranium atoms produces a great variety of fission products, radiation, as well as neutrons. The fission products can themselves be radioactively unstable leading to additional nuclides. Another important consequence of UO_2 fission is the creation of free oxygen since only a part of the O_2 recombines with the fission products. In the TRISO particle, an important parameter is that portion of this free oxygen which combines with carbon from the PyC coatings to form CO and CO_2 gases. Identification of those compounds (solid and gaseous) that can form in fuel during normal and off-normal conditions and which elements remain in elemental form, is known as fuel chemistry. This chemistry may lead to many important mechanisms affecting fuel performance, e.g., kernel size (swelling), kernel migration (amoeba effect), stresses in the

coatings (particle pressurization due to fission products and carbon oxide gases), thermal conductivity, creep properties modification, etc.

The oxygen potential, the pressure of oxygen in the gas phase within the fuel, is the critical parameter determining which elements in their competition for oxygen form oxides. Calculation of the oxygen potential is complex since it generally varies with distance from the particle center and with temperature, fuel burnup, fission product yields, chemical state of fission products including solid and gas phases and the effectiveness of the coating layers (notably the buffer) to absorb fission products and oxygen. Furthermore, in comparison with Light-Water Reactor (LWR) fuels, four parameters influencing the oxygen potential and fuel physical-chemistry are significantly different: the higher temperature prevailing in the kernel under normal conditions (between 1273 and 1473 K compared to around 773-1273 K for LWRs), higher enrichment, higher fission rate and higher final burnup (10 to 15 at% compared to about 5 at%). In addition, the fuel temperature in HTGRs is, for the vast majority of particles, fairly uniform, whereas in LWR fuel pellets a significant radial temperature gradient exist. Furthermore, the TRISO particle induces specific thermo-mechanical kernel behavior which in turn can modify fission product behavior (e.g., the local stresses may play a determining role).

In this Chapter, the relevant phenomenology focusing on the different aspects that affect the oxygen potential are summarized along with illustration of existing models used for evaluation. The complexity of the chemical system leads to a need to first consider unirradiated oxide fuel and then to highlight modifications due to formation and inclusion of fission products in the fuel-coating system.

10.2. Unirradiated fuel

The unirradiated fuel particle comprises a UO_2 fuel kernel, the porous-carbon coating, the IPyC layer, the silicon carbide coating and the OPyC layer. A detailed description of this chemical system was given in [90] and is summarized therein. At the nominal temperature of an HTGR, one can assume (in an initial approach) that the fuel within the coated particle reaches thermodynamic equilibrium with its surrounding coatings. The main product of the reaction between UO_{2+x} ($x>0$) and carbon is gaseous carbon monoxide, CO, by the following reactions:

$$UO_{2+x} \rightarrow UO_{2+y} + \tfrac{1}{2}(x-y)\,O_2 \qquad (10\text{-}1)$$

$$\tfrac{1}{2}(x-y)\,O_2 + (x-y)\,C \rightarrow (x-y)\,CO \qquad (10\text{-}2)$$

i.e., by the equation:

$$UO_{2+x} + (x-y)\,C \rightarrow UO_{2+y} + (x-y)\,CO. \qquad (10\text{-}3)$$

If reaction (2) has equilibrium constant K_p, one may write:

$$\text{Log } P(CO) = \text{Log } K_p + \tfrac{1}{2}\,\text{Log } P(O_2) \qquad (10\text{-}4)$$

where, K_p, is the oxidation constant of carbon up to carbon monoxide (which can be found, e.g., in [91]) and P_{CO} the pressure of CO gas (in atm.) and $P(O_2)$ the oxygen partial pressure (in atm.) linked with the oxygen potential, $\mu(O_2)$ (in J/mol). The oxygen potential is represented by the following relationship:

$$\mu(O_2) = RT \text{ Log } P(O_2) \qquad (10\text{-}5)$$

where, R is the Universal Gas Constant and T the absolute temperature (K). Stoichiometric UO_2 has an oxygen potential of roughly -400 kJ/mol at nominal HTGR operating temperatures.

Figure 50 shows U-O-C phase diagram at 1573K from [92].

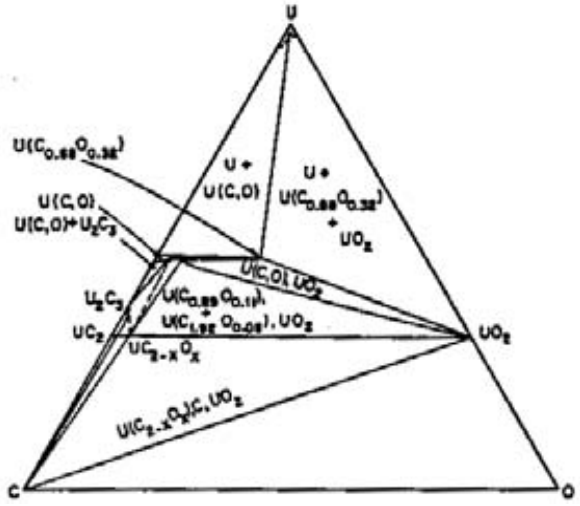

Fig.50. U-O-C phase diagram at 1573K.

According to the U-O-C phase diagram at 1573 K (Fig. 50) [92], if O/U>2 with an excess of carbon (which typically corresponds to the chemical system with the fuel kernel surrounding by the carbon buffer), there are only two condensed phases ($UO_{2+x}$and C). In this biphasic domain, the pressure of CO gas not only depends on temperature but also on the O/U ratio in UO_{2+x}, in other words on the oxygen potential variations in the $UO_{2\pm x}$ phase (a review of the $\mu(O_2)$ variations is available in [93], [94]).

Thermodynamic calculations (Fig. 51) shows that, at 1573 K, CO pressure dominates over the entire interval of oxygen potentials between –700 and –300 kJ/mol. At lower temperature CO_2 may dominate.

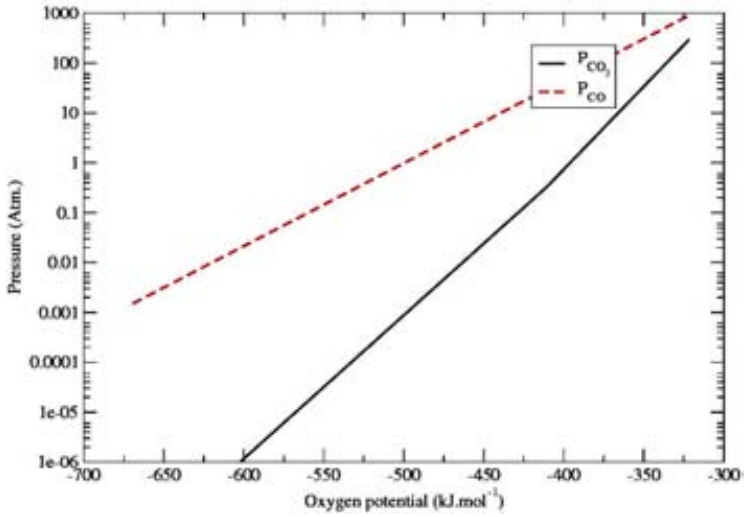

Fig. 51. Calculated thermodynamic pressures of CO, CO_2 as a function of oxygen potential for UO_2 kernel and a buffer volume fixed at 3.10^{-11} m^3 at 1573 K using the MEPHISTA thermodynamic database [95].

The result of CO (and CO_2) formation is internal pressurization of the particle coatings which may lead, in extreme conditions, to particle failure. To limit this pressurization other fuel-kernel concepts have been and are being studied. Of particular interest is the oxycarbide fuel (or UCO) comprising a mixture of UC_2 and UO_2 [116]. Gas formation is effectively reduced within the UCO particle as compared to a UO_2 particle due primarily to their lower oxygen inventory as well as to the gettering effect the UC_2 has on the oxygen released during UO_2 fission to form condensed oxide rather than CO gas. The presence of both oxide and carbide phases in the kernel allows chemical "buffering" of the oxygen potential and hence the CO pressure. The calculated oxygen potential along the composition line UC_2-O at 1573 K in the U-O-C phase diagram is represented in Fig. 52. It shows that the oxygen potential [$\mu(O_2)$] is effectively reduced to –700 kJ/mol in the triphasic domain UC_2-UO_2+C in comparison to the biphasic domain UO_{2+x}+C.

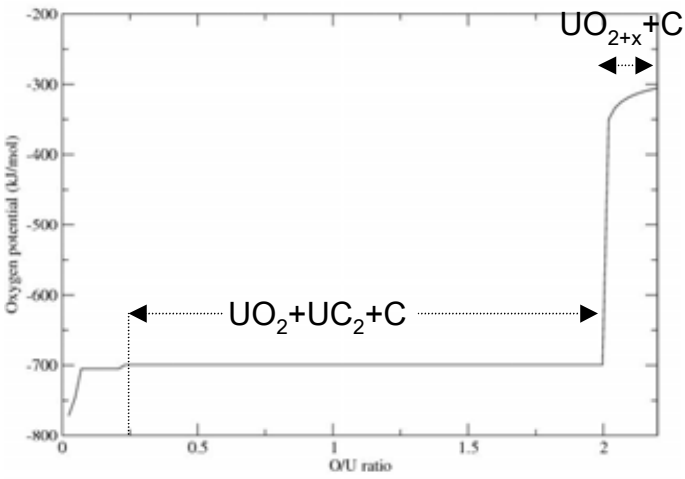

Fig. 52. Calculated oxygen potential as a function of O/U (along the composition line UC_2-O in the U-O-C phase diagram) at 1 573 K using the thermodynamic MEPHISTA database [95].

10.3. Irradiated fuel

10.3.1. Particle composition and fission product behavior

Element and isotope inventories for irradiated high burnup HTGR fuel are as well-known as they are for low burnup LWR fuel. The rate of change of each nuclide is a function of three processes:

- depletion of heavy nuclei by fission and corresponding production of lighter nuclei (fission products);
- production by radioactive decay (actinides and fission products) and/or by neutron capture (actinides); and
- loss by radioactive decay (actinides and fission products) and/or by neutron capture (actinides).

Nuclide production and inventory variations during irradiation are described by the Bateman equation which is, in fact, a coupled set of rate equations (one for each nuclide) as a function of neutron flux. To calculate HTGR core isotope inventories it is usual to apply general computer codes developed for depletion/decay in nuclear fuels such as ORIGEN2 [101] with an appropriate library of cross-sections for HTGR conditions; indeed, this depletion/decay code may be used, e.g., in a core analysis via the MONTEBURNS coupled neutronic/isotopic Monte Carlo code system [102]. For fuel chemistry, the isotopic details are of no interest since it is the relative quantities of each element that are really important. An element inventory for an irradiated HTGR particle is illustrated in Table 13 below.

Location of fission products in UO_2 fuel

Fission products exist in the fuel lattice as atoms and ions. Their location depends mainly on the fuel stoichiometry. Atomic-scale calculations performed for LWR fuel show Xe incorporated in uranium vacancies in UO_{2+x} (or divacancy in stoichiometric UO_2) [117]. The same is foreseen for Cs, Ba, Sr, Zr and the rare earths (Sm, La, Nd, Pr, Ce, Y). Molybdenum

might also be incorporated in uranium vacancies [118], [119] with Mo ionization varying with O/M ratio. Iodine, Br and Te are also found most stable in uranium vacancies in possibly different charge states including cationic ones.

Table 13. ELEMENTAL INVENTORY IN AN HTGR FUEL PARTICLE AT 5.5% FIMA (FROM [103])

Element	Amount (10^{-8} moles)	Element	Amount (10^{-8} moles)
UO_2	411	Zr	6.49
C	755	Ru	3.63
Kr	0.74	Ba	1.57
Xe	5.32	La	1.46
Sr	1.78	Ag	0.13
Se	0.12	Br	0.04
Rb	0.70	Y	0.91
Mo	5.74	Tc	1.47
Rh	1.03	Pd	1.08
Cd	0.06	Sn	0.06
Sb	0.03	Te	0.57
I	0.29	Cs	4.79
Ce	2.75	Pr	1.35
Nd	4.62	Sm	0.52
Eu	0.07	Gd	0.02

Solubility of fission products in UO_2 fuel

From atomic-scale calculations, it is also possible to derive estimates of fission product solubilities in irradiated UO_2 to be compared to the values obtained from experiments [120]. It is well acknowledged that noble gases exhibit almost total insolubility. Iodine, Br and Te are also highly insoluble whereas Cs and Ba exhibit only low solubility in the case of hyperstoichiometric fuel. Then the solubility increases from Zr (depending on temperature) to Sr, reaching very high solubilities for the rare earth elements, namely Ce, which is extremely soluble.

Behavior of gaseous fission products (Xe and Kr) in UO_2 fuel

Fission products in the fuel lattice can diffuse out of the UO_{2+x} to grain boundaries. The diffusion mechanism depends on the nature of the fission product trap sites and on the fission product intrinsic characteristics (size and charge, see [121]). Irradiation effects can greatly enhance or reduce this diffusion by trapping mechanisms on extended defects (dislocations, for example).

The behavior of fission-gases is unique because of their very low solubility and high volatility. The gases precipitate primarily as intragranular bubbles. These bubbles can grow by gas-atom and vacancy absorption [122]. Generally speaking, bubble mobility is limited (defects and impurities created by irradiation limit bubble diffusivity) [123]; nevertheless, because of high fuel temperatures, some bubble coalescence can not be excluded. Additional mechanisms for bubble growth are associated with interactions with dislocations, essentially at high burnup, that can induce high local stresses increasing bubble diffusivity, bubble trapping [124] and the possibility of bubble growth by dislocation-loop punching (mainly during transients) [125]. The thermodynamic state in the bubbles depends greatly on the

interaction with defects, mainly vacancies. Bubble relaxation is a function of the local vacancy concentration, and in the case of limited vacancy concentration, highly-over-pressurized bubbles can be observed [124]. For the UO_2 kernel in TRISO fuel particles, both fission-rate and temperature help to strongly limit bubble size and maintain a substantial fission-gas atom population in the fuel lattice by re-solution of gas from bubbles. Fission gases can migrate to grain boundaries by atomic or bubble diffusion to form intergranular bubbles (porosities) where they can grow by addition of gas and vacancies (thermally produced at grain boundaries) [126]. Like intragranular bubbles, high levels of irradiation-induced re-solution significantly limits this growth (and bubble-induced swelling of the kernel) while stresses in the particle may also limit the equilibrium bubble size. Once intergranular-bubble growth becomes significant causing interconnection of porosity, a path from within the kernel to the buffer is created leading to fission-gas release by a percolation mechanism. This release mechanism can be significant and can reach values from ~20% at 4% FIMA to ~35% at 10% FIMA at 1450 K [115].

Behavior of chemically active fission products in fuel

For the behavior of solid fission products one must consider solubility, possible oxidation (as expressed by the Ellingham diagram in Fig. 53 [127]) and diffusion. For oxygen potentials expected in HTGR fuel particles, the Rare Earths (RE) are highly soluble being incorporated in the fuel lattice as oxides (REO_2 or RE_2O_3) where they remain stable with the possible exception of Ce (seen to be significantly released at around 1743 K for 4% FIMA fuel [103]). With respect to UCO fuel, we note that as the UC_2/UO_2 ratio increases then so do the mobilities of the REs since their “trapping” in the kernel in oxide form is lessened. Zirconium, Nb and Sr have significant solubility in UO_2 (more at high temperature for Zr) and are easy to oxidize (ZrO_2, Nb_2O_3 and SrO). Barium is in the form of low-solubility BaO and can migrate to grain boundaries forming separate complex ternary compounds with Sr, Zr, REs (and small amounts of Cs and Mo, see below) of perovskite structure. This complex phase can only be observed at high temperature and high burnup (it was not observed at 4% FIMA by Minato et al. [103] even at high temperature; furthermore, significant Ba release out of the kernel was measured). Tellurium is also of low solubility and is difficult to oxidize; at grain boundaries it forms inter-metallic compounds (e.g., with Pd) and Cs_2Te (rarely observed) and is significantly released from the kernel [103]. Many of the other metallic elements also have rather low solubility and are difficult to oxidize except at high oxygen potentials and, after segregation at grain boundaries, form metallic inclusions. Noble metals (Mo, Ru, Rh, Tc and Pd) constitute the main type of inclusion. Other inclusions of Te, Sn or Pd, Ag, Cd are also observed. The size of inclusions is very temperature dependent [103]. Pd and Ag have high volatility and are significantly released out of the fuel kernel [103]. Molybdenum has a complex behavior because its oxidation potential is close to the value corresponding to stoichiometric fuel and a significant amount can be oxidized to MoO_2 (limiting increase of fuel stoichiometry), a low solubility oxide. At high temperature Mo can form molybdate compounds with Cs or Ba but even at high temperature (>1673K) these were not observed in [103] (but only for 4% FIMA fuel). Cesium also has low solubility and might be oxidized to Cs_2O depending on the fuel temperature and oxygen potential. This oxide also has low solubility. Once again, formation of complex ternary phases could be foreseen at high temperature and high burnup [151] but were not observed in [103] where significant release of Cs from the kernel was observed.

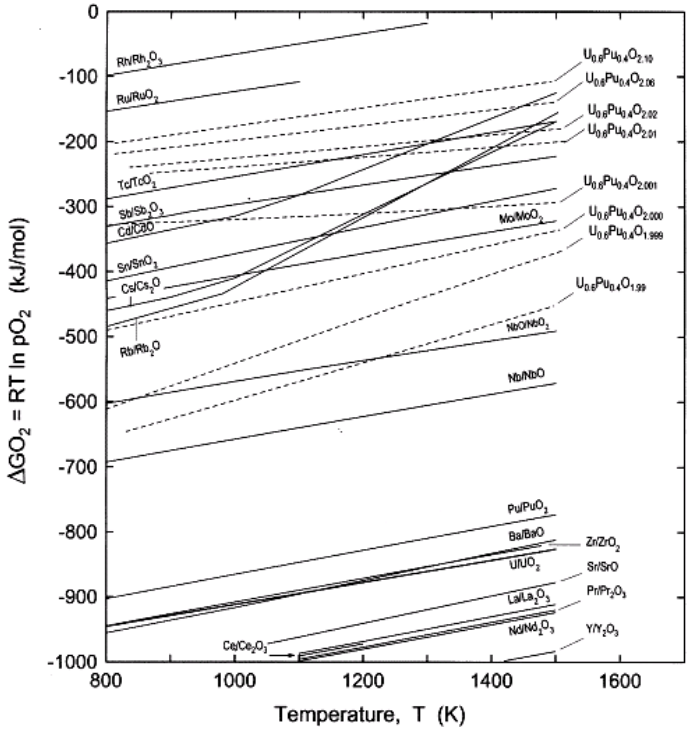

Fig. 53. Ellingham diagram for different oxides of fission products (from [107]).

In the UCO-type fuel kernel, oxygen liberated during the fission process of UO_2, first oxidizes the carbide UC_2 phase and then the RE fission products because of their high affinity for oxygen (Fig. 54). When the UC_2 phase is present in the kernel, the oxygen potential is maintained at a fixed value which is about –700 kJ/mol at 1573 K (Fig. 52). Under these conditions, the results shown in Fig. 54 indicate that those fission product elements with lower affinity for oxygen (Sr, Eu, Zr, Ba) exist as carbide compounds. As the burnup increases, the UC_2 phase in the kernel decreases. When UC_2 has fully disappeared, the oxygen potential then increases and oxygen is available to form oxide compounds with these fission products. A rather complete investigation of these chemical modifications in the UCO kernel as a function of burn up can be found in [109].

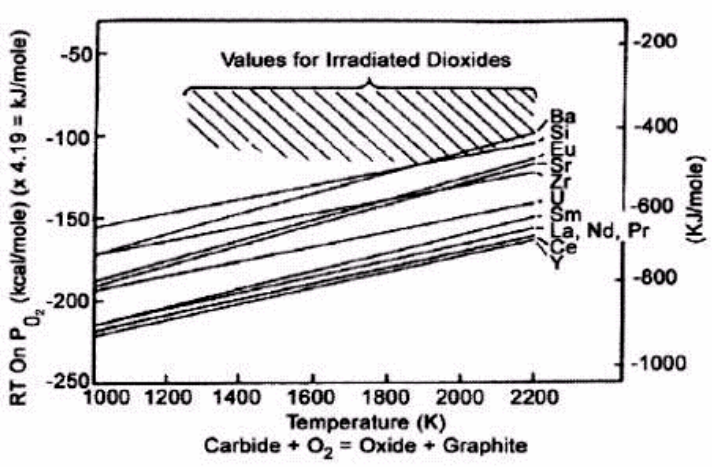

Fig. 54. Oxidation diagram for carbides of interest (from [96]).

10.3.2. Urania (UO2) kernel oxygen potential

Uranium-atom fissions (i.e., burnup) deplete the uranium content replacing each uranium atom with two fission products that, overall, have a slightly lower affinity for the oxygen of the urania (in particular, a large fraction of the noble gas xenon (~28%) is produced – see Table 13 – which has no affinity for oxygen). Thus, the fuel oxygen potential increases during irradiation and the fuel becomes slightly hyperstoichiometric (excess oxygen), a trend tempered by some of this oxygen reacting with the carbon buffer layer. Different approaches can be used to determine the oxygen potential in TRISO particles:

- tables of fission yields can be used to determine the amount of each fission product element and then calculate the oxygen requirements as metal monoxide (BaO, etc.), sesquioxide (La_2O_3, etc.) and dioxide (ZrO_2, etc.); this approach was used by Minato et al. [103] (or in [108]) who estimated an oxygen potential in an HTGR particle of 5.5% FIMA burnup at around –400 kJ/mol at 1573 K and –370 kJ/mol at 2000 K (Fig. 55);
- measure the CO trapped in the buffer layer by crushing a particle at elevated temperature in a mass spectrometer, as performed by Bildstein and Strigl [104] for 6% FIMA HTGR, irradiated in the temperature range of 1200-2100 K; Lindemer and de Nordwall [90] reviewed these data and derived an interval for the oxygen potential between –500 and –375 kJ/mol in the temperature range of 1200 and 2100 K (Fig. 56). The same values were later deduced by Homan et al. [109];
- analyze microprobe investigations conducted during post-irradiation examination if irradiated HTGR fuel particles to determine chemical speciation that are usually indicators of the oxygen potential range.

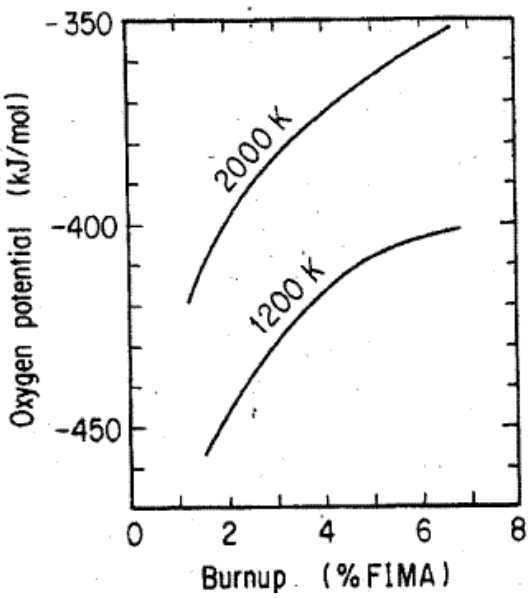

Fig. 55. Calculated oxygen potentials in HTGR UO_2 fuel as a function of burnup and temperature (from [103]).

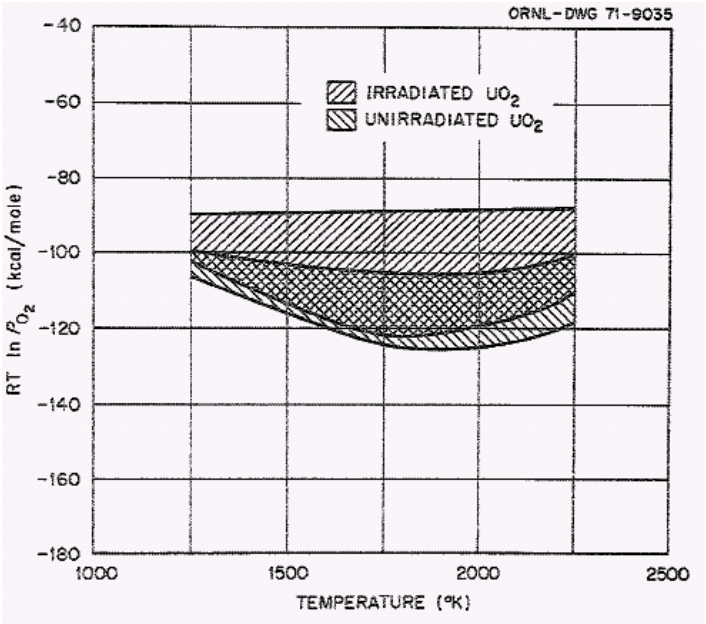

Fig. 56. Calculated oxygen potentials from UO_2 pressure measurements for HTGR UO_2 fuel (from [90]).

These results are fairly consistent with observations for LWR UO_2: Matzke showed [105] that, for 6% FIMA (equivalent to ~58 GWd/t_{HM}) fuel, between 900 and 1400 K, the oxygen potential was evaluated in the interval between –400 and –500 kJ/mol. At higher burnup (HTGR conditions), recent studies on LWR UO_2 [106], [107] indicate for a burnup of 16% FIMA (equivalent to ~161 GWd/t_{HM}), at 1273 K, the fuel oxygen potential is greater than –300 kJ/mol. This oxygen potential value is above the threshold for the oxidation of molybdenum (Fig. 57).

For such low-enriched LWR fuel, the burnup accumulated after the third irradiation cycle mainly results from the fission of ^{239}Pu which is known to be a more oxidizing process than the fission of ^{235}U. For the HTGR fuel kernel, the uranium fission is assumed to be preponderant during a longer time considering the higher initial enrichment. Consequently it is expected that HTGR UO_2 fuel kernels reach these oxygen potential values at higher burnup.

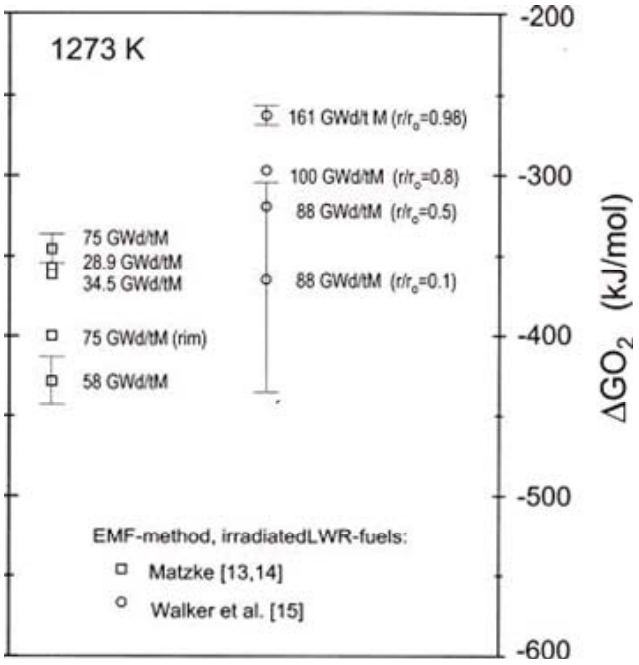

Fig. 57. Measured oxygen potentials for irradiated LWR and BWR UO_2 fuels (Figure from [107] and from experimental data in Matzke [105] and Walker et al. [106]).

10.3.3. CO/CO_2 formation and particle pressurization

The result of CO and CO_2 formation is internal pressurizing of the particle that increases with burnup and adds to the pressurization from fission gases.

For a burnup of 9% FIMA, at 1450 K, the pressure resulting from fission gases can represent one half of the contribution of CO and CO_2 in an HTGR TRISO coated particle (see Fig. 58). At lower burnup ($\leq$ 6 % FIMA), it must be stressed that pressurization of the particle arises principally from fission-gas release from the fuel kernel [114], [115]. The significant role played by the fission gases on the pressurization of the particle has to be tempered by the fact that the total pressure may be lower because some fraction of these noble fission gases may remain trapped within the fuel kernel.

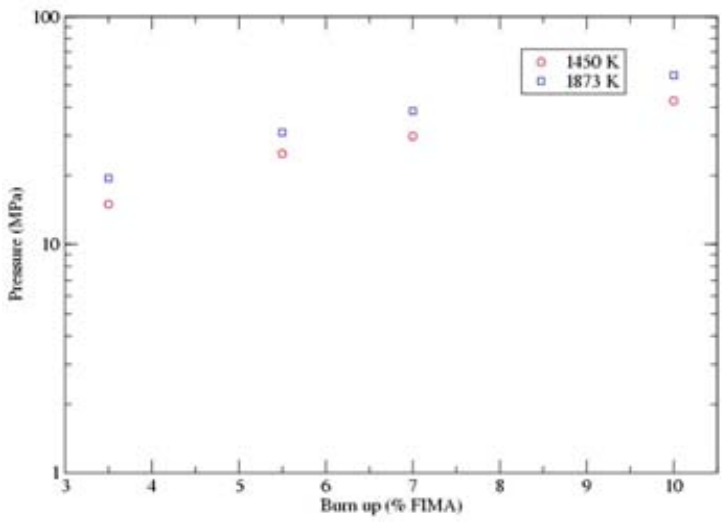

Fig. 58. Thermodynamic calculations of the Xe+Kr pressure as a function of burn up at 1450 K and 1873 K [115].

Thermodynamic calculations provide an upper bound for oxygen release as given by.

$$O/f < 0.40\ f_U + 0.85\ f_{Pu}\ , \qquad (10\text{-}6)$$

where, O/f is the atomic oxygen release per fission, f_U and f_{Pu} are the fractions for uranium and plutonium fissions, respectively.

The observed values are usually lower and can be described by the Proksch correlations [113]

$$\mathrm{Log}_{10}\,[(O/f)/t^2] = -0.21 - 8500/T \qquad (10\text{-}7)$$

where, O/f is the atomic oxygen release per fission, t, the irradiation time (in days) and T, the particle surface temperature (K). This equation is valid for $66 < t < 550$, $1223\ K < T < 1808\ K$.

The suppression of excessive CO formation during oxidation of a UO_2 based particle remains an important design objective at moderate and high burnup. The failure of the SiC layer may happen because of over-pressurization due to CO formation. However, the SiC layer may fail by other mechanisms where CO formation is implied. Corrosion of the SiC layer by CO [97], can occur as a result from failure of the IPyC coating caused by irradiation-induced shrinkage [98]. Carbon monoxide and CO_2 pressures are suspected of being partly responsible for the mechanical weakening of the IPyC coating by acting as the vehicle for mass transfer of carbon in presence of a thermal gradient [99], [100]. Uranium oxi-carbide fuel allows a significant reduction of CO and CO_2 pressurization, especially at high burnup, in comparison with UO_2 particles [116].

10.3.4. Silicon carbide corrosion by fission products

In the typical HTGR TRISO coating design, the silicon carbide layer serves as a critical fission product barrier. Nevertheless, it has been shown experimentally that the silicon carbide layer can be corroded by metallic fission products, in particular, palladium [128]. It was additionally found that silver [129], [130] could be transported through intact SiC layers.

These processes tend to limit the fuel life time, especially at high temperature. For this reason, considerable literature exists on the experimental study of interface reactions between metallic fission products and SiC [131], [132].

For Pd, the reaction with SiC can be qualitatively explained by phase-diagram arguments [133] (the Si-C-Pd system was experimentally investigated [134] and recently modeled by [135]). To prevent corrosion by Pd, new combinations of coating layers were proposed with success in [136]. The idea was to introduce a sacrificial layer inside the SiC coating able to retain the offending fission products. An alternative approach consists of replacing the SiC coating by a ZrC layer. Review and evaluation of the ZrC coating for HTGR fuel particles has been performed [137], [138]. In particular, experimental observations [139], [140] showed neither Pd attack nor thermal degradation of ZrC up to 1600°C. Zirconium carbide was also shown to have a high capacity to retain cesium [141]; however, Ru retention was not as good as for SiC. At higher temperatures, the deterioration of the ZrC particle is caused by failure of the IPyC [142]. The development of TRISO-coated particles with a ZrC-coating must be viewed as at an early stage compared to the development of the SiC-coated design for which many experiments have been performed.

Silver release has been observed [129], [130] from undamaged particles suggesting that Ag migrates through intact SiC layers at temperatures >1100°C. Today, the Ag migration mechanism remains not fully understood. A review of the possible explanations for this process is available [143]. In many situations of the past, Ag release was modeled as a diffusive mechanism since measurements of silver release exhibited temperature dependence. It seems that recent experimental results do not support this mechanism. McLean et al. [143] showed that, if grain-boundary diffusion is assumed, the expected value of the diffusion coefficient in SiC is inconsistent with the value derived from Ag release measurements. Nabielek et al. [129] speculate that Ag migration is due to the presence of free silicon at the grain boundaries. Recent experimental studies [143], [144] indicate that Ag migration by diffusion (intergranular or intragranular) does not occur up to 1300°C and alternative explanations are proposed.

Once cesium has migrated into the buffer, it can react with carbon [145]. The question of the stability of the C_nCs compounds at temperatures higher than 1100 K is an important concern. At nominal temperatures, cesium may be released and associated with carbon of the buffer layer to form compounds. These compounds, if they are not stable with increasing temperatures, may become a potential source of cesium release. The thermodynamic properties of these compounds, C_nCs (n=8,10,24,36,48,60), can be derived from vapor pressures measured in the temperature range between 670 and 1070 K [147], [148]. There are no data at higher temperatures as mentioned in different reviews [149], [150]. It was only shown that cesium-graphite compounds are not stable at 923 K under vacuum and decompose to give cesium vapor and graphite [151]. A method was developed [152] for estimating the conditions under which graphite reacts with cesium in HTGR conditions (high temperatures and low cesium pressures) to form compounds.

10.4. Some trends in accident conditions

Accident scenarios and conditions are presented in [16] along with some experimental results on oxidation of coatings (inducing particle failure) and fission product release. Severe accident scenarios involving air or water ingress, after sufficient erosion of the graphite fuel compact, could have a dramatic effect on failed particles (already-failed or oxidized during the accident) by allowing contact between the kernel and an air-helium, steam-helium or air-

steam-helium mixture. This situation is not unique to HTGR accidents as similar situations are possible in LWRs where extensive knowledge exists. Such situations are considered beyond the scope of the present book and the reader is referred to [16], [146]. For a loss-of-forced-circulation accident scenario (also called a "core conduction heatup" accident), a rapid depressurization occurs along with a flow coast down and reactor scram. The depressurization coolant is helium with no air ingress. The primary consequence of this accident is heating-up of the fuel beyond nominal conditions (about 1250°C) where modern core designs aim to limit the peak fuel temperatures to 1600°C. The principal result as far as the fuel is concerned is an enhanced release of fission products from the UO_2 kernel into (and through) the coating layers. For example, half or more of the inventories of the fission gases, I, Cs, Te and Pd could be released from the kernel. This is important in two aspects: one, increased release from the small number of defective and failed particles and, secondly, possible corrosion with SiC layer. Most fission products will still be retained by intact coatings.

11. PARTICLE MODELING

Mathematical modeling of the mechanical behavior of fuel in a nuclear reactor during the course of its irradiation is a useful tool, both as a guide for the manufacturer and also at the pre- and post-irradiation stages of in-reactor studies. At the fabrication stage, modeling can assist in optimizing the fuel design and in identifying permissible tolerances. For the purpose of planning test irradiations, modeling can assist in identifying appropriate fuel specifications and irradiation conditions. Modeling predictions may also be compared with the irradiation results. If they agree, then further extension of the calculations can check, with reasonable certainty, which a satisfactory irradiation was not on the brink of some catastrophic occurrence. If, on the other hand, they disagree, then the assumptions and/or limitations in the calculations have to be examined - a classic way by which scientific progress is made. One advantageous feature of modeling, which is why it should be used to the full, is that many calculations can be performed quickly and cheaply, in contrast with in-reactor irradiation experiments. In short, modeling studies are a way of gaining a scientific understanding of what is occurring when fuel is being irradiated - which is required by researchers, industry, utilities, and especially regulators.

To model the mechanical performance of coated particles it is necessary to calculate the tangential stresses within each of the three load bearing layers – the IPyC, the SiC and the OPyC - over the course of the irradiation. This enables one to explore whether at any stage the fracture stress in any of the layers has been exceeded. Therefore, we need to consider the various factors which affect these stresses.

During irradiation the kernel will release a proportion of the fission gases generated. If the kernel is uranium oxide, oxygen will also be released, which then reacts with pyrocarbon to form mainly CO and CO_2.This is not the case for UCO fuel kernels until very high burnup are achieved and the UC_2 phase is consumed.

The irradiation causes the kernel to swell and the buffer layer to shrink, thereby modifying the internal void volume available to the fission and reaction gases. Because of differential dimensional changes, from the early stages of the irradiation, the kernel and buffer layer are both mechanically uncoupled and in some cases the buffer layer may be cracked. Regardless if the crack occurs, the high porosity of the buffer layer implies that fission gases can

penetrate to the inner surface of the IPyC layer. As a result, the only force impinging on the three load bearing layers is the gas pressure on this surface.

If the IPyC and OPyC were absent, the gases produced in the fission process would simply stress the SiC layer and, if the pressure were high enough, cause it to fail. However, these tangential stresses are reduced by the presence of the two PyC layers because; under unrestrained conditions they would shrink during irradiation. Since this shrinkage will be largely restrained by the SiC layer, tangential stresses will be generated in both PyC layers and radial, inward acting forces imposed on the two surfaces of the SiC layer. In practice, these tangential stresses in the two PyC layers will attain a quasi-equilibrium stress state because their shrinkage is counter-balanced by irradiation creep. The SiC elastic modulus is at least an order of magnitude greater than that of PyC. During irradiation, dimensional changes and creep strains of SiC are comparatively much smaller than for PyC.

In short, modeling involves calculating stresses in the three load bearing layers created by the restraints due to attempted changes in the layer dimensions and also by the gas pressure exerted on the inner surface of the IPyC layer. This requires knowledge of various properties of the particle's constituent materials and also the manner in which these values vary over the course of the irradiation. The model must also be able to handle details of the irradiation history. Because a measure of protection from fission product release is obtained even after two of the three load bearing layers have failed, it is desirable to be able to model the fracture of one layer and then to continue the calculation up to the failure of all three layers. Moreover, a model must also be able to deal with gaps that may develop between the layers. Apart from the kernel-buffer and buffer-IPyC gaps, there is the possibility that in its attempt to shrink during the irradiation the IPyC will de-bond from the SiC layer. A description of a model that meets these requirements is presented below.

The whole irradiation history is divided into a sequence of consecutive finite neutron dose (or time, or burnup) steps. Values of stresses and strains in each layer are known at the beginning of each step (and assumed to be zero at the start of the calculation). It is, therefore, required to calculate changes in stresses and strains in each layer over the current neutron dose step which then enables stresses and strains to be up-dated for the start of the next step. The manner in which these stress and strain changes are calculated is as follows:

There are three sets of basic equations for each of the layers and the kernel [154]:

1. The displacement equations, state that the overall change in strain during a neutron dose step is the sum of the strain changes due to stress changes (elastic), irradiation creep, temperature change and irradiation induced dimensional changes. Because spherical symmetry is assumed, there are two equations, referring to the radial and tangential directions respectively.

$$\dot{\varepsilon}_1 = \dot{g}_1 + K(1-\nu)\sigma_1 - K\nu\sigma_1$$

$$\dot{\varepsilon}_3 = \dot{g}_3 + K\sigma_3 - 2K\nu\sigma_1$$

where $\dot{\varepsilon}$, $\dot{g}$, ν, and K are strain rate, creep rate, Poisson's ratio, and creep constant, respectively. σ_1 and σ_3 are radial and tangential stresses.

2. The compatibility equations (again two equations) are in spherical geometry which relate radial displacements to strains.

$$\varepsilon_1 = \frac{u}{x}, \quad \varepsilon_3 = u'$$

Where u is the radial displacement along the radial direction x and the prime denotes differentiation with respect to x.

3. The equation of equilibrium (only one equation) between tangential and radial stresses. Thus five simultaneous equations are derived for each layer.

$$\sigma_1 = \sigma_3 + \frac{1}{2} x \sigma_3'$$

From these a second order differential equation in one of the unknowns (e.g., changes in the radial displacement) is obtained by a process of elimination.

The solution has two constants of integration; these are evaluated from a set of simultaneous equations which define the boundary conditions for each of the layers (e.g. continuity of radial displacements and radial stresses at the interfaces). If the radial stress between two layers is found to exceed the de-bonding stress, the step is repeated with the boundary conditions suitably modified. If, on the other hand, the tangential stress in a layer is found to exceed the material's fracture stress, it is reduced to zero by a sequence of pseudo thermal creep time steps, thereby simulating failure; in subsequent neutron dose steps the tangential compliance constants of this failed layer are set extremely high.

Figure 59 illustrates the evolution of stresses in the three load bearing layers. Initially stresses in the SiC layer are compressive due to the attempted shrinkage of the two PyC layers, but as the gas pressure increases they become tensile until failure occurs at the fracture stress of 650 MPa. Material properties assumed for the two PyC layers were the same. However while stresses in the OPyC varied little during the course of the irradiation, they will decrease in the IPyC layer because of an increasing compressive component from the gas pressure.

So far only the endurance of an individual coated particle has been considered. However, in practice one is only concerned if some fraction, say 10^{-5}-10^{-4}, of particles from the whole population have failed (fracture of the SiC layer). Not all particles will fail at the same burnup value for two reasons. First, because the layers are considered to be brittle materials, their fracture stresses will be variable from particle to particle. This implies that as the tangential stress increases during irradiation so also will the fraction which has failed. The second reason why particles will not all fail at one burnup value is because of the statistical variations in the characteristics of individual particles.

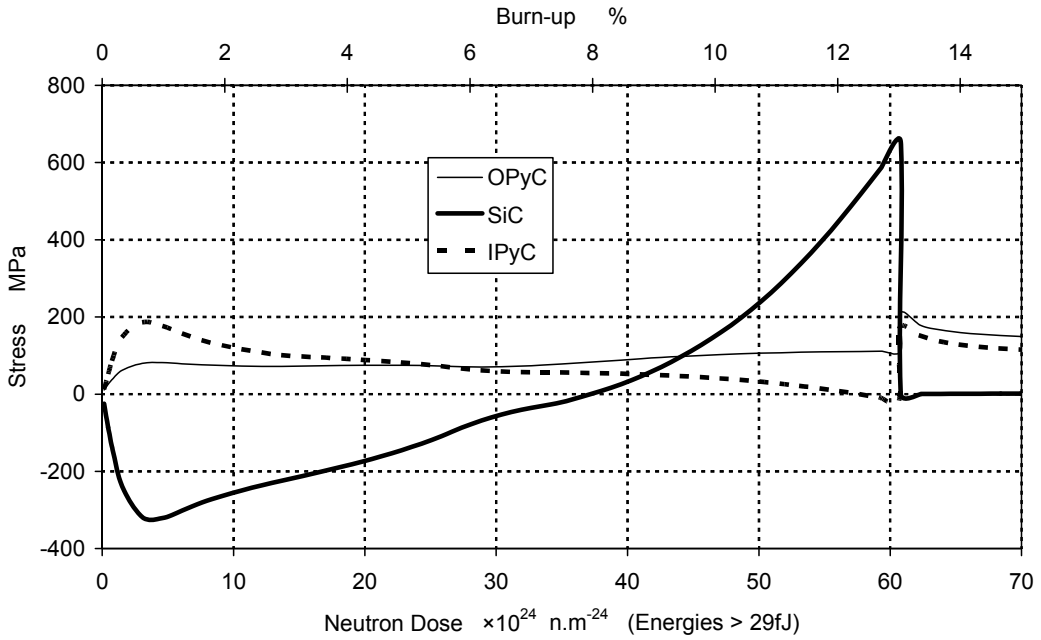

Fig.59.. Example of stresses in the three load-bearing layers during irradiation.

One way to calculate particle failure fractions as a function of the burnup is to employ Monte Carlo methods. Essentially this involves running the single particle computer code many times on a large number of particles, the specifications of each having been selected in accordance with the statistical variations of the various components. The burnup at which each particle fails is recorded, thereby enabling failure fractions as a function of burnup to be evaluated.

Uncertainties in some of the input data are a major source of uncertainties in the modeling results. In particular the properties of PyC can be highly variable, being strongly dependent on the manufacturing procedure. In simple terms, PyC may be regarded as a collection of imperfect graphite crystallites whose properties are highly anisotropic. To make their macroscopic properties as isotropic as possible the PyC layers must be manufactured with these crystallites in random orientations. This is necessary to avoid shrinkage rates in the tangential direction being so large that they cause fracture.

Along with computer codes, simple analytical models, which make the reasonable approximation that stress does not cause deformation of the SiC layer, enable identification of the most significant material properties affecting particle endurance. These models provide a useful, quick way of checking for gross errors in the more sophisticated computer codes.

Modeling is an invaluable tool for understanding the behavior of coated fuel particles during irradiation and further developments are in progress. More experimental work on material properties is necessary to reduce uncertainties in the input constituent materials property data. There needs to be a continual interaction between modelers and experimenters to ensure that what is observed is also being modeled. On the other hand, modeling may predict features (e.g., a failure mechanism) not previously observed which could be worth investigating experimentally.

Figure 60 is an example of the application of a simple model to predict SiC failure fraction as a function of temperature and burnup. The gas pressure at 10% FIMA used in generating this figure are given in Table 14.

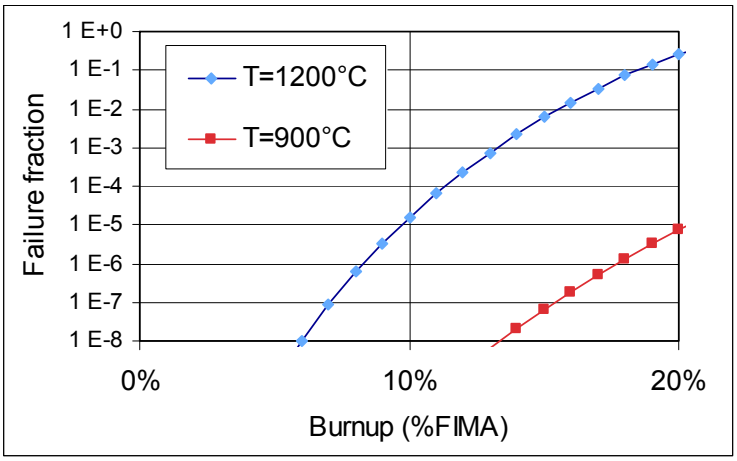

Fig. 60. Predicted failure fractions for irradiations at 900° and 1200°C up to 20% FIMA (German contribution to CRP6 normal operations benchmark calculations, Ref Phélip Mayeul). The acceptance level is in the range $2x10^{-5}$ to $6x10^{-5}$.

Table 14. PREDICTED GAS PRESSURES (MPA) AT 10% FIMA IN UO_2 LTI TRISO REFERENCE PARTICLE

Temperature	Fission Gas Pressure (MPa)	CO Pressure (MPa)	Total Pressure (MPA)
900°C	3.9	0.1	4.0
1200°C	15.7	5.8	21.5

12. FISSION PRODUCT TRANSPORT MODELING

For all modern nuclear reactor designs, safety is the most important consideration. The safety of a nuclear reactor design is measured by its ability to mitigate possible detrimental side effects of reactor operation from the public and operating staff under all foreseeable conditions. The main safety considerations for an HTGR power plant are radioactive material escaping from the fuel elements.

The source of radioactive materials is the large inventory of fission and activation products built up in the reactor fuel. A typical HTGR power plant design generates thermal power up to 600 MW, or ~2×10^{19} fissions per second. In a reactor's 40 yr operational lifetime, ~$5x10^{28}$ fission product atoms along with a large inventory of activation products are created. Fortunately most of the fission products have very short half-lives and decay quickly (in terms of a fuel element core residence time of three years), or form stable oxide compounds in the fuel kernel [16], [155]. Due to adequate shielding around the reactor core and spent fuel containers, fission products in the fuel elements pose no threat to either plant personnel or the nearby population.

The safety of a high temperature gas cooled nuclear power plant is therefore dependent on its fuel elements ability to retain fission products under all expected reactor operating conditions. The reactor design must be such that the fuel elements are never exposed to conditions in excess of their design qualification. Similarly, fuel designs must be such that fuel elements can be manufactured economically in large quantities, while maintaining fuel quality and integrity during manufacture and subsequent irradiation [16]. In modern HTGR reactors, the principal containment barrier is the TRISO coated particle, which has proven effective during various irradiation tests and real-time experiments.

Even under the best manufacturing conditions, a small fraction of coated fuel particles will be defective, which together with contamination in the fuel materials, are potential sources of fission product release into the coolant gas. Furthermore under abnormally high temperatures and power surges, coated fuel particles may start to fail and release fission products. Condensable radionuclides released from the core plate out in the cooler regions of the main power system causing radiation dangers to operating personnel, and if released from the closed coolant circuit, also to the public. It is therefore imperative to be able to predict, with a reasonable level of certainty, fission product release from the fuel elements and the plant under any expected operating or accident conditions. This is exactly the role of fission product release analyses.

12.1. Production

12.1.1. Sources

In a nuclear reactor, fissile fuel atoms (^{233}U, ^{235}U, ^{239}Pu, ^{241}Pu) capture thermal neutrons and undergo fission reactions that produce fission products, energy (~200 MeV or ~32 pJ per event in the form of heat, kinetic energy and radiation) and more neutrons to sustain a chain reaction. When these fissile nuclides undergo nuclear fission a large variety of fission products are formed. The probability of a specific fission product being formed during a fission reaction is known as its fission yield and is different for the various fissile nuclides. These differences may be quite significant; e.g. the yield of stable ^{109}Ag, the precursor of ^{110m}Ag, is an order of magnitude higher in ^{239}Pu fission than from ^{235}U fission. Thermal neutron fission product yields for ^{233}U, ^{235}U and ^{239}Pu are shown in Fig. 61.

Because nearly all fission fragments are produced neutron rich, they undergo successive radioactive decay by β-particle emission (β-decay) leading to the characteristic chains of radioactive decay products for a specific mass level. Thus, a large collection of fission product nuclides is created in a nuclear reactor by the fission of uranium and plutonium. Fortunately, most or the fission products have very short half-lives, and many others form chemically stable oxide compounds in the fuel kernel. Therefore, they are of little interest for fission product release analysis.

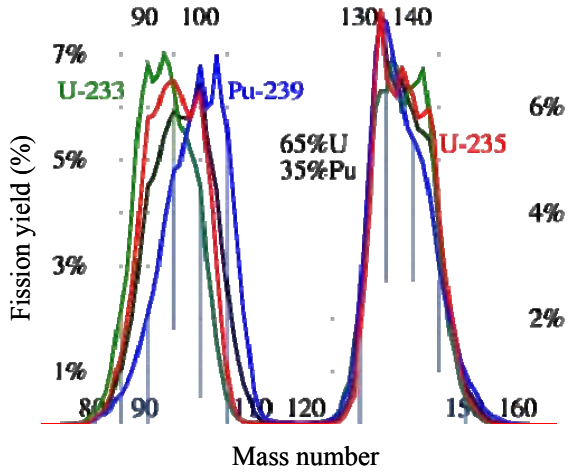

Fig. 61. Fission yield as a function of fission product mass number for ^{233}U fissions, ^{235}U fissions, ^{239}Pu fissions (Ref: Wikipedia 2009).

The fission product source term S_i (production from fission) for a specific isotope *i* can be calculated by the relationship

$$S_i = P_f \cdot t \cdot Y_i \tag{12.1}$$

where P_f is the fission power output of the fuel element (W),
t is the duration of each time step (decay corrected) (s), and
Y_i is the cumulative fission yield of the fission product.

The fact that one fission event results is the liberation of ~200 MeV of energy can be used to show the equivalency of 1 W of power to 3.12 x10^{10} fissions/s.

Activation products are formed when a fission product captures a neutron to form a new nuclide. Some of these activation products are very important for HTGR maintenance and safety, for example ^{134}Cs and ^{110m}Ag. The ^{110m}Ag production and decay chain is shown below:

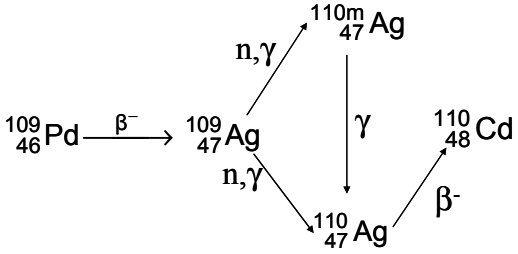

The activation product source term S_{AP} (production from activation) can then be calculated by the effective decay constants of the activation and mother products as follows:

$$S_{AP} = S_{MP} \cdot \frac{Y_{CUM}}{Y_{DIR}} \cdot R_{Br} \left[e^{-\lambda_{MP} t} - e^{-\lambda_{AP} t} \right] \cdot \left[\frac{\lambda_{AB}}{\lambda_{AB} - \lambda_{MP}} \right], \tag{12.2}$$

where S_{AP} is the activation product's source term (production from fission),
S_{MP} is the mother product's source term (production from fission),

Y_{CUM} is the cumulative fission yield of the mother product,
Y_{DIR} is the direct fission yield of the mother product,
R_{Br} is the branching ratio, (the fraction activation product formed),
λ_{AP} is the effective decay constant of the activation product,
λ_{MP} is the effective decay constant of the mother product.

The effective decay constants are calculated from the average neutron flux (Φ_{th}), and the neutron capture cross-section (σ_{th}) according to:

$$\lambda_{eff} = \lambda + \sigma_{th} \Phi_{th}. \tag{12.3}$$

12.2. Radionuclide selection

Since it is impractical (and unnecessary) to evaluate production, transport and release of all the fission and activation products generated in a nuclear reactor, only the most significant radiological nuclides are analyzed. Key radionuclides are selected based on the combination of their radiological hazard level, fission yield, and their transport and release properties.

Because radiological decay occurs during fission product transport and diffusion through the ceramic layers of a coated fuel particle, the radiologically important fission products released from fuel elements are divided into two groups: the relatively short-lived gaseous fission products, and the long-lived metallic fission products. Different theoretical models and sets of transport parameters (e.g. diffusion coefficients, correlations) describe both these two fission product group's behavior.

These models are applied in software codes that use the different sets of transport parameters to describe fission product behavior in fuel elements. A simple steady-state code can adequately describe gaseous fission product release during normal operation, but a transient code is needed to describe metallic fission product release. Although all the iodine, bromine, krypton and xenon fission products could be calculated, only six key nuclides from these four elements are necessary to provide the significance of the radiological risk. These six key radiological short-lived fission product nuclides are:

^{131}I, ^{133}I (especially accident conditions, heat-up during loss of forced coolant events),

^{88}Kr, ^{138}Xe, ^{133}Xe (normal conditions, leaking from main power system),

^{90}Kr, ^{137}Xe (as precursors for 90Sr and ^{137}Cs, respectively) and

^{132}Te (although a metal, its behavior and inventory is calculated very similar to that of iodine and xenon).

The inventory of any metallic fission or activation product can be calculated as long as the transport parameters of the nuclide are available. Currently six long-lived metallic fission and activation products have been identified as radiologically significant:

^{137}Cs, ^{111}Ag (normal operation and accident conditions),

^{134}Cs, ^{136}Cs, ^{110m}Ag (normal operation) and to a lesser extent,

^{90}Sr (principally formed by ^{90}Kr decay in the primary circuit).

The inventories of all twelve nuclides identified above are calculated for normal operation conditions, but only four of these nuclides are significant for off-normal event conditions: ^{90}Sr, ^{131}I, ^{137}Cs and ^{111}Ag. A fifth important nuclide ^{133}I is chemically the same as ^{131}I and the same release fractions are used for both nuclides. The list of radiologically significant nuclides is continuously reviewed and updated, and more nuclides may be added depending on the expected fuel conditions.

12.3. Transport modeling

There are three distinct and independent sources of fission product release from fuel elements. Fission products produced from each source have a different pathway to the surface of the fuel. The fission product transport route is graphically shown in Fig. 62.

- **Uranium and thorium contamination in the fuel constituent materials.** This contamination is both in the oPyC layer and in the matrix material of the fuel element. Fission products created by fission of this contamination only have to diffuse through the oPyC and the matrix material.

- **Defective and failed coated particles.** Even under the best manufacturing conditions, a small fraction of coated fuel particles will be defective. Furthermore, under abnormally high temperatures and power surges, some small fraction of the normal coated fuel particles may begin to fail. It is assumed that fission products from failed and defective particles do not have to travel through the particle's coating layers, but are released directly from the fuel kernel to the matrix material.

- **Intact TRISO coated particles.** Fission products formed in fully intact TRISO particles have to be transported through all the coating layers before they can diffuse through the matrix material. Diffusion parameters for krypton and xenon gases in the PyC coatings are very small. Therefore, the transport rates of gaseous fission products are extremely slow, and release fractions from intact coated particles are negligible. Consequently, only metallic fission product transport through intact coated particle layers needs to be considered.

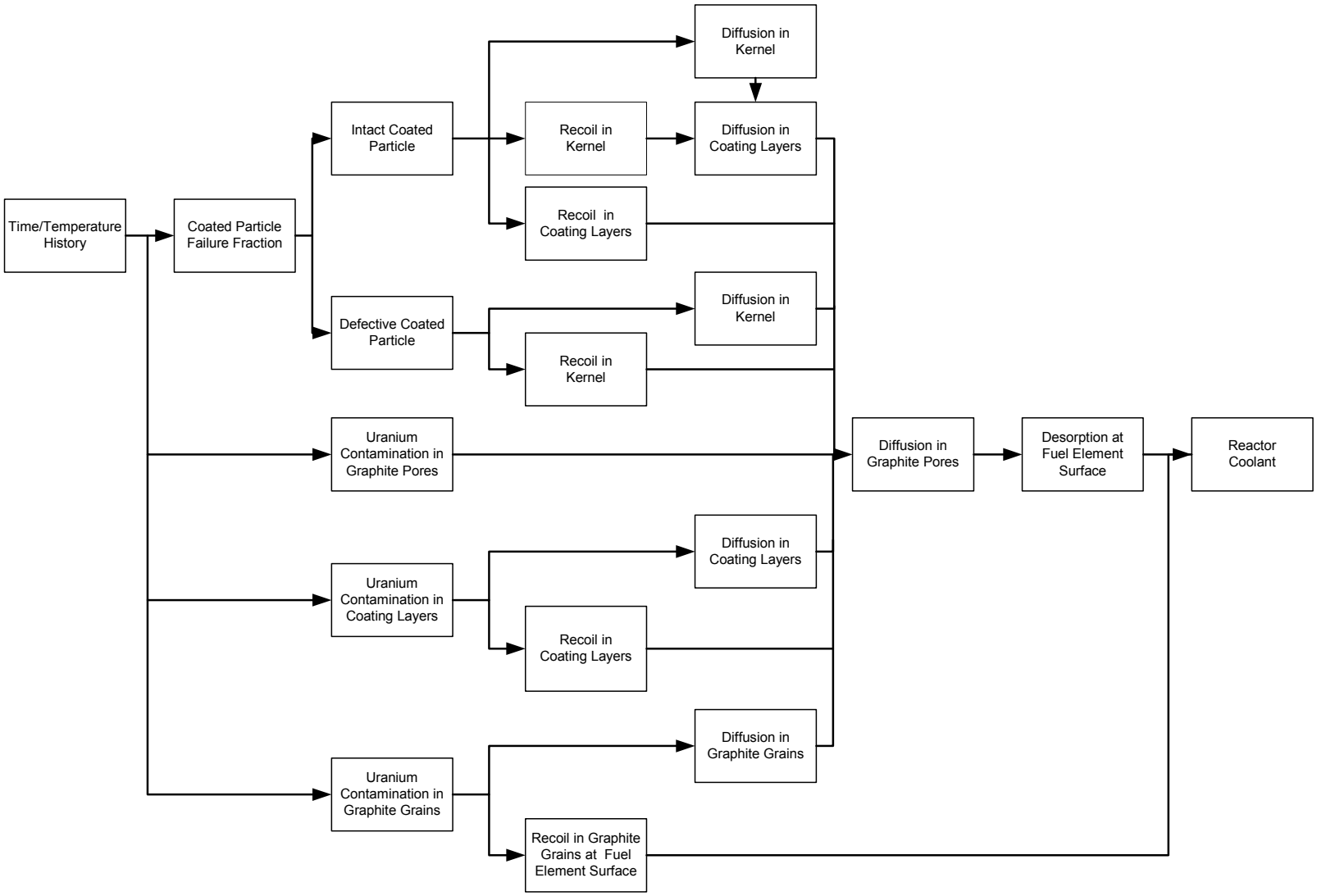

Fig.62. Fission product transport diagram.

12.3.1. Fission product recoil

Recoil refers to the distance, fission products travel after birth before they are stopped in the surrounding material. The recoil stopping range for each fission product nuclide is dependent on its mass, its kinetic energy and the material through which it penetrates. Initially, fission products have high kinetic energies and travel a finite distance before being stopped by the surrounding material. As a result, some of the fission products formed near the surface of a fuel kernel are released directly into the buffer region because of recoil.

Similarly, some fission products formed in the grains of the graphite matrix (because of heavy metal contamination) escape the grains directly without diffusion. Also, some of the fission products formed in the oPyC layer (due to uranium contamination) escape directly from the coating layer. Finally, some of the fission products generated by heavy metal contamination in the outer 5 mm-thick fuel-free zone of the spherical element can be released directly into the coolant without diffusion.

Fission products recoiling from fission sites may knock-out other imbedded fission products from the fuel materials. However, this mechanism only plays a role at very low temperatures, and is negligible at the normal operational temperatures of modern HTGRs.

The recoil fraction F_R released by fission in the fuel kernel into the neighboring buffer layer is calculated from geometrical considerations and is temperature independent [156]:

$$F_R = \frac{3}{4}\frac{r_0}{R_a}\left[1-\frac{1}{12}\left(\frac{r_0}{R_a}\right)^2\right], \tag{12.4}$$

where F_R is the recoil fraction into the matrix material,
r_o is the mean recoil range in the buffer layer,
R_a is the kernel radius.

12.3.2. Fission product release

The transport of fission metals through the fuel constituent materials is modeled as a transient diffusion process. The transient diffusion equation is typically solved numerically with appropriate boundary and interface conditions [157]. The transport of mobile fission metals, including Cs, Ag, Sr and Eu isotopes, is undoubtedly much more complicated than classical Fickian diffusion. These apparent migration coefficients are generally structure sensitive which indicates that their transport process is not a simple diffusion process but likely a combination of lattice diffusion, grain boundary diffusion, pore diffusion, etc., complicated further by effects like irradiation-enhanced trapping and adsorption. Consequently, any quoted diffusion coefficients should be called “effective” diffusion coefficients, which imply that the overall migration process can be approximately described by Fick’s laws [158].

The fission product speciation in the kernel changes with burnup, especially with UCO kernels as the oxygen potential changes, and these changes in chemistry could affect the mobility of oxide-forming species, including Cs and Sr. The probable exception is silver which appears to remain in elemental form for all kernel compositions and burnups of interest.

Atoms and molecules have the spontaneous tendency to disperse as a consequence of the second law of thermodynamics. The rate of migration of an atom through a medium is

measured by its mass flux ***J***, expressed as atoms $\cdot$ m^{-2} $\cdot$ s^{-1}. Atoms migrate down a concentration gradient as described in [158], [159]:

$$J_x = -D\frac{\partial c}{\partial x} \text{ or, more general, } \vec{J} = -D \cdot \vec{\nabla} c \tag{12.5}$$

with c [atoms $\cdot$ m^{-3}] being the concentration as a function of time and space coordinates.

The flux of atoms diffusing through a medium is proportional to the concentration gradient, which give us the balance equation in the absence of source and decay terms:

$$\frac{\partial c}{\partial t} = -\frac{\partial J}{\partial x} \text{ or } \iiint_V \frac{\partial c}{\partial t} dV = -\oint_S \vec{J} \cdot d\vec{S}\,, \tag{12.6}$$

where V and S are volume and surface under consideration.

Inserting the diffusion flux J in the balance equation gives us Fick's second law. Fick's second law of diffusion describes the time dependant diffusion process:

$$\frac{\partial c}{\partial t} = \nabla(D \nabla c) \text{ and this is } \frac{\partial c}{\partial t} = \frac{D}{r}\frac{\partial^2 (rc)}{\partial r^2} \text{ in spherical coordinates and constant D,} \tag{12.7}$$

where by r (m) is the radial position (in a kernel, in a particle, or in a spherical fuel element). This is known as the diffusion equation, and mathematically, it is a partial differential equation of parabolic type.

In a fuel element there is a source S of atoms (e.g. production from nuclear fission) and a removal term λc (radioactive decay) so that the diffusion equation becomes

$$\frac{\partial c}{\partial t} = D\left(\frac{\partial^2 c}{\partial r^2} + \frac{1}{r}\frac{\partial c}{\partial r}\right) - \lambda c + S. \tag{12.8}$$

With the following boundary conditions:

1. For reasons of symmetry, the concentration gradient is 0 at r = 0.

$$\left.\frac{\partial c}{\partial r}\right|_{r=0} = 0 \tag{12.9}$$

2. Continuity of concentration and flux at the interface between two adjacent materials with diffusion constants D_1, and D_2

$$c_L = c_R \text{, and } -D_1 \left.\frac{\partial c}{\partial r}\right|_L = -D_2 \left.\frac{\partial c}{\partial r}\right|_R \tag{12.10}$$

3. Mass transfer at the fuel surface.

$$-D\left.\frac{\partial c}{\partial r}\right|_{r=r_s} = \beta\left(\alpha c_s - c_g\right) \tag{12.11}$$

where, β is the mass transfer coefficient from the surface to the coolant,
α is determined by the sorption isotherm,
c_s and c_g are concentrations on the surface and in the coolant.

The third boundary condition defines the release rate from the surface of the fuel sphere ($\text{atoms} \cdot \text{cm}^{-2} \cdot \text{s}^{-1}$) [160]. At the coolant boundary, the mass flux from the surface into the flowing coolant is given by the product of a convective mass transfer coefficient and a concentration driving force which is the difference between the desorption pressure (expressed as a volumetric concentration) and the "free stream" or mixed mean concentration in the coolant. In practical terms, the assumption of free evaporation from the surface can be made, i.e.

$\beta \to \infty$, or, equivalently: $c_s \equiv 0$ (12.12)

The matrix material used in fuel compacts for the prismatic core designs is porous and provides little holdup of the fission gases which are released from the fuel particles, and any retention effect is generally neglected. However, this matrix is a composite material which has a high content of amorphous carbon, and this constituent of the matrix is highly sorptive of metallic fission products, especially Sr. While the matrix is highly sorptive of metals, it provides little resistance to diffusion/migration of fission metals because of its high interconnected porosity.

The matrix of a spherical fuel element is more dense and partially graphitized so it does provide more diffusion/migration resistance of fission metals.

Metallic fission product transport in matrix material is also modeled as a transient Fickian diffusion process: the transient diffusion equation is solved with an evaporative boundary condition. It is assumed that at equilibrium, the vapor pressure in the helium-filled gap and solid-phase concentration on the fuel-compact surface are uniquely related to one another by a sorption isotherm which is determined experimentally.

Sorption isotherms for Cs, Sr and Ag have been measured for a variety of nuclear graphites and matrix materials; the data are summarized in IAEA-TECDOC-978 [16]. Experimental data are generally correlated with a simple Henry isotherm (linear dependence) for low sorbate concentrations and with a Freundlich isotherm (exponential dependence) at higher sorbate concentrations [16].

The partial pressure is assumed to be the sum of the pressures calculated with the two isotherms:

$$p = p_H + p_F, \tag{12.13}$$

Henry:
$$p_H = c_s \exp\left[\left(A + \frac{B}{T}\right) + \left(D - 1 + \frac{E}{T}\right)\ln c_t\right], \tag{12.14}$$

Freundlich:
$$p_F = \exp\left[\left(A + \frac{B}{T}\right) + \left(D + \frac{E}{T}\right)\ln c_s\right], \text{ and} \tag{12.15}$$

transition at c_t: $\ln c_t = d_1 - d_2 T$, (12.16)

where T is the absolute temperature (K)

c_s is the mass concentration of sorbate (mol/kg of carbon or graphite)
A, B, D, E, c_t, d_1, d_2 are empirically derived constants.

In most cases, the concentrations are low and the equilibrium vapor pressure can be expressed by:

$$p_H = c_S \cdot e^{(A+B/T)}. \tag{12.17}$$

12.3.3. Fission product release from fuel materials

In the Equivalent Sphere Model [158], the primary fission product retaining object is a UO_2 or $(Th,U)O_2$ grain that is modeled as a sphere with radius *a*. With the initial and boundary conditions

$$c(0 \le r \le a, t = 0) = 0\,,\ \frac{\partial c(r = 0, \forall t)}{\partial r} = 0\,,\ c(r = a, \forall t) = 0\,. \tag{12.18}$$

Solving the diffusion equation

$$\frac{\partial c}{\partial t} = D\left(\frac{\partial^2 c}{\partial r^2} + \frac{1}{r}\frac{\partial c}{\partial r}\right) - \lambda c + S \tag{12.8a}$$

for concentration c as a function of radius r and time t reveals

$$c(r,t) = \frac{S}{\lambda}\left[1 - \frac{\sinh \rho\sqrt{\lambda/D'}}{\rho \sinh\sqrt{\lambda/D'}}\right] - \left[\frac{2}{\pi}\frac{S}{D'}\frac{e^{-\lambda t}}{\rho}\sum_{n=1}^{\infty}(-1)^{n+1}\frac{e^{-n^2\pi^2 D' t}}{n\left(n^2\pi^2 + \lambda/D'\right)}\sin n\pi\rho\right], \tag{12.19}$$

with reduced radius $\rho = \frac{r}{a}$ and (12.19a)

reduced diffusion coefficient $D' = \frac{D}{a^2}$. (12.19b)

For short-lived fission gases, $\lambda \ge 10^{-6}$s, and

only the steady state first term of equation (12.19) needs to be used. Thus, Eq (12.19b) becomes

$$\frac{R}{B} = 3\sqrt{\frac{D'}{\lambda}}\left(\coth\sqrt{\frac{\lambda}{D'}} - \sqrt{\frac{D'}{\lambda}}\right) \approx 3\sqrt{\frac{D'}{\lambda}} \propto \sqrt{\tau}\,, \tag{12.20}$$

where R/B is the ratio of release-rate (R) over birth-rate (B) is approximately proportional to the square root of the half life, $\tau^{1/2}$. Figure 63 shows the good agreement of this model with a calibration experiment for gas release rates. The diffusion coefficient used here is given by

$$D = D'_0\, e^{-\frac{Q}{RT}} \text{ with} \tag{12.21}$$

$D'_0 = 2.1\times10^{-5}\,s^{-1}$, $Q = 126\ kJ/mol$ activation energy,

$R = 8.3145\ J/mol/K$ universal gas constant, and $T(K)$ fuel temperature.

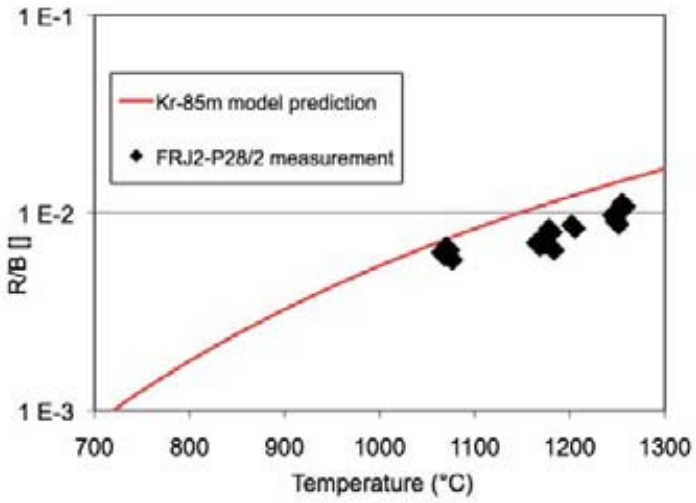

Fig. 63. ^{85m}Kr release rate from UO_2: model predictions and measurements during the calibration experiment FRJ2-P28/2.

The accumulated diffusive fractional release, *F,* of long lived or stable fission products, $\lambda \approx 0$, is given by the transient solution of the diffusion equation to yield

$$F = 1 - \frac{6}{\tau}\sum_{n=1}^{\infty}\frac{1-e^{-n^2\pi^2\tau}}{n^4\pi^4} \quad = \quad 4\sqrt{\frac{\tau}{\pi}} - \frac{3}{2}\tau + 48\sqrt{\tau}\sum_{n=1}^{\infty} \mathrm{i}^3\,\mathrm{erfc}\frac{n}{\sqrt{\tau}}. \tag{12.22}$$

The fractional release is shown as the lower curve in Fig. 64 as a function of diffusion time τ; it can be efficiently approximated by

$$F \approx \quad 4\sqrt{\frac{D't}{\pi}} - \frac{3}{2}D't \text{ for } \tau \le 0.35, \text{ and} \tag{12.22a}$$

$$F \approx \quad 1 - \frac{1}{15D't} \text{ for } \tau > 0.35. \tag{12.22b}$$

In these expressions, the diffusion time $\tau = D't$.

12.3.4. Kernel release from post-irradiation heating tests

Kernel release of long-lived or stable fission products (λ = 0) during accident condition heating tests (no source term, S = 0) can be approximated by solving the diffusion equation (13.8)

$$\frac{\partial c}{\partial t} = D\frac{1}{r}\frac{\partial^2(rc)}{\partial r^2} \tag{12.8b}$$

with the boundary conditions $\left.\frac{\partial c}{\partial r}\right|_{r=0} = 0,\ c(r=a,t) = 0$. (12.23)

The initial condition $c(r, t=0) = \text{constant}$ for $0 \le r < a$ approximates the case of a prior cold-irradiation.

The out-of-reactor fractional release [158] $F_{out-of-reactor}$ from the fuel kernel is

$$F_{out-of-reactor} = 1 - 6\sum_{n=1}^{\infty} \frac{e^{-n^2\pi^2 D't}}{n^2\pi^2}, \tag{12.24}$$

where $D'(s^{-1}) = D/a^2$ the reduced diffusion coefficient. The out-of-reactor fractional release is efficiently approximated as

$$F_{iyt-of-reactir} \approx 6\sqrt{\frac{D't}{\pi}} - 3D't \text{ for } D't \le 0.15, \text{ and} \tag{12.24a}$$

$$F_{out-of-reactor} \approx 1 - \frac{6e^{-\pi^2 D't}}{\pi^2} \text{ for } D't > 0.15. \tag{12.24b}$$

The release curve, applicable to a heating test of a bare kernel or broken particle, is shown as the upper term in Fig. 64. The predicted release curves for the out-of-reactor (top) and in-reactor (bottom, without recoil) fractional release versus a dimensionless kernel diffusion time given by the product of the reduced diffusion coefficient with heating or irradiation time.

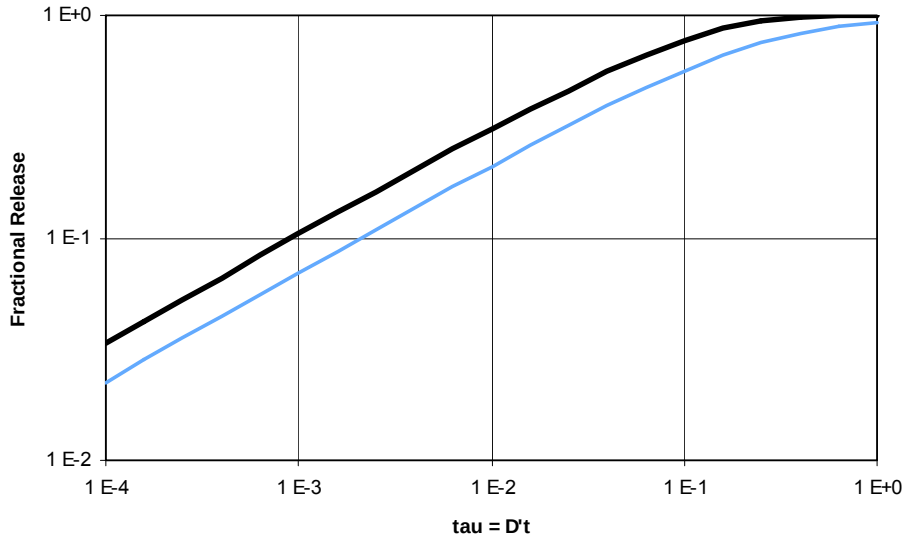

Fig. 64. Fractional release of long-lived fission productions during heating (top) and during irradiation (below) as a function of diffusion time $\tau = D't$ according to the equivalent sphere model.

The cesium release fraction shown in Fig. 65 is the good agreement with experimental data when using the following diffusion coefficient of cesium in UO_2:

$$D'_{Cs-in-UO_2}(s^{-1}) = 0.90e^{-209 kJ/mol/RT} + 8320e^{-362 kJ/mol/RT}. \tag{12.25}$$

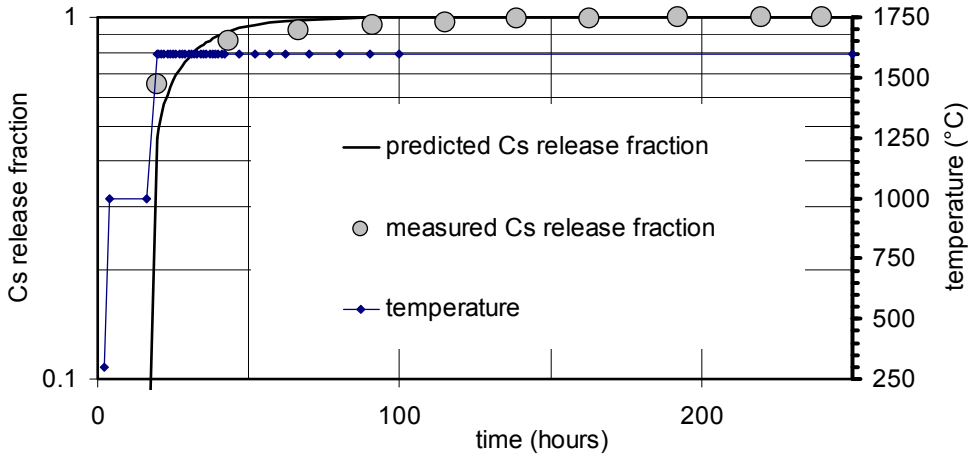

Fig. 65. Predicted and measured cesium release from irradiated kernels in a 300-1000-1600°C accident condition simulation test. Five UO_2 kernels in coupon C6 had been irradiated in FRJ2-P28 to 8.1% FIMA, were reactivated in FRJ1, and subjected to KUEFA heating tests.

Figure 65 displays the predicted release curves for the out-of-reactor and in-reactor (without recoil) fractional release versus a dimensionless kernel diffusion time given by the product of the reduced diffusion coefficient with heating or irradiation time.

12.3.5. Diffusion coefficients

Kernel retention is mainly due to fission product slow-down in UO_2 grains; further delays in grain boundaries, intergranular bubbles etc. are usually neglected in high burnup (>10% FIMA) HTGR fuel. Because numerical diffusions codes like GETTER and FRESCO treat the whole kernel as one unit, the fuel kernel radius being equated to the equivalent grain radius

$$D' = \frac{D_{grain}}{a^2} = \frac{D_k}{r_k^2}, \qquad (12.26)$$

with a being the equivalent grain radius and $r_k = 250 \mu m$ kernel radius. Usual tables like Table 15 below contain D_k [$m^2 s^{-1}$] values.

12.3.6. Retention by a single layer

In a situation typical of a heating test, an estimate of the breakthrough time for the release of long-lived or stable fission products through a thin spherical shell can be made with the expression

Table 15. DIFFUSION COEFFICIENTS, FROM [16]

	Diffusion Coefficients			
	D_1 [m^2/s]	**Q_1 [kJ/mol]**	**D_2 [m^2/s]**	**Q_2 [kJ/mol]**
Cesium in UO_2	$5.6*10^{-8}$	209	$5.2*10^{-4}$	362

in buffer	$1*10^{-8}$	0		
in PyC	$6.3*10^{-8}$	222		
in SiC	$5.5*10^{-14} * e^{\Gamma/5}$	125	$1.6*10^{-2}$	514
in matrix A3-3	$3.6*10^{-4}$	189		
in matrix A3-27	$3.6*10^{-3}$	189		
Strontium				
in UO_2	$2.2*10^{-3}$	488		
in buffer	$1*10^{-8}$	0		
in PyC	$2.3*10^{-6}$	197		
in SiC	$1.2*10^{-9}$	205	$1.8*10^{6}$	791
in matrix	$1.0*10^{-2}$	303		
Silver				
in UO_2	$6.7*10^{-9}$	165		
in buffer	$1*10^{-8}$	0		
in PyC	$5.3*10^{-9}$	154		
in SiC	$3.6*10^{-9}$	215		
in irradiated matrix A3-3	1.6	258		
Krypton (Iodine)				
in UO_2	$8.8*10^{-15}$	54	$6.0*10^{-1}$	480
in buffer	$1*10^{-8}$	0		
in PyC	$1*10^{-30}$	0		
in SiC	$1*10^{-30}$	0		
in matrix	$6.0*10^{-6}$	0		

$$t_0 = \frac{\ln\left(1+\gamma/2\right)}{3\gamma D^*}, \tag{12.27}$$

which for small γ can be approximated by

$$t_0 \approx \frac{1}{6D^*}, \tag{12.28}$$

whereby γ is the ratio of layer thickness d to the inner radius, r_2, of the layer, D is the diffusion coefficient in the retaining layer, and $D^* = D/d^2$. The underlying assumption is that the only delay in release is determined from the slow diffusion through this coating layer.

Assuming that a fixed number of molecules are completely mobile inside r_2 and there is an infinitely fast release from the surface at R = r_2+d, mathematically expressed by C(r=R)=0. The breakthrough time estimate comes from the long-time, large release approximation for the release fraction F:

$$F \approx 1-\left(1+\frac{\gamma}{2}\right)\exp\left(-3\lambda D^* t\right), \tag{12.29}$$

and its zero-crossing F=0. This release fraction ranges from a few percent release to 100% release and comes from the solution of the diffusion equation below with its boundary conditions.

In the thin, retaining coating layer $r_2 \le r \le R$, characterized by diffusion coefficient D, the diffusion equation (13.8b) describing concentration c as a function of time t and radius r for given spherical geometry. Within the coating layer, the initial condition is the concentration is zero, $C(r,t=0) \equiv 0$. The boundary condition at the outer surface, r = R, is $c(r=R,t) \equiv 0$ for all times, i.e. infinitely fast evaporation from the surface. Initially, inside the spherical shell, there are N freely movable atoms, i.e. an initial concentration $c_0(r,t=0) = N \Big/ \frac{4}{3}\pi r_2^3$, that can be depleted only by diffusion into the spherical shell

$$-\frac{4\pi r_2^3}{3}\frac{\partial c_o}{\partial t} = -4\pi r_2^2 D \left.\frac{\partial c}{\partial r}\right|_{r=r_2} \tag{12.30}$$

Also, it is assumed that the partition coefficient between inner volume and the spherical shell is equal to 1, i.e. $c_o = c(r=r_2,t)$ for all times.

Of interest is the cumulative fraction release defined by

$$F = \frac{\int_0^\infty -4\pi R^2 D \left.\frac{\partial c}{\partial r}\right|_{r=R} dt}{N} . \tag{12.31}$$

The solution in Laplace space yields the fractional release $\widehat{F}$ whereby s is the Laplace transformed time variable:

$$\widehat{F} = \frac{1+\gamma}{s} \cdot \frac{1}{\left(q^2 \Big/ 3\gamma + \gamma\right)\frac{\sinh(q)}{q} + \cosh(q)} \tag{12.32}$$

or alternatively

$$\widehat{F} = \frac{1+\gamma}{s} \cdot \frac{3\gamma q \Big/ \sinh(q)}{q^2 + \gamma^2 + 3\gamma q \cdot \coth(q)} , \tag{12.32a}$$

where, $q \equiv \sqrt{\frac{s}{D^*}}$.

Transformation into real space gives:

$$F = 1 - \sum_{m=0}^{\infty} T_m \cdot \exp\left(-y_m^2 \tau\right) , \tag{12.32b}$$

where $\tau \equiv D^* t \equiv \frac{Dt}{d^2}$ and coefficients

$$\tan y_m = \frac{3\gamma y_m}{y_m^2 - 3\gamma^2} \;,\; y_m > 0 \quad , \tag{12.33a}$$

$$T_m = \frac{1+\gamma}{\cos y_m} \frac{1}{\frac{y_m^2}{6\gamma} + \frac{1}{2} + \gamma + \frac{3\gamma^2 + 4.5\gamma^3}{y_m^2 + 3\gamma^2}} \quad . \tag{12.33b}$$

For short diffusion times $\tau < 0.07$, the fractional release can be approximated by

$$F \cong \frac{24\gamma(1+\gamma)}{\sqrt{\pi}} \exp\left(-\frac{1}{4\tau}\right) \tau^{1.5} \left[1 - 6\tau(1+\gamma) + 12\tau^2\left(5 + 6\gamma + 6\gamma^2\right) - + \ldots\right] \quad . \tag{12.34}$$

Figure 66 is a comparison of the release fraction calculated using the exact solution and the approximation for short diffusion times. The fractional release values are nearly identical for diffusion times < 0.07.

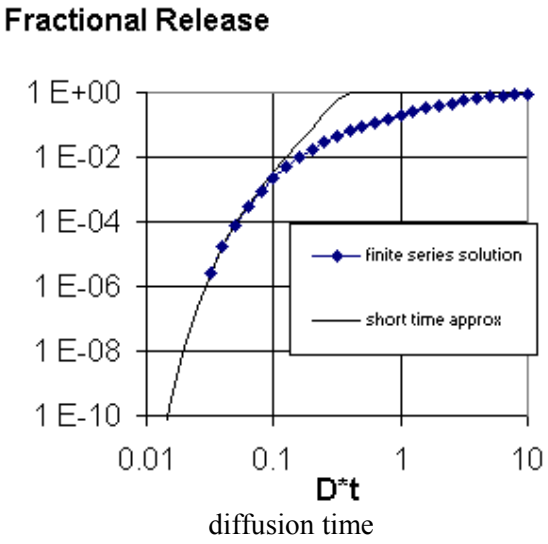

Fig. 66. Fractional release calculations based upon the exact solution and the solution for short diffusion times $\left(\tau = D^* t = {}^{Dt}\!/_{d^2} < 0.07\right)$.

For large diffusion times $\tau > 0.2$, the variables s and q in Laplace space are small and can be approximated by

$\frac{q}{\sinh q} \approx 1 - \frac{q^2}{6}$ and

$q \coth q \approx 1 + \frac{q^2}{3}$ Substituting them into Eq. (13.33a) the approximation in Laplase space is

$$\hat{F} \cong \frac{1}{2}\frac{\gamma(1+\gamma)}{s}\frac{6-q^2}{q^2+3\gamma^2+3\gamma+\gamma q^2} = -\frac{1}{2}\frac{\gamma}{s}\frac{q^2-6}{q^2+3\gamma} = -\frac{1}{2}\frac{\gamma}{s}\frac{s-6D^*}{s+3\gamma D^*} = \frac{1}{s} - \frac{1+\gamma/2}{s+3\gamma D^*} \quad (12.35)$$

For large diffusion times, i.e. $\tau > 0.2$, this approximation becomes

$$F \cong 1-\left(1+\gamma/2\right)\exp\left(-3\gamma\tau\right) \quad (12.36)$$

A comparison of the release fraction calculated using the exact solution and the approximation for long diffusion times is shown in Fig. 67. The fractional release values are nearly identical for diffusion times > 0.2.

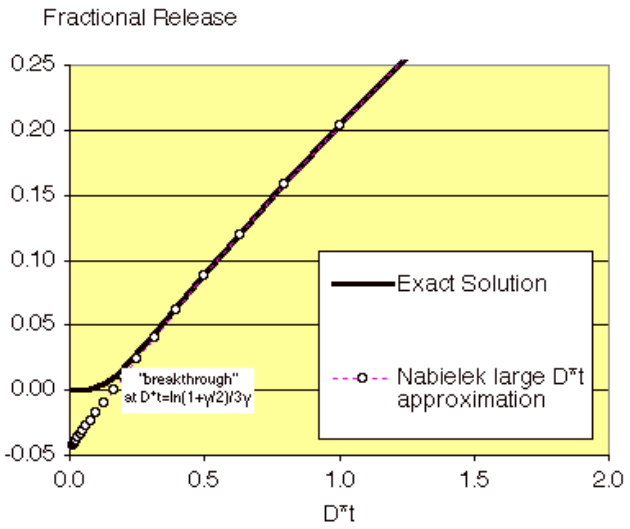

Fig. 67. Fractional release calculations based upon the exact solution and the solution for long diffusion times $\left(\tau = D^* t = Dt/d^2 > 0.2\right)$.

12.4. Verification and validation

The verification and validation status of calculation models and software used in safety calculations for design and licensing purposes are critical to the success of such an application. The terms verification and validation are defined below:

Verification: Verification is the assurance that the operations specified in a numerical model are correctly performed.

Validation: Validation is the assurance that a computational method is a correct and independent representation of the process or system for which it is intended.

12.4.1. Verification

The first step in any verification effort is to ensure that the theory and principles underlying the software product or model are clearly understood. For legacy calculation models, this usually requires reverse engineering of software and re-evaluation of parameters used. After the theory is understood, it must be ascertained that the theory has been correctly applied, followed by mathematical verification of numerical solutions.

Additionally, alternative calculation models may be used in comparisons and benchmarking exercises, for example comparison between the analytical solutions namely 'Booth equation' [161] and numerical solution for Fick's laws for short lived fission products. A comparison between different codes completes the verification effort.

In general, the computer codes used to predict fission product transport in HTGR cores are judged to have been properly verified.

12.4.2. Validation

Validation usually requires more effort, as real life experiments and benchmarks must be evaluated. A thorough evaluation of independent data available from suitable irradiation and post-irradiation heating tests is required. For spherical fuel, the irradiation tests performed in the High Flux Reactor in Petten, HFR-K5, and -K6, are highly valuable data for validation purposes. The evaluation of the heatup investigations performed in the cold finger apparatus (KÜFA) after HFR-K3 irradiation gives valuable information for metallic fission product transport validation. Measurements done during the HFR-K5 and -K6 irradiations provide good data for gaseous fission product release validation [164].

12.5. Pebble bed reactor/spherical fuel example: PBMR calculation model

12.5.1. Information required

Fuel analyses require an understanding of almost all the fields of nuclear engineering. An understanding of the fuel design and the reactor design in which it will be used are vital. The data and parameters required can be summarized as follows:

- **Core data.** The core geometry, expected core power under various operating conditions, fuel residence times and different enrichments used are required.

- **Neutronics and thermal-hydraulics.** Neutron fluxes and their corresponding cross sections for the specific nuclides of interest, along with their fission yields, must be known. In addition, removal due to neutron absorption and decay must be considered. The temperatures, pressures and flow rated of the coolant medium are also required.

- **Material data.** A thorough understanding of the fuel specifications, heat transfer and transport parameters of all fuel materials.

- **Coated particle performance.** Coated particle performance may be estimated by a calculation model or a statistical evaluation may be used. The PBMR example shown in Fig. 68 is based on a statistical evaluation of all German irradiation and heat-up testing results [165].

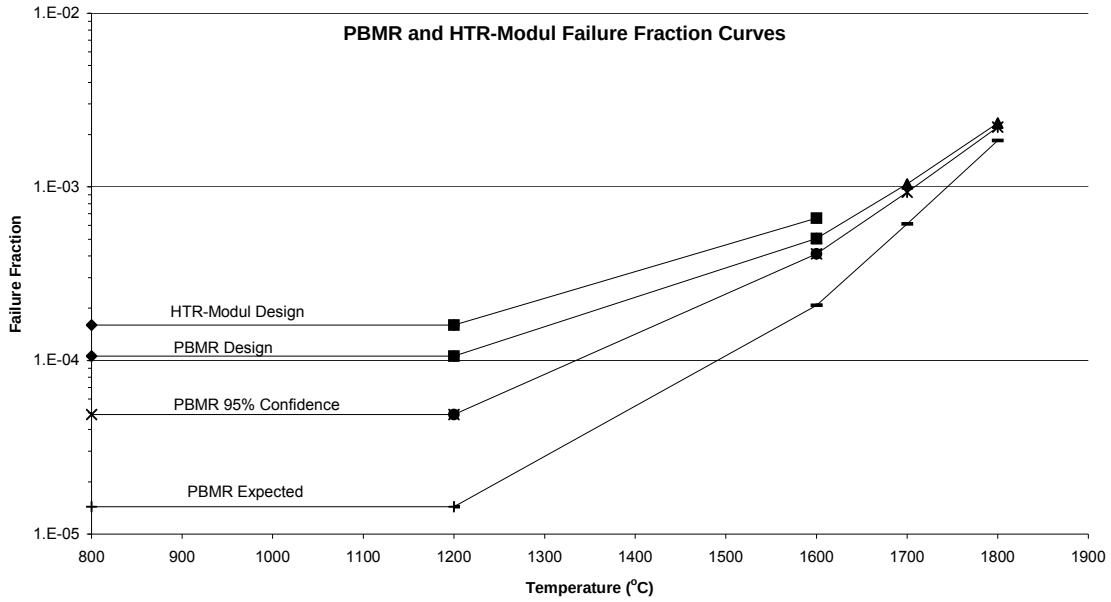

Fig. 68. PBMR and HTGR-module failure fraction vs. temperature curves.

12.5.2. Calculation models - PBMR example

The diffusion coefficient for gaseous fission product transport through a PyC layer is $\sim 2 \times 10^{-18}$ m^2/s. Then for all practical purposes, PyC can be considered impervious to fission gases [166]. Hence the gaseous fission product source term for intact coated particles can be ignored. Furthermore, the half-lives for most fission gases are relatively short and only steady-state conditions can realistically be assessed. However, this is not the case for long-lived metallic fission products. Two separate calculation models are therefore required to predict all the radiological significant fission products released from the fuel.

12.5.2.1. Short-lived fission products

The short-lived fission product calculational model is presented in Fig. 69. Releases are calculated with the NOBLEG software program, a legacy code from the German fuel development program. It is in principal based on Booth's "equivalent sphere" model, and calculates the steady state releases of fission gases from fuel [162].

It contains a thermo-hydraulic routine that calculates fuel temperatures based on the power produced and coolant temperatures in each core region. Fission product production is determined by the power produced in each core region. Transport of gaseous fission products are calculated from contamination sources in the matrix material and from defective coated particles source. Defective coated particles are treated as bare kernels. The NOBLEG transport model describing the release of fission gases from defect particles and contamination is shown in Fig. 70.

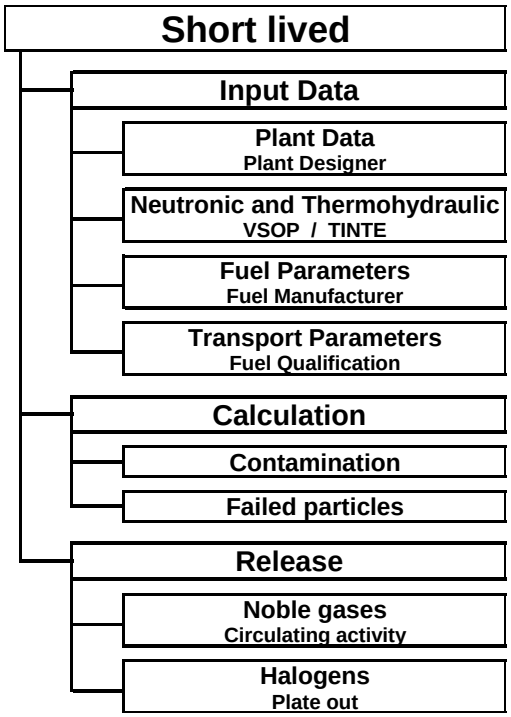

Fig. 69. PBMR short-lived fission product calculational model.

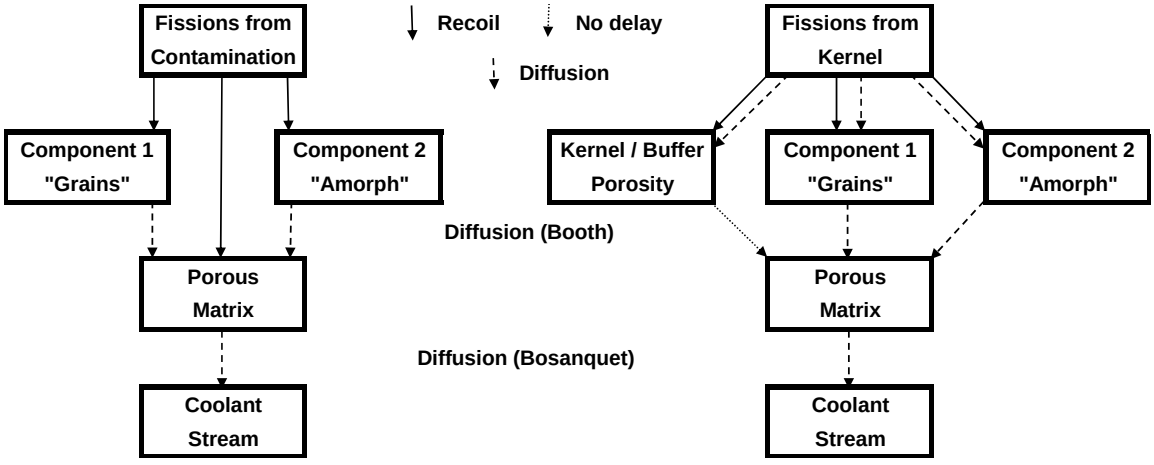

Fig.70. NOBLEG model for fission gas release calculations, after [162].

For the release of fission gases from uranium and thorium contamination in the matrix material, the graphitic material is treated as a three-component system. Component 1 may be attributed to the graphite grains of the raw material, and component 2 to the amorphous, non-graphitized binder coke between the grains. The open pore system filled with helium constitutes the gaseous component 3. Primary fission products are distributed homogeneously in these components by direct recoil. Gas atoms diffuse from the recoil sites in the grains of the solid components to the open porosity of the fuel sphere.

For the release of fission gases from defective coated particles, a four-component system is used. It consists of kernel 'grains', two material components of the buffer layer ('grains' and 'amorphous constituents'), and helium-filled open pores in the kernel and in the porous buffer layer. The birth rates of primary fission products in the four components are calculated with the known relations for the recoil stopping ranges in different materials. In the NOBLEG code these transport processes are solved separately for each model, and combined over all regions of the core. An R/B calculation for all relevant fission gases (Kr + Xe) is shown in Fig. 71 as a function of half-life.

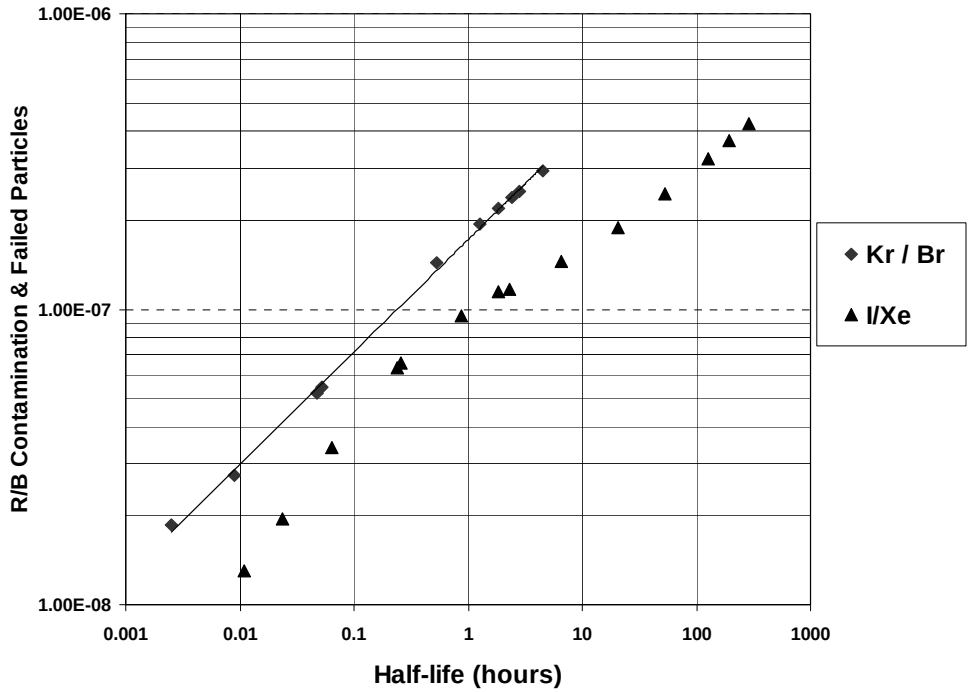

Fig. 71. Total R/B at 1000°C fuel temperature, 9 MPa helium pressure.

12.5.2.2. Long lived fission products

The long-lived fission product calculation model is presented in Fig. 72. Releases are calculated with the GETTER code [166]. It is based on Fick's laws of diffusion, and calculates the dynamic release of fission products from fuel. Differential equations are solved numerically with specific boundary conditions.

The GETTER code includes subroutines that calculate the burnup and the power history of a fuel sphere in the core and the temperature distribution in the spheres on the bases of given neutron cross sections and gas temperatures. Fission product production is determined by the power produced in each core region. Transport of metallic fission products are calculated for contamination sources in the matrix material, intact coated particles and from failed coated particles. Defective coated particles are treated as bare kernels, and intact coated particles according to the specific fuel design.

In case of activation products (^{134}Cs, ^{110m}Ag), GETTER is run two times: first for the release of the parent nuclide (^{133}Cs, ^{109}Ag); and a second time for the activation products whereby the time dependent concentration profiles of the parent nuclides define the source term for the

second run. For gas precursors (^{137}Xe -> ^{137}Cs or ^{90}Kr -> ^{90}Sr), a Booth type calculation similar to the NOBLEG model is applied.

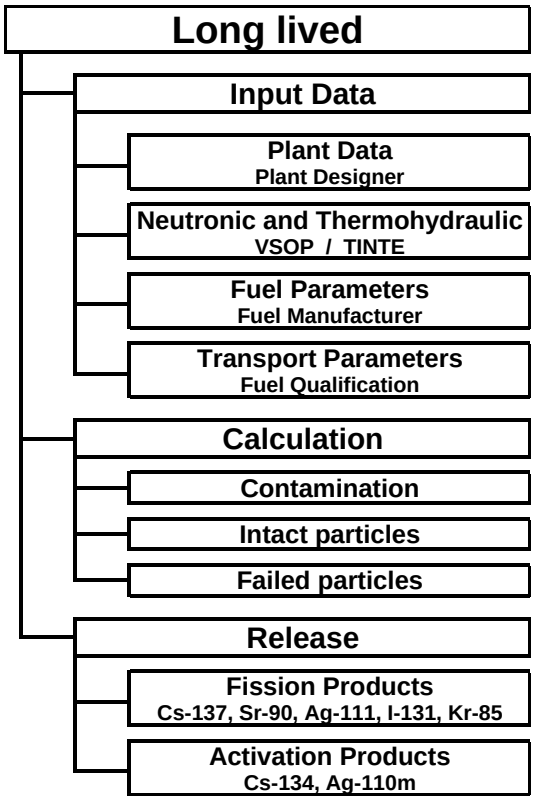

Fig. 72. PBMR long-lived fission product calculational model.

The metallic fission product section has been expanded to include non-metallic fission product analyses as well. In order to determine iodine release during accident conditions, GETTER was also equipped to handle branched diffusion coefficients. Special storage condition equations were also derived from AVR fuel element storage tests to perform ^{85}Kr release analyses under similar storage conditions.

Figure 73 describes the release of ^{110m}Ag from a fuel element (sphere) for 6 passes through an illustration PBMR core. The release increases for each subsequent pass as the fission product inventory grows and silver is transported through the fuel constituent materials.

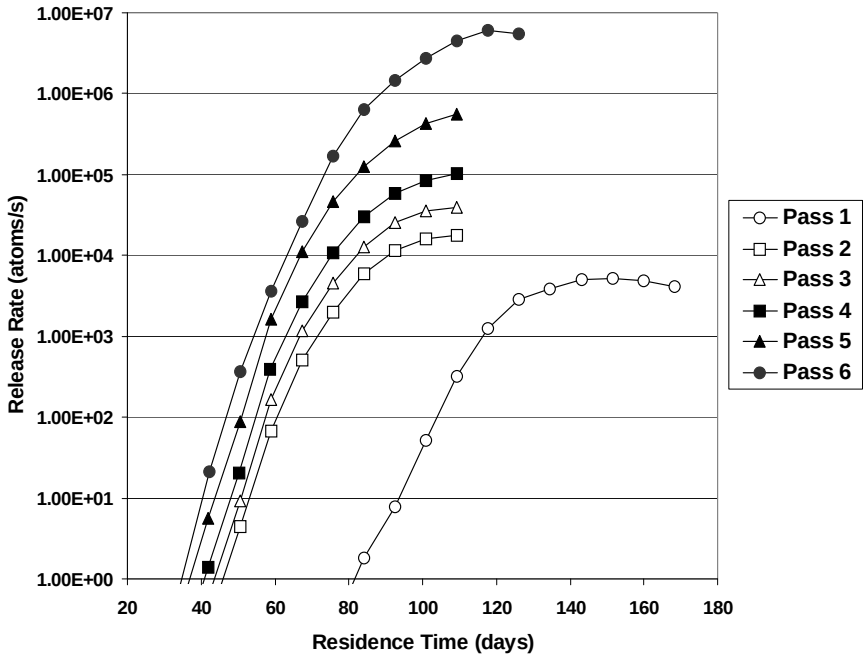

Fig. 73. Expected ^{110m}Ag release from a spherical fuel element.

12.5.2.3. Full core analyses

The PBMR core consists of a bed of spherical fuel elements. The fuel elements are introduced at the top of the core, flow downwards and exit from the base of the core. This flow pattern is modeled using a number of vertical flow channels, each flow channel being axially subdivided into core regions. A typical PBMR core is modeled as 4 to 6 flow channels, with each channel consisting of between 10 and 20 axial subdivisions, resulting in 70 to 120 core regions. The axial subdivisions are chosen so that the residence times for the fuel elements in all core regions are equal, typically 8 to 12 days. These core regions, not necessarily of equal volume, are used by the core neutronics, thermo-hydraulic and fission product release codes to model the entire core.

Depending on the fuel-loading scheme, the fuel elements may pass through the pebble bed core up to 16 times before finally being discarded. The core, therefore, consists of a random mixture of fuel elements with different irradiation histories.

The GETTER code calculates the fission product release rate for a single fuel element at each time-step throughout its residence history in the core. In order to accurately represent the entire core (approximately 450 000 fuel elements in the 400 MW_{th} design), individual fuel-element histories are sampled and a GETTER calculation performed for each. The results are then combined using arithmetic averaging and normalization to determine total core release rates.

This implies that GETTER must calculate all the fuel element release histories in the core for all the possible irradiation histories, given that the irradiation and temperature conditions in each flow channel of the core are unique. Performing GETTER calculations for each of the 450 000 elements in the reactor core are not feasible. Furthermore, exact calculation of

DLOFC-type accidents would be virtually impossible because the accident can occur at any time-step in a specific fuel element's irradiation history.

However, it was found that significantly smaller sample sizes give satisfactory statistical convergence. Multiple independent calculations using sample sizes of 10 000 fuel elements, for example, showed a variance in calculated release rates of <1%. The FIPREX-GETTER software was developed to generate GETTER input files for both normal operation and accident conditions [166]. Accident conditions can be defined and the time of accident specified.

Figure 74 presents the predicted ^{111}Ag release from the illustration PBMR core during four different accident events. A medium pipe break with very short coolant depressurization and small pipe breaks with depressurization times of 24, 48 and 72 hours.

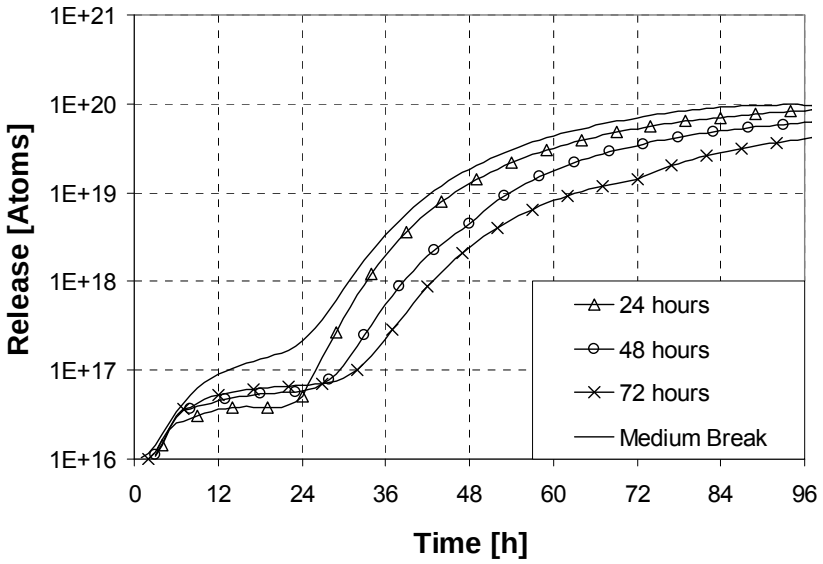

Fig. 74. Predicted ^{111}Ag releases from fuel during small and medium pipe break accident events as a function of accident duration.

12.5.2.4. Uncertainty analyses

Input parameters, values and data sets that include uncertainty in their derivation are investigated to determine a design value for fission product release under the specified operating conditions. Uncertain parameters and values can be categorized and described as follows:

- The diffusion coefficients describing metallic fission product transport through the fuel materials were derived from irradiation experiments conducted on TRISO particles, fuel compacts and complete fuel spheres. Due to uncertainties in the measurements taken during irradiation and in irradiation conditions, uncertainty factors of between two and eight were suggested for metallic diffusion constants.
- The fuel specification allows maximum values for the uncontained uranium fraction of 6×10^{-5} and the thorium contamination of 0.4 mg thorium per spherical fuel element. This defines upper limits for the failed particle fraction, the uranium

contamination and the thorium contamination of 5.6×10^{-5}, 4.0×10^{-6} and 6.0×10^{-6} (effective), respectively.

- The uncertainty in the sorption isotherm was calculated by assuming a variation in the partial pressures by a factor of four.
- Thermo hydraulic uncertainties in the material properties and correlations used lead to uncertainties in fuel temperatures.
- The statistical evaluation of German irradiation experiments with TRISO UO_2 particles showed that due to the restricted sample size (Poisson distribution), growing failure fractions cannot be excluded at burn-ups above 5% FIMA. The uncertainty in the failure fraction under excessive temperature is derived from statistical evaluations of experimentally measured failure fractions. These expected curves and their uncertainty ranges were modeled and are used in design calculations.
- Neutronic uncertainties are cross section and neutron fluxes that lead to uncertainties in power production, temperatures, burn-up and inventories.

Three types of uncertainty analyses have been developed:

- S**tacked uncertainty analyses**. All uncertain parameters are simply set to their design parameters and the calculation is performed. This method is most conservative, relatively simple to perform, and easy to defend.
- **Monte Carlo analyses**. For each parameter, a suitable probability distribution is chosen and values are randomly sampled (example shown in Figure 74. After the Monte Carlo calculations are done, the upper 95% confidence limit is determined from the sampled output. This complicated method calculates the lowest design values, but is very difficult to defend.
- **Least squares analyses.** Each uncertain parameter is evaluated separately. The result is squared and added to the squared results of all the other parameter evaluations. The square of this sum gives the design value. Most information is extracted from this method, but is extremely time consuming.

All three uncertainty analyses methods have their place in core design and analyses. Monte Carlo analyses is quick and can be used to compare different core designs, least square analyses tells us what parameters are most important for different conditions, and stacked analyses provides the upper limit for design calculations for licensing applications.

12.6. Prismatic core reactor/graphite block - HTR-GT example

12.6.1. Introduction

A characteristic feature of HTGRs is the essential role of the coated fuel particle acting as miniature containment and serving as the main barrier against radionuclide release under all operational and accidental conditions. The performance of TRISO fuel particles and other types of coated fuel particles has been extensively investigated and a number of performance models developed. Previously published fuel performance models were largely developed in the US, the UK and Germany [167]. A detailed compilation of these models has been published as an IAEA-TECDOC-978 [16].

The following present a description and gives some preliminary results of the fission product diffusion model, developed at AREVA NP.

Objective

The main purpose of this work is to estimate, as an example, the inventory of the fission product ^{137}Cs released into helium coolant of the core of the Japanese 600 MW_{th} HTR-GT concept. These results are then compared with the available calculated values from the JAEA Japanese team [168] for their 600 MW_{th} HTR-GT concept.

12.6.2. Diffusion model hypothesis in the particle

Fick's diffusion with an equivalent diffusion coefficient that generalizes all diffusion mechanisms is adopted. The source term in the kernel and radioactive decay must be added to complete the mass balance:

$$\frac{\partial c}{\partial t} = \nabla \cdot D\nabla c - \lambda c + \dot{S} \tag{12.8}$$

c: fission product concentration (m^{-3})
λ: decay constant ($7.297.10^{-10}$ s^{-1} for ^{137}Cs)
S: source term ($m^{-3}.s^{-1}$)
D: equivalent diffusion coefficient of the considered layer, $D = D_0 \exp\left(-\frac{Q}{RT}\right)$
Do: pre exponential term ($m^2.s^{-1}$)
Q: activation energy ($J.mol^{-1}$)
R = 8.3145 J/mol/K
T: temperature (K)

Equivalent diffusion coefficients :

According to the IAEA publication reference [16], the values for the pre-exponential term (D_0) and the activation energy (Q) which defines the ^{137}Cs diffusion in the fuel constituent materials in this study are shown in Table 16.

Table 16. PRE-EXPONENTIAL AND ACTIVATION ENERGY COMPONENTS OF THE EQUIVALENT DIFFUSION COEFFICIENT FOR CESIUM IN FUEL CONSTITUENT MATERIALS FOR THE HTR-GT CONCEPT [168]

	Equivalent Diffusion Coefficients (m^2/s)						
	UO_2	Buffer	iPyC	SiC	oPyC	Compact Matrix	Graphite Block
Pre-exponential (m^2/s)	$6.75x10^{-6}$	$6.69x10^{-6}$	$6.69x10^{-9}$	$6.75x10^{-12}$	$6.69x10^{-9}$	$3.6x10^{-4}$	$9\ x10^{-6}$
Activation Energy J/(mol)	177 000	197 880	197 880	177 000	197 880	189 000	157 140

12.6.3. Fraction of defective fuel particles

Three types of particle have to be considered:

1. **Particle with A Failed SiC Layer** (Fig. 75). The diffusion coefficient of the defective layer is replaced by the PyC value. The fraction of coated particles with this defect in the total particle population is equal to $5x10^{-4}$ according to reference [168].

2. **Exposed UO_2 Fuel Kernels** (Fig. 76). These particles have all their coatings completely failed allowing fission products to migrate directly and rapidly outside the particle. The fraction of coated particles this type of particle is equal to 2.10^{-5} according to reference [168].

3. **Intact Particles** All the coatings of these particles are unbroken.

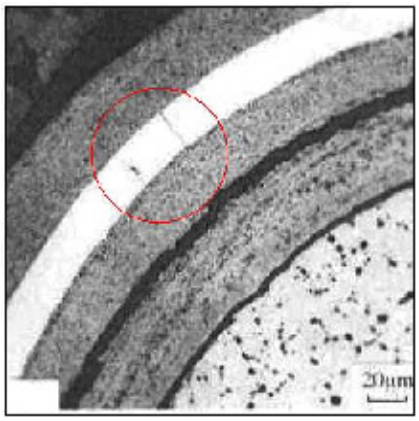

Fig. 75. Photomicrograph of an irradiated particle with a through-crack in the SiC layer.

Fig. 76. Irradiated particle with through cracks in all of its coating layers (iPyC, SiC, oPyC, and an outer protective layer).

12.6.4. Diffusion from the fuel compact or graphite block to the coolant

It is necessary to know the fraction of fission products that pass through the graphite block to the helium coolant. At the boundary between a solid and a gas, the transition of diffusing atoms occurs by the processes of sorption and evaporation. In most cases, these two processes are so fast that a local equilibrium between the concentration of atoms adsorbed at the solid surface and the concentration of atoms in the neighboring layer of gas ("vapor pressure") may

be assumed. This means that the phenomenological data of importance is the sorption equation which relates these two equilibrium values.

Generally the equilibrium vapor pressure in the gas phase is expressed as a function of the fractional coverage of the solid surface by adsorbed atoms. In practice, adsorption is mainly of importance in the case of porous solids which have a large internal surface area per unit weight. The vapor pressure is expressed as an exponential function of temperature and adsorbed concentration.

The transition of metallic fission products between fuel element surface and the turbulent coolant is described by sorption isotherms. Figure 77 [16] is an example of the sorption isotherms in the case of cesium on H-451 graphite.

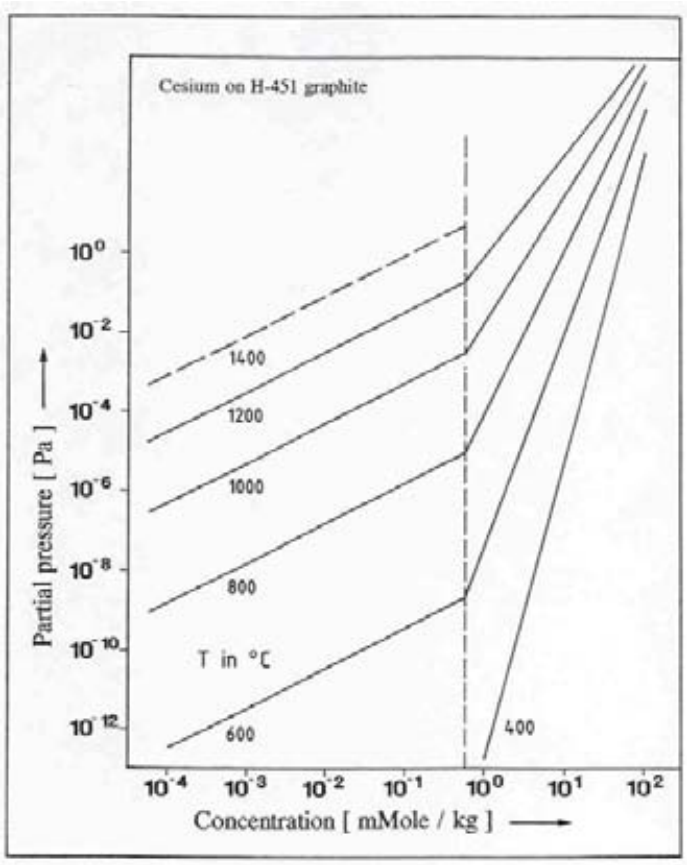

Fig. 77. Sorption isotherms for cesium on H-451 graphite [16].

To determine the concentration of fission products in the helium when it is known in the graphite, the relevant equations are the Henry's law, the Freundlich's law and the ideal gas law. The partial pressure is assumed to be the sum of the pressures calculated with the two isotherms (see Fig. 77):

$$p = p_H + p_F, \tag{13.14a}$$

Henry's law dominates at low concentrations and which supposes an adsorption heat directly proportional to the pressures and the concentrations of the adsorbed species and is given by the expression:

$$p_H = c_s \exp\left[\left(A + \frac{B}{T}\right) + \left(D - 1 + \frac{E}{T}\right) \ln c_t\right], \tag{12.15}$$

Freundlich's law dominates at higher concentrations and assumes a decreasing adsorption heat and an increasing concentration is given by the expression:

$$p_F = \exp\left[\left(A + \frac{B}{T}\right) + \left(D + \frac{E}{T}\right) \ln c_s\right], \text{ and} \tag{12.16}$$

transition at c_t: $\ln c_t = d_1 - d_2 T$, (12.17)

where T is the absolute temperature (K)
c_s is the mass concentration of sorbate (mol/kg of carbon or graphite)
A, B, D, E, c_t, d_1, d_2 are empirically derived constants given in [16].

The ideal gas law is applied to the sum of both Henry and Freundlich pressures.

From the boundary helium gas layer, fission products are transported into the coolant. The governing equation in the helium coolant is given by:

$$\frac{\partial c_{He}(x,t)}{\partial t} = -\frac{\partial v(x) c_{He}(x,t)}{\partial x} - \frac{k_m(x,t).p_L(x)}{A_f(x)}(c_{He}(x,t) - c_b(x,t)) \tag{12.38}$$

where:

c_{He}:	concentration of fission product in turbulent helium gas stream;
c_b:	concentration of fission product in boundary layer;
A_f:	sectional flow area (m^2);
k_m:	mass transfer coefficient ($m.s^{-1}$);
p_L:	wetted perimeter (m);
v:	helium velocity ($m.s^{-1}$).

In the Japanese model [168], a global parameter "α" is introduced and used as the ratio of an absorbed fission product concentration to a transported fission product concentration.

Figure 78 shows the global parameter "α" as a function of temperature over the range of 100°C to 900°C for the fission product ^{137}Cs and the activation product ^{110m}Ag. Above temperatures of 700°C, the concentration ratio for key fission products between the helium coolant and graphite is given by $c_{He} = 0.9\ c_{Gr}$. These simplified functions are based on measurements made at Peach Bottom HGR Nuclear Power Plant.

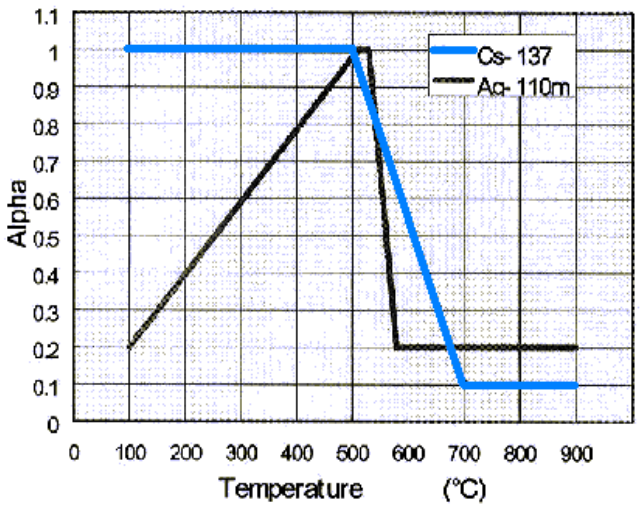

Fig. 78. The global parameter "α" which represents the concentration ratio of absorbed fission product to a transported fission product as a function of temperature [168].

12.6.5. Fuel loading scheme

During its lifetime within the prismatic core, a hexagonal fuel assembly occupies three different locations within the core and experiences three different ranges of temperature before being removed from the plant. Modeling this subassembly redistribution within the core is complicated. In order to simplify, and at this step of evaluation, a so called Daruma-Otoshi fuel loading scheme is adopted. This is a simplified scheme which well represents the more complicated real one. It models and shares the whole core in nine equivalent blocks which are grouped by three. This Daruma-Otoshi scheme is employed in the Japanese code FORNAX [168] and for the HTR-GT is represented in Fig. 79 below:

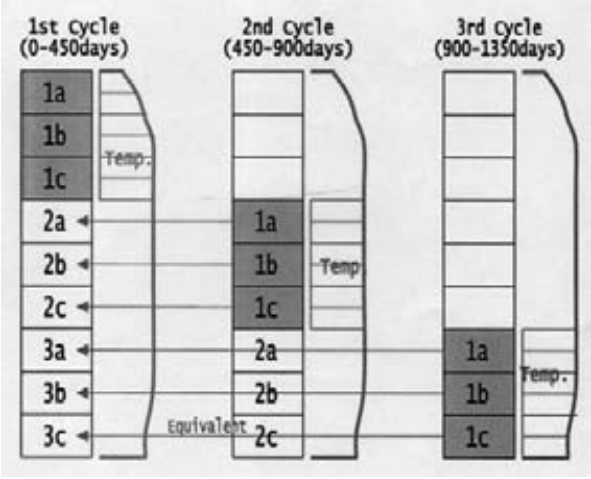

Fig. 79. The HTR-GT Daruma-Otoshi fuel loading scheme employed in the Japanese code FORNAX [168].

12.6.6. Temperature maps

12.6.6.1. In TRISO coated fuel particles

For the TRISO particles of HTR-GT project, the temperature profile shown in Fig. 75 is representative of steady- state normal operating conditions.

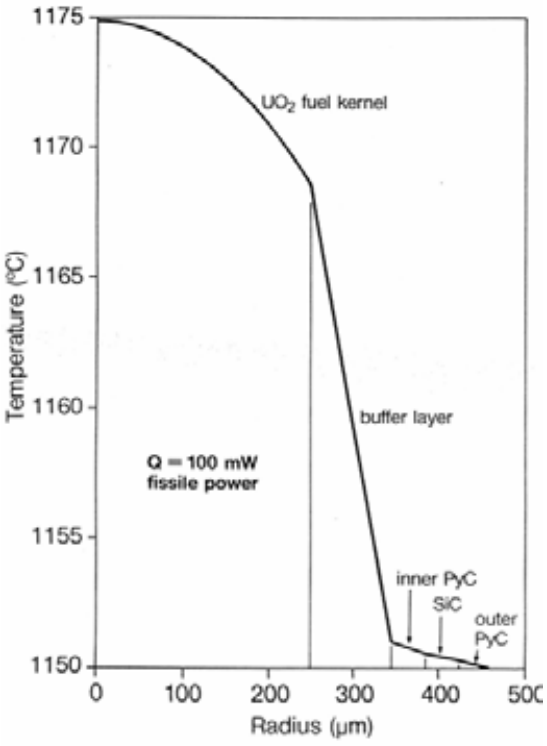

Fig. 80. Temperature profile across the UO_2 TRISO coated particle in a typical high temperature reactor operation.

12.6.6.2. In the compact matrix and graphite blocks

The temperature distributions in the fuel compact matrix and graphite blocks of the HTR-GT, calculated in the AREVA NP studies, have been adopted for steady- state normal operating conditions. These temperature distributions are shown below in Fig. 81. A comparison of the temperatures experienced in the helium coolant, fuel compacts and hexagonal block graphite as a function of core height are shown in Fig. 82. These temperatures are also from the AREVA NP studies.

In order to apply a "Daruma Otoshi" Fuel Loading Scheme [168], the hexagonal graphite columns are divided in nine fictitious blocks and for each column an exponential average temperature has been calculated as it is done for the different layers of a TRISO particle. Nine equivalent diffusion coefficients linked to the height in the core are then obtained.

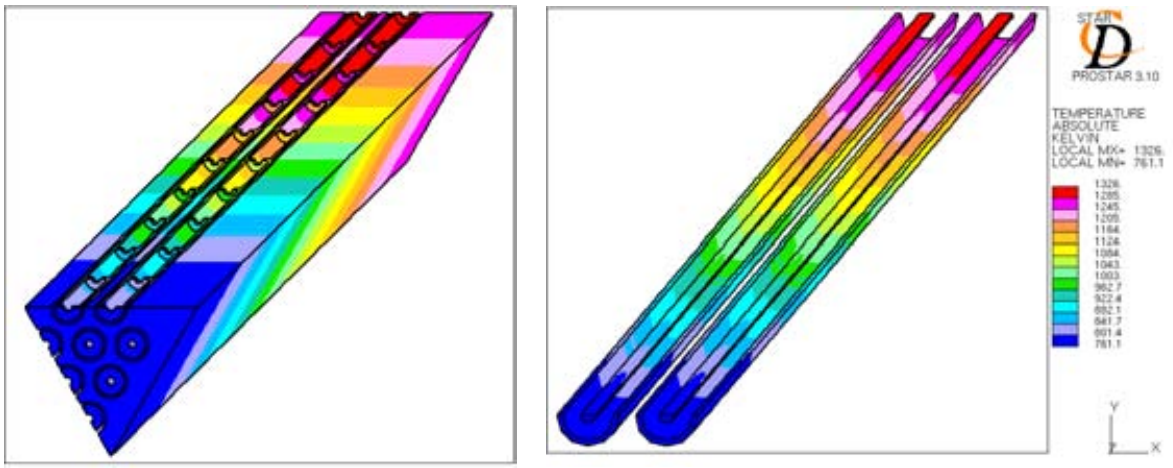

HTR-GT temperature distribution in a graphite column

HTR-GT temperature distribution in helium

Fig. 81. Temperature distributions in the fuel compact and hexagonal block graphite for the NTGR-GT concept based on analyses performed by AREVA-NP.

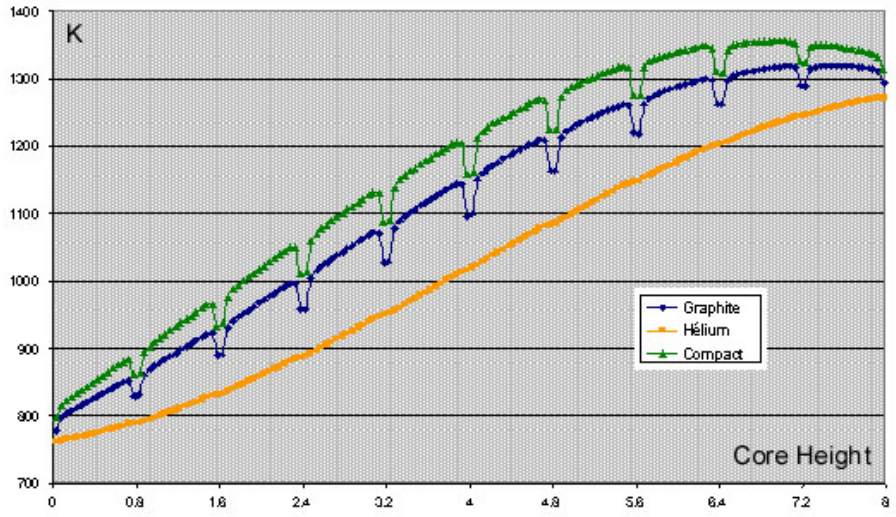

Fig. 82. Temperature comparison as a function of core height for the He coolant, fuel compacts and graphite blocks in the HTR-GT concept.

12.6.7. Finite difference code description

The code developed for calculating the release of a single metallic fission product nuclide (e.g., ^{137}Cs) from the core of a HTGR is a one-dimensional, finite difference computer program. It calculates the diffusive transport of fission products through multi-layered coated particles, graphite matrix (compact and hexagonal block or spherical elements), equilibrium evaporation and condensation at the graphite surfaces, and diffusion across the coolant boundary layer. The code is based on the discretization of the selected Fickian Diffusion Law by means of the Forward Time Centered Space scheme.

The adopted equations are:

$$\frac{\partial c}{\partial t} = D \cdot \left[\frac{\partial^2 c}{\partial x^2} + \frac{\partial^2 c}{\partial y^2} + \frac{\partial^2 c}{\partial z^2} \right] - \lambda c + \dot{S} \tag{12.8a}$$

in Cartesian co-ordinates (for graphite block geometry),

$$\frac{\partial c}{\partial t} = D \cdot \frac{1}{r^2} \frac{\partial}{\partial r} \left(r^2 \frac{\partial c}{\partial r} \right) - \lambda c + \dot{S} \tag{12.8b}$$

in spherical co-ordinates (for TRISO particles geometry), and

$$\frac{\partial c}{\partial t} = D \cdot \frac{1}{r} \frac{\partial}{\partial r} \left(r \frac{\partial c}{\partial r} \right) - \lambda c + \dot{S} \tag{12.8c}$$

in cylindrical co-ordinates (for compact geometry).

The explicit scheme employed can be unstable if the parameters ∂t and ∂r do not verify stability criteria. The Von Neumann Stability Analysis is a stability criterion that is applied to all the calculations. For the three systems of co-ordinates, the Forward Time Centered Space scheme applies to our equation is stable if:

$$\frac{2D \cdot dt}{dr^2} + \lambda \cdot dt \leq 1 \tag{12.39}$$

.

Thus, the values of ∂t and ∂r chosen in the code are always verified by this criteria.

12.6.8. Results

Table 17 summarizes the ^{137}Cs release results obtained with the AREVA NP evaluation and compares it to the results obtained in by the JAEA [168].

In the AREVA NP modeling analysis, nearly all of the main Japanese hypotheses (fuel loading scheme, TRISO particle design and core dimensions, sorption - desorption simplified function, diffusion coefficients, etc.) were used as in the JAEA in-house code FORNAX [168]. Since the diffusion coefficients are being exponentially dependant on the temperature, a relatively small difference in the selected temperatures can explain the difference between the two evaluations.

Table 17. COMPARISON OF THE ^{137}CS INVENTORY RELEASED TO THE COOLANT FOR THE HTR-GT CONCEPT FROM THE AREVA NP ANALYSIS WITH THE JAEA RESULTS [168]

HTR-GT Concept	AREVA NP Result	JAEA Result
^{137}Cs Released to Coolant after 450 days of operation	11.25 x10^{12} Bq	15.84 x10^{12} Bq

13. HTGR FUEL CYCLES

13.1. Introduction

This chapter examines the HTGR fuel cycle from the “front-end” perspective. The available fuel cycle-related options are examined along with the basis for the subsequent choice of fuel type and cycle from the “back-end” perspective. The generation and management of spent fuel and graphite waste are examined in Chapter 15.

The HTGR has the inherent flexibility to accommodate many fuel types and to permit full cost-effective optimization. The reasons for this flexibility are presented and the main advantages and disadvantages of the various fuel cycles are discussed.

The amount of spent fuel and graphite waste generated by the HTGR is governed by the burnup capability of the fuel. The near-term and long-term options for dealing with the waste streams are also examined.

The HTGR is a promising concept that can meet the requirements of enhanced safety, higher efficiency, fuel cycle flexibility, competitiveness and waste management in an environmentally responsible and sustainable manner. Evaluations performed by the Generation IV International Forum concur with this assessment [169]. Fuel cycle issues of HTGRs in general assessing nuclear materials flow is described in detail by Shropshire [170].

13.2. An assessment of HTGR fuel cycle flexibilities

Due to their unique features, graphite moderated HTGRs can accommodate many types of fuel cycles. The fundamental reasons for this flexibility are presented below.

The advantage that makes the HTGRs particularly attractive and distinguishes them from other reactor types is its fuel: a refractory fuel with sealed coated particles embedded in a graphite matrix cooled by helium. Because of this unique arrangement of fuel, moderator, and coolant, HTGRs can accommodate a variety of mixtures of fissile and fertile materials without significant modification to the core design. This flexibility comes mainly from the near perfect uncoupling of the parameters that determine cooling geometry, and the fundamental parameters that characterize neutronic optimization; that is, the moderation ratio or the concentration and space distribution of heavy nuclei which determine the self shielding effect. It is possible to modify the packing fraction of coated particles (up to a value of ~60%) within the graphite matrix without changing the basic dimensions of the fuel elements. It is also possible to change the size of the fuel kernels, or the relative proportions of the various particle types containing different nuclear materials. Hence, many degrees of freedom exist to optimize the HTGR core that facilitates achievement of fuel cycle management objectives.

There are other more physical reasons that contribute to the fuel cycle adaptability in the HTGRs as compared with reactors using liquid moderators, such as light water reactors (LWRs). As an example, the moderator void coefficient limits the plutonium content of pressurized water reactor (PWR) mixed-oxide (MOX) fuels. In the event of complete loss of coolant in a PWR, the neutron spectrum becomes very "fast" (the neutrons exhibit a very high average speed since they are no longer slowed down). Under these conditions, the neutron multiplication factor due to plutonium isotopes increases considerably (the reproduction factor increases significantly for fast neutrons). Clearly, this is not a constraint for graphite-moderated reactors. Note also that an HTGR core has a significantly better neutron economy than a PWR core because there is much less parasitic capture in: (1) the moderator (the

capture cross section of graphite is 100 times less than that of water), (2) internal structures (there are no metal materials to capture neutrons); and (3) fission products (the spectrum is harder and fission products tend to capture more neutrons as they become thermalized).

The performance of TRISO-coated particle plutonium or uranium fuels is such that they are capable of attaining very high burn-ups, ranging upwards of hundreds GWd/tHM. This capability has been confirmed through irradiation tests conducted since the inception of the particle fuel concept [171]. While not pushed to these higher burnup capabilities, actual experience with particle fuel in the Fort St. Vrain, AVR, THTR and, more recently at the HTTR and HTR-10 has validated the particle fuel concept at an operational level.

The flexibility that the HTGR particle fuel form extends to the choice of fuel cycle hinges on the performance of the particle fuel itself. The ability of coated particle fuel to reliably retain fission products over a wide range of conditions is of fundamental importance to modular HTGR designs. Fuel performance and fission product behavior was the subject of an IAEA Coordinated Research Project which begun in 1992 and lasted four years, with participating countries including China, Germany (G), Japan, Poland, the Russian Federation, the United Kingdom (UK) and the United States (USA). This significant work on particle fuel performance, reported in IAEA-TECDOC-978 [16], summarized the nearly 30-years of particle fuel experience in existence at that time. In addition to surveying the national program activity in progress, this report comprehensively summarizes the operating experience relative to fuel performance for the following HTGRs: Dragon (UK) [172], Peach Bottom Unit 1 [173] and Fort St. Vrain (USA) [174], and AVR (G) [175] and THTR (G) [176].

Despite the collective amount of irradiated particle fuel performance data, additional performance data, specific to modern HTGR fuel, needs to be developed so that acceptable performance of the fuel under normal and accident conditions can be confirmed. Unlike any prior reactor design, the safety case for the HTGR relies on the retentive capability of the particle fuel. That retention capability, along with the thermo-limiting characteristic of the core-reactor vessel system, is the key, not only to inherent safety, but economic success as well.

13.3. A review of possible HTGR fuel cycles

A general assessment of the fuel cycles that may be used in an HTGR is presented in [177]. The starting point is to find a comprehensive set of possible fuel cycles in a nuclear reactor by considering all combinations of the basic components of a nuclear fuel: that is: (1) fissile material, which may be ^{235}U, ^{233}U or plutonium; and, (2) fertile material, which may be ^{238}U or ^{232}Th. This systematic approach leads to a list of seven possible fuel cycles, which can be grouped into four categories:

- "**L**ow **e**nriched **u**ranium" (LEU) fuel cycle;
- "**M**ixed oxide (MOX) fuel cycle;
- "Plutonium only" fuel cycle; and
- "Thorium based" fuel cycle.

Each of these categories is examined below.

13.3.1. Low-enriched uranium (LEU) cycle

Despite its name, applied to distinguish it from the highly-enriched uranium (HEU) cycle, the LEU cycle actually uses uranium with enrichments up to 20% depending on the reactor type.

These are actually high enrichment levels as compared to other thermal reactors. This is primarily due to a rather diluted and homogeneous uranium distribution in HTGR fuels which favors resonance captures by fertile nuclei (in this case ^{238}U nuclei). This situation reduces the self-shielding effect due to these resonances. Self-shielding arises when an isotope that exhibits absorption resonances (capture or fission) is concentrated in a given medium. The result is that the neutron flux is depressed both in space and energy at the level of the resonances, considerably reducing the effective absorption rate of the resonances. Naturally, the reverse happens when the isotope becomes increasingly diluted. These captures are, moreover, increased by the under-moderation of HTGR cores to limit their size. In older gas-cooled, graphite-moderated reactors, the moderation ratio had to be set at the optimum to avoid excessive resonant capture, because of the very "tight" neutron balance of such reactors using natural uranium (no enrichment).

The LEU cycle was studied in the USA, Germany, UK and France during the 1960s and 1970s. As a result of studies performed by the French Commissariat à l'Énergie Atomique (CEA) in the late 1970s as part of their contribution to the "International Nuclear Fuel Cycle Evaluation" carried out under IAEA leadership, France officially selected as the LEU cycle as the reference cycle for HTGR development 1979 [178]. This decision was made moot by France's decision to stop HTGR related programs in order to pursue other reactor technologies at that time. Germany continued with HTGR technology development and selected the LEU cycle in 1980. Today, all current commercial projects are based on this fuel cycle with the exception, naturally, of the GT-MHR Project [179] being developed in cooperation between the U.S. and Russia that is dedicated specifically to the consumption of weapons-grade plutonium.

The LEU cycle appears as the most appropriate cycle for near term commercial deployment and it has already been used in HTGRs. Its main advantage is the large commercial experience base as uranium oxide fuels are in use in almost all of the power reactors in operation worldwide. Consequently, the LEU cycle has been selected as the reference cycle for all the HTGRs on-going projects.

13.3.2. Mixed oxide (MOX) cycle

As in pressurized water reactors (PWRs), deployment of a mixed plutonium/depleted uranium fuel can also be envisioned. This mixture currently takes the form of a mixed oxide (MOX), but it could also take a different form, such as carbides, or even nitrides for example.

In practice, for both strategic and historical reasons, MOX was developed after the cessation of earlier HTGR programs and this type of fuel cycle has never really been studied for HTGRs. However, the CEA in France conducted some exploratory neutronic studies about ten years ago. The results were published in reference [180].

Studies show that this cycle in HTGRs performs similarly to MOX fuel cycles in LWRs with regard to plutonium consumption, and in HTGRs it offers more flexibility for better optimization. However, concerning plutonium consumption, the MOX cycle for HTGRs does not offer a significant advantage compared to the "plutonium-only" cycle.

13.3.3. Plutonium-only cycle

As part of the search for solutions enabling improved "control" of plutonium, current efforts are focused on maximizing plutonium consumption. Studies [171], [181] have been conducted to assess the feasibility and performance of plutonium cores containing no fertile

material at all. This solution of “plutonium-only” cores, a unique feature of HTGRs, was investigated by the U.S. and Russia as part of the GT-MHR program to examine consumption of excess weapons-grade plutonium.

The plutonium-only cycle would need an extensive research and development program to develop and qualify a fuel capable of reaching the burn-up levels envisaged by current projects, although experimental fuels have already been tested at such burn-up levels in reactors in the past (for example the DRAGON reactor [172] and the Peach Bottom Reactor [173]). The costs and lead times involved in developing plutonium fuels for HTGRs were the main reasons behind the U.S. Department of Energy’s (US-DOE) decision not to consider this solution as a means of “burning” weapons-grade plutonium in the USA. (see reference [182] for assessment). Moreover, the neutronic-related difficulties which could potentially arise with "plutonium-only" cores should not be underestimated. Studies for prismatic element cores illustrate this. Difficulties such as control of changes in reactivity (using erbium-type poisons), moderator temperature coefficient (risk of positive coefficient), low fraction of delayed neutrons, and increased residual heat were encountered.

13.3.4. Thorium-based cycles

a) Thorium – high enriched uranium (Th / HEU) cycle

Thorium generates ^{233}U, which is by far the best fissile isotope for thermal spectrum reactors. This is because of ^{233}U’s nuclear characteristics in terms of neutrons released in the fission process. In a thermal spectrum reactor like that of HTGRs (and PWRs), the neutron multiplication factor η (the average number of neutrons produced for each neutron absorbed in the fissile isotope) is 2.29 for ^{233}U, but only 2.05 for ^{235}U, and only 1.80 for ^{239}Pu. This makes breeding theoretically possible in a thermal reactor with fuel using ^{233}U. This possibility was demonstrated under experimental conditions in the Shippingport reactor (USA) [183] in the early 1970s, although the technological configuration used would be difficult to transfer to power reactors.

The main advantage of the HEU/Thorium fuel cycle, which has been extensively studied for HTGRs, is reduced natural uranium consumption when operating in a closed cycle. The HEU/thorium cycle is particularly well-suited to this type of fuel because it can potentially reach very high conversion factors and, with ^{233}U recycling, reduce natural uranium requirements by a factor of 2 or more.

For the above reasons, the HEU/Thorium cycle was the reference fuel cycle during early HTGR development in both the USA and Germany. These two countries initially led the research in this reactor type. Four HTGR prototype power reactors were designed, constructed and operated with this type of fuel cycle: the AVR and the THTR in Germany, the Peach Bottom and the Fort Saint Vrain in the USA. All are now shutdown. It should be noted that the AVR, in contrast to the other cited reactors, was not solely dedicated to the use of HEU/Thorium fuel but was used to test other fuel types as well.

Despite the HEU/Thorium cycle’s advantages cited above, it has not been developed commercially beyond the reactors mentioned above for a number of reasons: its competitiveness, the attendant recycling difficulty due to the high radiation level of ^{232}U daughter products (^{208}Tl, ^{212}Bi), and proliferation concerns. These factors are definitely subordinate to the primary reason - the widespread adaptation of LEU light water reactor

technology and the accompanying development of the significant LWR-supporting infrastructure.

The future re-deployment of the HEU/Thorium cycle on a grand scale will undoubtedly require significant research and development along with heavy industrial investment. Furthermore, barring a shortfall of natural uranium supply, commercial development of the HEU/Thorium cycle will be isolated to countries with very unique nuclear situations. A prime example of this is India, a country that has several factors favoring development of the HEU/Thorium cycle: (1) nuclear energy is vital to India's economic growth; (2) the current political situation that bars India from access to the global uranium market; (3) India has very little natural uranium resources; and (4) India has significant thorium resources, estimated at about 600 000 tonnes. Given these factors, India is embarking on a program to ultimately integrate, symbiotically, the HEU/Thorium cycle into its commercial nuclear market. In the absence of any of the cited factors above, India most probably would not embark upon such a course.

The competitiveness of this cycle is questionable today, particularly given the considerable uncertainty regarding estimates of thorium cycle costs, not the least of which is the cost of thorium itself, since the market for this material is practically non-existent. Its main technical hurdle is ^{233}U recycling due to difficulties arising from the significant gamma activity emitted by some daughter products of ^{232}U, which are present as an admixture with ^{233}U. This means, in practice, that the fuel has to be re-fabricated remotely in shielded facilities (hot-cells). Technically, such operations are feasible but significant research and development effort would be necessary to implement it on an industrial scale and make it profitable. Finally, it is clear that, regardless of the potential merits of this cycle, it would be nearly impossible to market in the current climate, given the use of highly-enriched uranium (HEU) and the associated problem of proliferation.

b) Thorium - medium-enriched uranium (Th / MEU) cycle

Studies of the intermediate MEU/Thorium cycle began in the U.S. in the late 1970s as a result of the non-proliferation policy initiated by President Carter. At that time, the aim was to investigate fuel cycles capable of minimizing proliferation risks associated with the use of fissile materials suitable for the manufacture of nuclear weapons. The HEU cycle for HTGRs was considered to be highly proliferating. Therefore "denatured" cycles with limited uranium enrichment levels of <20% ^{235}U (or <12% ^{233}U), with a certain quantity of thorium continued to be investigated.

This cycle complicates the management of heavy nuclei, given that all of the thorium chain isotopes are being brought together with the uranium chain isotopes. It, therefore, does not appear to offer any significant advantages compared to other fuel cycles.

c) Thorium-plutonium (Th/Pu) cycle

The idea of using plutonium as the only fissile material in place of highly-enriched uranium (but still with ^{232}Th as a fertile material) was considered at a very early stage in HTGR development. Initial studies were conducted in the UK in the early 1960s as part of the DRAGON European project [172]. General Atomic continued the studies in the USA in 1968 in a joint program with Edison Electric Institute that included the manufacture of a test plutonium fuel element and its irradiation in the Peach Bottom HTGR [173]. From a physics standpoint, because of the very large capture resonances of some plutonium isotopes at low

energy, the reactivity of plutonium and the evolution of its fissile and fertile isotopes depend greatly on the initial concentration of plutonium as well as its geometric distribution in the fuel (self-shielding effect). Therefore, HTGR fuel allows designers considerable margins for optimizing fuel cycle characteristics.

The Th/Pu Cycle could be of interest in a transition period to the full use of a thorium fuel cycle. Plutonium from available stockpiles or from reprocessing LWR fuels (or from both sources) could serve as a feeding fissile material to initiate a closed thorium cycle. Justifying such an option in today's market is not possible; therefore, this cycle could be considered as a possible long term option. It is to be noted, however, that HTGR cores, operating with such a cycle, may have attractive features such as a more uniform power distribution (thus an increase of outlet temperature), an increase of average power density, and a reduction of reactivity control means.

14. SPENT HTGR FUEL MANAGEMENT

14.1. Introduction

The disposal of fuel cycle and decommissioning wastes from existing gas-cooled reactors (GCR) and future HTGR plants are covered by generic International Standards issued by the IAEA and ISO, completed by national standards and codes. They are applicable to all nuclear systems, but do not necessarily address the specific issues associated with the treatment and disposal of waste from GCRs. For the further management of the waste inventories (classification, disposal routes, etc.), the radiological characteristics and thermal output of the conditioned waste are decisive.

The back end of the HTGR fuel cycle is primarily governed by the large amounts of graphite, as shown in Fig. 83, of which 92% is from fuel elements plus ~2% from the pyrocarbon (PyC) layers of the particle's TRISO coating. The amount of spent fuel and graphite waste generated is governed by the burnup capability of the fuel. The options for dealing with these waste streams are examined in this Chapter.

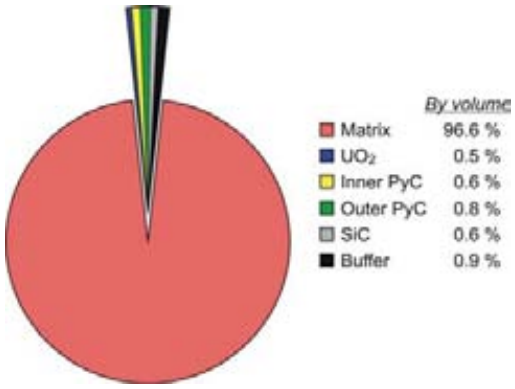

Fig. 83. Shares of HTGR spherical fuel element components (by volume).

14.2. Spent fuel management options

Strategically, there are three primary options for spent fuel: (1) reprocessing, (2) disposal in a monitored geologic repository (MGR), or (3) long-term on-site storage. In the ideal situation, the spent fuel would be shipped offsite soon after discharge from the reactor to either a reprocessing facility or an MGR for disposal. However, the availability of these options varies on a national or regional level. In the case where shipment offsite is not an available option, then the spent fuel will have to be stored on-site until such an option becomes available.

14.2.1. Spent fuel reprocessing countries

Upon discharge from the HTGR, the uranium in the spent fuel elements will have a residual ^{235}U enrichment which makes its recovery attractive. One of the first steps in reprocessing HTGR fuel is the separation of the fuel particles from the graphite matrix. The steps to do this are challenging due to extremely tough nature of the TRISO-coated fuel particle. The feasibility and constraints of reprocessing HTGR fuels are explored in [184]. Should thorium based fuels be used, an alternate process such as the THOREX process would have to be implemented. Once recovered, the remaining uranium is reprocessed in standard fashion with the PUREX process.

The refinement of the fuel separation process depends on the ultimate disposition of the graphite after the fuel is removed. If the graphite is destined for disposal as waste, the process to separate out the fuel can be destructive. If there is a potential to re-use the graphite, then the separation process will need to be non-destructive.

While investigative work has focused on the separation techniques, much remains to be done on assessing the impact of HTGR fuel reprocessing on the existing fuel reprocessing infrastructure. Furthermore, reprocessing offers the opportunity to separate the respective waste streams, allowing the irradiated graphite to be treated totally separate.

14.2.2. Non- reprocessing countries

The example of the U.S. is described here. The absence of reprocessing options combined with the lack of a disposal site for spent nuclear fuel (SNF) and high level waste (HLW) continues to hamper the U.S. commercial nuclear power industry. Many U.S. nuclear sites have Independent Spent Fuel Storage Facilities that are used to temporarily store spent fuel and HLW until that time when the U.S. Department of Energy (DOE) accepts delivery. And that day may still be very far in the future because, even now, there is an ongoing risk that resolution of long standing political, social and technical issues may result in delays that could significantly affect the start of repository operations at Yucca Mountain. Furthermore, the U.S. Nuclear Waste Policy Act of 1983 limits the amount of waste at the repository to 70 000 metric tons heavy metal (MTHM) of which 63 000 MTHM is allocated to commercial spent nuclear fuel (LWR fuel). The remaining 7000 MTHM is allotted to the U.S.-DOE for HLW and non-standard fuels, such as Fort. St. Vrain spent fuel. This allotted capacity to commercial spent nuclear fuel, DOE spent fuel and HLW at Yucca Mountain is currently acknowledged to be insufficient to accommodate existing waste streams, let alone the waste generated from a new fleet of HTGRs or any other kind of reactors. The SNF and HLW wastes that will be generated by new reactors have not been included in the Yucca Mountain Program (YMP) waste stream assumptions [185]. Hence, more repository space will be needed, either at Yucca Mountain or at a second MGR.

Even with repository space available; there may be little or no incentive for a plant operator to reduce the volume of HTGR waste by separating the fuel from the graphite.

The current situation will most certainly have to change to accommodate any resurgence in the U.S. nuclear industry expected over the next few decades. If a fleet of HTGRs or any other kind of new reactors are built, then reprocessing will probably be made available; if not, then an expanded YMP or another MGR must be made available. In the interim, and, prudently, the HTGR will include expandable storage capacity sufficient to accommodate all the spent fuel generated by each reactor module throughout the lifetime of the plant. This is necessary to be consistent with the New Generation Nuclear Plant (NGNP) functions and requirements document [186]. The compatibility of on-site dry cask storage systems and shipping containers will be maximized with repository requirements. However, these requirements are in a state of flux and the risk of incompatibility may be present for some time. As an example, the final method of packaging and transferring Fort St. Vrain spent fuel to the repository, from either of its storage locations in Idaho or Colorado remains to be decided. Nevertheless, repository cask requirements for HTGR fuel need to be well defined. The DOE has an opportunity to finalize these requirements in fulfilling their obligation to transfer Fort St. Vrain fuel to the YMP; however, the timing of that transfer may not be compatible with HTGR development. The U.S.-DOE is mandated by law to remove all Fort St. Vrain fuel from its Colorado storage site by January 1, 2035. In order to solidify requirements for HTGR repository fuel disposal, DOE decisions on transfer method, repository storage form, etc. will have to be made significantly earlier than the mandated date.

14.2.3. Irradiated graphite options

While characteristically similar, it is unlikely that spent fuel element graphite will be dispositioned together with spent non-fuel graphite. For reasons previously stated, fuel and fuel element separation is not considered a site operation. Hence, the disposition of spent fuel element graphite will most likely be the responsibility of the entity accepting the spent fuel element (i.e. either a repository or the fuel reprocessor). In this situation, the accepting entity will face the same choices for dispositioning spent fuel graphite as the plant operators do for the graphite element.

Spent non-fuel graphite can be dispositioned in a surface repository (should that option be available) or, in a geologic repository, space permitting. Other options, such as incineration, re-use and recycling may exist; however, like reprocessing; such options will only become available as the respective technology becomes available and as the market for the service develops. Furthermore, such options have to be environmentally and politically acceptable. Reference [187] presents the options for graphite disposal with particular emphasis on acceptability. In the U.S., graphite waste can be disposed of in a surface repository providing that the waste is classified as U.S. Class C or less. Hence, it is critical to keep graphite impurities low and to track neutron exposure to preclude the creation of greater than Class C waste to insure the surface repository disposal option remains viable.

14.2.4. Spent fuel and graphite waste strategy

The basic strategy for the HTGR is to minimize the creation of spent fuel and graphite wastes through design, and then to minimize the impact of the unavoidable wastes that will be generated. Fuel and core designs will continue to be improved as the HTGR design matures, yielding an optimum combination of operating parameters. That optimum combination must be that which allows the plant to achieve its high level objectives - safety, power production,

economics, waste generation and proliferation resistance. Furthermore, efficient management of HTGR spent fuel and graphite wastes will dictate an infrastructure that gives plant operators' confidence that solutions for the back-end of the fuel cycle are real and workable. The development of this infrastructure is a key part of the HTGR strategy and includes the infrastructure for fuel handling systems, fuel storage and transportation systems, fuel reprocessing, and the creation of additional options for graphite waste. Many of the elements that make up this infrastructure exist today; however, some significant items remain to be developed.

14.3. Characterization of spent HTGR fuel

14.3.1. Nuclide inventory of spent fuel

Most of the radiological activity in spent HTGR fuel exists as a solid, non-releasable form. From the gaseous fission and activation products, only the long-lived isotopes are of importance with regard to spent fuel storage. The radioactive isotopes of ^{3}H, ^{14}C and ^{85}Kr have been identified as the only significant contributors to radioactive release from spent HTGR fuel at inert storage conditions [188].

The origin of tritium (^{3}H) is primarily from B and Li impurities in the matrix material and from ^{3}He activation. Therefore, it is released at rates basically independent of the fuel type. Only a small fraction of ^{3}H is produced in ternary fission and this fraction remains inside the coated fuel particles. The ^{85}Kr is also a fission product that is primarily contained inside the coated fuel particles. The amount of ^{85}Kr released is directly related to the number of failed particles and to the uranium contamination in the fuel element matrix.

Measurements on the release of ^{3}H and ^{85}Kr were conducted using specially prepared canisters filled with GK type (carbide fuel, average burnup 15% FIMA) or GO type (oxide fuel, 12.4% FIMA) spherical fuel elements, all discharged from the AVR at the end of 1976. The canisters were equipped with valves to allow sampling of the interior gas atmosphere. Ranges of the activity release rates from AVR spherical fuel elements into the canister gas atmosphere are shown in Fig. 84 in an Arrhenius-type diagram [189].

With regard to ^{14}C, which is an activation product from ^{14}N and ^{13}C, high concentrations are typically found near the spherical element surface resulting from coolant deposition. It can be released as CO_2 during oxidation processes. The ^{14}C is bound to the binder material in the matrix graphite and, in the presence of moisture in the storage container, is liberated as gaseous CO_2 during corrosive reactions.

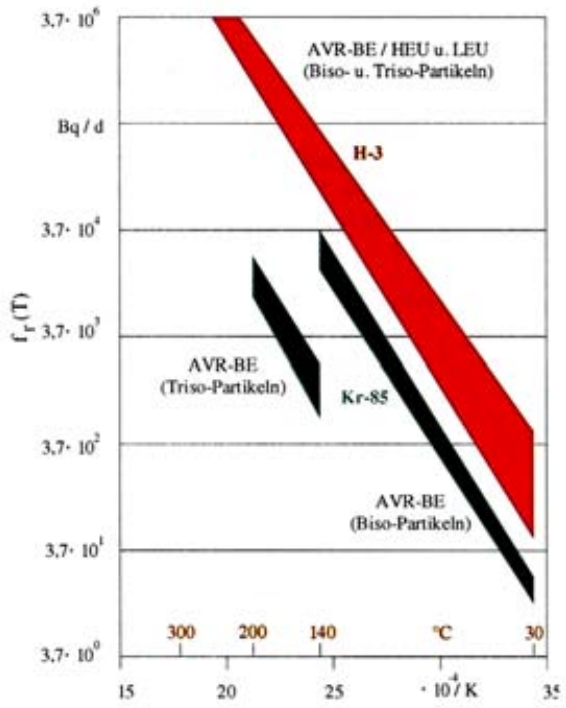

Fig. 84. Arrhenius diagram of ^{3}H and ^{85}Kr release rates from experimental data [189].

The decreasing amount of O_2 and the concomitant increase of CO_2 in the canister atmosphere show the corrosive origin of ^{14}C. The accumulated CO_2 corresponds to a carbon loss on average of 7.7 mg per GK fuel element (after 5.3 yrs) and 6.5 mg per GO fuel element (after 6.4 yrs), respectively. Considering an average ^{14}C inventory of 5.5 MBq per fuel sphere, the fractional release rate of ^{14}C into the canister atmosphere is 8.6×10^{-4} Bq/yr. This is a conservative value used for the first 10 years of storage. For longer periods, the depletion of oxygen in the container atmosphere can be taken into account [190].

A ^{3}H inventory of 0.53 GBq per spent spherical fuel element was calculated with the ORIGEN-S 2 code for THTR fuel with a target burnup of 11.4% FIMA and 3 years of cooling time [185]. The ^{3}H activity inventory in an AVR HEU fuel element has an upper limit estimated to be 2.5 GBq with about 20% inside the coated fuel particles and 80% inside the fuel matrix material. The ^{85}Kr inventory in a HEU fuel element, has an upper limit value estimated at 17.3 GBq and is considered a reasonable estimate for all AVR fuel spheres. Almost the entire ^{85}Kr inventory is inside the coated fuel particles. The estimated inventory value for ^{14}C in the fuel matrix material is 0.045 GBq [189].

The release from the two AVR canisters inside a CASTOR cask, into the cask atmosphere has also been experimentally investigated. In the period 1987-1992, one CASTOR THTR/AVR cask and one TN-AVR 2 cask were each externally heated up to 55°C. The higher temperature resulted in the release of moisture and thus, of ^{3}H in form of HTO. The released activities after a six month period are provided in Table 18 [189]. Because leakage rates from a cask lid are three orders of magnitude lower than those from a canister plug, activity release into the environment from CASTOR casks, which are closed with two lids, is expected to be negligibly low.

Table 18. COMPARISON OF ACTIVITY RELEASE INTO CONTAINER ATMOSPHERE FOR TWO DIFFERENT CASK TYPES CONTAINING AVR SPENT FUEL ELEMENTS

Casks with a total of 1900 elements (each cask contains two AVR canisters)	Activity released to cask atmosphere [Bq]		
	^{3}H	^{14}C	^{85}Kr
CASTOR THTR/AVR	1.7×10^{5}	8.5×10^{3}	6.6×10^{3}
TN-AVR 2	8.1×10^{4}	1.4×10^{4}	1.5×10^{4}

14.3.2. Heat production from spent fuel

Calculations of thermal power production were aloe made with the ORIGEN-S 2 code for the CASTOR casks used for storage of THTR fuel elements within the licensing process for storage and transport casks. Assuming a canister for damaged fuel is filled with 2320 THTR spherical fuel elements, calculations were made for the so-called average target burnup[1] of 11.4% FIMA as a conservative coverage for all casks. These results were compared to the case of an average measured burnup of 5.3% FIMA for discharged THTR fuel elements. The results after 3 years of cooling (referring to a time around 1990) showed an acceptable level of 246 W per cask for the target burnup case and 118 W per cask for the measured burnup case [189].

Thermal power production for the total, ~700 000 THTR fuel elements today is estimated to be around 8 kW. For the total, ~290 000 AVR sphere elements, the thermal power is around 6 kW. These values will further decrease to less than half of these estimates by 2038, 50 years after shutdown of the reactors.

14.4. Strategies of spent HTGR fuel treatment

Various options of spent fuel treatment are conceivable (see Fig. 85). Direct disposal of the complete HTR spent fuel elements (Path A) leads to rather high masses, 6000 to 10 000 t depending on the fuel cycle over the 60 year lifetime of a single HTR module. A significant reduction in disposal volume can be achieved using new head-end processes. Here, the large volume of only slightly contaminated moderator graphite is separated from the highly radioactive coated particles or fuel compacts thereby, avoiding cross-contamination and C-14 releases, as much as possible. The separated compacts or coated-particles can either be conditioned for direct disposal (Path B) or further treated to recover the LEU fuel kernels from which plutonium and residual uranium can be extracted in existing reprocessing plants. These fissile materials could then be recycled as MOX in LWR or other reactors (Path C).

[1] Target burnup is the burnup, for which the generated isotopes U-233, Pu-239, Pu-241 reach maximum values.

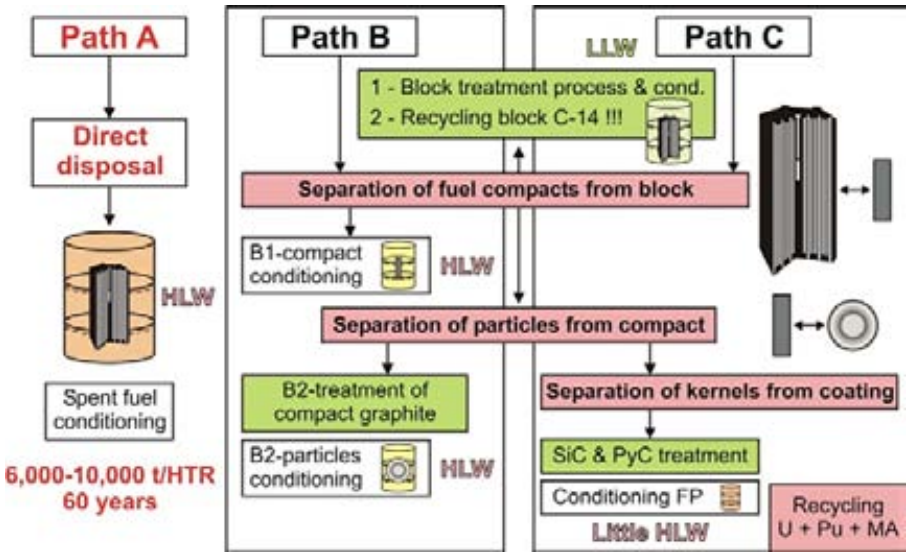

Fig. 85 Back-end options for HTGR fuel.

14.4.1. Direct disposal

Direct disposal is the currently pursued option for the waste management of spent HTGR fuel elements. There are a number of positive features for the HTGR concept that are effective not only during normal operation and during accidents, but also under conditions of intermediate storage and final disposal; these include:

- efficient use of uranium and in-situ generated plutonium in LEU fuel due to high burnup;
- isotopic composition in the spent fuel which is non-proliferation friendly;
- the TRISO coating of the fuel particles provides an effective long-term barrier against fission product transport and reduces the need for additional barriers;
- due to the low power density of the fuel, passive air cooling systems are sufficient from the beginning of intermediate storage;
- disposal techniques developed for medium active waste can be applied to spent HTGR fuel;
- homogeneous graphite matrix minimizes any spent fuel conditioning effort; and
- corrosion resistance of both the matrix graphite and the particle coatings against repository relevant salt brines allows simple fuel disposal packaging concept.

In particular, the different barriers to radionuclide mobilization in HTGR fuel represent an important advantage for HTGR fuel with respect to its long-term safety. The major disadvantage is the large volume required for storage of spent HTGR fuel.

Visco-plastic behavior in rock salt will eventually close gaps/voids, so-called convergence, around the storage arrangement and imposes a hydrostatic pressure build-up according to the depth of the disposal location which, after all the gaps are closed, corresponds to the total mountain pressure. Convergence is enhanced with increasing temperature. For a depth of 800-

1000 m and a maximum temperature of 200°C, a temporarily and locally limited maximum pressure of about 30 MPa has to be taken into consideration. Convergence was measured in the ASSE salt mine at a rate of about 0.3 mm/yr. The annular gap around the waste barrels in a bore hole was estimated to be closed after approximately 200 yrs [191].

An *in-situ* demonstration test of direct final storage with spherical fuel elements was planned in the MHV Project (MAW and HTR Fuel Element Test Storage in Bore Holes) in Germany starting in 1983. It was focused on demonstrating applicable radioactive handling techniques for the retrievable *in-situ* disposal. A bore hole with a depth of 10 m was to be drilled in the ASSE salt mine and loaded with four gas-tight stainless steel canisters, each with 950 spent AVR fuel elements and a total of ~403 g of uranium. The test was planned for a five-year duration [192]. This project was, however, discontinued for financial reasons and the demonstration storage test never materialized. These same canisters were later used in a demonstration test program for the verification of two transport and storage cask designs, the TN-AVR-2, and the GNS-CASTOR-AVR [193].

An accident scenario to be considered for final storage of spent fuel is the event of water ingress into the salt mine, where the evolving salt brine would start corroding the waste package and possibly reach the fuel particles. For intact coatings, no corrosion effect has been observed; thus, coated particles are assumed to have excellent long-term chemical resistance.

The graphite matrix is the first barrier in spent HTGR fuel elements to aqueous phase penetration and radionuclide release. The next barrier between the fuel kernel and the aqueous phases is the PyC layers on the fuel kernel. Therefore, it is necessary to understand the long term behaviour of graphite and PyC under final disposal conditions. An aqueous solution can penetrate the A3 matrix graphite of a fuel element through its open pore system. Under normal conditions, a spherical fuel element takes up about 8 ml of brine solution. Under pressurized conditions and dissolution of the pore gases in the liquid, this amount increases to a conservatively estimated volume of 23 ml [194].

The leak resistance of complete spent AVR fuel elements of different fuel types, along with one non-heated spheres from the HFR-K3 experiment, in a quinary alkaline solution (Q-brine) [2] representative of salt repository conditions was experimentally investigated at pressures up to 30 MPa and temperatures up to 150°C for up to 1230 days. Leached activities were measured for ^{137}Cs, ^{134}Cs, ^{90}Sr, ^{144}Ce, ^{133}Ba, ^{154}Eu and ^{60}Co. The tests revealed a gradual release of the matrix contamination into the brine, for Cs about 10-20% of its inventory was in the fuel matrix. The leaching process at 90°C temperature and 13 MPa pressure exhibited two distinct phases: first, removal of surface activity on a short-term basis (~ weeks), and second, removal of activity from uranium contamination and defective/failed particles on a longer term. Major differences in the release behaviour were observed between BISO-coated and TRISO-coated fuel (see Fig. 86). Release from defective particles was by orders of magnitude higher than from intact coated particles. Long-lived relevant nuclides like ^{129}I, ^{99}Tc, ^{237}Np, are expected to exhibit much lower release rates [193], [195].

---

2 The term ‘Quinary’ means ‘consisting of five parts’, or ‘occurring in sets of five’. The majority of the corrosion tests related to the quinary Q-brine because this brine is considered to be the most relevant solution encountered in an accident in a repository in rock salt. The test media were selected on the basis of common knowledge of brines possibly occurring in the Zechstein bodies of rock salt in Lower Saxony in the FRG. NaCl-KCl-MgCl2-MgSO4-H2O (Q-brine): 1.4 NaCl, 4.7 KCl, 26.8 MgCl2, 1.4 MgSO4, 65.7 H20 (pH = 4.9). In order to simulate the additional uptake of NaCl in a HLW borehole at the higher disposal temperatures (200°C at the maximum), 1.7 g NaCl was added per 100 g of solution. The saturation oxygen content of the salt brines between 25 °C and 55 °C was in was in the range from 0.2 mg/1 to 5 mg/1.

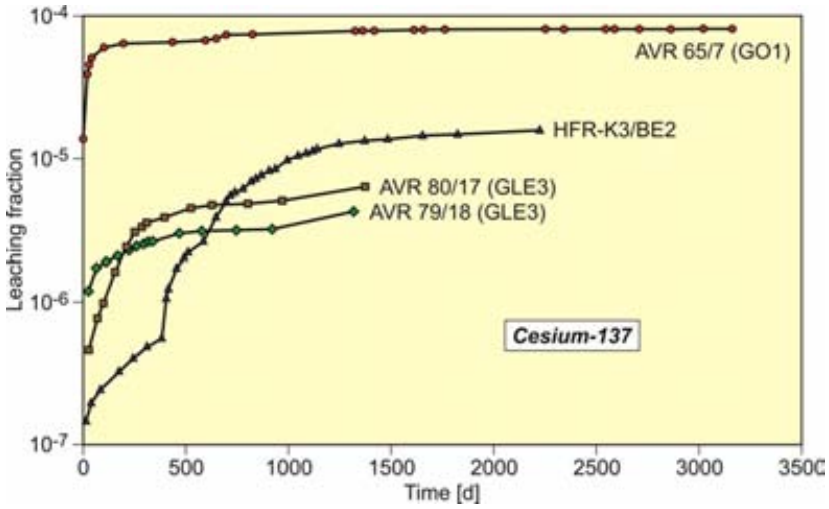

Fig. 86 ^{137}Cs release fraction leached in Q-brine [193].

Apart from the above "integral" tests, further investigations are concentrated on the understanding of the behavior of the single components under corrosive conditions. These studies included the measurements of corrosion rates for the fuel constituent materials - matrix, PyC, SiC, as well as the leaching of uranium and thorium from particle fuel kernels. Results based on a leaching time of 40 d have shown that corrosion rates for the A3 matrix are higher in the presence of oxygen. The significant increase in an argon atmosphere under γ-radiation conditions is due to the generation of radiolysis products. Results for PyC are similar to those for the A3 matrix material. Corrosion rates for SiC were found to be strongly related to the corrosive environment and the temperature. Leaching tests with different types of unirradiated kernels in Ar at 90°C for more than one year exhibited lower dissolution rates for (Th,U)O_2 kernels, by up to 2 orders of magnitude, compared to UO_2 kernels [194].

14.4.2. Reprocessing of HTGR fuel

The association of the uranium/thorium fuel cycle with an HTGR was for reprocessing of bred fissile ^{233}U material. Reprocessing of spent HTGR fuel was formerly developed in the U.S. and Germany based on incineration and mechanical technologies. In Germany, the development of economic reprocessing methods, initiated in 1966, led to the so-called THOREX process scheme. The THOREX process was based on a liquid-liquid extraction method using the immiscible liquid nitric acid as the aqueous phase and a mixture of tributylphosphate and kerosene as the organic phase. The process was verified at the Research Center Jülich (FZJ) in a semi-technical facility called JUPITER. Work in Germany on reprocessing of HTGR fuel, however, were abandoned in 1985. Beyond this date the favored option was interim storage over several decades with a future final disposal favored [196].

Mechanical methods like grinding and crushing have also been investigated and used in the U.S. in the 1970s, but were found to lead to a cross-contamination of the moderator graphite with high-level waste from the spent fuel. Therefore, future processes have to fulfill the following criteria or performance:

- separation of graphite from coated particles without damaging them and without significant contamination transfer;
- techniques for removing particle coating layers without damage to the kernels; and

- optimizing the process of waste management and conditioning (including secondary wastes).

Formerly, combustion processes were used to extract the coated particles from the HTGR fuel element matrix. These processes can no longer be used because of the possibility of releasing ^{14}C to the environment.

For block-type fuel, methods have to be developed and demonstrated for extracting the fuel compacts from the hexagonal fuel block. The Idaho National Laboratory (INL) has conducted actual reprocessing of similar graphite as well as the removal of fuel compacts from spent Fort St. Vrain fuel blocks in remote testing facilities.

14.5. Spent fuel management for AVR and THTR-300

By the end of the 1970s, the HTGR fuel strategy in Germany was guided by the need to meet non-proliferation aspects and to find a convincing publicly accepted spent fuel concept. At present, the only accepted method of HTGR spent fuel management in Germany involves the two steps of:

1. intermediate dry storage in appropriate containers and facilities, and
2. transfer to a deep-mined salt dome repository for final disposal utilizing techniques of treatment similar to heat generating medium active waste.

14.5.1. AVR

The 46 MW(th) AVR reactor in Jülich was operated from 1967 to 1988. Prior to granting the license for decommissioning, the reactor was held at "zero-power operation". Safestore[3] decommissioning of the AVR began in 1994 with defueling of the reactor and the dismantling of plant systems outside the reactor building. In 2003, the decommissioning strategy was changed in that it was decided not only to have a safe enclosure of the AVR reactor, but to have the site returned to green-field status by the year 2012.

Defueling began in 1994, at first with only the removal of the HEU fuel. The defueling process was interrupted after having discharged ~35 000 HEU fuel elements and resumed in 1996, when the LEU license was granted. The defueling process was completed by middle of 1998 [197]. In total, more than 290 000 spherical fuel elements of 5 different types and 15 variants (carbide/oxide, BISO/TRISO, HEU/LEU) (see Table 19) were inserted into the AVR. This number of spherical elements contains more than 6 billion coated fuel particles. In addition, ~80 000 graphite (moderator) balls were also inserted into the core during its lifetime.

Steel cans, each with a capacity of 50 spherical fuel elements, were filled at the AVR site and transported to the Hot Cells at FZJ, where they were sealed and stored in a water pool serving as a buffer storage facility. Later the steel cans were re-opened and the fuel from those cans which did not indicate water penetration, was repacked into larger, dry storage canisters with a capacity of 950 elements (see Fig. 87) [188]. Those fuel elements which were found to be wet due to leaky seals on the steel cans, were also loaded into the dry storage canisters, but then sealed with a particular leak-tight weld.

---

3 The term 'Safestore' is the name of the decommissioning concept used in Germany and the UK. Refer to reference [15.14] for additional information

For the intermediate storage, both canister storage behind concrete shielding and storage directly in shielded containers concepts are being applied. A natural convection type of dry storage facility, which has operated since 1981 without any disruptions, took 72 of the dry storage canisters and placed them in 36 positions up to now. Heat removal, designed for 7.2 kW, is provided by an air venting system of 2000 Nm^3/h capacity (Nm^3/h stands for normal $meter^3$ per hour). For the second intermediate storage concept, two AVR canisters were inserted into a CASTOR THTR/AVR type storage cask and closed with a double lid system. The CASTOR casks are stored at the FZJ in an intermediate dry storage facility licensed to take up to 158 casks. The maximum heat production of 15 kW (if completely filled) is passively removed by natural convection [198]. All 290 000 fuel spheres discharged during reactor operation and after reactor shutdown were stored in (presumably) 153 CASTOR casks.

14.5.2. THTR-300

The Thorium High Temperature Reactor, THTR-300, in Hamm-Uentrop has a thermal power of 750 MW and was operated for a total of 16 410 h or 423 full power days in the years 1983 to1988. Licensing, technical and political obstacles eventually resulted in the decision by the operator in 1989 to decommission the reactor.

Table 19. AVR AS TEST BED FOR DIFFERENT TYPES OF SPHERICAL FUEL ELEMENTS, FUEL TYPES AND FUEL PARTICLE DESIGNS [197]

Fuel Type	No. of Fuel Spheres
Fuel element design	
Shell type	37 700
Pressed type	253 000
Fuel design	
HEU, $(Th,U)C_2$	87 600
HEU, $(Th,U)O_2$	129 400
HEU, fissile/fertile	20 300
LEU, UO_2	53 400
Coating design	
BISO	202 900
TRISO	74 300
Mixed (fissile TRISO/fertile BISO)	13 500

The decommissioning procedure [199] began the steps of shutdown operation with the primary circuit depressurized, helium substituted for nitrogen, and the shutdown rods fully inserted and locked. Decay heat (< 20 kW) was removed by natural convection and radiation.

The next step was unloading fuel elements from the reactor and spent fuel storage as a prerequisite for safe enclosure. Fuel for the THTR was a HEU $(Th,U)O_2$ kernel surrounded by a HTI_BISO coating. Each spherical fuel element contains ~34 100 of such coated particles. During unloading, operating fuel elements were sorted by means of graphite moderated 500 W “Solid Moderated Reactor” (SMR) and these elements transferred to steel canisters.

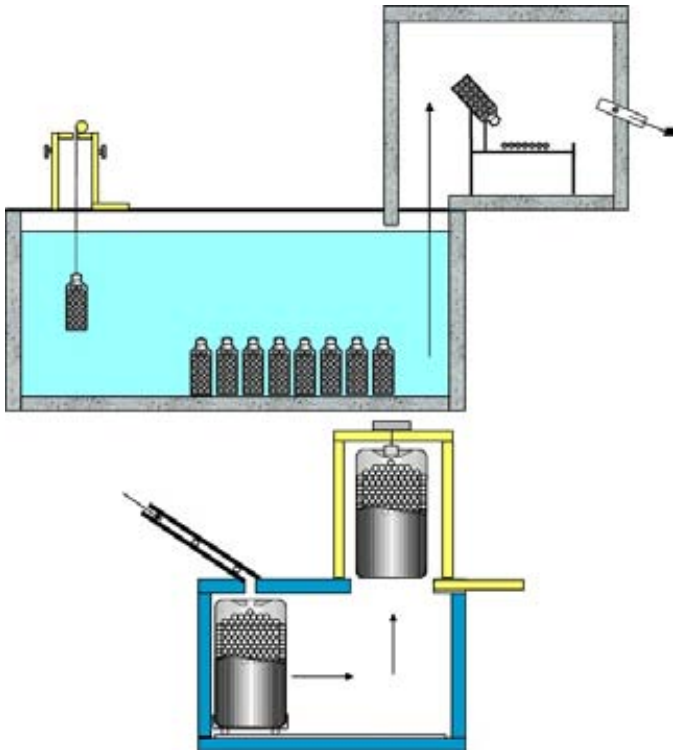

Fig. 87 AVR spent fuel management.

The diagram in Fig. 88 shows the number of discharged absorber elements (AE) and graphite elements (GE), respectively, per each of the 268 "unloading steps", which corresponds to 2100 discharged fuel elements or one filled steel canister. Furthermore, the mean burnup curve of the fuel elements removed exhibits different phases during the unloading process. The minimum in burnup occurs around unloading step 150 and is a result of the large number of relatively "fresh" fuel elements with a short-irradiation history, taken from the pebble-bed surface of the outer upper core. The increase in burnup in the latter unloading steps is from highly irradiated fuel removed from the bottom edge of the core [200]. The unloading process was completed within 10 months achieving a "nuclear fuel free" state for the reactor. The inventory of fissile material remaining in the core was estimated to be 0.976 kg, significantly lower than the required value of 2.5 kg.

A safe enclosure configuration was achieved in 1997 (comparable to the IAEA passive SAFE STORAGE option). All buildings except for the reactor hall, the reactor building, and the auxiliary building were released from the validity of the Atomic Act. Operation of the safely enclosed plant will last for 30 years with largely no maintenance, before a complete dismantling can take place. Each canister with 2100 fuel spheres was then placed into a CASTOR THTR/AVR type cask and shipped to an external interim storage facility at Ahaus (BZA). By 1995, a total number of ~620 000 spent fuel elements had been transported in 306 CASTOR casks, by 57 shipments from the THTR site to the BZA.

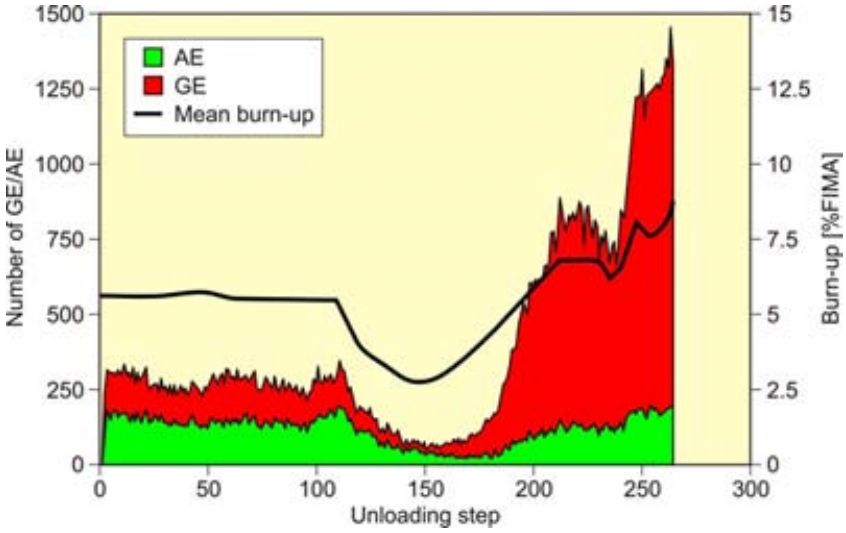

Fig. 88 Discharged absorber (AE) and graphite elements (GE) per unloading step (= 2100 fuel elements) and mean burnup of THTR fuel elements [200].

The THTR fuel will remain in intermediate storage until a final disposal site is available. The graphite and absorber elements, because of their low radioactivity and heat generation, will most likely go to a low-active waste repository [199].

14.6. Outlook on Generation-IV reactors (VHTR)

With the discussion about the VHTR as the next generation HTGR, new concepts for waste treatment strategies others than direct disposal are necessary to achieve a minimization of radioactive waste streams and further closure of the fuel cycle. This is a minimum requirement for environmentally benign nuclear energy. Recycling of spent fuel, partitioning and transmutation of actinides and long-lived fission product species, plus the immobilization of the remaining wastes are the steps which will eventually result in a reduction of radioactive waste in the short-term. During this period, which is on the order of hundreds rather than millions of years, the wastes may represent a risk to the public and to the environment. Very high temperature reactors (VHTR) may play an important role in lowering the toxicity level of the waste through “deep burning” (ultra-high burnup) of plutonium and the long-lived actinides by applying recycling only once to the driver fuel.

Partition and transmutation, and the reduced generation of long-lived radiotoxic waste will have a significant impact on geological disposal. The goal of transmutation is to transform long-lived, highly radiotoxic minor actinides (MA) into mostly short-lived and less toxic species by their by reaction with neutrons. This process, however, does not change heat production of the waste nor does it reduce the quantity of wastes. Current and future research and development is concentrating on efficient methods for the necessary isotope separation and the subsequent preparation of “new” fuels with a wide variety of potential kernel compositions. These include Pu or MA, as well as the feasibility of transmutation either in specially designed nuclear reactors or in accelerator driven systems (ADS). Symbiotic fuel cycles of LWRs and HTGRs could lead to a significant reduction in Pu inventories.

ANNEX I.

I-1. NUCLEAR HYDROGEN PRODUCTION

I-1.1. Introduction

A strong increase in the demand for the energy carrier hydrogen is foreseen in the near future. Not only are there rapidly growing markets for hydrogen anticipated in the chemical industries as a raw material for upgrading mined oil resources, but it may also play a significant role as an environmentally benign fuel in the transportation sector. Essential questions are therefore, how to generate and supply hydrogen in sufficient quantities.

Currently, the annual production of hydrogen worldwide amounts to approximately 550 billion Nm^3, corresponding to 50 million tons per year, of which more than 95% are generated on the basis of fossil fuels. Given the serious impact on the climate of using fossil fuel, clean alternatives must be developed and gradually substituted for their use. Water and biomass are expected to become the main sources for hydrogen in the future with the necessary process heat for extracting hydrogen to be provided by CO_2 emission free energy sources. With respect to hydrogen production on a large scale at a constant rate, nuclear energy may play an essential role.

Nuclear power is generally considered a safe, reliable, clean, and economic energy source with a huge to be discovered potential beyond dedicated electricity production. In particular, hydrogen production based on nuclear generated process heat sources could represent an important contribution to the goal to develop a domestic energy sources for the purpose of energy security and stability. And at the same time, reduce national dependencies on imports of fossil fuels.

I-1.2. The nuclear generation of hydrogen

In principal, all methods of hydrogen production, except for the photolytic processes, can be linked to a nuclear reactor that can deliver electricity and process heat, respectively. Not every type of nuclear plant, however, is as equally appropriate for coupling with a hydrogen production technique. Conventional light water reactors (LWRs) have too low a coolant exit temperature to be able to supply process heat; they rather could be employed for hydrogen production via the electrolytic water splitting process. This low temperature, alkaline electrolysis process would immediately be feasible. It is a well established technology and does not require being located in close vicinity to the nuclear plant. It would be economical only in the case of a cheap electricity source (e.g., off-peak). Much more appropriate are high temperature gas-cooled reactors (HTGRs) with helium coolant exit temperatures of up to 950°C. The achievement of high coolant exit temperatures for the direct utilization of process heat was impressively verified in the German AVR reactor under long-term operation, and most recently in the Japanese HTTR.

The connection between nuclear generated process heat and a heat application plant is principally independent of the method of hydrogen production. The hot coolant transfers its heat to the chemical process via an intermediate heat exchanger (IHX). The main purpose of the intermediate circuit is to clearly separate the nuclear heat source from the chemical island. The IHX serves the safety related purpose of precluding the direct access of the reactor primary coolant to the chemical plant and, in the reverse direction, preventing product gases from penetrating the reactor building. Thus it is possible – and that is the intention – to design

the chemical side as a purely conventional facility and to have routine maintenance operations performed under non-nuclear conditions.

Of particular significance is the consideration of possible accident scenarios in such a combined nuclear and chemical facility. Apart from their own specific categories of accidents, a qualitatively new class of events will have to be taken into account, characterized by interacting influences. Problems to be covered by a relevant overall safety concept are: the question of safety of the nuclear plant in case of a flammable gas cloud n explosion on the chemical side, or vice versa; and the question of what influence an accident-induced release of radioactivity will have on the continued operation of the chemical plant. But there are also more frequently expected events involving thermo-dynamic feedback in case of a loss of heat source (nuclear) and heat sink (chemical), respectively. For the specific example of the HTTR coupled with a steam-methane reforming device, the hazardous potential has been identified and evaluated, and resulted in a relevant proposal for a safety concept.

I-1.3. Methods for hydrogen production using HTGR as a primary heat source

Reforming of hydrocarbons as transition solution

The processes of splitting hydrocarbons are presently widely applied production methods for hydrogen. The most important ones established on an industrial scale are steam reforming of natural gas, extraction from heavy oils, and the gasification of coal. Biomass gasification is currently being tested on a pilot plant scale.

Worldwide steam reforming of natural gas covers about half of the hydrogen demand. This process was subjected to a long-term research and development program in Germany with the aim to utilize the process heat required for the methane splitting from a HTGR. The Research Center Juelich (FZJ) has developed, in cooperation with the respective industries, a design for a process heat HTGR as well as the necessary heat exchanging components, which according to their dimensions, belong to the 125 MW power class. A particular 10 MW component test loop was constructed and successfully operated for over 18 400 hours, 38% of which was at temperatures above 900°C. Components tested in terms of reliability and availability included two designs of an IHX, steam generator, decay heat removal cooler, hot gas ducts, and hot gas valves.

The steam reforming of methane was investigated in experiments conducted under the typical conditions of a nuclear reactor, i.e., in reformer tubes heated with helium of 900°C at 4 MPa with industrial-scale dimensions (15 m in length, 130 mm inner diameter). The first test facility was a single splitting tube (EVA); the follow-on facility consisted of a tube bundle (EVA-II) (see Fig. 89). A similar experimental program was recently conducted in Japan where the main focus was on the mutual thermo-dynamic interaction. Also EVA's counterpart, ADAM, a facility for the re-methanation of the synthesis gas generated in EVA, was constructed and operated, thus completing the system to a closed cycle and verifying the principle of a long-distance energy transportation system based on hydrogen as the energy carrier.

Within the framework of the project "Prototype Nuclear Process Heat" (PNP), the coal gasification processes for hydrogen production was also investigated in Germany. These activities eventually resulted in the construction and operation of pilot plants for coal gasification utilizing nuclear heat source. Catalytic and non-catalytic steam-coal gasification of hard coal was verified in the 1.2 MW WKV facility using 950°C helium as the energy

source. The process of hydro-gasification of brown coal (lignite) was realized in the 1.5 MW HKV plant operated for ~27 000 h with a total amount of 1800 tonnes of lignite being gasified.

Fig. 89. Reformer tube test bundle for the generation of synthesis gas under simulated nuclear conditions in the EVA-II facility at the Research Center Juelich.

I-1.3.1. Splitting of water

The electrolytic decomposition of water is also a widely applied technology on the industrial scale accounting for ~4% of the world's hydrogen production. It has, however, a comparatively low efficiency and is economic only, if cheap electricity is available. The electrolysis of water in the vapor phase at high temperatures, 800-1000°C, has the advantage of a lower total energy input and, in particular, an electricity input reduced by about 30% compared to "normal" electrolysis. Research and development efforts in various countries are concentrating on the development and optimization of planar or tubular electrolysis cells, the composition of cell stacks, and the selection of appropriate materials. The development may benefit from the efforts in the area of solid oxide fuel cells representing the reverse process of high temperature electrolysis.

In Germany, the high temperature electrolysis process became known in the 1990s under the project "HOT ELLY" demonstrated in tubular cells in a 2 kW pilot plant. Japan's approach, based on planar cells, achieved hydrogen production rates of 3-6 l/h per m^2 of cell surface at a temperature of 850°C. Idaho National Laboratory (INL) in the USA is presently conducting an experimental program to test solid oxide electrolysis cell stacks combined with materials research and detailed Computational Fluid Dynamics (CFD) modeling. In a 2005 test, a H_2 production rate of 162 Nl/h (Nl/h stands for normal liter per hour) over 197 hours could be verified using a 22 cell stack and no problem in stack performance was observed. A 1000 h test was planned for 2006.

Direct splitting of water is usually not practicable because of the extremely high temperatures required. Thermo-chemical cycles, on the other hand, are composed of several reaction steps which run at much lower temperatures and, in the sum, lead to a decomposition of water into hydrogen and oxygen. The supporting chemical substances are regenerated and recycled, and remain – ideally – completely inside the system. The only input is water and heat.

Numerous cycles have been proposed in the past and investigated in terms of their characteristics like reaction kinetics, thermodynamics, separation of substances, stability, processing flow scheme, and cost analysis. Only a few, however, were deemed to be sufficiently promising and worth further investigation. Among those whose partial reactions are being investigated in more detail, also with respect to their coupling to an HTGR or a solar heat source, is the sulfur-iodine (S-I) process originally developed in the USA by the General Atomics (GA) company and later pursued and modified by various research groups. Presently, research on the S-I process is underway in many research institutions including: JAEA (Japan Atomic Energy Agency, former JAERI), GA, SNL (Sandia National Laboratory), CEA (Commissariat à l'énergie atomique), and KAERI (Korean Atomic Energy Research Institute). Among these, JAEA is most advanced in this technology.

The process scheme of the S-I cycle is composed of three principal steps.

1.	$I_2 + SO_2 + 2\,H_2O$	→	$2\,HI + H_2SO_4$	+ 165 kJ	@ 70-120°C
2.	$2\,HI$	→	$H_2 + I_2$	- 173 kJ	@ 400-500°C
3.	H_2SO_4	→	$H_2O + SO_2 + 0.5\,O_2$	- 371 kJ	@ 850-950°C

Equation (1) corresponds to the so-called Bunsen reaction where in the presence of the substances SO_2 and I_2, water is added. The products of this exothermal reaction are the two acids hydro-iodide (HI) and sulphuric acid (H_2SO_4), which appear as HI and H_2SO_4-rich phases. After separation, purification and concentration, these acids are then decomposed by adding heat according to equations (2) and (3), respectively, to finally liberate hydrogen and oxygen. A schematic of the S-I thermo-chemical process is shown in Fig. 90.

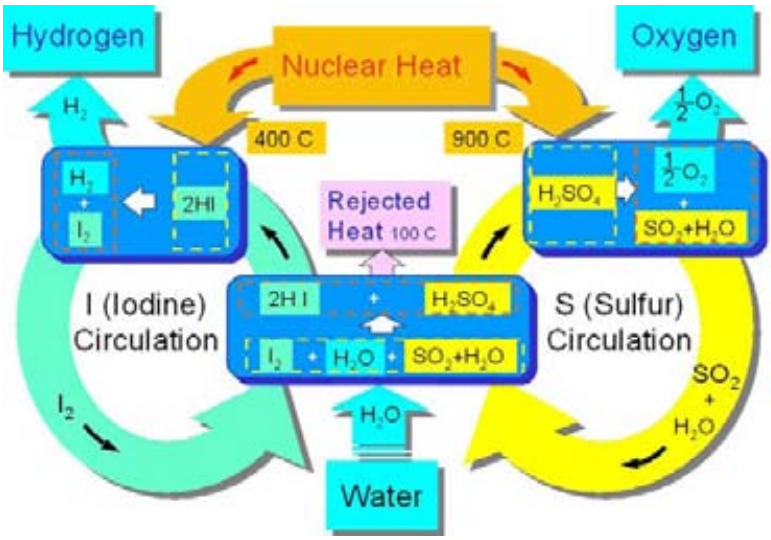

Fig. 90 Principal schematic of the sulfur-iodine (S-I) thermo-chemical cycle investigated at JAEA, Japan.

This process was verified at JAEA and was successfully demonstrated in a closed cycle in continuous operation over one week. The facility was composed of more than 10 process units made of glass and quartz, achieving a hydrogen production rate of 30 Nl/h. The next step, which began in 2005, is the design and construction of a pilot plant operated under the simulated conditions of nuclear generated heat source (i.e. electrically heated) of helium coolant, 880°C at 3 MPa. The expected yield of this pilot plant was 30 Nm^3/h. After 2010, it is planned to connect the S-I process to the HTTR for hydrogen production at a rate of 1000 Nm^3/h; thus, realizing the world's first nuclear hydrogen production.

I-1.4. Nuclear reactors of the next generation

Several partner countries including the EURATOM have joint to form the "Generation IV International Forum" (GIF) with the main objective to develop nuclear reactors of the next – fourth – generation by 2030. Not only are such reactors expected to be safer, more reliable, more economic, and more proliferation-resistant than those from the previous and present generations, they are also most likely to penetrate non-electric markets like the supply of process heat / steam or hydrogen on a large scale. From the suggested Gen-IV concepts, the so-called "Very High Temperature Reactor" (VHTR) appears to have the most likely chance of taking the lead role. A schematic of the VHTR is provided in Fig. 91. Its characteristic features are: a gas turbine Brayton cycle for high efficiency, coolant exit temperatures of 1000°C, a long lifetime and the possibility of large-scale hydrogen production. However, with such extremely ambitious goals, it appears wise to proceed in steps.

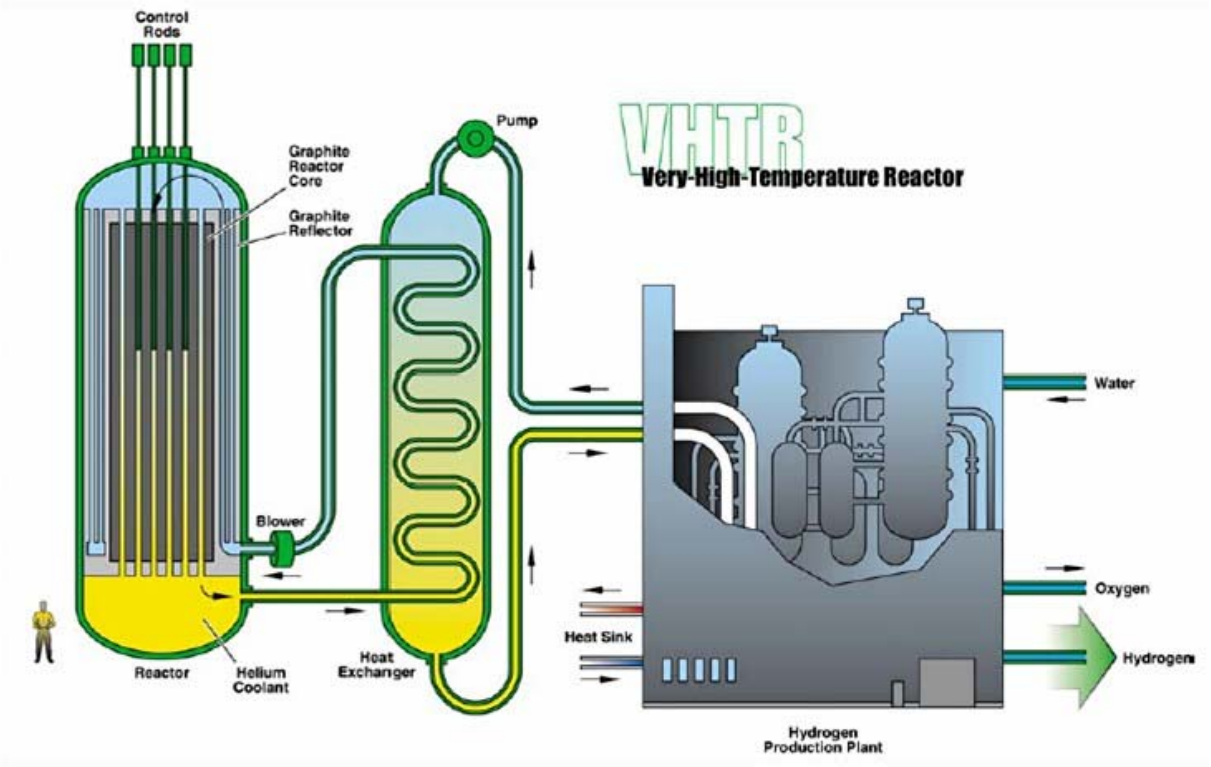

Fig. 91. Schematic of the VHTR as an option for a nuclear plant of the fourth generation used for the large scale generation of hydrogen.

Excellent starting points are the currently operated HTGRs in Japan and China as testing and research instruments to further demonstrate the safety features of an HTGR. Concepts of prototype plants with VHTR like properties also exist. In this respect, the most advanced is the PBMR (Pebble Bed Modular Reactor), a 400 MW(th) direct-cycle plant, under development in South Africa. The United States is currently designing the "Next Generation Nuclear Reactor" (NGNP). This U.S.-DOE sponsored demonstration program is based on an HTGR with a thermal power of 400 to 600 MW for the cogeneration of electricity and process heat at 900° to1000°C. A fraction, 100 MW(th), is being considered for hydrogen production employing the S-I thermo-chemical water splitting cycle as the reference production technology. High temperature electrolysis is an alternative or backup solution for hydrogen production. In Europe, the French concept ANTARES corresponds to a medium-sized modular HTGR with an indirect cycle, a gas outlet temperature of 850° to 900°C, a fuel burnup of about 16% FIMA (150 GWd/t_{HM}), as well as an IHX for the potential coupling to high temperature processes (e.g., for hydrogen production).

I-1.5. Outlook

New reactor concepts offer the ideal chance of delivering, apart from the "classical" electricity, the primary energy for the production of hydrogen or other fuels. Nuclear, with its virtually no air-borne pollutant emissions, appears to be the natural option for large centralized hydrogen production. In a future energy economy, hydrogen could play an important role as storage medium to adjust the variable demand for electricity via fuel cell power plants ("hydricity") and also serve as the so-called "spinning reserve". Prerequisites for

such scenarios would be a competitive nuclear hydrogen production, large-scale (underground) storage of the hydrogen at low cost and, last but not least, cost-effective fuel cell power plants. However, since production processes have not yet been tested beyond pilot plant scale, the technical and economic feasibility remains to be demonstrated.

Additional Reading Materials

Additional reading materials: (belongs to Chapter 1)

- WORLD NUCLEAR ORGANIZATION, Education Papers on 'Nuclear Energy Made Simple' refer to World Nuclear association web-page http://www.world-nuclear.org/education/education.htm

- COMMISSARIAT À L'ÉNERGIE ATOMIQUE, Gas-cooled nuclear reactors, A monograph of the Nuclear Energy Directorate, e-den, CEA, France (2006), ISBN 2-281-11343-4, http://den-dans.extra.cea.fr/Phocea/file.php?class=page&reload=1224236340&file=25/Gas_cooled_nuclear.pdf

Additional Reading Materials: (belongs to Chapter 7)

- David Petti, An Overview of the DOE Advanced Gas Reactor Fuel Development and Qualification Program, Proc. of OECD / NEA's Workshop on Advanced Reactors With Innovative Fuels, 16-18 February 2005, Oak Ridge National Laboratory, Oak Ridge, Tennessee, USA (2005).
- Next Generation Nuclear Plant Research and Development Program Plan, INEEL/EXT-05-02581 Idaho National Engineering and Environmental Laboratory, USA (2005).
- Preliminary Assessment of Existing Experimental Data for Validation of Reactor Physics Codes and Data for NGNP Design and Analysis, ANL-05/05, Argonne National Laboratory, USA (2005) (gives nice description of several GCR reactors).

Additional Reading Materials: (belongs to Chapter 12 & 13)

- For a more detailed version of this article, see D.G. Martin, Considerations pertaining to the achievement of high burn-ups in HTR fuel, Nucl. Eng. Des., 213 (2002) 241-258.
- For a simple analytical model, see D.G. Martin, An analytical method of calculating, to a reasonable accuracy, stresses in the coatings of HTR fuel particles, J. Nucl. Mater. 48 (1973) 35-46.
- For a review of PyC properties see Chapter 7 of "Irradiation damage in graphite due to fast neutrons in fission and fusion systems", IAEA-TECDOC-1154, [refer 45].
- US NUCLEAR REGULAROTY COMMISSION, TRISO-Coated Particle Fuel Phenomenon Identification and Ranking Tables (PIRT) for Fission Product Transport Due to Manufacturing, Operations, and Accidents, NUREG/CR-6844, US NRC, Washington, DC., (2004).

REFERENCES

[1] Energy to 2050 - Scenarios for a Sustainable Future, Organization for Economic Co-operation and Development (OECD) & International Energy Agency (IEA) Publication, Paris, France (2003) ISBN: 92-64-01904-9.

[2] INTERNATIONAL ATOMIC ENERGY AGENCY, International Status and Prospects of Nuclear Power, IAEA, Vienna (2008) http://www.iaea.org/Publications/Booklets/NuclearPower/np08.pdf.

[3] HOWARD, R.M., PRICE, M.S.T., SHEPHERD, L.R., A Summary and Evaluation of the Achievements of the Dragon Project and its Contribution to the Development of the High Temperature Reactor, Dragon Report DP-1000, OECD High Temperature Reactor Project (1978).

[4] IVENS, G., WIMMERS, M., "The AVR as Test Bed for Fuel Elements," in: Association of German Engineers (VDI) (Ed.), "AVR – Experimental High Temperature Reactor, 21 Years of Successful Operation for a Future Energy Technology," VDI-Verlag Dusseldorf (1990).

[5] SAITO, S., et al., Design of High Temperature Engineering Test Reactor (HTTR), Report of the Japan Atomic Energy Research Institute, JAERI 1332 (1994).

[6] SIMON, W., General Atomics, Gas Turbine-Modular Helium Reactor, Proceedings: American Nuclear Society (ANS) Winter Conference, Reno/Nevada, USA, Nov. 11-15, 2001.

[7] STEWARD, K.P., Final Summary Report on the Peach Bottom End-of-Life Program, Report GA-A14404, General Atomic Company (1978).

[8] ROLLIG, K., "The THTR Coolant Gas Activity, an Indicator of Fuel Performance, Behaviour of GCR Fuel under Accident Conditions", Proc. IAEA Specialists' Mtg, Oak Ridge, 1990), IWGGCR/25, IAEA, Vienna (1991) 99-108.

[9] BAXTER, A.M., et al., FSV Experience in Support of the GT-MHR Reactor Physics, Fuel Performance, and Graphite, Report GA-A21925, GA Technologies Inc. (1982).

[10] Matzner, D. (2004), "*PBMR Project Status and the way ahead",* Proc. 2nd Int'l Topical Mtg on High Temperature Reactor Technology, Beijing, China, Sept 22-24, 2004, paper A03.

[11] TANG, C., *"Current Status of HTR-PM Fuel,"* Third CRP-6 Research Coordination Meeting on Advances in HTGR Fuel Technology, June 18-22, 2007, IAEA, Vienna.

[12] Next Generation Nuclear Plant-Research and Development Plan, INEEL/EXT-05-02581, January 2005.

[13] RODRIGUEZ, C., et al., Deep-Burn: making nuclear waste transmutation practical, Nuc. Eng. and Design **222** 2-3 (June 2003) 299-317.

[14] INTERNATIONAL ATOMIC ENERGY AGENCY, Energy, Electricity and Nuclear Power Estimates for the Period up to 2030, 2008 Edition, Reference Data Series No. 1, IAEA-RDS-1/28, 53, IAEA, Vienna (2008)

[15] SOKOLOV, Y.A., Status of Nuclear Power: A global view, presented at Global 2005, 9-13 Oct 2005, JAEI (2005).

[16] INTERNATIONAL ATOMIC ENERGY AGENCY, Fuel Performance and Fission Product Behaviour in Gas Cooled Reactors, IAEA-TECDOC-978, IAEA, Vienna (1997).

[17] INTERNATIONAL ATOMIC ENERGY AGENCY, Status and Prospects for Future Gas Cooled Reactor Fuels, IAEA-TECDOC-1614, IAEA, Vienna (2009).

[18] HOWARD, R.M., PRICE, M.S.T., SHEPHERD, L.R., (Ed.), A Summary and Evaluation of the Achievements of the Dragon Project and its Contribution to the Development of the High Temperature Reactor, Dragon Report DP-1000, OECD High Temperature Reactor Project (1978).

[19] VOICE, E.H., LAMB, D.N., The Deposition and Structure of Pyrolytic Silicon Carbide, Dragon Report DP-667, OECD High Temperature Reactor Project (1969).

[20] ALLEN, P.L., FORD, L.H., SHENNAN, J.V., Nuclear Fuel Coated Particle Development in the Reactor Fuel Element Laboratories of the U.K. Atomic Energy Authority, Nucl. Techn. **35** (1977) 246-253.

[21] KADNER, M., BAIER, J., Production of Fuel Kernels for High-Temperature Reactor Fuel Elements, Kerntechnik **18** (1976) 413-420.

[22] NAEFE, P., ZIMMER, E., Preparation of Uranium Kernels by an External Gelation Process, Nucl. Techn. **42** (1979) 163-171.

[23] MÜLLER, A., "Establishment of the Technology to Manufacture Uranium Dioxide Kernels for PBMR Fuel", Proc. from the Third Int'l Topical Mtg on High Temperature Reactor Technology, Johannesburg, South Africa, October 1 -4, 2006, Paper B00000070.

[24] HUNT, R.D., COLLINS, J.L., Uranium Kernel Formation via Internal Gelation, Radiochim Acta **92** (2004) 909-915.

[25] STINTON, D.P., LACKEY, J.L., SPENCE, R.D., Production of Spherical UO_2-UC2 for Nuclear Fuel Applications using Thermochemical Principles, J. Am. Ceramic Soc. **65** (1982) 321.

[26] ABLITZER, C, et al., "CVD Coating in Fluidized-Bed Furnace: Pyrolytic Carbon and SiC Deposition", Eurocourse on coated particle fuel, Petten, NL, December 2007.

[27] PETTI, A., et al., Key Differences in the Fabrication, Irradiation and Safety Testing of U.S. and German TRISO-coated Particle Fuel and Their Implications on Fuel Performance, INEEL/EXT-02-00300 (June 2002).

[28] HUNN, J.D., Quality Assurance and Quality Control for Coated Particles and Fuel Compacts, Eurocourse on coated particle fuel, Petten, NL, December 2007.

[29] NABIELEK, H., et al., Fuel for Pebble-Bed HTRs, Nucl. Eng. Des. **78** (1984) 155-166.

[30] SAITO, S., et al., Design of High Temperature Engineering Test Reactor (HTTR), JAERI-1332, Tokyo (1994).

[31] KATO, S., et al., Fabrication of HTTR first loading fuel, IAEA-TECDOC-1210, IAEA, Vienna (2001).

[32] SAWA, K., et al., Fabrication of the First-Loading Fuel of the High Temperature Engineering Test Reactor, J. Nucl. Sci. Techn. 6 (1999) 83.

[33] UETA, S., et al., "Database of Fabrication Characteristics of the Second-loading-fuel for the High Temperature Engineering Test Reactor (1) – Fuel kernels, Coated fuel particles and fuel compacts –", JAEA-Data/Code 2006-009 (2006) (in Japanese).

[34] VITALI, M.P., Very/High Temperature Reactor Technology -Fuel bodies: rods/ sticks/ blocks, compacts/ pin-in-block, in EuroCourse 2007, Petten, The Netherlands, December 4-7, 2007, NRG, IAEA, RAPHAEL, PUMA and Institut fuer Kernenergetik und Energiesysteme (IKE), Universitaet, Stuttgart, Germany (2007) http://lehre.ike.uni-stuttgart.de/eurocourse2/index.html.

[35] PETTI, D.A., et al., "Technical Program Plan for the Advanced Gas Reactor Fuel Development and Qualification Program," Idaho National Laboratory Report INL/EXT-05-00465, Revision 1 (Aug. 2005).

[36] PAPPANO, P.J., BURCHELL, T.D., HUNN, J. D., TRAMMELL, M.P., A novel approach to fabricating fuel compacts for the Next Generation Nuclear Plant (NGNP), J. Nucl. Mater. 381 (2008) 25.

[37] FORTESCUE, P., BELL F.R., DUFFIELD, R.B., "Hexagonal Fuel Element", US Patent Application No. 485,811, Filed September 8, 1965.

[38] DAHLBERG, R. C., TURNER, R.F., GOEDDEL, W.V., FSV Core Design Characteristics, Nucl. Eng. Int'l **14** 163 (December 1969).

[39] MELESE, G., KATZ, R., Thermal and Flow Design of Helium-Cooled Reactors, American Nucl. Soc., La Grange Park (1985).

[40] KOUTZ, S. L., TURNER, R.F., FORTESCUE, P., Fuel Element for a Neutronic Reactor, US Patent No. 3,135,665, Issued June 2, 1964.

[41] TURNER R. F., DUFFIELD, R.B., HTGR Fuel Element Performance in Peach Bottom Reactor, Report GA-8113 (July 1967).

[42] STEWARD, K. P., Final Summary Report on the Peach Bottom End-of-Life Program, DOE Report GA-Al4404, General Atomic Company (1978).

[43] BRESNICK S., et al., MHTGR Fuel Process and Quality Control Description, Document No. DOE-HTGR-90257 (Sept. 1991).

[44] BAXTER, A.M., et al., FSV Experience in Support of the GT-MHR Reactor Physics, Fuel Performance, and Graphite, GA-A21925, General Atomics (Nov. 1994).

[45] INTERTANIONAL ATOMIC ENERGY AGENCY, Irradiation Damage in Graphite Due to Fast Neutrons in Fission and Fusion Systems, IAEA-TECDOC-1154, IAEA, Vienna (2000).

[46] INTERTANIONAL ATOMIC ENERGY AGENCY, Graphite Moderator Lifecycle Behavior, IAEA-TECDOC-901, IAEA, Vienna (1996).

[47] BURCHELL, T., BRATTON, R., WINDES, W., NGNP Graphite Selection and Acquisition Strategy, ORNL/TM-2007/153 (2007).

[48] ODEYCHUK, *M.P.,* ZELENSKIY, V.F., YAKOVLEV, V.K., The current state of HTGR core components fabrication technologies in Ukraine and some properties of the materials and products, Proc. of Techical Meeting on Current Status and Future Prospects of Gas Cooled Reactor Fuels, IAEA Vienna, 7-9 June 2004, Status and Prospects for Future Gas Cooled Reactor Fuels, IAEA-TECDOC-1614, IAEA, Vienna (2009).

[49] ISHIHARA, M., et al., "Effects of Superplastic Deformation on Thermal and Mechanical Properties of 3Y-TZP Ceramics", The Second Information Exchange Mtg on Basic Studies in the Field of High Temperature Engineering, at OECD, Paris, 10-12 October 2001, p. 17, http://www.nea.fr/html/science/htemp/iem2/abstracts/httr2-abstracts-for-dist-r0.pdf.

[50] SOWDER, W.K., Quality Assurance Program Plan for AGR Fuel Development and Qualification Program, INEEL/EXT-04-01825, Idaho National Engineering and Environmental Laboratory, Idaho Falls, Idaho (Oct. 2003).

[51] HUNN, J.D., "Quality Assurance and Quality Control for Coated Particles and Fuel Compacts," presented in Eurocourse on coated particle fuel, Raphael Project, Petten, NL, December 2007.

[52] JELLISON, Jr., G.E., HUNN, J.D., LOWDEN, R.A., Optical Characterization of Tristructural Isotropic Fuel Particle Cross-sections Using Generalized Ellipsometry (Proc. E-MRS 2005 Spring mtg, Symp), J. Nucl. Mater. **352** (2006) 6-12.

[53] JELLISON, Jr., G.E., HUNN, J.D., Optical Anisotropy Measurements of TRISO Nuclear Fuel Particle Cross-sections: The Method, J. Nucl. Mater. **372** (2008) 36-44.

[54] ASTM INTERNATIONAL, Standard Test Method for Density of Plastics by the Density Gradient Technique, ASTM D1505-98, ASTM International, West Conshohocken, PA (1999).

[55] KIM, W.K., et al., "Non-destructive Measurement of the Coating Thickness in the Simulated TRISO-Coated Fuel Particle for the HTGR", 3nd International Topical Meeting on High Temperature Reactor Technology, Johannesburg – South Africa, 2006.

[56] PRICE, J.R., et al., New Developments in Image-based Characterization of Coated Particle Nuclear Fuel (Proc. Machine Vision Applications in Industrial Inspection XIV), SPIE Vol. 6070 (2006) 153-162.

[57] WALLISCH, K., KOSS, P., Automatic Size Analysis of Coated Fuel Particles, Nucl. Techn. **35** (1977) 279-283.

[58] BASINI, V., CHAROLLAIS, F., New Techniques Dedicated to the Characterization of Future Nuclear Fuels, Revue de métallurgie **96** (1999) 641-648.

[59] LE HOUËDEC, H., et al., Superlattices and Microstructures **35** (2004) 401-408.

[60] ROCHAIS, D., LE MEUR, G., BASINI, V., DOMINGUES, G., "Microscopic Thermal Characterization of HTR Particle Layers", Proc. 3nd International Topical Meeting on High Temperature Reactor Technology, Johannesburg – South Africa, 2006.

[61] ROCHAIS, D., LE MEUR, G., BASINI, V., DOMINGUES, G., Microscopic thermal characterization of HTR particle layers, Nucl. Ener. and Design **238** (2008) 3047-3059.

[62] BARIN, I., KNACKE, O., Thermochemical Properties of Inorganic Substances, Berlin; New York: Springer-Verlag, (1973).

[63] MILLER, G. K., et al., Current Capabilities of the Fuel Performance Modeling Code PARFUME, Proc. of Second International Topical Meeting on High Temperature Reactor Technology, Beijing, CHINA, September 22-24, 2004, INET, Beijing, (2004) Paper B10.

[64] MARTIN, D.G., "Physical and Mechanical Properties of the Constituents of Coated Particles and the Effects of Irradiation", HTR-F WP3 Meeting, Lyon (2001).

[65] HOFMANN, G., et al., An Investigation of the Relationship Between Position Within Coater and Pyrolytic Carbon Characteristics Using Nanoindentation, Carbon 38 (2000) 645-653.

[66] CONTARD, R., NABIELEK, H., Performance Evaluation of Modern HTR TRISO Fuels, HTA-IB-05/90 (July 1990).

[67] FELTUS, M.A., et al., US Advanced Gas Reactor Fuel Program, The Netherlands, December 4-7, 2007, NRG, IAEA, RAPHAEL, PUMA and Institut fuer Kernenergetik und Energiesysteme (IKE), Universitaet, Stuttgart, Germany (2007) http://lehre.ike.uni-stuttgart.de/eurocourse2/index.html

[68] FELTUS, M.A., et al., Overview of the DOE Advanced Gas Reactor Fuel Development and Qualification Program and Gas Reactor R&D, Proc. of Techical Meeting on Current Status and Future Prospects of Gas Cooled Reactor Fuels, IAEA Vienna, 7-9 June 2004, Status and Prospects for Future Gas Cooled Reactor Fuels, IAEA-TECDOC-1614, IAEA, Vienna (2009).

[69] BELL, G.L., et al., Technical Program Plan for the Advanced Gas Reactor Fuel Development and Qualification Program, Oak Ridge National Laboratory Report ORNL/TM-2002/262 (April 2003).

[70] PETTI, D.A., GROVER, S.B., MAKI, J.T., "Status of the First Advanced Gas Reactor Fuel Irradiation Experiment in the Advanced Test Reactor," in Proc. of 4th International Topical Meeting on High Temperature Reactor Technology – HTR 2008, September 28 – October 1, 2008, Washington, D.C., USA, Paper HTR2008-58024.

[71] FÜTTERER, M.A., et al., "Irradiation of High Temperature Reactor Fuel Pebbles at VHTR Conditions in the HFR Petten", 2nd International Topical Meeting on High Temperature Reactor Technology, Paper B12, Beijing, China, September 22-24, 2004.

[72] REMPE, J.L., et al., "Evaluation of Specialized Thermocouples for High-Temperature In-Pile Testing," Proceedings of the International Congress on Advances in Nuclear Power Plants, Paper 6068, Reno, NV, USA, June 4-8, 2006.

[73] OLANDER, D.R., Fundamental Aspects of Nuclear Reactor Fuel Elements, National Technical Information Service, U.S. Department of Commerce, Springfield, Virginia, Publication No. TID-26711-P1 (1976).

[74] MİLLER, G.K., PETTİ, D.A., VARACALLE, D.J., MAKİ, J.T., Consideration of the Effects on Fuel Particle Behavior from Shrinkage Cracks in the Inner Pyrocarbon Layer, J. Nucl. Mater. **295** (2001) 205-212.

[75] MİLLER, G.K., PETTİ, D.A., MAKİ, J.T., Consideration of the Effects of Partial Debonding of the IPyC and Particle Asphericity on TRISO-coated Fuel Behavior, J. Nucl. Mater. **334** (2004) 79.

[76] KETTERER, J.W., BULLOCK, R.E., Capsule HRB-15B Postirradiation Examination Report, GA-A15940 (June 1981).

[77] Projektleitung Hochtemperaturreaktor-Brennstoffkreislauf (HBK),"Projektbericht 1984," 1984.

[78] MARTİN, R.C., Compilation of Fuel Performance and Fission Product Transport Models and Database for MHTGR Design, ORNL/NPR-91/6 (Oct. 1993).

[79] MİLLER, G.K., PETTİ, D.A., MAKİ, J.T., KNUDSON, D.J., An Evaluation of the Effects of SiC Layer Thinning on Failure of TRISO-coated Fuel Particles, J. Nucl. Mater. **355** (2006) 150-162.

[80] PRİCE, R.J., Properties of Silicon Carbide for Nuclear Fuel Particle Coatings", Nucl. Tech. 35 (1977) 320-336.

[81] RUGGIRELLO G., TOSCANO, E.H., Modelling of V/HTR fuel elements and coated particles: needs of PIE in support to the European RAPHAEL and GEN-IV projects, in Proc. of HOTLAB, Petten, Netherlands, May 23-25, 2005, SCK.CEN, (2005) http://www.sckcen.be/HOTLAB/events/proceedings/2005/session2.pdf.

[82] COEN, V., et al., "Cesium Migration in Silicon Carbide", Jou. Nucl. Mater., **45** (1972/1973) 96.

[83] COEN, V., et al., "Interaction Between Silicon Carbide, Cesium and Strontium," in Proc. BNES Int. Conf. Nuclear Fuel Performance, P. 19.1, British Nuclear Energy Society, London (1973).

[84] MİNATO, K., et al., "Fission Product Behavior in TRISO-coated UO_2 Fuel Particles", J. Nucl. Mater. **208** (1994) 266-281.

[85] CONTARD R., NABİELEK H., "Performance Evaluation of Modern HTR TRISO Fuels," HTA-IB-05/90, July 1990.

[86] SCHENK, W., Nachbestrahlungsausheizverfahren für Kügelbrennelemente und andere Brennstoffproben, Jülich Report 1454 (July 1977).

[87] SCHENK, W., PİTZER, D., NABİELEK, H., Fission Product Release Profiles from Spherical HTR Fuel Elements at Accident Temperatures, Jülich Report 2234 (Sep. 1988).
[88] SCHENK, W., GONTARD, R., NABİELEK, H., Performance of HTR Fuel Samples under High-Irradiation and Accident Simulation Conditions, with Emphasis on Test Capsules HFR-P4 and SL-P1, Forschungszentrum Jülich Report Jül-3373, April 1997.
[89] OLANDER, D.R., Fundamental aspects of nuclear reactor fuel elements, TID-26711-P1, Technical Information Center, US-DOE, Washington D.C. (1976).
[90] LINDEMER, T.B., DE NORDWALL, H.J., An Analysis of Chemical Failure of Coated UO_2 and other Oxide Fuels in the High Temperature Gas-Cooled Reactor, Tech. Rep. ORNL-4926, Oak Ridge National Laboratory, Oak Ridge (1974).
[91] STULL, D.R., PROPHET, H. JANAF, Thermochemical Tables, NSRDS-NBS-37, U.S. Government Printing Office, Washington D.C. (1971).
[92] JAVED, N.A., Phase relations in the uranium-carbon-oxygen system at 1573 K, J. Nucl. Mater. **37** (1970) 353-354.
[93] CHEVALIER, P.-Y, CHEYNET, B., FISCHER, E., Progress in the thermodynamic modelling of the O–U binary system, J. Nucl. Mater. **303** (2002) 1-28.
[94] GUÉNEAU, S., et al., Thermodynamic assessment of the uranium-oxygen system, J. Nucl. Mater. **304** (2002) 161-175.
[95] CHEYNET, B., FISCHER, E., MEPHISTA: A Thermodynamic Database for Next Generation Nuclear Fuels, http://hal.archives-ouvertes.fr/hal-00222025/fr/
[96] PETTI, D.A., et al., Key differences in the fabrication, irradiation and high temperature accident testing of US and German TRISO-coated particle fuel, and their implications on fuel performance, Nucl. Eng. Des. **222** (2003) 281.
[97] MINATO, M., et al., Carbon monoxide-silicon carbide interaction in HTGR fuel particles, J. Mater. Sci. **26** (1991) 2379-2388.
[98] KAAE, L.J., STERLING, S.A.; YANG, L., Improvements in the Performance of Nuclear Fuel Particles Offered by Silicon-Alloyed Carbon Coatings, Nucl. Tech. **35** (1977) 359.
[99] M. WAGNER-LOFFLER, Amoeba behavior of UO_2 coated particle fuel, Nucl. Techn. **35** (1977) 392.
[100] MAKI, J.T., PETTI, D.A., KNUDSON, D.L, MILLER, G.K., The challenges associated with high burnup, high temperature and accelerated irradiation for TRISO-coated particle fuel, J. Nucl. Mater. **371** (2007) 270-280.
[101] CROFF, A.G., A user's manual for the ORIGEN2 computer code, ORNL/TM-7175 (1980).
[102] POSTON, D.L., TRELLUE, H.R., User's Manual, Version 2.0 for MONTEBURNS Version 1. LA-UR-99-4999, Los Alamos National Laboratory (1999).
[103] K. MINATO, et al., Fission product behavior in Triso-coated UO_2 fuel particles, J. Nucl. Mater. **208** (1994) 266-281.
[104] BILDSTEIN, H., STRIGL, A., Determination of gases in low enriched coated particles, OECD High Temperature Reactor Project (England), D.P. Report 728 (1970).
[105] MATZKE, H.J., Oxygen potential measurements in high burnup LWR $U0_2$ fuel, J. Nucl. Mater. **223** (1995) 1-5.
[106] WALKER, C.T., et al., On the oxidation state of UO_2 nuclear fuel at a burn-up of around 100 MWd/kgHM, J. Nucl. Mater. **345** (2005) 192-205.

[107] SPINO, J., PEERANI, P., Oxygen stoichiometry shift of irradiated LWR-fuels at high burn-ups: Review of data and alternative interpretation of recently published results, J. Nucl. Mater. **375** (2008) 8-25.

[108] DIECKER, J.T., "Development of high temperature gas cooled reactor TRISO coated particle fuel chemistry model", MIT Nuclear Engineering, Master Thesis (United States) (2005).

[109] HOMAN, F.J., et al., Stoichiometric Effects on performance of high temperature gas-cooled reactor fuels from the U-C-O system, Nucl. Techn. **35** (1977) 428-441.

[110] GOSSÉ, S., et al., "Kinetic study of the UO_2/C interaction by high temperature mass spectrometry", 3rd Intern. Topical Meeting on High Temperature Reactor Technology, October 1-4, 2006, Johannesburg (South Africa).

[111] LINDEMER, T.B., ALLEN, M.D., LEITNAKER, J.M., Kinetics of the graphite-uranium dioxide reaction from 1400°C to 1756°C, J. Amer. Ceram. Soc. **52** (1969) 233-237.

[112] MUKERJEE, S.K., DEHADRAYA, J.V., VAIDYA, V.N, SOOD, D.D., Kinetics and mechanism of UO_2 + C reaction for UC/UC_2 preparation, J. Nucl. Mater. **210** (1994) 107-114.

[113] PROKSCH, E., STRIGL, A., NABIELEK, H., Production of carbon monoxide during burn-up of UO_2 kerneled HTR fuel particles, J. Nucl. Mater. **107** (1982) 280-285.

[114] SCHRAM, R.P.C., CORDFUNDKE, E.H.P., VAN HEEK, A.I., "High-temperature reactor developments in the Netherlands", Contribution to the 3rd JAERI Symposium on HTGR Technologies, 15-16 February 1996, Japan.

[115] BARRACHIN, M., DUBOURG, R., KISSANE, M., OZRIN, V., Progress in understanding fission-product behaviour in coated uranium dioxide fuel particles, J. Nucl. Mater. **385** (2009) 372-386.

[116] MORRIS, R.N., PETTI, D.A., POWERS, D.A., BOYACK, B.E., TRISO-coated fuel particle phenomenon identification and ranking tables for fission product transport due to manufacturing, operations, and accidents, NUREG/CR-6844, US NRC (2004).

[117] GRIMES, R., CATLOW, C.R.A., The stability of fission products in uranium dioxide, Phil. Trans. R. Soc. Lond **A335** (1991) 609-634.

[118] NICOLL, S., MATZKE, H.J., GRIMES, R.W., CATLOW, C.R.A., The behaviour of single atoms of molybdenum in urania, J. Nucl. Mater. **240** (1997) 185.

[119] MARTIN, P., et al., A study of molybdenum behaviour in UO_2 by X-ray absorption spectroscopy, J. Nucl. Mater. **326** (2004) 132.

[120] KLEYKAMP, H., The solubility of selected fission products in UO_2 and (U, Pu)O_2, J. Nucl. Mater. **206** (1993) 82.

[121] BUSKER, G., GRIMES, R., BRADFORD, M.R., The diffusion of iodine and cesium in the $UO_{2\pm x}$ lattice, J. Nucl. Mater. **279** (2000) 46.

[122] TIWARI, G., SINGH, J., Consideration of swelling and thermodynamic stability of inert gas bubbles in solids, J. Nucl. Mater. **195** (1992) 205.

[123] M. S. VESHCHUNOV, V. E. SHESTAK, "An advanced model for intragranular bubble diffusivity in irradiated UO_2 fuel", Jou. Nucl. Mater. **376** (2008) 174-180.

[124] THOMAS, L.E., BEYER, C.E., CHARLOT, L.A., Microstructural analysis of LWR spent fuels at high burnup, J. Nucl. Mater. **188** (1992) 80.

[125] TRINKHAUS, H., In Fundamental aspects of inert gases in solids (DONNELY, S.E., EVANS, J.H., Eds), Plenum, New York (1991) 369.

[126] WHITE, R.J., The development of grain-face porosity in irradiated oxide fuel, J. Nucl. Mater. **325** (2004) 61-77.

[127] KLEYKAMP, H., The chemical state of the fission products in oxide fuels", J. Nucl. Mater. **131** (1985) 221.
[128] MINATO, K., et al., Fission product palladium-silicon carbide interaction in HTGR fuel particles, J. Nucl. Mater. **172**, (1990) 184.
[129] NABIELEK, H., BROWN, P.E., OFFERMANN, P., Silver release from coated particle fuel, Nucl. Techn. **35** (1977) 483.
[130] K. MINATO, et al., Release behavior of metallic fission products from HTGR fuel particles at 1600 to 1900°C, J. Nucl. Mater. **202** (1993) 47.
[131] LAUF, R.J., LINDEMER, T.B., PEARSON, R.L., Out-of-reactor studies of fission product-silicon carbide interactions in HTGR fuel particles, J. Nucl. Mater. **120** (1984) 6.
[132] OGAWA, T., IKAWA, K., Reactions of Pd with SiC and ZrC, High Temp. Sci. **22** (1986) 179.
[133] LINDEMER, T.B., Thermochemical analysis of gas-cooled reactor fuels containing Am and Pu oxides, Tech. Report ORNL/TM-2002/133, Oak Ridge National Laboratory (2002).
[134] BHANUMURTHY, K., SCHMID-FETZER, R., Experimental study of ternary Pd-Si-C phase equilibria and Pd/SiC Interface Interactions", Z. Metallkd **87** (1996) 244.
[135] DU, Z., GUO, C., YANG, X., LIU, T., A thermodynamic description of the Pd-Si-C system, Intermatallics, **14** (2006) 560.
[136] MINATO, K., FUKUDA, K., ISHIKAWA, A., MITA, N., Advanced coatings for HTGR fuel particles against corrosion of SiC layer, J. Nucl. Mater. **246** (1997) 215.
[137] KASTEN, P.R., CORUM, M.R., RITTENHOUSE, P.L., Research on very high temperature gas reactors, Report EPRI ER/NP-7372, Electric Power Research Institute (1991).
[138] MINATO, K., OGAWA, T., FUKUDA, K., Review of experimental studies of zirconium carbide coated fuel particles for high temperature gas-cooled reactors, Report JAERI-Review 95-004, JAERI, Tokyo (1995).
[139] MINATO, K., et al., Fission product release from ZrC coated fuel particles during postirradiation heating at 1600°C, J. Nucl. Mater. **224** (1995) 85.
[140] MINATO, K., Irradiation experiment on ZrC-coated fuel particles for high-temperature gas-cooled reactors", Nucl. Techn. **130** (2000) 272.
[141] MINATO, K., et al., Retention of fission product cesium in ZrC-coated fuel particles for high-temperature gas-cooled reactors, J. Nucl. Mater. **279** (2000) 181.
[142] MINATO, K., et al., Deterioration of ZrC-coated fuel particle cuased by failure of pyrolitic carbon layer, J. Nucl. Mater. **252** (1998) 13.
[143] MACLEAN, H.J., et al., The effect of annealing at 1500°C on migration and release of ion implanted silver in CVD silicon carbide, J. Nucl. Mater. **357** (2006) 31.
[144] JIANG, W., et al., Thermal and dynamic responses of Ag implants in silicon carbide, Nuclear Instr. and Methods in Phys. Research B, **219-220** (2004) 642.
[145] GUDKOV A.N., et al., Behavior of solid fission products in coated fuel particles of a high-temperature gas-cooled reactor, Atomic Energy, Volume 67, Number 2 / ((1989) pp 1063 {Translated from Atomnaya Énergiya, Vol. 67, No. 2, pp. 93–97, August, 1989}).
[146] SEHGAL, B.R. (ed.), LWR severe accident safety. SARNET deliverable (to appear) (2008).
[147] SALZANO, F.J., ARONSON, S., Thermodynamic properties of the cesium-graphite lamellar compounds, J. Chem. Phys. **43** (1965) 149.

[148] SALZANO, F.J., ARONSON, S., Stability of Phases in the Cesium-Graphite System, J. Chem. Phys. **45** (1966) 2221.
[149] NOVIKOV, Y.N., VOL'PIN, M.E, Lamelar Compounds of Graphite with Alkali Metals, Russian Chem. Rev. **40** (1971) 733.
[150] SANGSTER, J., C-Cs (Carbon-Cesium) System, J. Phas. Equil. and Diff. **29** (2008) 93.
[151] SALZANO, F.J., ARONSON, S., Kinetic Study of the Decomposition of Cesium-Graphite Lamellar Compounds, J. Chem. Phys. **45** (1965) 1323.
[152] SALZANO, F.J., ARONSON, S., The compatibility of Graphite with Cesium", Nucl. Sci. and Engin. **28** (1967) 51.
[153] KLEYKAMP, H., Mikrosondenuntersuchungen zum Verhalten der Spaltprodukte in hochabgebrannten HTR-Brennstoffen, Tech. Rep. KfK-2213 (1975).
[154] WALTHER, H., Stress analysis in coated fuel particles: part I – theory and examples, Dragon Project Report 604, August 1968.
[155] BAUMER, R., et al., AVR – Experimental High-Temperature Reactor: 21 Years of Successful Operation for a Future Energy Technology, Association of German Engineers (VDI) – The Society for Energy Technologies, Dusseldorf (1990).
[156] KROHN, H. et al., FRESCO II: Ein Rechenprogramm zur Berechnung der Spaltproduktfreisetzung aus kugelförmigen HTR Brennelementen in Bestrahlungs- und Ausheizexperimenten, Jül-Spez-212, Forschungszentrum Jülich, June 1983.
[157] HANSON, D.L., A Review of Radionuclide Release from HTR Cores during Normal Operation, EPRI Report 1009382, Electric Power Research Institute (Feb. 2004).
[158] NABIELEK, H., et al., Performance Limits of Coated Particle Fuel; Part III: Fission Product Migration in HTR Fuel, DP-828 (Pt. 3), Dragon Project (June 1974).
[159] CRANK, J., The Mathematics of Diffusion, Oxford University Press (1975).
[160] INCROPERA, F., DEWITT, D., Fundamentals of Heat and Mass Transfer, J Wiley and Sons, 5th ed. (2002).
[161] BOOTH, A., A method of calculating fission gas diffusion from UO2 fuel and its application to the X-2-F loop test, Report CRDC-721, Atomic Energy of Canada Ltd (1957).
[162] RÖLLIG, K., Release of Rare Fission Gases from Spherical Elements with Coated Fuel Particles, Nucl. Techn. 35 (Sept. 1977) 516.
[163] MYERS, B.F., MORRISSEY, R.E., Licensing Topical Report: The Measurement and Modeling of Time-Dependent Fission Product Release from Failed HTR Fuel Particles under Accident Conditions, GA-A15430, General Atomic (Apr. 1980).
[164] VAN DER MERWE, J.J., Development and validation of fission product release models and software at PBMR, Proc. Int. Conf. on HTR's, HTR-2004, Beijing, China, September 2004.
[165] VENTER, J.H., VAN DER MERWE, J.J., HTR Fuel Design, Qualification and Analysis at PBMR, Proc. Int. Conf. From American Nuclear Society's Topical Meeting on Reactor Physics, PHYSOR 2006, Vancouver, BC, Canada, September 10-14, 2006.
[166] VAN DER MERWE, J.J., Development of a Fission Product Release Model and its Application at PBMR, Proc. Int. Conf. on HTR's, HTR-2006, Johannesburg, South Africa, October 2006.
[167] MAKI, J.T., et al., NP-MHTR Fuel Development Program Results, Idaho National Engineering and Environmental Laboratory Report, INEEL/EXT-2002-1268 (1992).

[168] MUTO, Y., ISHIYAMA, S., SHIOZAWA, S., Study of Fission Product Release, Plate-Out and Maintenance in Helium Turbomachinery, Japan Atomic Energy Research Institute, IAEA Committee Meeting on Gas Turbine Power Conversion Systems for Modular HTRs, Palo Alto, (14-16 Nov 2000).
[169] U.S. DOE Nuclear Energy Research Advisory Committee and the Generation IV International Forum, "A Technology Roadmap for Generation IV Nuclear Energy Systems," GIF-002, December 2002.
[170] SHROPSHIRE, D.E., HERRING, J.S., Fuel-Cycle and Nuclear Material Disposition Issues Associated with High-Temperature Gas Reactors, in Proc. of the Americas Nuclear Energy Symposium: Building Bridges for Greater Cooperation (ANES 2004), October 3-6, 2004, Miami Beach, Florida, ANS, USA, Session 1.05B.
[171] MHTGR PU Consumption Study – Final Report, General Atomics, May 1993.
[172] HOWARD, R.M., PRICE, M.S.T., SHEPHERD, L.R., A Summary and Evaluation of the Achievements of the Dragon Project and its Contribution to the Development of the High Temperature Reactor, Dragon Report DP-1000, OECD High Temperature Reactor Project (1978).
[173] STEWARD, K.P., Final Summary Report on the Peach Bottom End-of-Life Program, Report GA-A14404, General Atomic Company (1978).
[174] BAXTER., A.M. et al., FSV Experience in Support of the GT-MHR Reactor Physics, Fuel Performance, and Graphite, Report GA-A21925, GA Technologies Inc. (1982).
[175] IVENS, G., WIMMERS, M., The AVR as Test Bed for Fuel Elements," in: Association of German Engineers (VDI) (Ed.), AVR – Experimental High Temperature Reactor, 21 Years of Successful Operation for a Future Energy Technology, VDI-Verlag Dusseldorf (1990).
[176] ROLLIG, K., The THTR Coolant Gas Activity, an Indicator of Fuel Performance, Behaviour of GCR Fuel under Accident Conditions, Proc. IAEA Specialists' Meeting, Oak Ridge IWGGCR/25, IAEA, Vienna (1991) 99-108.
[177] GRENECHE, D., HTR Fuel Cycles: A Comprehensive Outlook of Past Experience and an Analysis of Future Options, ICAPP Conference 2003.
[178] INTERNATIONAL ATOMIC ENERGY AGENCY, "Advanced fuel cycle and reactor concepts: report of INFCE Working Group 8, International Fuel Cycle Evaluation (INFCE), STI/PUB/534, IAEA, Vienna (1980).
[179] SIMON, W., General Atomics, Gas Turbine-Modular Helium Reactor, Proc. American Nuclear Society (ANS) Winter Conference, Reno/Nevada, USA, Nov. 11-15, 2001, (2001).
[180] MITAUT, P., Cycles Combustibles U-Th, Pu-U Appauvri et Pu-Th dans les Réacteurs Modulaires à Haute Température, – CEA Report, DMT/93-291 (June 1993).
[181] BONIN, B., GRENECHE, D., Prospective Studies of HTR Fuel Cycles Involving Plutonium," International conference HTR-2002 –Petten (Netherland), April 22/24, 2002.
[182] Management and Disposition of Excess Weapons Plutonium," Report of the American National Science Academy, 1999 – Vol. 2: Reactor Related Options.
[183] OLSON, G.L., MCCARDELL; R.K., ILLUM, D.B., Fuel Summary Report: Shippingport Light Water Breeder Reactor, INEEL/EXT-98-00799, Rev. 2 (Sept. 2002).
[184] Greneche, D., Masson, M., Brossard, P., "The Reprocessing Issue for HTR Fuels: An assessment of Its Interest and Its Feasibility", Global 2003 Conference, New Orleans, LA November, 2003.

[185] 2002 Operational Waste Stream Assumptions, TDR-CRW-SE-000024 Rev 00, prepared by Bechtel SAIC Company LLC, Las Vegas, NV for US DOE, OCRWM (Sept. 2002).
[186] Next Generation Nuclear Plant – High Level Functions and Requirements," INEEL/EXT-03-01163, Idaho Nation Engineering and Environmental Laboratory, (Sept. 2003).
[187] WICKHAM, A.J., NEIGHBOUR, G.B., DUBOURG, M., "The Uncertain Future for Nuclear Graphite Disposal: Crisis or Opportunity," IAEA Technical Committee Meeting on "Nuclear Graphite Management," Manchester, United Kingdom, 18-20 October 1999.
[188] KRUMBACH, H., DUWE, R., RÖDIG, M., Handling and Behaviour of AVR Fuel Elements for Interim Storage, HOTLAB 2004, Halding, Norway, 2004.
[189] NIEPHAUS, D., Referenzkonzept zur direkten Endlagerung von abgebrannten HTR-Brennelementen in CASTOR THTR/AVR Transport- und Lagerbehältern, Report Jül-3734, Research Center Jülich, Germany, 2000.
[190] RÖLLIG, K., C-14 Freisetzung von abgebrannten THTR-BE, Technical Note 413-211-BF3521, Hochtemperatur-Reaktorbau (HRB) GmbH, Mannheim (1989).
[191] REBMANN, A., DUWE, R., Das Belastungsverhalten von HTR-Brennelementen im salinären Endlager, Internal Report KFA-IRW-IB-3/88, Research Center Jülich (1988).
[192] KIRCH, N., BRINKMANN, H.U., BRÜCHER, P.H., Storage and Final Disposal of Spent HTR Fuel in the Federal Republic of Germany, Nucl. Eng. Des. **121** (1990) 241-248.
[193] DUWE, R., SCHRÖDER, R., Temperatur und Dosisleistung abgebrannter HTR-Brennelemente in Transport- und Lagerbehältern (GNS-Castor, TN-AVR-2), Internal Report KFA-IRW-IB-2/93, Research Center Jülich (1993).
[194] FACHINGER, J., et. al., Behaviour of Spent HTR Fuel Elements in Aquatic Phases of Repository Host Rock Formations, Nucl. Eng. Des. **236** (2006) 543-554.
[195] GANSER, B., et.al., FuE-Arbeiten zur Endlagerung von HTR-Brennelementen, Proc. Status Seminar about Works on High Temperature Reactor Fuel Elements, Graphite, and Disposal, held at Jülich, Germany, May 18, 1987, FZJ Report Jül-Conf-61 (1987) 147-160.
[196] MERZ, E., BRÜCHER, H., HALASZOVICH, S., Lösung der Entsorgungsfrage beim Hochtemperatur-reaktor, in: Fortschritte in der Energietechnik, Monographien des Forschungszentrums Jülich **8 (1993)** 336-348.
[197] POHL, P., AVR Decommissioning, Achievements and Future Programme, in Proc. Tech. Mtg, Jülich, 8-10 Sept, 1997, IAEA-TECDOC-1043, IAEA, Vienna (1998) 41-53.
[198] RÖLLIG, K., et.al., Entsorgung von Hochtemperaturreaktoren, Proc. Status Seminar about Works on High Temperature Reactor Fuel Elements, Graphite, and Disposal, Jülich, Germany, May 18, 1987, Report Jül-Conf-61, Research Center Jülich, Germany (1987) 109-134.
[199] SCHRÖDER G., et.al., Aspekte der Entsorgung des THTR-300, in: Fortschritte in der Energietechnik, Monographien des Forschungszentrums Jülich, Germany, Vol. 8, pp. 301-308, 1993.
[200] PLÄTZER, S., MIELISCH, M., Unloading of the Reactor Core and Spent Fuel Management of THTR-300 (Proc. Tech. Mtg, Jülich, 8-10 Sept, 1997), IAEA-TECDOC-1043, IAEA, Vienna (1998).

ABBREVIATIONS

ADS	Accelerator Driven Systems
ADU	Ammonium Diuranate
ADUN	Acid Deficient Uranyl Nitrate
AERE	Atomic Energy Research Establishment
AGR	Advanced Gas Cooled Reactor
ASTM	American Society for Testing Materials
ATR	Advanced Test Reactor
AVR	Arbeitsgemeinschaft Versuchsreaktor
BAF	Bacon Anisotropy Factor
BISO	Bi-coated Isotropic
BOL	Beginning of Life
BZA	Brennelemente Zwischenlager Ahaus (Fuel Element Interim Storage)
CCD	Charge Coupled Device
CFD	Computational Fluid Dynamics
CERCA	Compagnie pour l'Etude et la Réalisation de Combustibles Atomiques
CVD	Chemical vapour deposition
DLOFC	Depressurized - Loss of Forced Cooling Accident
dpa	Displacements per atom
DRE	DRAGON Reactor Experiment
efpd	Effective full power days
EPMA	Electron-probe Micro Analysis
EOL	End-of-Life
EVA	Einzelspaltrohr-Versuchsanlage (Single Splitting Tube Test Facility)
FIMA	Fissions per Initial Heavy Metal Atom
FPMS	Fission Product Monitoring System
G-IV	Generation-IV reactor
GLCC	Great Lakes Carbon Company
GT-MHR	Gas Turbine- Modular Helium Reactor
FRJ-2	Forschungsreaktor Jülich (Research Reactor Jülich)
FSV	Fort St. Vrain Nuclear Power Station
GA	General Atomics, San Diego, USA

HEU	High Enriched Uranium
HFIR	High Flux Isotope Reactor at Oak Ridge National Laboratory
HFR	High Flux Reactor at Petten
HLW	High Level Waste
HMTA	Hexa-methyl-tetramine
HPGe	High Purity Germanium
HTGR	High Temperature Gas-Cooled Reactor
HTR	High Temperature Reactor
HTTR	High Temperature Engineering Test Reactor
HTR-PM	High Temperature Reactor - Pebble Modular
ICP-MS	Induced Couple Plasma - Mass Spectrometry
IHX	Intermediate Heat Exchanger
IMGA	Irradiated Microsphere Gamma Analyser
INL	Idaho National Laboratory
IPyC	Inner Pyrocarbon Layer
IVV-2M	Research pool-type water-moderated water-cooled reactor of the 2nd series modernized (in Russuian "ИВВ-2М").
ITU	Institute for Transuranium (Karlsruhe, Germany)
JAEA	Japan Atomic Energy Agency
KCMI	Kernel Coating Mechanical Interaction
KUEFA	Kuehlfingerapparatur (Cold Finger Apparatus)
LEU	Low Enriched Uranium
LOCA	Loss of coolant accident
LWR	Light Water Reactor
MA	Minor Actinides
MAGNOX	Magnesium non-oxidizing
MAW	Medium Active Waste
MOX	Mixed (U, Pu) Oxide Fuel
MTHM	Metric Tons Heavy Metal
MTR	Material Test Reactor
MWe	10^6 Watt electrical
MWt	10^6 Watt thermal
NGNP	New Generation Nuclear Plant
nvt	flux (neut·m^{-2}·s^{-1}) · time (s) ≡ fluence (neut·m^{-2})
OAF	Optical Anisotropy Factor

ODS	Oxide Dispersion Strengthened
OPyC	Outer Pyrocarbon Layer
ORNL	Oak Ridge National Laboratory
O/U ratio	Oxygen to Uranium ratio in oxide materials
PBMR	Pebble Bed Modular Reactor
PSA	Particle Size and Shape Analyzer
PWR	Pressurized Water Reactor
PyC	Pyrocarbon Layer
PUREX	Plutonium – URanium EXtraction
IPyC	Inner Pyrocarbon Layer
OPyC	Outer Pyrocarbon Layer
QA/QC	Quality Assurance / Quality Control
R/B	Release Rate to Birth Rate ratio
SCA	Share Cost Action
SMR	Small medium sized reactor
SNF	Spent Nuclear Fuel
SNL	Sandia National Laboratory
TCE	Trichloroethylene
THOREX	THORium Extraction
THTR	Thorium High Temperature Reactor
TRISO	Tri-coated Isotropic
VHTR	Very High Temperature Reactor
YMP	Yucca Mountain Program

CONTRIBUTORS TO DRAFTING AND REVIEW

Barrachin, M.,	IRSN, France
Basini, V.,	CEA, France
Basak U.,	IAEA
Colak, Ü.,	Hacettepe University, Turkey
Dubourg, R.,	IRSN, France
Feltus, M. A.,	US-DOE, USA
Greneche, D.,	AREVA, France
Guillermier, P.,	AREVA, France
Hansen, U.,	University of Rostock, Germany
Hanson, D. L.,	General Atomics, USA
Hunn, J. D.,	ORNL, USA
Kania, M. J.,	(Retired from) ORNL & KAPL USA
Kissane, M.,	IRSN, France
Martin, D. G.,	Consultant-Nexia Solutions PLC, UK
McEachern, D. W.,	General Atomics, USA
van der Merwe, J. J.,	PBMR, South Africa
Nabielek, H.,	(Retired from) FZJ, Germany
Nawada, H. P.,	IAEA, Austria
Nothnagel, G.,	NESCA, South Africa
Petti, D.A.,	INL, USA
Shenoy, A.,	General Atomics, USA
Tang, C.,	Tsinghua University, China
Toscano E. H.,	(Retired from) CEC-ITU Karlsruhe, Germany
Turner R. F.,	(Retired from) General Atomics, USA
Ueta, S.,	JAEA, Japan
Venter, S.,	PBMR, South Africa
Verfondern, K.,	FZJ, Germany
Szymczak, W. J.,	AREVA, France

Consultancy Meetings

Dec 2006, Vienna, Dec. 2007, NRG, Petten and Nov 2008, Vienna